Novel Initiators for the Production of Copolymers

Forder, Thomas

Award date:
2014

Awarding institution:
University of Bath

Novel initiators for the production of copolymers

Thomas R. Forder

A thesis submitted for the degree of Doctor of Philosophy

Department of Chemistry

University of Bath

January 2014

This thesis is dedicated to my parents, Susan and Richard,

and,

in memory of Martha Kay Sangster

Contents

Acknowledgements

Firstly, I would like to express my deepest thanks to my PhD supervisor, Dr Matthew Jones. His continual support and guidance towards my research and wider aspects of the PhD program have made the training experience very enjoyable. I would also like to extend my gratitude to Dr Marianne Ellis and Professor Matthew Davidson for their contribution to the project - placing the research in context and the potential for further applications.

My experience at the University of Bath was one of continual fun and exciting opportunities, I was very lucky to join the DTC in Sustainable Chemical Technologies in its first year and would like to thank all members of the Centre for their hard work and belief in creating a fast-paced and dynamic hub that has provided a great launch pad to my future career. The whole experience would not have been the same without my cohort; a fantastic bunch of chemists and chemical engineers, and those who are a bit of both! I'm forever indebted to their supply of research ideas, encouragement and distraction when needed.

I would like to thank Emma, Carlo, Kirsty, Daniel and Cathy, among others, for warmly welcoming me into the lab and showing me the ropes. Over the years, members of the Jones and Davidson research groups have kept spirits high and it has been a pleasure to work in the lab with them all. Special thanks must go to Stuart, Chris, Heather and Sarah; with an added salute to Ben, Lois and Rhodri, my thesis writing buddies.

My thanks to Drs Mary Mahon and John Lowe for their respective expertise in X-ray crystal structure determination and NMR spectroscopy, and I acknowledge the EPSRC and University of Bath for funding during my studies.

Finally, I would like to thank my family for always providing support and interest in my continued studentdom. I can never come close to thanking my parents enough for all the encouragement and faith they have shown me in all aspects of life; they are my inspiration to succeed in all I do. To my brother, Andrew, I thank you for all your brotherly love and competition; I look forward to seeing our lives develop in the future.

Abstract

The development and improvement of biodegradable plastics from renewable resources is a hot topic in chemical research. One example is the ring-opening polymerisation (ROP) of the cyclic ester *rac*-lactide to give polylactide (PLA). Current industrial metal initiators are non-stereoselective and this thesis investigates a range of catalytic initiators for the ROP of lactide and its copolymerisation with ε-caprolactone.

Chapter 1 presents an introduction to the polymerisation of lactide to yield PLA with insights into polymer tacticity and associated polymer analytical techniques. A current review of the literature, with respect to the controlled polymerisation of lactide using metal initiators, is followed by a discussion of lactide copolymerisation and a review of kinetic studies.

Chapter 2 consists of a series of imine bis(phenolate) ligands, with variation in phenol substituents, that have been coordinated to aluminium (III) and titanium (IV) metal centres. For the aluminium-based initiators ligand steric bulk was found to influence the coordination motif; whilst with the larger titanium metal centre the experimental methodology was also influential. Trialling as initiators for the ROP of lactide found the initiators to be non-stereoselective but with rate constants an order of magnitude higher than similar aluminium initiators in the literature.

Chapter 3 describes the development of a synthetic route to tripodal unsymmetrical amine tris(phenolate) ligands. Complexes with zirconium (IV) and hafnium (IV) were characterised and a monomer-dimer equilibrium is proposed. An in-depth study for the ROP of lactide suggested that dimer dissociation into an active species, and aggregation during propagation, is influential in determining rate and molecular weight control. The unsymmetrical nature resulted in a step-reduction in stereoselectivity providing more evidence of the enhanced chain-end control previously reported for a C_3-symmetric zirconium amine tris(phenolate) initiator.

Chapter 4 looks to apply the aforementioned group IV initiators in the one-pot copolymerisation of lactide and ε-caprolactone. Microstructure is analysed and quantified by different methods, with tapered block copolymers being produced similar to that previously reported for aluminium isopropoxide. Few examples of zirconium-based initiators for the copolymerisation of lactide are present in the literature.

Chapter 5 compiles the procedures followed for the synthesis of ligands, complexes and polymers. Conditions for the polymerisation kinetics experiments and reactivity ratios are also provided, along with details of all analytical techniques used.

Glossary of Abbreviations

ROP	ring-opening polymerisation
LA	lactide
PLA	polylactide
CL	ε-caprolactone
PCL	polycaprolactone
VL	δ-valerolactone
PVL	polyvalerolactone
NMR	nuclear magnetic resonance
s	singlet
d	doublet
dd	doublet of doublets
t	triplet
td	triplet of doublets
q	quartet
sept	septet
m	multiplet
δ	chemical shift
ppm	parts per million
J	coupling constant
DSC	differential scanning calorimetry
T_g	glass transition temperature
T_m	polymer melting temperature
T_c	polymer crystallisation temperature
GPC	gel permeation chromatography
PDI	polydispersity index
M_w	weight average molecular weight
M_n	number average molecular weight
$M_{n\ (calc)}$	theoretical number average molecular weight
P_r	probability of *racemic* enrichment
P_m	probability of *meso* enrichment
"i"	isotactic
"s"	syndiotactic
$[LA]_o$	initial concentration of lactide
$[LA]_t$	concentration of lactide at a specific time, t

CHAPTER 1

INTRODUCTION

1 Introduction

1.1 Polylactide

Polylactide (PLA) is a biodegradable polymer that can be produced from renewable resources.[1 2] It can be processed and machined by similar methods to that used for traditional petroleum based plastics; making it a viable replacement for many commodity products. It is also used in high-value biomedical applications; such as orthopaedics, stents, sutures and dissolvable stiches.[3] PLA, a polyester, can be hydrolysed to a reduced polymer molecular weight and then further biodegraded *via* the Krebs cycle to CO_2, H_2O and humus (Figure 1.2). This biocompatibility and *in vivo* absorption has led to the FDA (U.S. Food and Drug Administration) approval of PLA for therapeutic treatments.[4]

Commercial lactic acid is acquired through the fermentation of sugars found in agricultural waste such as cornstarch. Poly(lactic acid) can be produced *via* a direct condensation method, however, this yields a low molecular weight polymer due to the hydrolysis equilibrium imposed by the water by-product.[5] High molecular weight PLA can most effectively be achieved by the ring-opening polymerisation (ROP) of lactide (3,6-dimethyl-1,4-dioxane-2,5-dione); a cyclic dimer of lactic acid (Figure 1.1).

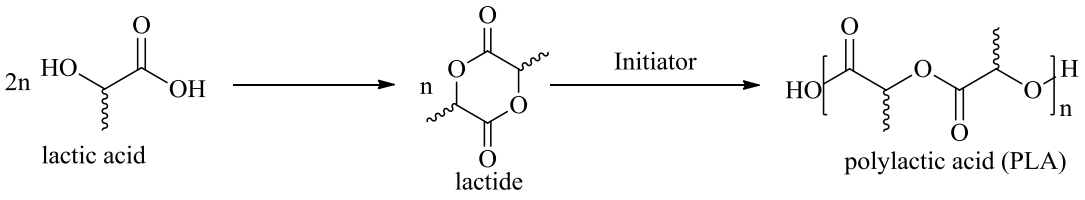

Figure 1.1 Production of PLA *via* the cyclic monomer lactide

The process of generating PLA *via* the ROP of lactide is both an environmentally and economically viable alternative to direct polycondensation of lactic acid due to both the monomer and polymer being synthesised in the melt.[1] In order to produce lactide, lactic acid is continuously polymerised to give low molecular weight PLA. Tin catalysis is then utilised to enhance intermolecular cyclisation reaction to produce a mixture of lactide stereoisomers. These are then isolated *via* vacuum distillation.[1]

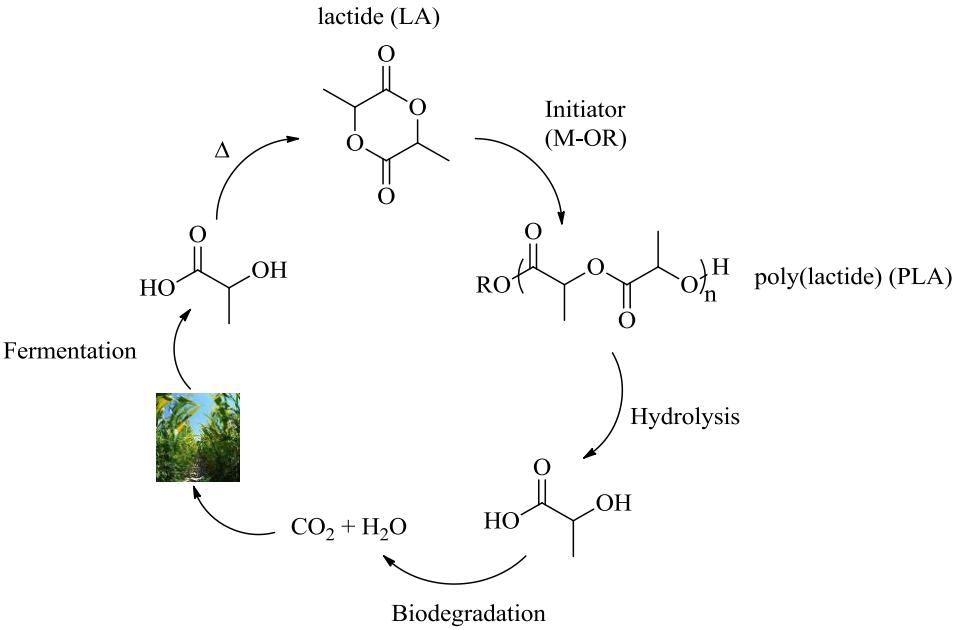

Figure 1.2 The 'life cycle' of polylactide (PLA) as adapted from the literature [4]

Whilst lactic acid is a renewable feedstock the cost of this platform chemical is a hurdle to the wider application of PLA. Lactic acid can be produced by the fermentation of aqueous glucose under anerobic conditions.[6] However, for every tonne of lactic acid produced approximately an equivalent amount of gypsum ($CaSO_4$) is generated as waste.[7] With esterification to methyl lactate often required to aid purification, work is under way to generate methyl lactate direct from sugars, which will enhance the sustainable credentials of PLA.[8-10]

The inherent sensitivity of the aliphatic backbone of PLA makes it susceptible to hydrolysis resulting in lower molecular weight material. In a recent report NatureWorks have suggested that chemical recycling of PLA to replenish feedstocks of lactic acid is a highly attractive approach. Whilst depolymerisation can be achieved akin to the PET industry through the treatment with strong acid,[11] noticeable alternatives are emerging in the literature. Alcoholysis of PLA under microwave irradiation has been reported at 130 °C whilst at a similar temperature and bulk conditions 4-dimethylaminopyridine (DMAP) has been utilised as a depolymerisation catalyst.[12, 13] More recently Jones *et al.* have reported on a number of unsymmetrical group IV complexes that are active for the conversion of commercially available PLA to methyl lactate in the presence of methanol.[14] The controlled biodegradation of PLA is also highly desirable for biomedical applications and the use of NaOH and HCl for depolymerisation has also received attention.[3, 15]

1.2 Ring-opening polymerisation (ROP) of lactide

The ring-opening of lactide (LA) is preferential in the production of PLA as it provides good molecular weight control yielding not only high molecular weight but also a narrow polymer weight distribution.[16] Control over such polymer properties is essential when attempting to tune the thermal and mechanical properties of the resulting polymeric material. The process can be described as a 'living polymerisation' as there is no inherent termination step. The overall polymer molecular weight can be controlled by altering the monomer-to-initiator ratio;[17] this makes the presumption that the rate of initiation is considerably faster the rate of propagation of the polymer, which will be discussed later in section 1.7. The ROP of lactide typically requires the presence of a metal-based initiator, although organo-catalysis is possible,[18-25] and occurs *via* one of three suggested mechanisms: anionic, cationic or coordination-insertion.

Anionic polymerisation (Figure 1.3) proceeds *via* cleavage of the acyl bond of the lactide due to nucleophilic attack at the carbonyl. An alkoxide ion is generated at the end of the polymer chain and it is this that acts as the new initiating species.[3]

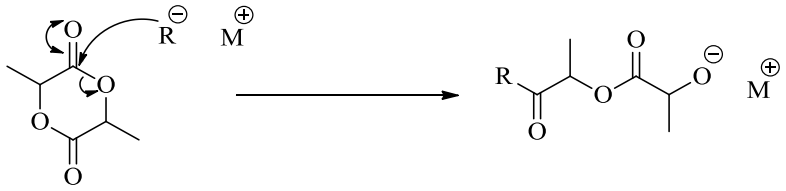

Figure 1.3 Anionic ROP of lactide

The cationic mechanism (Figure 1.4) is initiated by nucleophilic attack at the methine carbon and subsequent cleavage of the alkyl-oxygen bond.[16]

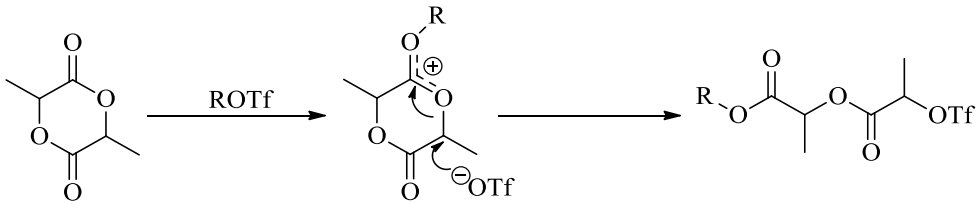

Figure 1.4 Cationic ROP of lactide (OTf = $^{-}O_3SCF_3$)

Coordination-insertion polymerisation of lactide provides good molecular weight control and chain-end stereo-control. Many metal alkoxide and carboxylate initiators proceed *via* this

mechanism; including tin (II) 2-ethylhexanoate (tin octanoate), which is widely used in industry.[1] Carboxylate initiating species require the presence of an alcohol as a co-initiator, providing further routes to molecular weight control.[3] The mechanism (Figure 1.5) is believed to begin with carbonyl activation due to coordination to the Lewis acidic metal centre. The lactide monomer is then inserted into either the M-OR or co-initiator H-OR bond with ring-opening occurring due to cleavage of the acyl-oxygen bond, thus forming a new alkoxide species. Further lactide incorporation occurs (propagation) until the polymerisation is terminated by the addition of alcohol.[26]

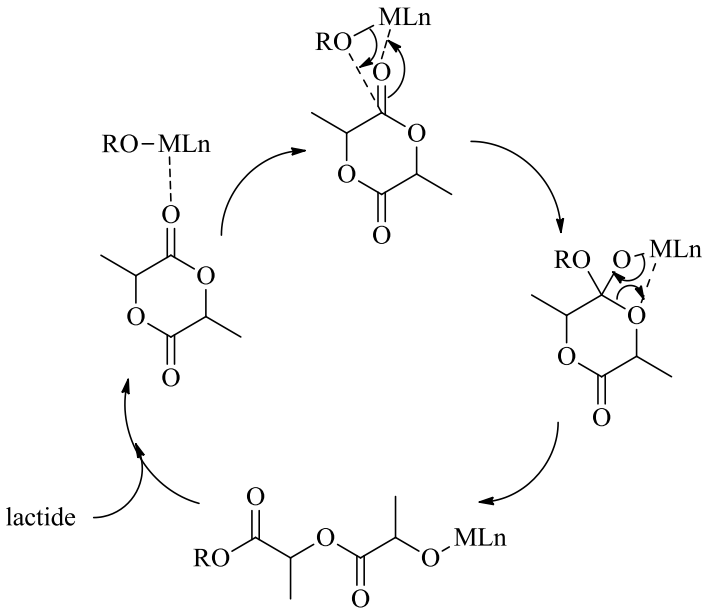

Figure 1.5 Coordination-insertion ROP of lactide

1.3 Polylactide stereochemistry

Lactide has two stereocentres and the stereochemistry of its resulting polymer has a significant effect on the physical and mechanical properties of the material. The two stereocentres of lactide lead to the occurrence of three stereoisomers: the *RR* configuration is referred to as D-lactide whilst its entantiomer, with the *SS* configuration, is L-lactide; the third form is the diastereomer of the previous two, *RS*-lactide (*meso*-lactide) (Figure 1.6).

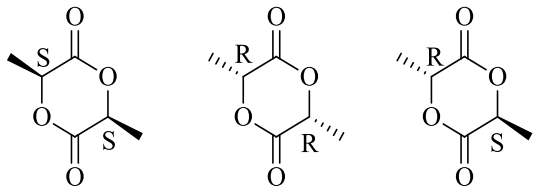

Figure 1.6 Three possible stereoisomers of lactide

With L-lactic acid being its natural form L-lactide is easily produced. However D-lactide is now also commercially available and is an attractive addition as controlled polymerisation of a mixture of the two enantiomers can lead to polymers with significantly different stereochemistry.[27, 28] Whilst polymerisation of L-lactide would yield stereoregular isotactic poly-(L-lactide) (PLLA), the polymerisation of a racemic mixture of L-lactide and D-lactide, refered to as *rac*-lactide, could yield a range of polymeric material (Figure 1.7). [27] Random polymerisation would give atactic PLA, polymerisation alternating from L-LA to D-LA would yield heterotactic PLA, and finally the complete polymerisation of one enantiomer before the polymerisation of the remaining would afford stereoblock isotactic PLA. Due to the lack of epimerisation during the polymerisation process with *rac*-lactide, syndio-tactic PLA is only achievable *via* the polymerisation of *meso*-lactide.

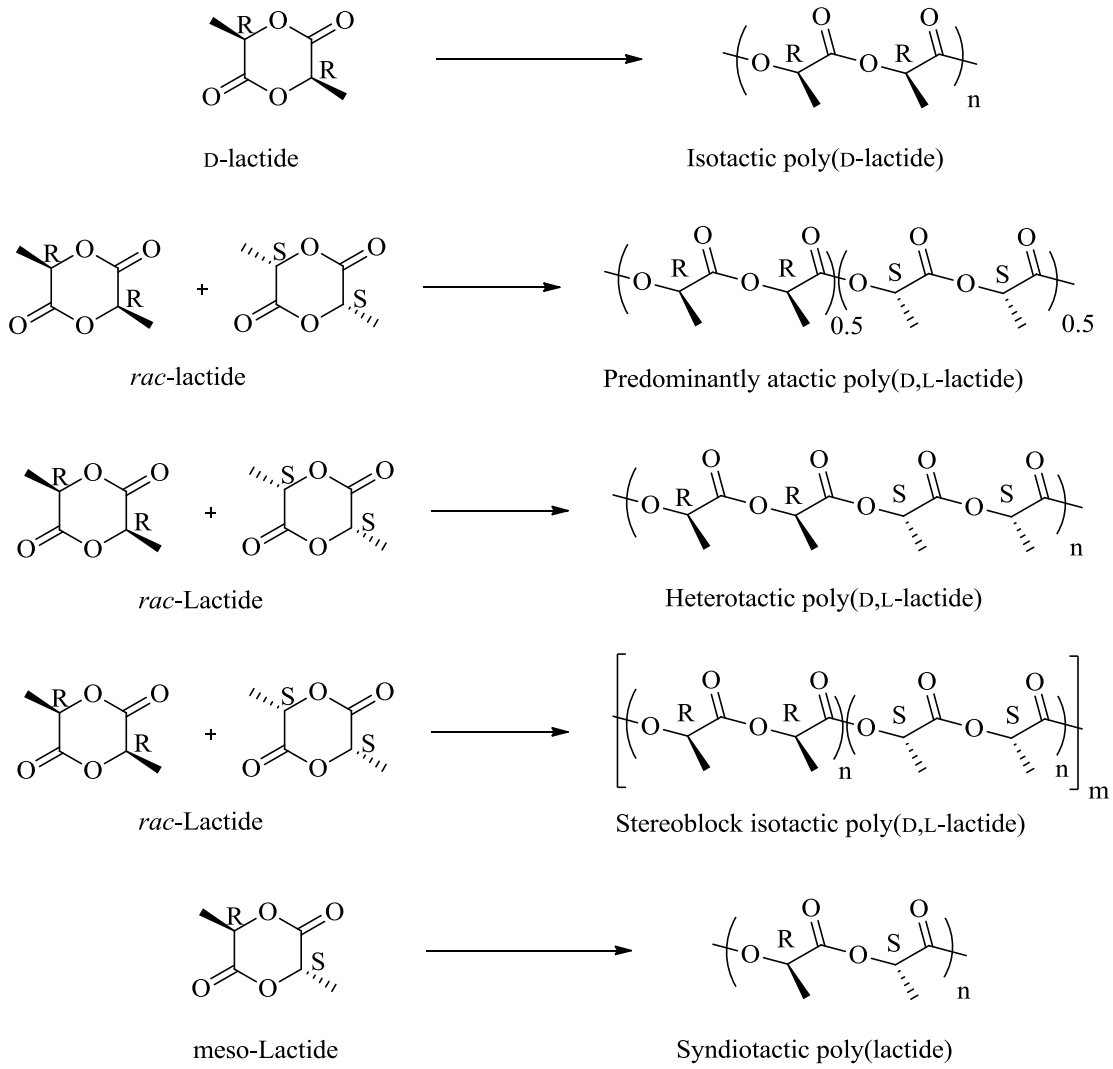

Figure 1.7 Lactide stereochemistry and PLA microstructures[27]

The stereosequences in PLA can be defined to aid characterisation, with equivalent adjacent stereocentres denoted *i* (isotactic) and inequivalent centres denoted *s* (syndiotactic) (Figure 1.8).[27]

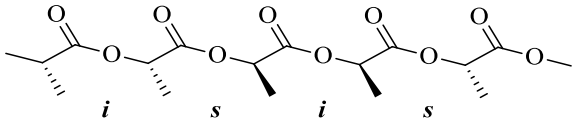

Figure 1.8 Assignment of stereosequences in PLA[27]

Stereo-regular isotactic poly(L-lactide) (PLLA) and poly(D-lactide) (PDLA) have the ability to form a polymer-polymer stereocomplex enhancing thermal stability.[28] Interaction takes place

between the left-handed and right-handed helices of adjacent macromolecular chains of PLLA and PDLA through CH_3··O=C and $C_\alpha H$···O=C H-bonding forces.[29, 30] This results in an increase in both melting temperature (T_m) and glass transition temperature (T_g). Stereoblock PLA, that is accessible through the sequential polymerisation of L-lactide and D-lactide or the controlled ROP of *rac*-lactide, offers a convenient route to stereocomplexed PLA with block length influencing the extent of thermal enhancement.[31, 32]

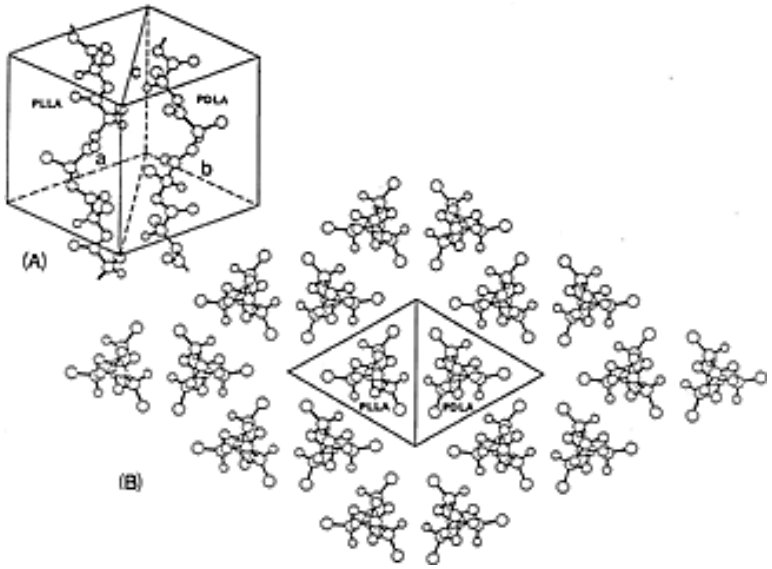

Figure 1.9 Crystal structure of stereocomplex PLA, taken from the reference[30]

1.4 Polymer Characterisation

1.4.1 Overview

With the characteristics of polymeric material, such as stereochemistry, molecular weight, and its distribution, having great effect on the materials performance, it is essential to have well developed methods for analysis of polymers. This section outlines the workings of various analytical methods and highlights the information they can provide on samples tested. The list is by no means exhaustive and is centred on techniques used in the under-taking of this research.

1.4.2 NMR Spectroscopy

NMR spectroscopy can yield significant information about both a polymerisation reaction and the subsequent polymer produced. ^{1}H NMR spectroscopy is commonly used due to the presence of protons in most polymer chains (including polylactide) and the fast relaxation times that

allow rapid analysis of freshly produced polymeric material. Proton environments often exhibit slightly different chemical shifts in the momeric environment compared to when incorporated in the polymer chain. For examples such as polylactide, where both the polymer and monomer are soluble in a deuterated sovent, ^{1}H NMR spectroscopy can be used to calculate monomer conversion.

For polylactide in $CDCl_3$, the quartet resonance due to the methine proton (coupled to the CH_3) undergoes a downfield shift as it is incorporated into the polymer chain. This shift from 4.95 ppm to approximately 5.1 ppm allows for conversion to be calculated (Figure 1.10). The loss of the clean quartet is due to the stereochemistry of the *rac*-lactide and subsequent polymer tacticity.

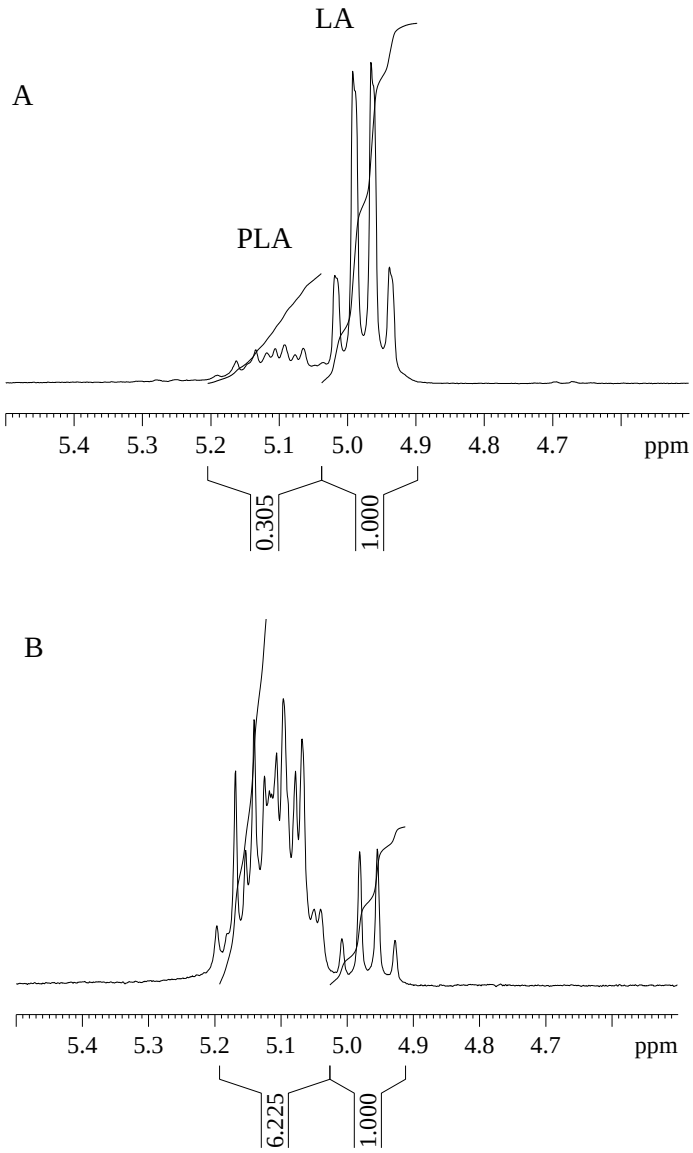

Figure 1.10 Extracts of ^{1}H NMR spectra ($CDCl_3$) for poly(lactide) showing: A – low conversion (23 %), B – high conversion (86 %) for samples using initiators presented in this thesis

Protons within the end group of a polymer chain are likely to have a different resonance with respect to those within the repeat units (Figure 1.11). Assignment and quantification allows a polymer molecular weight to be calculated. In the case of polylactide, where a benzyl alcohol or isopropoxide initiating group is often used, as long as the number of end groups introduced to the polymerisation is known then an accurate polymer molecular weight can be determined.

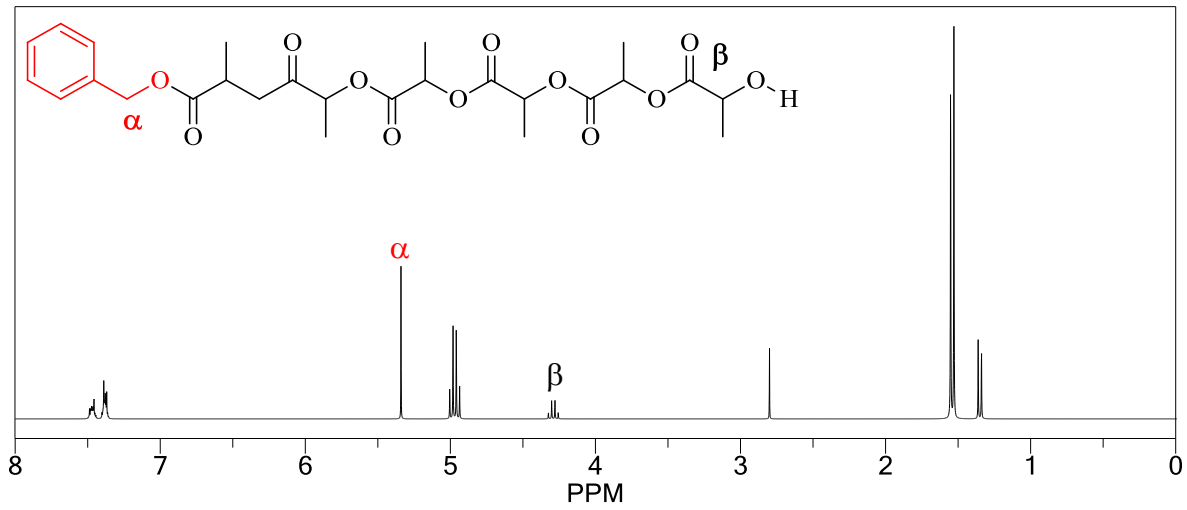

Figure 1.11 Theoretically generated ^{1}H NMR spectrum for oligomeric polylactide highlighting the difference in chemical shift (ppm) for mid-chain and end-group repeat units

The use of NMR spectroscopy for the determination of polymer molecular weight does have its limitations. A presumption has to be made that ROP occurs with good molecular weight control and there is no loss of end groups through intramolecular transesterification. This process can lead to formation of cyclic polymers and the reduced presence of end groups in the NMR spectrum misleading towards higher molecular weights. MALDI mass spectrometry offers another route to identifying the presence of end groups, or lack thereof, as well as branching and macrocyclic formations.[33-35]

1.4.3 Homonuclear-decoupled NMR

The stereochemical microstructure of polylactide can be quantified *via* analysis using homonuclear decoupled ^{1}H NMR spectroscopy. Multiple resonances of the methine proton can be observed due to the different stereochemical environments experienced in the polymer.[36] These resonances can be assigned to different stereosequence combinations which are named using the previously mentioned '*i*' and '*s*' notation. The number of possible combinations for a stereosequence of *n* stereocentres is defined by $2^{(n-1)}$; for example a tetrad of four stereocentres has $2^3 = 8$ combinations, one such being *iii* that would denote four stereocentres of equivalent

stereochemistry (RRRR or SSSS). The probability of each of these combinations occurring in the polymer chain can be calculated based on Bernoullian statistics (Table 1.1).[37]

	Probability	
tetrad	*rac*-lactide	*meso*-lactide
[*iii*]	$P_m^2 + P_rP_m/2$	0
[*iis*]	$P_rP_m/2$	0
[*sii*]	$P_rP_m/2$	0
[*sis*]	$P_r^2/2$	$(P_m^2 + P_rP_m)/2$
[*sss*]	0	$P_r^2 + P_rP_m/2$
[*ssi*]	0	$P_rP_m/2$
[*iss*]	0	$P_rP_m/2$
[*isi*]	$(P_r^2 + P_rP_m)/2$	$P_m^2/2$

Table 1.1 Tetrad probabilities based on Bernoullian statistics [37]

Significant work and heated debated surrounded the initial assignment of homodecoupled ^{1}H NMR resonances to the tetrads of the polylactide microstructure. Initial work was carried out in 1992 by Kricheldorf *et al.* and through the comparison of ^{1}H and ^{13}C NMR spectra of poly(D,L-lactide) from *meso*- and *rac*-lactide initial assignments were made.[36] With the increasing magnetic field strengths available in spectroscopic analysis, work continued into microstructure analysis with Thakur *et al.* reporting sensitivity at the hexad level.[38] However, this was quickly followed by evidence from Chisholm *et al.*, with the aid of HETCOR NMR that previous assignments at the tetrad level were incorrect.[39] HETCOR NMR allowed for the 2D correlation of homodecoupled methine protons with the corresponding ^{13}C{^{1}H} NMR signals. Counter arguments were generated on both sides of the Atlantic by Thakur *et al.* [40] and Kasperczyk [41] before the assignment presented by Chisholm *et al.* was generally accepted; assignment of stereochemical sequences was reasonably constrained to the tetrad level.[39] Decoupling removes the quartet splitting due to the adjacent methyl group and allows straightforward identification and quantification of the 5 tetrads seen for PLA formed from L-lactide, D-lactide or mixtures thereof.[37] Concentration of the *sis* tetrad can be calculated *via* integration of the five tetrad peaks observed in the homonuclear decoupled ^{1}H NMR spectrum. P_r can then be calculated using the formula: $P_r = \sqrt{2 \times [sis]}$ where P_r equals the probability of racemic enchainment. For heterotactic PLA, P_r tends to a value of 1, atactic PLA a value of 0.5, whilst isotactic PLA tends

towards 0. P_m equals the probability of meso enchainment ($P_m = 1 - P_r$). Representations of tetrad homonuclear decoupled signal intensities are shown in Figure 1.12.

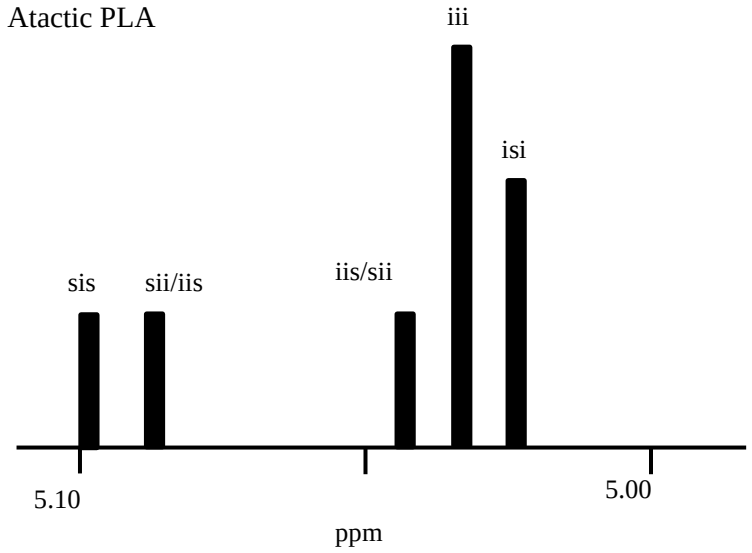

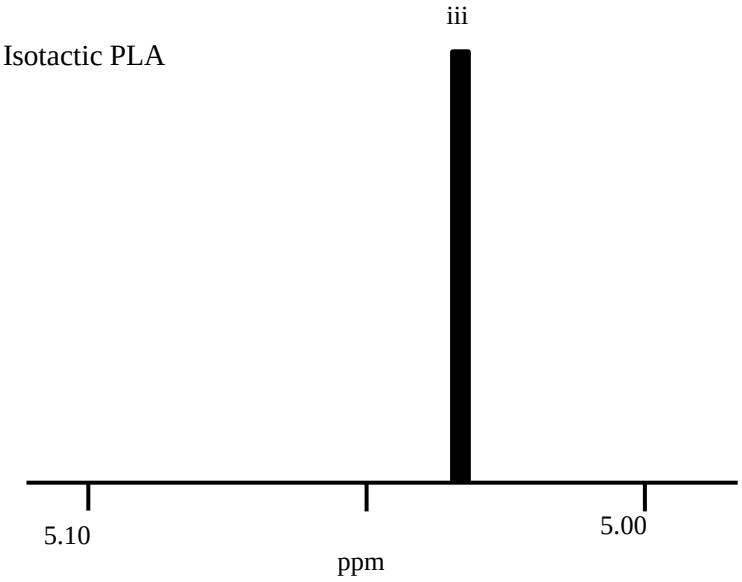

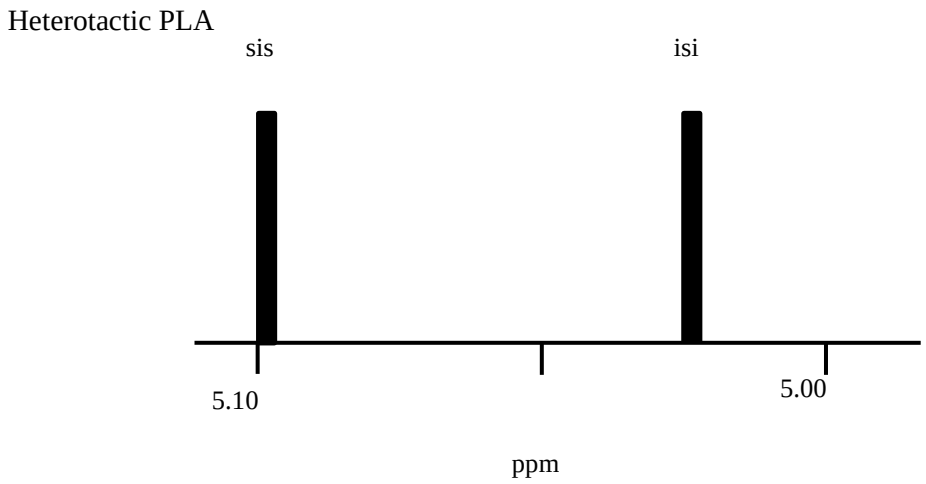

Figure 1.12 Graphical representation of the relative tetrad intensities for atactic, isotactic and heterotactic polylactide

1.4.4 MALDI-ToF Mass Spectrometry

Molecular weight control can be limited due the presence of transesterification processes. This can occur *via* intramolecular transesterification, known as back-biting that causes the formation of macrocylic PLA. Intermolecular transesterification causes molecular weight redistribution (Figure 1.13).

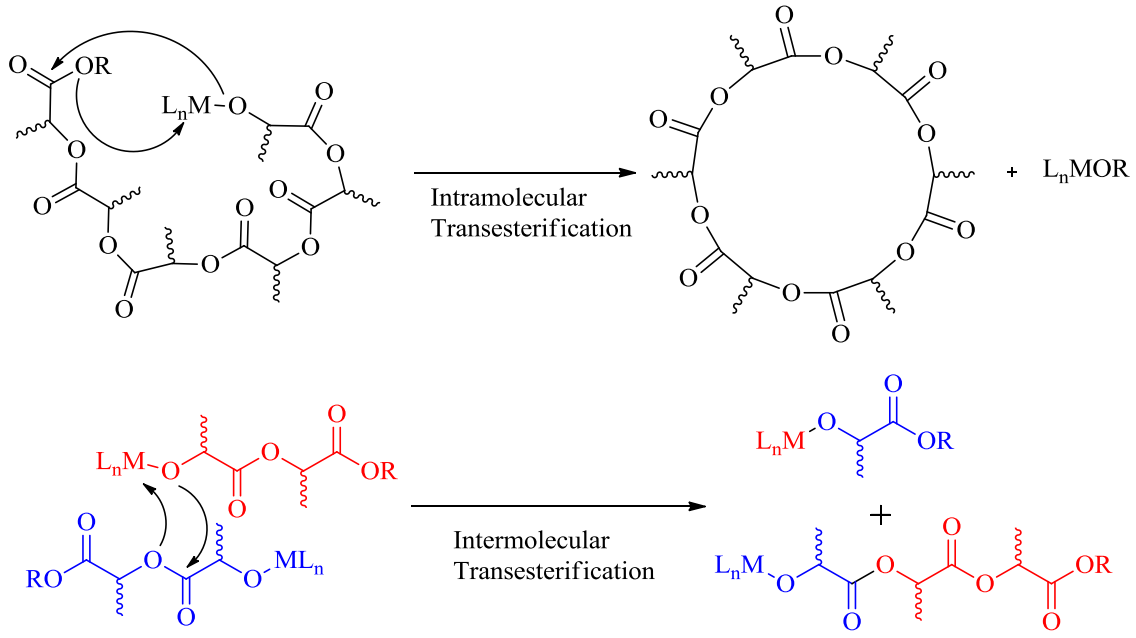

Figure 1.13 Intramolecular and intermolecular transesterification of PLA, causing macrocyclic rings and chain redistribution

The extent of transesterifcation can be monitored by analysis of MALDI-ToF mass spectra of the resulting polymers. This soft ionisation technique uses a pulsed laser beam to cause a desorption of a matrix from a sample plate that includes ions of the analyte.[42] The technique is widely used for analysis of polymer and biomolecules such as proteins.[33-35, 43] MALDI-ToF mass spectrometry data of PLA is capable of showing the repeat unit molecular weights of the polymer chains (Figure 1.14).

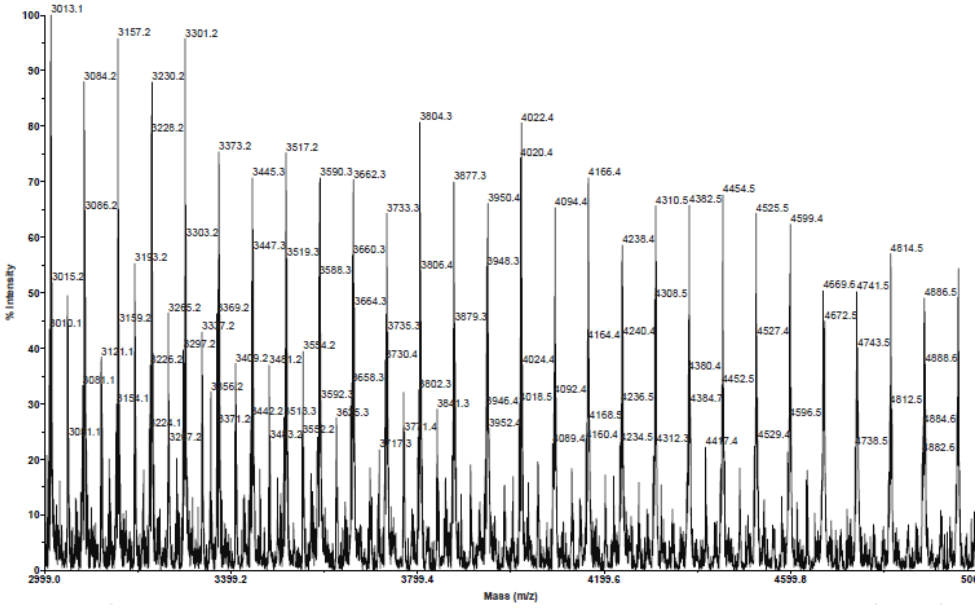

Figure 1.14 MALDI-ToF mass spectrum of PLA

In the spectrum shown (Figure 1.14) the mass differences between each peak give an indication of the degree of transesterification. With a repeat unit of 144 g mol^{-1} if no transesterification was present there would be one set of peaks with each having a mass difference of 144 g mol^{-1}. Due to the presence of two esters bonds per repeat unit, transesterification causes the appearance of multiple extra sets of peaks with mass spacing of 72 g mol^{-1}, a half-lactide unit. MALDI-ToF can also be used to identify the presence of polymer end groups, which can aid in determining the mechanism of polymerisation. Lack of expected end groups can be indicative of the presence of macrocyclic PLA due to intramolecular transesterification.

1.4.5 Gel Permeation Chromotography

Gel permeation chromatography (GPC) is a size-exclusion technique that can be used to characterise polymeric material. A solution of the polymeric sample can be passed through

columns of porous beads that separate the polymer chains based on size. Smaller molecular weight material passes into the beads and takes longer to elute than the larger chains that pass around the material (Figure 1.15).

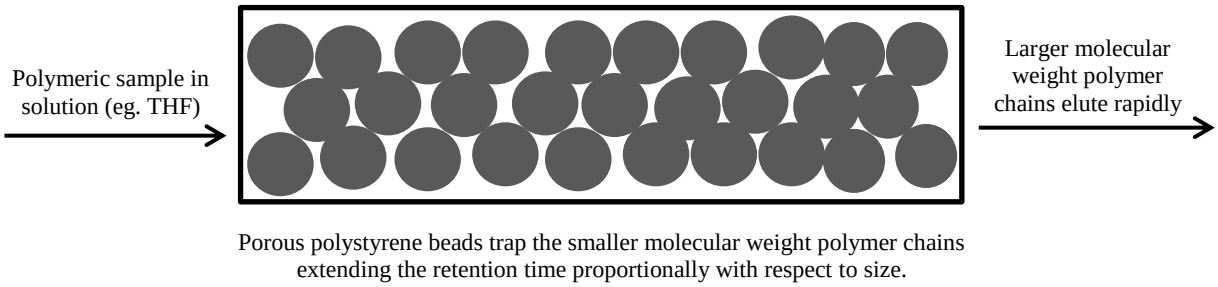

Figure 1.15 Principles of size exclusion chromotograph as untilised in gel permeation chromatography (GPC) for determining relative polymeric molecular weight (M_n and M_w) and polydespersity index (PDI)

The elutant concentration is measured using a detector; these are usually either ultra-violet (UV), refractive index (RI) or infra-red (IR) sensitive. Light scattering and viscometry can also be used as a method of detection. Standards of known molecular weight, such as polystyrene, are used to generate a calibration curve of retention time against molecular weight. GPC data can be used to calculate number-based average molecular weight (M_n), weight-based average molecular weight (M_w) and a polymer weight distribution index (PDI). It is essential to acknowledge that polymer analysis *via* a size-exclusion technique generates relative data due to the use of a standard calibration curve. Weights achieved are not absolute due to differences in hydrodynamic volume of the sample polymer to the standard and can only be compared for samples of equivalent material using the same column set and method.

1.4.6 Differential Scanning Calorimetry

Differential Scanning Calorimetry (DSC) can measure the thermal transitions of a material. Thermal transitions, such as phase changes, are accompanied by a change in heat capacity. A sample of the material is placed in a pan and heated at the same rate as a blank reference. At a phase change, a greater or less heat input will be required to ensure the temperature of both pans remains constant; this difference in heat flux can be plotted against temperature.

There are two types of calorimeter: power compensation DSC and heat flux DSC. In the power compensation method if a difference in temperatures between the blank and sample is detected

increased energy is then supplied to the sample to reduce the difference between the two. This provides a difference in heat flux for that temperature. Heat flux DSC records the difference in temperature between the material sample and blank for increased temperature; this difference is proportion to change in the heat flux.[44]

DSC can provide a number of thermal properties. T_g is the glass transition temperature of a material. A baseline shift in the endothermic direction on the DSC trace is caused by an increase in the heat capacity of the material. An amorphous polymer will be glassy and brittle below its T_g and softer above. T_c is the temperature of crystallisation. This is an exothermic transition and is signified by a peak in the exothermic direction on the DSC trace. Crystallisation occurs when the material is given enough energy to enter its regular crystalline state and thus reduces its heat capacity. T_m is the melting temperature of the material. Enough energy is provided to the sample to allow the endothermic transition from solid to liquid.[44]

1.5 Initiators for the ROP of lactide

1.5.1 Tin initiators

The tin based initiator tin (II) bis(2-ethylhexanoate), commonly referred to as tin octoate (Figure 1.16), is widely used for the industrial production of poly(lactide). It is an attractive species due to its ease of handling and commercial availability. Tin octanoate exhibits high activity in both solution and bulk polymerisations with low rates of epimerisation and transesterification.[1]

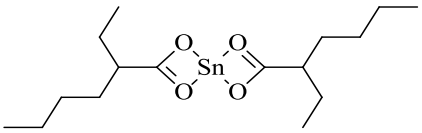

Figure 1.16 Tin (II) bis(2-ethylhexanoate)

A protic co-initiator is often used to provide increased control of molecular weight.[45] Mechanistically, it has been reported that the ROP of lactide proceeds by either the initial formation of tin alkoxide and 2-ethylhexanoic acid[46] or by direct coordination of the lactide to the tin octoanate followed by monomer activation by the alcohol.[47] Both routes can be classed as a coordination-insertion mechanism and result in the polymer terminated with the alkyl group of the alcohol co-initiator. It has also been reported that the ROP of lactide can be co-initiated by an amine *via* the same mechanism. After the initiation of the polymer chain there is still the

formation of a tin-oxygen bond, the oxygen being from the monomer, and thus coordination insertion propagation continues.[48]

Whilst the use of tin octoate has FDA approval, the toxicity of many resulting tin compounds limits the resulting polymers use in biomedical applications.[4] Along with the lack of stereocontrol provided by this initiator, it creates a drive for the development of new selective initiators for the ROP of lactide that use benign metals, even metal-free[21, 25] or heterogeneous,[49] that minimise the risk of heavy metal build up in the body.

Gibson *et al.* have synthesised a range a Sn (II) complexes with bidentate nitrogen-donor ligands.[50-52] When coordinated to β-diketiminate ligands, Sn (II) isoproxide was found to be active for the ROP of *rac*-lactide providing good molecular weight control and slight heterotactic enrichment of the polymer (Figure 1.17).[50, 51]

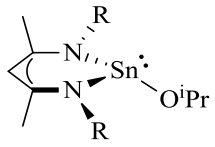

1; R = Ar
2; R = DIPP (diisopropylphenol)

Figure 1.17 Sn (II) β-diketiminate complexes[50, 51]

With R = Ar (**1**), high conversion (> 90 %) of *rac*-lactide was achieved at ambient temperature in CH_2Cl_2 after 96 hours. Increasing the reaction temperature to 60 °C yielded polymeric material and a conversion of 85 % in four hours when carried out in toluene.[50] Replacing the nitrogen substituent with DIPP (2,6-di-isopropylphenyl) (**2**) provided access to high conversion at ambient temperature in 50 hours with equivalent conversion at the higher temperatures (60 °C, toluene) achieved in only 4 hours.[51]

With a bidentate *tert*-butylamidinate ligand Gibson *et al.* explored the effect of initiating group on the activity of Sn (II) complexes for the ROP of *rac*-lactide (Figure 1.18).[52]

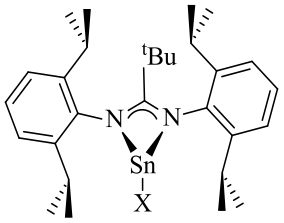

1; X = O^{i}Pr
2; X = NMe_2
3; X = $N(SiMe_3)_2$

Figure 1.18 Sn (II) *tert*-butylamidinate complexes[52]

With all initiating groups reported, a linear relationship was found between conversion and molecular weight at 60 °C in toluene. This suggests rapid initiation and good molecular weight control and, in the case of the alkoxide initiating group (Figure 1.18, **1**), high activity with a conversion > 90% being achieved in 90 minutes. Whilst the complexes with NMe_2 and $N(SiMe_3)_2$ (Figure 1.18, **2** and **3**) also exhibited higher activity than the β-diketiminate complexes (shown in Figure 1.17) they were significantly slower than **1**.[52] Kinetic investigations with respect to initiator loading found that **1** had a non-first-order dependence of 0.21, attributed to aggregation of the initiator in solution.[52]

At a similar time Gibson *et al.* also explored the potential of tridentate Schiff base ligands when coordinated to a Sn (II) amide complex (Figure 1.19).[53] A fluxional migration was identified involving the attack of the amide on the imine of the ligand creating a tetradentate ligand species that was susceptible to lactide coordination; leading to polymeric material with good control and a low polydispersity (PDI = 1.2). Variation in the ligand architecture was found to have little effect on the high activity observed (> 90 %, toluene, 60 °C).[53]

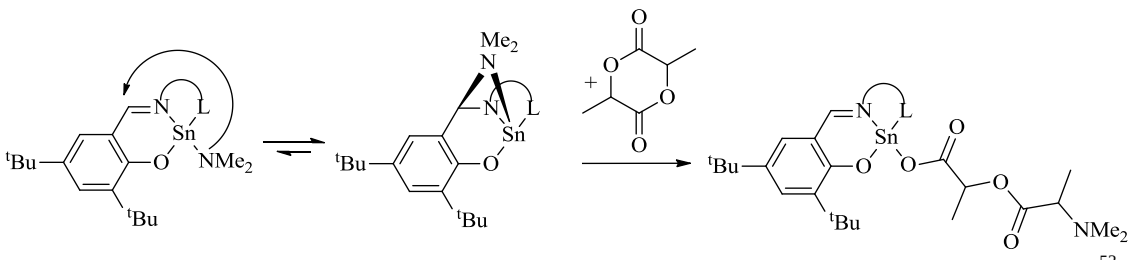

Figure 1.19 Sn (II) Schiff-base complex isolated by Gibson *et al.* and there use for the ROP of lactide[53]

Away from polydentate complexes Chisholm *et al.* presented a group of Sn (IV) complexes with the general formula Ph_2SnX_2 or Ph_3SnX.[54] When used as initiators for the polymerisation

of L-lactide at 80 °C in toluene the bisphenyl analogue, where X = O^iPr, was found to be faster than the triphenyl analogue. Analysis of the polymeric material found that with X = NMe_2 mainly cyclic polymers were formed, however replacing with the initiating group with O^iPr reduced the degree of intramolecular transesterication.[54]

1.5.2 Aluminium initiators

Early work into the suitability of trimers and tetramers of aluminium isopropoxide for the polymerisation of L-lactide showed it to be active and that complexation of bulky ligands such as porphyrins affords tighter molecular weight control.[46, 55] Aluminium isopropoxide has also been shown to be suitable for the ROP of other lactones and the copolymerisation with lactide.[56] Early work published by Spassky stated that chiral spectator ligands based on Schiff's base, when coordinated to aluminium (Figure 1.20), were found to give highly isotactic enchriched PLA from *rac*-lactide.[57] At low conversion isotactic enrichment was as high as 88% and, with longer reaction times, the formation of stereocomplexed PLA was observed due to the formation of stereo-block PLA. This stereocomplexed PLA has a higher melting point due to the preferential interaction been the blocks of PLLA and PDLA.[28]

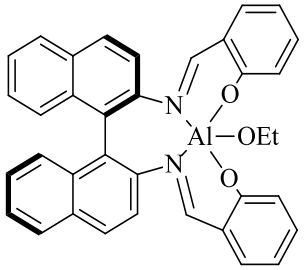

Figure 1.20 (SalBinap)Al(Et)

As an early example of isotactic selectivity in the ROP of *rac*-lactide, Spassky's complex provided the basis for further studies by many research groups. Nomura *et. al.* carried out an in-depth study into the extent of selectivity by changing the backbone linkage between the salen groups and varying the steric bulk of the phenyl substituents close to the alkoxide (Figure 1.21).[58]

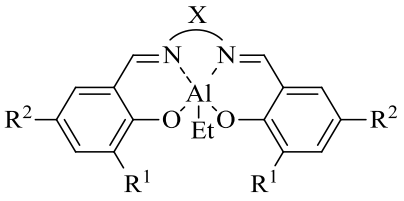

1; R^1 = Ph, R^2 = H, X = **-**C_3H_6**-**
2; R^1 = R^2 = ^{t}Bu, X = **-**C_3H_6**-**

Figure 1.21 Achiral aluminium salen complexes reported by Noruma *et al.*[58]

Polymerisation of *rac*-LA using complex **1** and **2** required the presence of one equivalent of BnOH and were carried out in toluene at 70 °C. Conversions of 94 % were achieved after 1.3 hours with **1** whilst with the bulkier-substituted complex (**2**), 95 % was achieved in 14 hours. Both yielded highly isotactic material with a narrow PDI.[58] Nomura *et al.* also reported that that reducing the length of the alkyl backbone to –C_2H_4– also reduced catalytic activity.[58]

Feijen reintroduced the chiral aspect through use of the Jacobsen ligand that incorporated a cyclohexyl backbone.[59] The use of the (*R*,*R*) stereoform for the ROP of *rac*-lactide provided highly isotactic PLA via an entaniomorphic site control mechanism in both solution (toluene, 70 °C) and melt conditions (Figure 1.22).[59, 60]

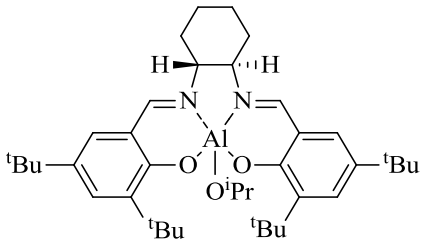

3

Figure 1.22 (*R*,*R*)-salen aluminium alkoxide complex (**3**) utilising the Jacobsen ligand [59]

Gibson *et al.* created salan analogues of complexes **1** and **2** (Figure 1.21) that were industrially attractive due to colourless nature of the polymeric material produded.[2] The alkyl group at the amine nitrogen could be varied (Me or CH_2Ph) as well as the phenolate substituents (H, Me, ^{t}Bu or Cl). The complexes were formed from coordination of the free ligand to trimethyl aluminium and thus *in situ* alcoholysis was carried using one equivalent of benzyl alcohol.[2] It was reported that activity of the dichloro-subsituted complex for the ROP of *rac*-LA was significantly slower than the unsubstituted analogue, k_{app} = 37.9 × 10^{-6} s^{-1} compared to 79.8 × 10^{-6} s^{-1}. Furthermore,

the unsubstituted analogues yielded isotactically enriched PLA (P_r = 0.32) whilst di-chloro-substitution gave rise to heterotactic PLA (P_r = 0.88). This was further enhanced when the amine nitrogen substituent was CH_2Ph with P_r values of 0.21 and 0.96 respectively.[2]

Work followed by Feijen *et al.* that presented a salan-analogue of the Jacobsen ligand with variation of the phenolate substituents providing a range of monoethyl aluminium complexes (Figure 1.23).[61]

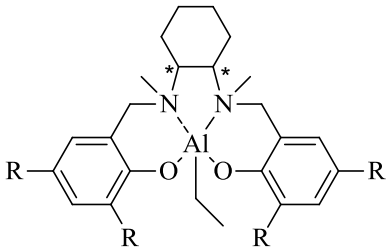

1; R = H, *(*R,R*)
2; R = Cl, *(*R,R*)
3; R = Me, *(*R,R*)
4; R = H, *(*rac*)
5; R = Cl, *(*rac*)
6; R = Me, *(*rac*)

Figure 1.23 Aluminium complexes with a chiral phenoxyamine ligand isolated by Feijen *et al.*[61]

Studies of the activity and selectivity of complexes in Figure 1.23 for the ROP of *rac*-LA were carried out by the *in situ* generation of an aluminium alkoxide species using propan-2-ol and all were found to have good molecular weight control. It was summarised that whilst the precence of chirality in the ligand was important for the isotactically enhanced stereocontrol observed, the specific stereochemistry had little effect on the catalytic activity or the tacticity of the PLA produced.[61] When R = H, the optically pure (*R,R*) ligand complex (**1**) was used, isotactically enriched PLA was produced with a conversion of 70 %; whereas with the racemic analogue (**4**) 89 % conversion was achieved in the same time. Substitution of the phenolate (R = Me) lead to production of atactic PLA that required longer reaction time to achieve high conversions: **3** = 69 hours, **6** = 53 hours.[61] Both the optically pure and *racemic* complexes with R = Cl (**1** and **5**) produced heterotactic PLA.[61]

Mechanistic studies into the coordination-insertion ROP of lactide using both salen- and salan-type aluminium initiators established that the polymer was terminated by the initiating alkoxide and that chirality of the polymer chain adjacent to the metal centre influenced subsequent selectivity.[62] This indicated a living polymerisation with chain-end control. Other studies highlighted that the more flexible coordination geometry of the sp^3 salan-type ligands would also effect overall activity and selectivity.[61]

Bis(phenoxy)amine aluminium complexes were reported by Gibson *et al.* that varied the ortho and para substituents of the phenolate arms (Figure 1.24).[63] For these complexes it was found

that electron-withdrawing chloro groups did not affect the rate of ROP of *rac*-lactide, however substituents that varied in steric bulk caused a dramatic decrease in activity, presumably due to the energy barrier to monomer binding.[63]

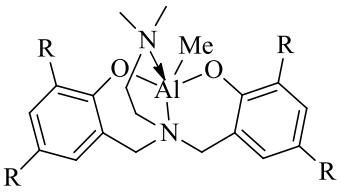

R = Me, ^{i}Pr, Cl or ^{t}Bu

Figure 1.24 Bis(phenoxy)amine alumiumium complexes isolated by Gibson[63]

With R = ^{t}Bu for the initiator in Figure 1.24, a reaction time of 280 hours was required to achieve essentially atactic PLA with 80 % conversion. Reduction in substituent steric bulk (R = Me) increased activity, with 91 % conversion achieved in 12 hours with high selectivity to isotactic PLA (P_r = 0.27). It was reported that for this ligand architecture the group on the nitrogen had little effect on stereoselectivity.[63]

Over the last few years significant research has been performed by the Jones group developing a range of tetradentate (ONNO)-type phenoxy ligands. Ligand backbones included ethylene diamine, piperazine and 1,4-diamino-cyclohexane (Figure 1.25).[64-66] Complexes with the ethylene diamine backbone (**1**) utilised a previously unreported salalen tetradentate ligand that offered substituent variation on both the phenolate rings and amine nitrogen.[64] All required benzyl alcohol for the complexes to be active for the ROP of *rac*-lactide.[64-66] Alkoxide derivatives of the complexes with the piperazine backbone (**2**) were generated prior to polymerisation through the addition of 3-5 equivalents of benzyl alcohol.[65]

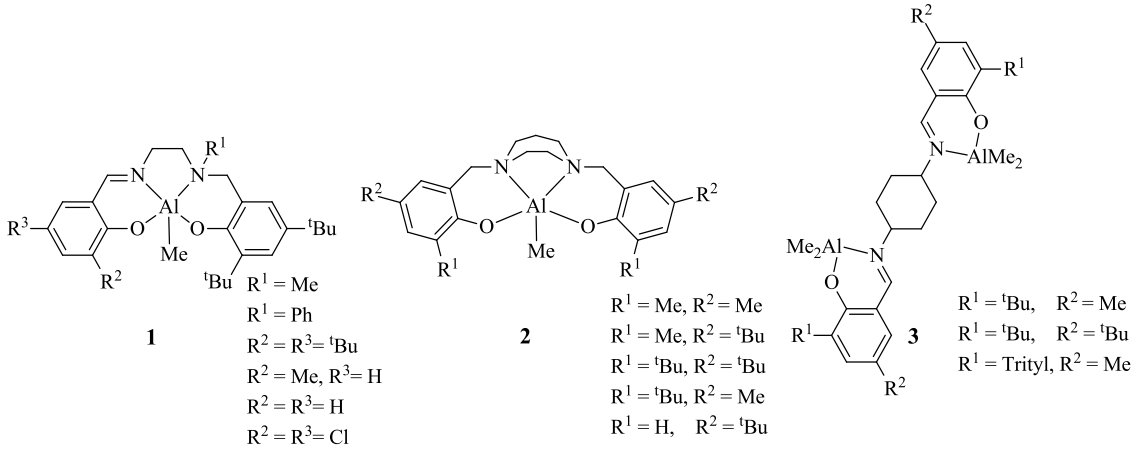

Figure 1.25 (ONNO)-type ligands coordinated to trimethyl aluminium as isolated by Jones *et al.*[64-66]

Unlike the bis(phenoxy)amine complexes reported by Gibson, variation of substituents of **1** found that the amine nitrogen group did influence polymer tacticity with slight heterotactic enrichment when R^1 = Me and isotactic enrichment when R^1 = Ph.[64] All aluminium salalen complexes gave high conversion to PLA with narrow PDI in a reaction time of 24 hours at 80°C in toluene; except for the complex (**1**), where R^1 = Me, R^2 = Me and R = H, which was significantly less active. Molecular weights were predictable based on metal-to-ligand ratio of 2:1 with a [LA]:[I] = 100:1 producing PLA of M_n ~ 10,000 – 14,000 Da.[64]

The Al (III)-homopiperazine complexes (**2**) offered changes in the ortho- and para- substiutents of the phenoxy groups. As the alkoxide was isolated prior to polymerisation activity testing, trials were carried out under more industrially relevant solvent-free conditions at 130 °C.[65] Whilst no stereoselectivity was reported for these complexes they proved efficiently active for the ROP of *rac*-lactide, providing access to > 80 % conversion for all but where R^1 = H.[65]

With a metal-to-ligand ratio of 2:1, two equivalents of benzyl alcohol were used per complex **3**. All complexes were reported to have good molecular weight control (PDI = 1.08 – 1.27) and provided isotactic enrichment to the PLA produced (P_r = 0.33). The addition of increased equivalents of benzyl alcohol reduced M_n in a predictable manner. With increased steric bulk (R^1 = trityl) rate was found to decrease. Further kinetic study reported the reaction was first order with respect to initiator.[66]

Darensbourg has shown that less sterically demanding half-salen ligands coordinated to aluminium still achieved high isotactic enrichment (82%) but with a relatively slow overall

activity.[67] Unlike the larger complexes, the smaller tridentate ligands resulted in the formation of dimeric complexes (Figure 1.26).

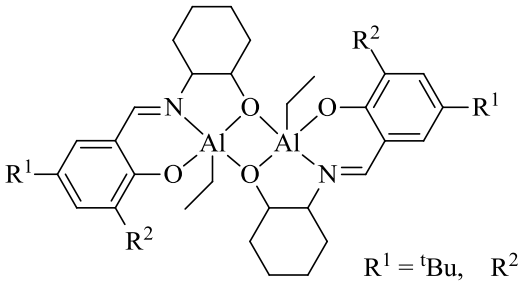

Figure 1.26 Al_2(half-salan)$_2$ complexes as reported by Darensbourg [67]

These dimers were also used to produce copolymers of lactide with caprolactone. A number of aluminium-based initiators have been used for the controlled copolymerisation of lactide and will be discussed further in later sections.[67-69]

Williams *et al.* have isolated complexes of Al(III) with bis(8-quinolinolato) and reported them to be active for the well-controlled production of PLA from *rac*-lactide (Figure 1.27).[70]

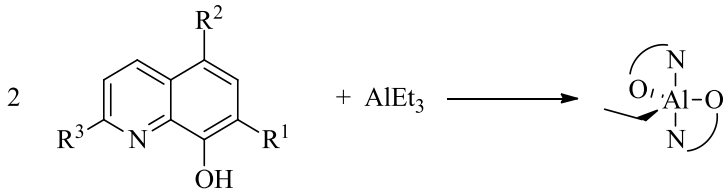

Figure 1.27 Bis(8-quinolinolato)aluminium ethyl complexes as published by Williams *et al.*[70]

Extensive substituent variation was achieved with steric bulk altered at the 2-position (R^3 = H or Me) and electron-withdrawing groups at the 5- and 7-postion (R^1 , R^2 = H, Cl, Br, I). Activity for polymerisation of *rac*-lactide was slow with high conversion being achieved only after several days in the presence of one equivalent of benzyl alcohol per metal centre. However there was good molecular weight control and polymer tacticity was enriched towards isotactic (P_r = 0.24).[70]

Most recently Hormnirum *et al.* have published a series of monomethyl and dimethyl aluminium pyrolylaldiminates of general formual L_2AlMe and $LAlMe_2$ respectively (Figure

1.28). Variation of the aldimine substituent was achieved using a range of benzyl rings with substituents at the 2- and 4- positions. This offered both electronic and steric influence to the ligand.[71]

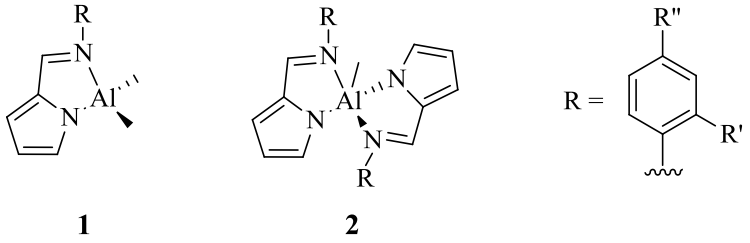

1 **2**

Figure 1.28 Dimethyl and monomethyl aluminium pyrolylaldiminiate complexes reported by Hormnirun *et al.* [71]

Ligand variation was found to alter both activity and stereoselectivity with respect to the ROP of *rac*-LA in the presence of one equivalent of benzyl alcohol. In general, higher activities were observed for the monomethyl analogues, presumed to be due to less steric hindrance about the metal centre when only one ligand is coordinated.[71] Selectivity was only apparent when larger steric bulk was present in the 2- position. When R' = *tert*-butyl, polymer was heterotactically enriched ($P_r \sim 0.6$) and when R' = adamantyl, isotactic PLA was produced ($P_r \sim 0.3$). Activity with the larger adamantyl substituent was significantly lower with high conversion only being achieved after 108 hours compared to 8 hours for the less hindered analogues. All initiators showed good molecular weight control with M_n values predicted by monomer-to-initiator ratio for both dimethyl (**1**) and monomethyl (**2**), suggesting one growing chain per metal centre.[71]

Also of group XIII, dinuclear indium halide complexes with bulky chiral diaminoaryloxy ligands have been reported by Mehrkhodavandi *et al.* as active for the ROP of lactide.[72, 73] After the first example was reported in 2008,[72] a family of complexes was reported with variation in the para-substituent of the phenolate, bridging species and terminal halides. The dinuclear geometry was identified in the solid state and found to persist in solution.

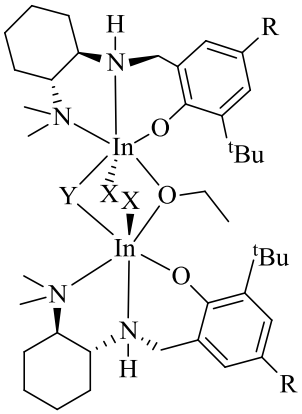

1; R = ^{t}Bu, Y = X = Cl
2; R = Me, X = Y = I
3; R = ^{t}Bu, X = I, Y = μ-OEt

Figure 1.29 Dinuclear Indium halide complexes with chiral diaminoaryloxy ligands as reported by Mehrkhodavandi *et al.*[73]

The complexes were found to be active for the ROP of lactide at room temperature with complex **3** proving significantly more active than complex **1**. This was attributed to the increased electrophillicity of Indium with terminal chloro substituents.[73] Kinetic studies found that after an initiating period the reaction was first order with respect to [LA] and also first order with respect to the dinuclear complex, suggesting one propagating species. Experimentally acquired rate constants were similar for both the mono-alkylated (**2**) and dialkylated (**3**) complexes providing further evidence of the active species maintaining the dinucelar structure in solution. Analysis of the stereoselectivity found that there was no halide effect and that with complex **3**, which produced isotactically enriched PLA (P_r = 0.35), the chirality of the cyclohexyl moiety equally had no effect. Conversely, increasing the amount of optically pure (*R,R/R,R*)-**1** compared to a racemic mixture caused the loss of a slight isotactic enrichment (P_r ~ 0.40) to essentially atactic material.[73] This significant difference in stereoselectivity would not be expected if the propagating species was a monomeric species. Mehrkhodavandi *et al.* reported extensive spectroscopic studies of **1** in the presence of donor species (pyridine, ethyl acetate, ethanol) with observations suggesting that dissociation of these dinuclear Indium species does not play a role in the polymerisation of lactide.[73]

1.5.3 Group IV initiators

The metals of group IV are an attractive target of research due to their similar coordination behaviour to tin-based initiators whilst being considerably more benign. Early work with group IV complexes found homoleptic Ti($O^{i}Pr$)$_4$ and Zr($O^{i}Pr$)$_4$ to be active for the ROP of L-lactide.[74, 75] A large number of group IV heteroleptic complexes have been reported with ancillary anionic ligands. The retention of a well-defined alkoxide group makes then an attractive target for potential initiators with the type of ligand proving influential for rate of polymerisation, which

generally follow the trend: salen > amine bis(phenolate) > amine tris(phenolate).[76] Most studies have been carried out with Ti(IV), however increased rates and enhanced stereoselectivity have been reported with Zr(IV) and Hf(IV).[77]

Ti(IV)-salen complexes, analogous to the aluminium complexes discussed previously, have been isolated and their performance as initiators for the ROP *rac*-lactide reported in the literature.[78] As with the aluminium series, the tetradentate ligands were varied at both the phenolate substituent position and the salen backbone linking group (Figure 1.30).

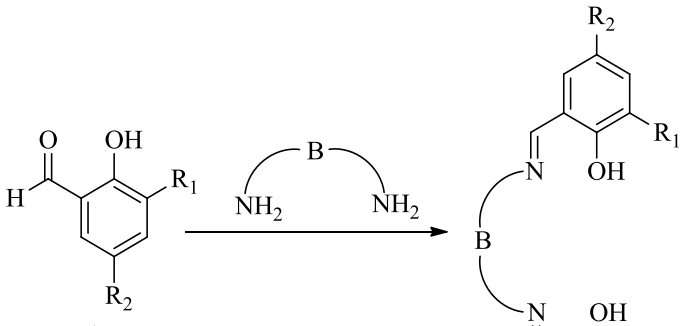

1: $R_1 = {}^t$Bu, R_2 = OMe, B=CH_2CH_2
2: $R_1 = {}^t$Bu, R_2 = H, B=CH_2CH_2
3: $R_1 = {}^t$Bu, $R_2 = {}^t$Bu, B=CH_2CH_2
4: $R_1 = {}^t$Bu, R_2 = I, B=CH_2CH_2
5: $R_1 = {}^t$Bu, R_2 = Cl, B=CH_2CH_2
6: $R_1 = {}^t$Bu, $R_2 = {}^t$Bu, B=(*R,R*)-cyclohexyl

Figure 1.30 Preparation of (ONNO)-type tetradentate ligands for subsequent coordination to Ti(IV)(O^iPr)$_4$ generating Ti(IV)-salen complexes[78]

Complexes were monomeric and adopted an octaheadral geometry with the tetradentate ligand able to wrap about the metal centre in one of three possible geometries (Figure 1.31).[79]

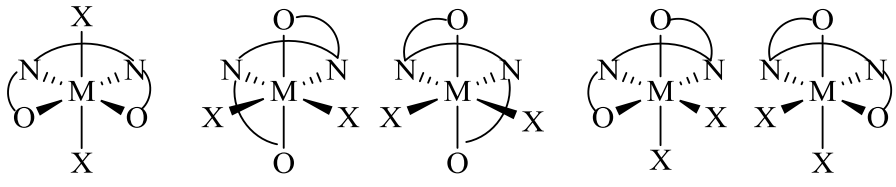

Λ Δ Λ Δ

mer-mer *fac-fac* *fac-mer*

trans *(α-cis)* *(β-cis)*

Figure 1.31 Possible geometries for tetrahedral Ti(IV)-salen complexes[79]

Polymerisations carried out in toluene at 70 °C behaved as a living polymerisation, with narrow polymer weight distribution and linear relationship between molecular weight and conversion. Activity was seen to be comparable to, if not faster than, that seen for the aluminium equivalents; with the *tert*-butyl substituted displaying activity an order of magnitude higher.[79] Polymer molecular weight was well controlled with M_n values suggesting one growing polymer chain per-metal centre.[78] Interestingly, it was noted that activity was highest for initiators with electron-donating groups (**1**) on the phenyl groups, whilst electron-withdrawing (**4** and **5**) lowered the overall activity; this is in contrast to the aluminium analogues.[78]

Kol *et al.* reported titanium and zirconium complexes with a (ONNO)-type phenylenediamine bis(phenolate) ligand.[80] Whilst the zirconium complex was dinuclear with a metal-to-ligand ratio of 2:1, the titanium complex was also isolated as a monomeric octahedral complex (Figure 1.32). A dinuclear complex containing titanium was also isolated with the equivalents of $Ti(O^iPr)_4$ added dictating the coordination behaviour.

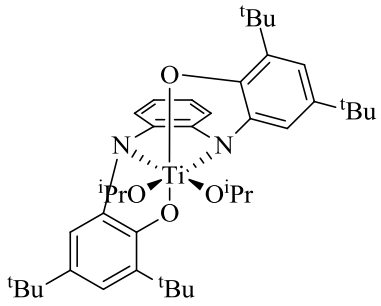

Figure 1.32 Titanium phenylenediamine complex presented by Kol et al. [80]

The complexes were found to be active for the ROP of lactide. Infact, they are the only example where titanium is faster than the zirconium analogues, providing heterotactic selectivity and melt-based levels of activity for titanium complexes that is un-paralleled in the literature.[80]

Chakraborty *et al.* isolated dinuclear, salen compounds of zirconium and hafnium alkoxide with the (*R*,*R*) configuration of Jacobsens ligand (Figure 1.33).[81]

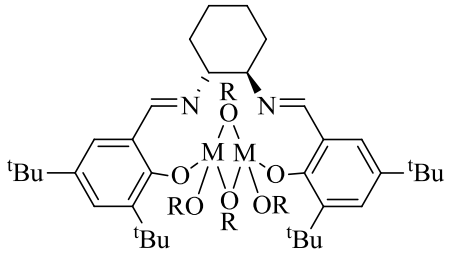

1; M = Zr, R = ^{i}Pr
2; M = Hf, R = ^{t}Bu

Figure 1.33 Binuclear salen complexes of zirconium and hafnium isolated by Chakraborty *et al.* [81]

The complexes were synthesised by the 2:1 reaction of the ligand with the respective metal alkoxide precursor. Both **1** and **2** showed activity for the ROP of *rac*-lactide with > 90 % conversion to atactic PLA in 48 minutes for **1** and 66 minutes for **2** in bulk conditions at 140 °C.[81] Both complexes generated polymeric material with a PDI = 1.02 and molecular weight (M_n) comparable to that calculated from conversions and [M]/[I]. Whilst this suggested good molecular weight control, MALDI-ToF analysis of low conversion material identified extensive transesterification; coupled with the dinuclear nature of the complexes, it has been mooted that this may be the cause of loss of stereoselectivity compared to the mononuclear aluminium species.[81]

At the beginning of the 21st century, Nakamura coordinated a bulky bis(phenolate) ligand to titanium isopropoxide and showed it to be active in the ROP of caprolactone.[82] The system exhibited good molecular weight control, with the alkoxide present at the terminal of the polymer chain; suggesting a coordination insertion mechanism similar to that seen for stannous initiators. Davidson *et al.* complexed titanium, zirconium and hafnium to two different types of bis(phenolate) ligand with variation in substituents (Figure 1.34). Resulting complexes were tested for activity of the ROP of *rac*-LA.[83]

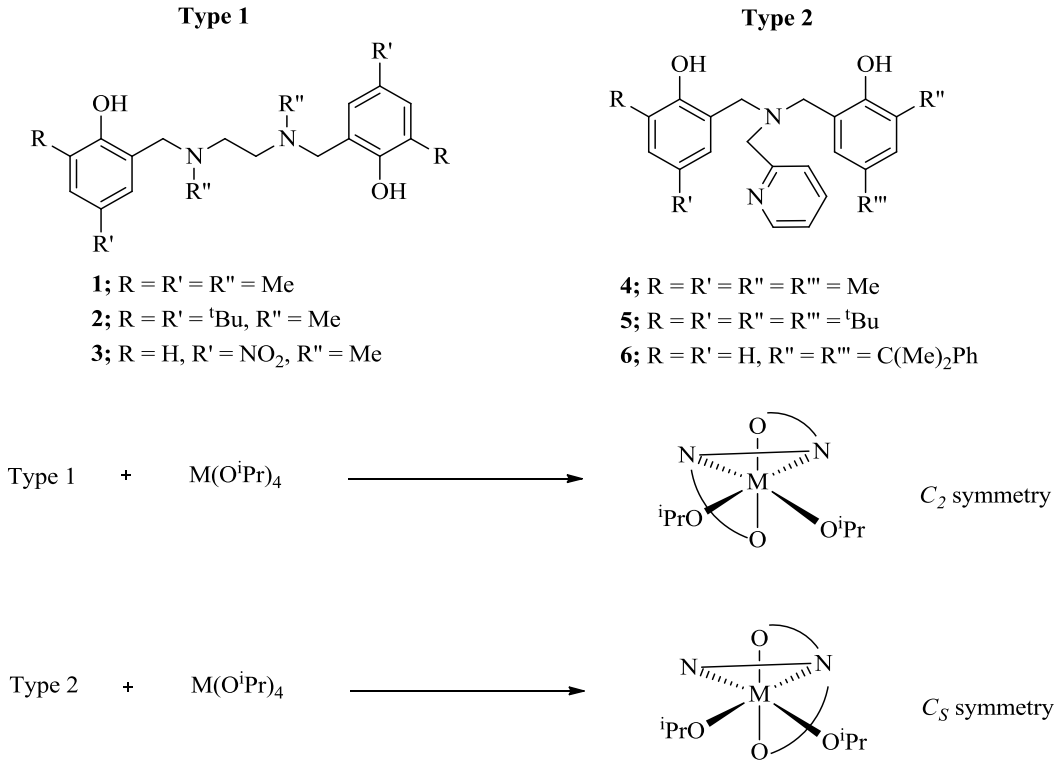

Figure 1.34 Two types of tetradentate amine bis(phenolate) ligands utilised by Davidson *et al.* to generate octahedral group IV complexes [84]

Both sets of complexes were pseudo-octahedral with type 1 complexes having C_2 symmetry whilst type 2 having C_s symmetry due to the labile nature of the M-N bond with the pyridine. It was reported that for the smaller Ti(IV) metal centre, bulkier ligand substituents were required to initiate polymerisation of lactide to produce even atactic PLA. With the larger Zr(IV) and Hf(IV) metal centres isotactic block PLA was produced from *rac*-lactide under solvent-free conditions when slightly less sterically demanding ligands were used.[83]

Early work into group IV metals with tripodal ligands as single-site initiators for the ROP of lactide was limited due to the formation of polynuclear aggregates. Verkade *et al.* identified titanium isopropoxide formed a tetramer with a tripodal tris(alkoxide) ligand.[85] Whilst it was found to be active for the polymerisation of L-lactide in bulk conditions, the polymerisation was not well controlled; which was attributed to poor thermal stability of the tetramer.[85] Verkade *et al.* also went on to publish a trinuclear titanium isopropoxide complex with a tripodal tris(phehonalte) ligand.[86] This was reported to have much better molecular weight control, with high conversion achieved in 12 hours with 200 equivalents yielding polymeric material with M_n = 14720 g mol^{-1} and PDI = 1.35.[86]

Concurrently, Verkade *et al.* also explored the coordination behaviour of tetradentate tripodal ligands in the form of amine tris(alkoxide) and amine tris(phenolate) species (Figure 1.35).[87-89]

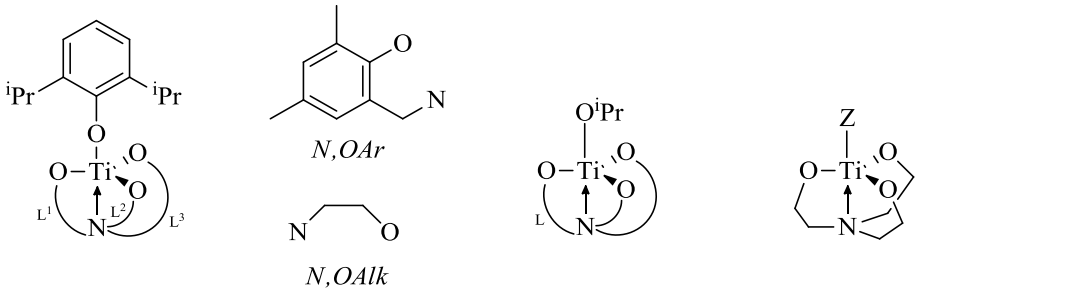

1; $L^1 = L^2 = L^3 = N,OAr$
2; $L^1 = N,OAlk$, $L^2 = L^3 = N,OAr$
3; $L^1 = N,OAr$, $L^2 = L^3 = N,OAlk$
4; $L^1 = L^2 = L^3 = N,OAlk$

5; $L = N,OAr$

6; $Z = O^iPr$
7; $Z = OPh$
8; $Z = O(C_6F_5)$
9; $Z = O(p\text{-}NO_2Ph)$
10; $Z = O(2,4,6\text{-}Me_3Ph)$

Figure 1.35 Tripodal tetradentate amine tris(phenolate)/tris(alkoxide) complexes with titanium (IV) as presented by Verdake *et al.*.[87-89] Summarised in the reference [77]

Complexes **1-4** were reported by Verkade *et al.* to effectively polymerise L-lactide and *rac*-lactide to high conversion in 24 hours under bulk conditions. However, resulting material was broadly dispersed with PDIs ranging from 1.42 to 1.97.[87] A coordination insertion mechanism was proposed due to the presence of both OH and OAr ester groups on the ends of the PLA chains and relatively, activity was found to be higher for complexes with a greater number of alkoxide donors (**1**→ **4**).[87] Replacing the di-isopropylphenoxide with a isopropoxide initiating group (**5**) was reported as providing much more efficient and well-controlled polymerisation than the alternative **1**. PDI was reduced to less than 1.5, attributed to less transesterification with the less bulky O^iPr group.[88] Further investigation was carried out by Verkade *et al.* into the effect of the initiating group for a five-coordinate titanium amine tris(alkoxide) complex (Figure 1.35, **6-10**).[89] As previously observed, the increased steric bulk of the initiating groups of **9** and **10** caused greater transesterification and broader polydispersity values. Whilst **6** was known to be dimeric in the solid state it was postulated by Verkade *et al.* that it readily dissociated under ROP-conditions to provide relatively unhindered mononuclear species that showed the greatest activity of the series.[89] With steric crowding appearing to play a crucial role in activity, the unsubstituted **11** (Figure 1.36) was found to be significantly more active than the bulkier **5** (Figure 1.35) and **12** (Figure 1.36) in bulk polymerisation. However, when trialled as initiators in solution (130 °C, toluene) it was found that the bulkier **11** and **12** were inactive.[89]

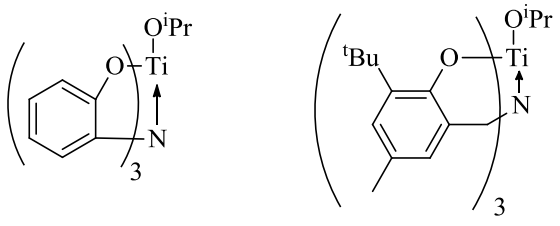

11 **12**

Figure 1.36 Further titanium isopropoxide complexes with amine tris(phenolate) ligands of varying steric bulk

The coordination of methyl and *tert*-butyl substituted amine tris(phenolate) ligands (Figure 1.37) to titanium isopropoxide was reported to yield a C_3-symmetric five-coordinate trigonal bipyramidal complexes.[90] These Ti(IV) complexes were seen to facilitate a living polymerisation of lactide with the phenyl substituents having a great effect on activity.[89]

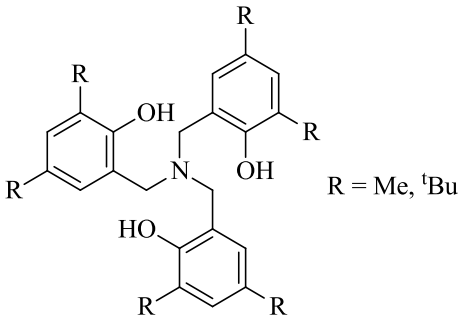

Figure 1.37 C_3-symmetrical amine tris(phenolate) ligands first synthesised by Kol[90]

The potential for significant study into the substituent-activity/selectivity relationship saw extensive work by the Davidson research group, with numerous amine tris(phenolate) ligand systems.[83,84,91] C_3-symmetry was present in the isolated five-coordinate complex with the complex adopting a propeller-type arrangement with a bulky amine tris(phenolate) ligand (Figure 1.38).

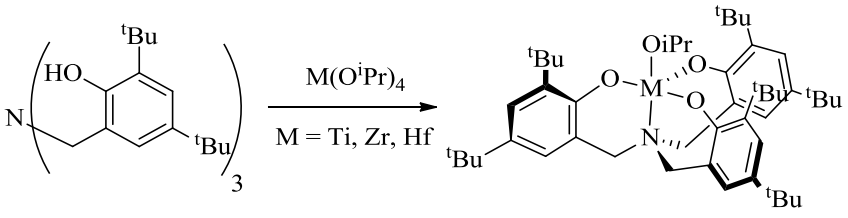

Figure 1.38 Group IV amine tris(phenolate) complexes as presented by Davidson *et al.*[91]

The substituted amine tris(phenolate)s coordinated to Ti(IV) afforded atactic PLA from *rac*-lactide, whilst the zirconium and hafnium analogues produced highly heterotactic PLA under melt conditions; similar to that required for industrial production (130 °C). High activity was observed with 97% conversion achieved in 6 minutes under melt conditions using the zirconium amine tris(phenolate). This short reaction time, compared to aluminium initiators, also gave high selectivity with P_r = 0.96 (M = Zr) and P_r = 0.88 (M = Hf).[91] Activity was seen to be seven times slower for enantiopure L-lactide compared to *rac*-lactide.

To investigate the nature of the high stereoselectivity of these C_3-symmetric amine tris(phenolate) complexes, work was carried out by Davidson *et al.* with the synthesis of a single-site germanium alkoxide initiator with a di-methyl-substituted amine tris(phenolate) ligand.[92] As with the highly selective aforementioned zirconium analogue (Zr-$C_3{}^tBu$), the propeller-like complex was found to be fluxional in axial chirality at room temperature, with rapid conversion between the *P* and *M* isomers (Figure 1.39).

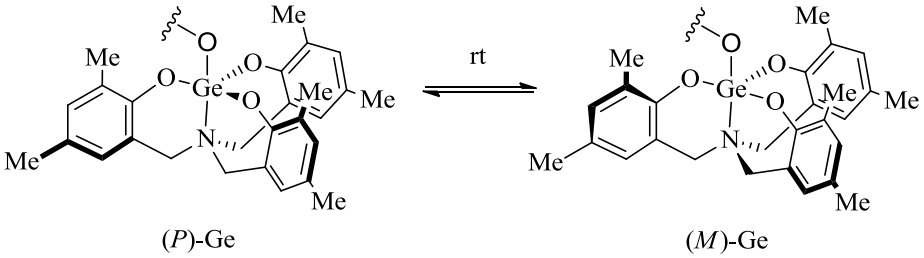

Figure 1.39 Inversion of chirality at the Germanium metal centre[92]

The Davidson group postulated that, whilst stereoselectivity has previously been classified as either chain-end control (CEC) or enantiomorphic site control (ESC), for this type of complex both aspects were involved providing an 'enhanced chain-end control'.[92] CEC defined monomer selectivity to be determined by the stereochemistry of the previously inserted monomer, Scheme 1.1 **(i)**, whereas ESC was indicative of a complex with dynamic chirality influencing the subsequent monomer selectivity, Scheme 1.1 **(ii)**.[93] For the enhanced chain-end control, a preferential pairing of stereochemistry of both the previously inserted monomer and the complex, with the (*R*,***R***)-(***M***)-Ge enantiomer selective towards L-lactide insertion and the (*S*,***S***)-(***P***)-Ge enantiomer selective towards D-lactide, Scheme 1.1 **(iii)**.[92]

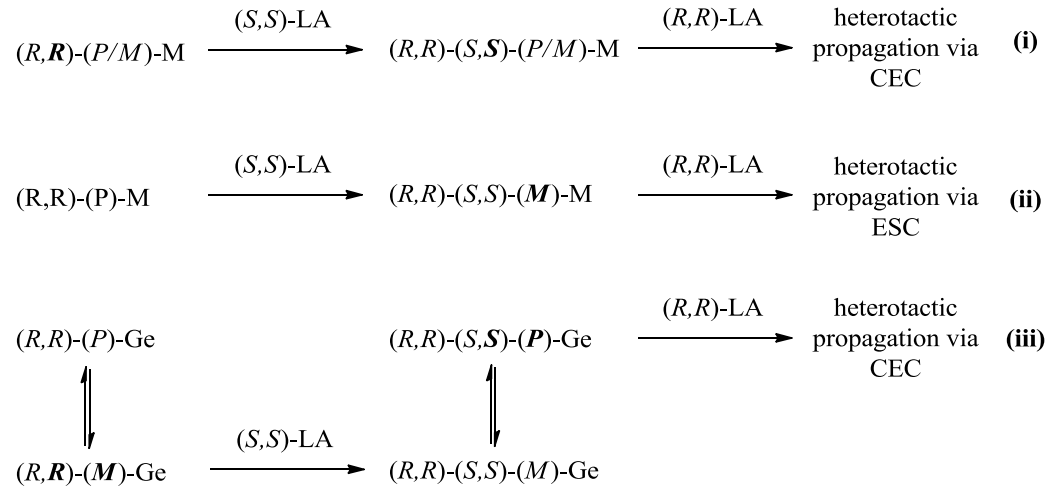

Scheme 1.1 Possible mechanisms of stereocontrol – **(i)** chain-end control (SEC), **(ii)** dynamic enantiomorphic site control (ESC), **(iii)** enhanced chain-end control [92]

Attempts were made by Davidson *et al.* to confirm the proposed mechanism by the synthesis of a chiral zirconium complex which, through the substitution of a methyl group on to one of the methylene bridges of the ligand, the C_3-symmetry was disrupted without changes to electronics and minimal alteration to the steric of the ligand.[94-96]It was found that the chiral complex had reduced fluxionality that had subsequent adverse effect on the addition of every other monomer. The lack of fluxionality led to a certain diastereotopic pairing, of monomer and metal, not occurring at room temperature due to the relative stability of the (*R,M*)-Zr form over the (*R,P*)-Zr form; this corresponded to that which was selective towards the insertion of L-lactide and thus polymerisation did not occur over the observed timescale.[97]

Work by Davidson *et al.* has also seen titanium and zirconium alkoxides coordinated to chiral Schiff base ligands.[96] Coordination of the bidentate ligand led to a metal-centred octahedral complex with general formula $L_2M(O^iPr)_2$ (Figure 1.16).

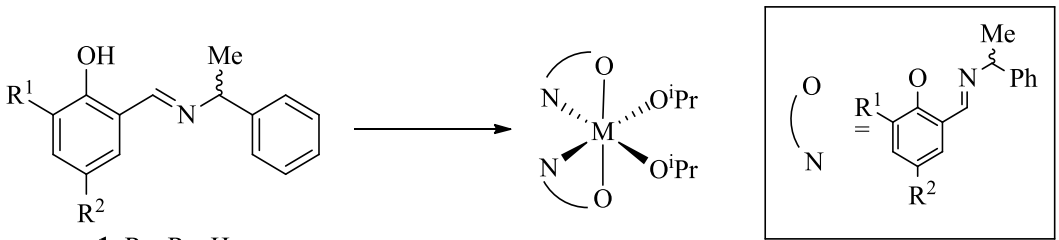

1: R_1=R_2=H
2: R_1=H, R_2=OMe
3: R_1=H, R_2=Me
4: R_1=R_2=Cl

M = Ti, Zr

Figure 1.40 Coordination of chiral Schiff base ligands to group IV isopropoxides

The titanium complex proved inactive for solution based lactide polymerisation, however, yielded atactic PLA under melt conditions. The zirconium analogue proved to be a very robust initiator with heterotactic enrichment seen at 20 °C and 80 °C for polymerisation in both toluene and the melt. Selectivity was not as high as seen for the C_3 amine tris(phenolate)s discussed previously. Unlike most metal alkoxide initiators, polymerisation continued after the addition of water.[96]

Jones *et al.* disrupted the C_3-symmetry of the amine tris(phenolate) ligands previously reported through the removal of the methylene bridge for one phenolate arm (Figure 1.41).[98] Complexation with Ti(IV) and Zr(IV) produced monomeric five-coordinate species for the titanium analogues, whilst coordination to a larger zirconium metal centre gave rise to dimeric species with one isopropoxide per metal centre and the phenolate without a methylene bridge occupying the bridging role.[98]

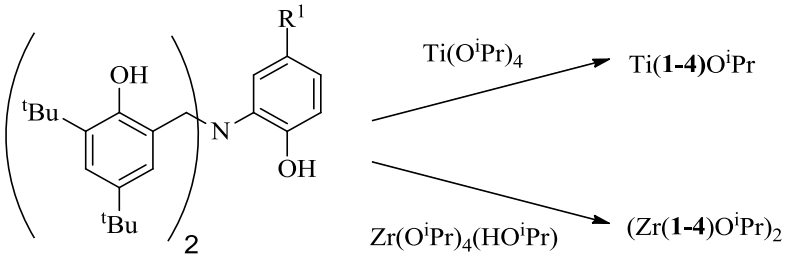

1; R^1 = H
2; R^1 = Me
3; R^1 = tBu
4; R^1 = Cl

Figure 1.41 Titanium (IV) and zirconium (IV) amine tris(phenolate) complexes as reported by Jones *et al.*[98]

All complexes, except Ti(**3**)O^{i}Pr, were found to be active for the ROP of *rac*-lactide in solution (toluene, 80 °C); all were found to be active in the melt (130 °C). Activity in the melt was much higher with high conversion achieved in 15 minutes for Zr(IV) complexes, whilst reaction times of 120 minutes were required for the Ti(IV) analogues. Polydispersity was slightly higher than reported for the C_3-symmetric Zr(IV) amine tris(phenolate) initiators. As with all titanium complexes, PLA afforded was atactic whilst slight heterotactic enrichment (P_r = 0.6) was observed for (Zr(**3**)O^{i}Pr)$_2$ and (Zr(**4**)O^{i}Pr)$_2$.

More recent work by Jones *et al.* has isolated group IV complexes with a range of unsymmetrical (ONNO)-salalen-type ligands that incorporate both Schiff base and amine character about an ethylene backbone (Figure 1.42).[14, 99]

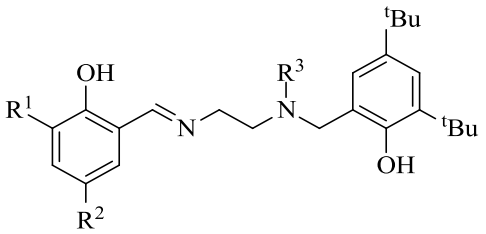

1; $R^1 = R^2 = {}^tBu$, $R^3 = Me$
2; $R^1 = R^2 = {}^tBu$, $R^3 = Ph$
3; $R^1 = Me$, $R^2 = H$, $R^3 = Me$
4; $R^1 = R^2 = H$, $R^3 = Me$

Figure 1.42 Salalen-type ligands as coordinated to Ti(IV), Zr(IV) and Hf(IV)[14, 99]

Substituents on the salen-phenyl ring and amine were varied and complexed with Ti, Zr and Hf from respective isopropoxide precursors. All complexes, except Hf(**3**)$(O^iPr)_2$ were found to have a *β-cis* configuration in the solid state, with complementary data from solution-state NMR spectroscopy.[99]

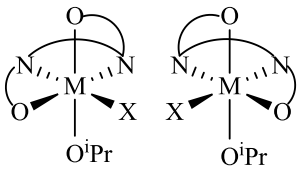

Figure 1.43 *fac-mer β-cis* geometry isolated in the solid state for group IV salalen complexes reported by Jones *et al.*[99]

Complexes were trialled as initiators for the ROP of lactide in both solution (toluene, 70 °C) and melt conditions (130 °C). Titanium complexes yielded atactic PLA in both the melt and solution whilst their zirconium analogues provided slight heterotactic enrichment. The hafnium salalen complex, with a methyl group on the amine, could not provide polymeric material on the similar time-scale to its Ti and Zr equivalents, however the oligomeric material isolated was significantly isotactic (P_r= 0.2). Extended reaction times yielded polymeric material but with slightly decreased isotactic enrichment (P_r= 0.3).[99] Further investigations into this type of ligand by the same group has revealed that a hafnium complex with slightly less sterically demanding groups on the salen-phenyl are active for not just the ROP of lactide but also the subsequent degradation to methyl lactate.[14]

In 2011 Okuda *et al.* published a new (OSSO)-type ligand coordinated to Ti(IV) and Zr(IV), reporting it active for the ROP of *meso*-lactide.[100] Ligand architecture was varied in both aromatic substituents and the bis(phenolato) backbone linker (Figure 1.44)

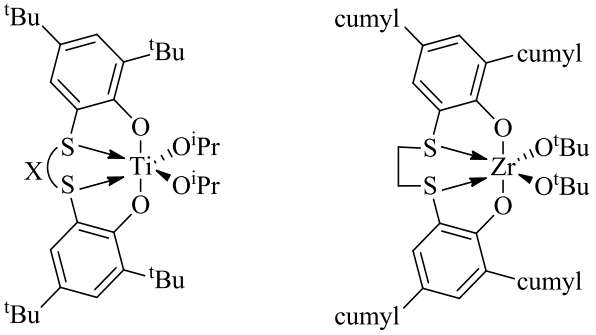

1; X = $(CH_2)_2$
2; X = *c*-C_6H_{10}
3; X = $(CH_2)_3$

4

Figure 1.44 (OSSO)-type bis(phenolato) ligands coordinated to group IV alkoxides, as presented by Okuda *et al.*

The complexes were found to be octahedral with the two remaining alkoxide group arranged *cis* to one another and the tetradentate ligand orientated *fac*-*mer*. Trials for the ROP of *meso*-lactide found that, in toluene at 100 °C with a reaction time of 24 hours, the nature of the ligand backbone affected catalytic activity with **3** achieving 71 % conversion whilst **1** and **2** only reached 38 % and 8 % respectively. All complexes produced syndiotactic PLA with a percentage-syndiotactic enchainment ~60-70 %.[100] A zirconium (IV) analogue, with *tert*-butyl alkoxides groups and cumyl phenolato substituents (**4**), was found to be significantly more active with > 99 % conversion achieved in 24 hours.[100]

Further work by the same group, and in collaboration with Kol, generated another new set of tetradentate ligands with (ONSO)-type bonding.[101] The resulting complexes with Zr(IV) were reported as fluxional, with the imine adopting the more rigid *meridional* orientation and the thio donor the *facial* orientation of the octaheadral geometry. Barriers to interconversion were found to be dependent on the phenolate substituents with considerable steric bulk of the adamtyl groups of **2** proving the most rigid whilst complex **1** with chloro substituents on the thio phenolate arm, displayed greatest fluxional behaviour (Figure 1.45).[101]

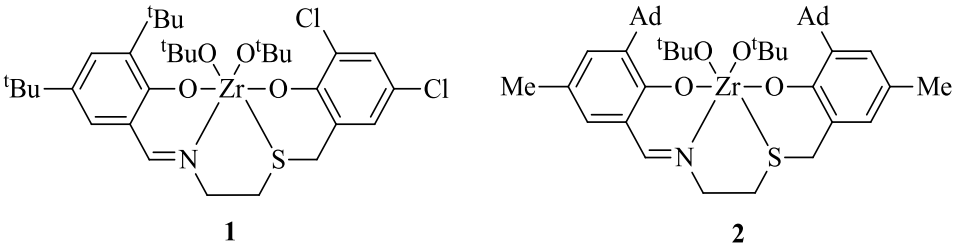

1 **2**

Figure 1.45 Fluxional complexes of Zr(IV) with (ONSO)-type bis(phenolate) ligands[101]

It was also reported that the more fluxional complex **1** directed towards heterotactically enriched PLA (P_r = 0.72) when used as an initiator for the ROP of *rac*-lactide at 70 °C in toluene. The rigid nature of complex **2** was conversely found to provide isotactically enriched PLA (P_r = 0.33), albeit at much lower activity, with only 18 % conversion over 24 hours compared to 98 % for complex **1**.[101] Whilst providing insight into the role of fluxional species in determining stereoselectivity it is important to note that molecular weight was not as well controlled as reported with other ligand systems and that all stereoselectivity was essentially lost under more industrially relevant solvent-free conditions.[101]

Whilst numerous salan and salen complexes incorporating phenolate donors have received considerable attention in the literature, recently Pampaloni and Repo *et al.* have published mechanistic studies into the use of group IV tetracarbamto complexes with general formula $M(O_2CNR_2)_4$.[102] Titanium, zirconium and hafnium analogues were all isolated with variation in the cambamto substituent as well (R = Et for Ti, R = Et or ^{i}Pr for Zr and Hf). The structure of the carbamto ligand had significant influence over molecular weight; with the highest weigh of 94000 Da being with ^{i}Pr-substituted complexes.[102] Studies of the generation of the ROP-active species for these complexes were carried out at low conversion with complementary DFT calculations. It was postulated that the mechanism for Zr and Hf was somewhat different to that for Ti with the larger group IV complexes (Zr and Hf) initiating *via* the protonation of the carbamto *O*-atom before the generation of an active alkoxy species and the release of CO_2 and NHR_2. The titanium species on the other hand, proceeds by initial formation of a racical fragment $[R_2NCOO]^\bullet$ and a Ti(III) complex with a coordinated lactide. This lactide acts as the initiating group for the ROP of a subsequently coordinated lactide and is observed as a chain end group.[102]

1.5.4 Group I, II, Zinc and other initiators

1.5.4.1 Group I

Early work into the suitability of lithium *tert*-butoxide as an initiator for the polymerisation of lactide showed that high molecular weights were obtainable with little transesterification and slight heterotactic selectivity.[103] Further work carried out by Bero *et al.*, showed that rapid polymerisation occurred as low as -20 °C; however extended reaction times would allow transesterification of the polymer chains. Whilst heterotactically enriched, small atactic segments in the polymer lowered the observed glass transition temperature (T_g).[104] Recently, Carptentier *et al.* have reported aminoether-phenolate complexes of lithium and potassium with

a large range of coordination motifs that were active for the immortal-like ROP of L-lactide *via* an activated monomer mechanism in the presence of benzyl alcohol as an initiator and chain transfer agent.[105]

1.5.4.2 Group II and Zinc

As a biocompatible metal, zinc is an attractive target for the development of initiators for the production PLA. Early examples of zinc-based initiators were published by Coates *et al.* and incorporated a *β*-diiminate bidentate ligand.[106 37] Coates also presented Magnesium analogues, whilst Chisholm *et al.* altered the backbone of the ligand and coordinated to zinc and magnesium (Figure 1.46).[107]

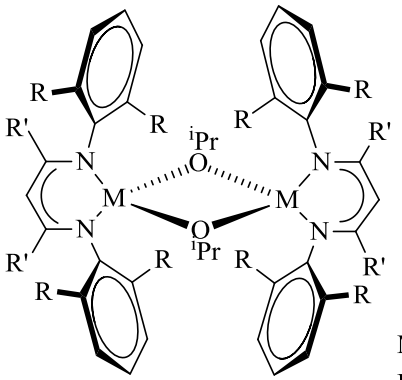

Figure 1.46 Single-site β-diiminate zinc and magnesium complexes[37, 106, 107]

Magnesium complexes trialled by Coates *et al.* for the ROP of *rac*-LA found that with R = ^{t}Bu complete conversion was achieved to atactic PLA in CH_2Cl_2 at 20 °C in only two minutes. However, the polydispersity was found to be broad (PDI = 1.59) that could be improved with the addition of propan-2-ol as a co-initiator.[37] Polymerisation was much more controlled with the zinc analogue where R = ^{i}Pr, with a PDI = 1.10. Activity was lower with equivalent conversion achieved in 20 minutes but analysis of polymer mictrostructure identified highly heterotactic PLA (P_r = 0.90).[106] Alteration to the R groups (isopropyl to ethyl) for the zinc complexes found stereoselectivity to decrease along with rate of polymerisaiton.[37] Chisholm *et al.* replaced the methyl substituents of the backbone with *tert*-butyl groups. The increased bulk was thought to enhance the end group control for both zinc and magnesium complexes, thus increasing selectivity. However, trials showed an actual decrease for the zinc complexes with all

producing atactic PLA.[107] Chisholm *et al.* carried out studies into the effect of the solvent system used on stereoselectivity for magnesium and zinc β-diiminate complexes. Polymerisations carried out in THF afforded high selectivity, with heterotactic PLA isolated. This selectivity was deemed to be due to the coordinative nature of the THF to the metal centre.[108, 109]

Hillmyer and Tolman *et al.* coordinated a tridentate phenolate ligand with diethyl zinc (Figure 1.47, **1a** and **1b**). On addition of ethanol it was found that in the solid-state the complex adopted a ethoxy-bridge dimeric structure (**2**a and **2b**). Analysis in CD_2Cl_2 found monomeric, dimeric and rapidly equilibrating mixture of the structure that were not slowed by reduction in the temperature.[110]

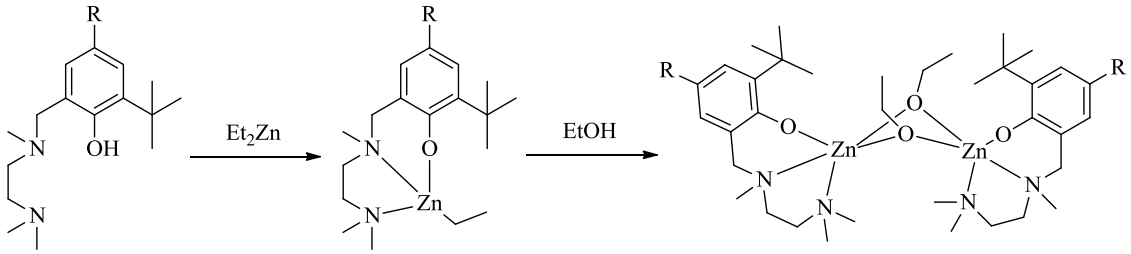

Figure 1.47 Monomeric and dimeric zinc complexes isolated and studied for the ROP of lactide by Hillmyer and Tolman *et al.* [110]

Hillmyer and Tolman *et al.* presented considerable experimental data to support that **2a** did predominately not remain as a dimer in solution, including PGSE NMR and calculated diffusion coefficients. Trialling of the complexes as initiators for the ROP of lactide found them highly active with good molecular weight control. Conversion to high molecular weight was also possible at lower catalytic loading, with a [LA]:[I] proving polymeric material of 130 kDa with a PDI = 1.4. Molecular weights were found to be slightly lower than expected and Hillmyer and Tolman postulated that this was due to impurities.[110] With respect to impurities, they acknowledged that impurities causing catalyst degradation/inactivity would cause an increase in molecular weight, whilst impurities acting as chain transfer agents would lower the observed molecular weight. Studies also found that **2a** retained high activity in the presence of benzyl alcohol whilst observations at high catalytic loadings implied that initiation was slower than propagation. In-depth kinetic studies were carried out for the ROP of lactide using initiator **2a**. The rate law was found to be first order with respect to LA and, whilst a plot of $\ln(k_{obs})$ versus ln[I] had a non-integer gradient, a linear releationship of k_{obs} versus [I] lead to the conclusion

that the rate equation was second order overall: $-\frac{d[LA]}{dt} = k_p[LZnOEt][LA]$. The non-zero intercept of the k_{obs} versus [I] with the y-axis suggested that a threshold catalyst concentration was in place. This was confirmed by experiments that involved the addition of extra catalysis to an inactive mixture of monomer and catalyst below the threshold concentration.[110]

Work published by Gibson *et al.* presented an *β*-diiminate ligand that was tridentate through the inclusion of a methoxy group on one of the phenyl rings. This was coordinated to both magnesium and zinc (Figure 1.48).[111]

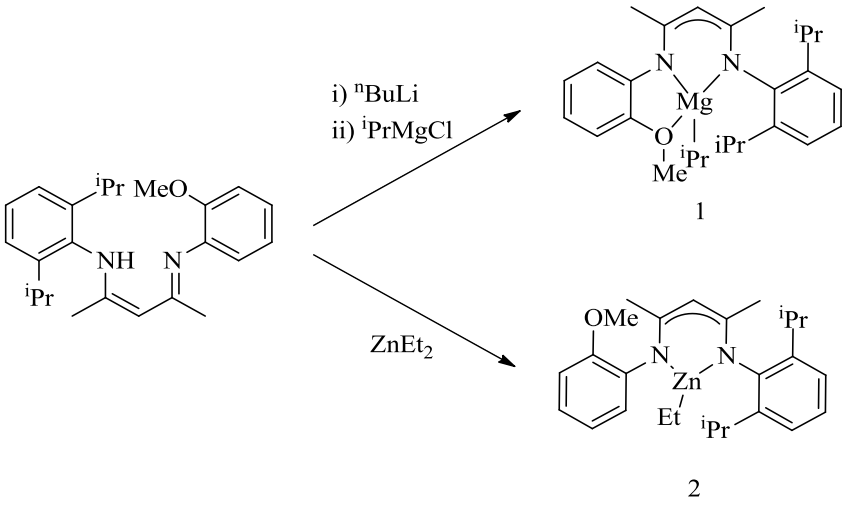

Figure 1.48 Magnesium and zinc complexes to a potentially tridentate β-diiminate ligand[111]

Complex **1** and **2** were trialled for the ROP of *rac*-lactide with an amide initiating group replacing the alkyl group on the metal centre. Complex **2** was also altered to a have a siloxide initiating group. All proved to have high activity, yielding PLA with 80 % conversion within 30 minutes. The magnesium initiator was found to be much less well-controlled than the zinc analogues with PDI > 1.6. The zinc species were found to be much more active than the bidentate *β*-diiminate complexes already discussed, however a trade-off for reduced stereoselectivity was reported.[111]

Gibson *et al.* also made attempts to justify the selectivity seen for the magnesium bidentate *β*-diiminate complexes through computational studies. This led to suggestions that heterotactic selectivity occurred due to preferential coordination alignment of the lactide nucleophillic attack by the M-O bond on the acyl carbon of the lactide.[112]

Work presented by Herres-Pawlis *et al.* introduced the use of bis(guanidine) ligands to generate monomeric tetrahedral zinc complexes. Complexation to $ZnCl_2$ or $Zn(acetate)_2$ formed species with a bis(guanidine)-to-metal ratio of 1:1 (**1** and **2**, Figure 1.49). The use of $Zn(triflate)_2$ as the metal source resulted in double coordination of the bidentate ligand with the complex adopting a geometry distorted between tetrahedral and square planar.[113]

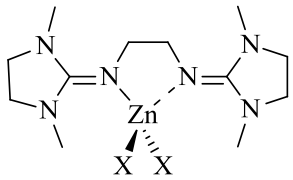

1; X = Cl
2; X = $OOCH_3$

Figure 1.49 Monomeric zinc bis(guanidine) complexes, $Zn(DMEG_2)X_2$ isolated by Herres-Pawlis *et al.*[113]

Complex **1** and the $Zn(DMEG_2e)_2(CF_3SO_3)_2$ complex, **3**, were air-stable at ambient temperatures; complex **2**, whilst hydroscopic, was air-stable on the hour-scale. Activity for the ROP of *rac*-lactide was undertaken at 150 °C and solvent free. All three complexes were found to be active with highest yield to industrially useful large molecular weights (83 %, 38200 Da) achieved using **3**. Increasing the reaction time from 24 to 48 hours was found to be unadvantageous, with lower yields and reduced molecular weights, attributed to increased transesterification. Performance was lowest for ROP trials undertaken for **2**, exhibiting relatively lower molecular weights and yields.[113]

In light of polymerisation activity and attractive air-stability, work was also done by Herres-Pawlis *et al.* utilising guanidine-pyridine hybrid ligands (Figure 1.50). These were coordinated to $ZnCl_2$, $Zn(acetate)_2$ and $Zn(triflate)_2$.[114]

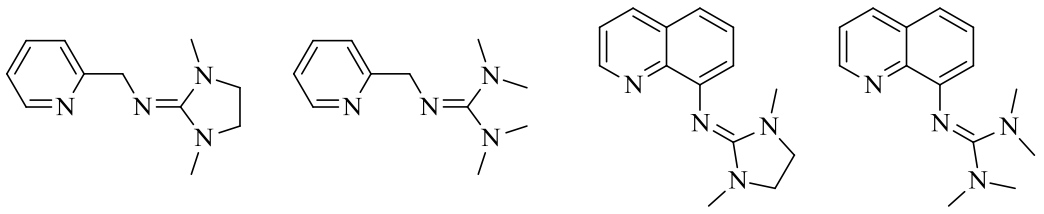

1 **2** **3** **4**

Figure 1.50 Guanidine-pyridine hybrid ligands used for the coordination with $ZnCl_2$, $Zn(acetate)_2$ and $Zn(triflate)_2$ by Herres-Pawlis *et al.*[114]

Complexes of all ligand were isolated, except for ligands **1** and **2** with Zn(triflate)$_2$. Structures with **1** and **2** were found to be akin to that previously reported for complexes with bis(guanidine) ligands; tetrahedral with one guanidine-pyridine hybrid ligand and two acetate or chloro ligands.[114] Complexes of **3** and **4** with the Zn(triflate)$_2$ precursor were found to be six-coordinate, consisting of two ligands and a triflate binding through two oxygen atoms.[114] Zn(**3**)Cl$_2$ and Zn(**4**)Cl$_2$ were found to be inactive for the ROP of *rac*-lactide whilst all acetate complexes were successful. Greatest activity was reported for the triflate complexes, attributed to the weak coordination of the triflate and thus increased Lewis acidity of the metal centre. With ligands **3** and **4** the Zn triflate complexes displayed the highest activity with polymeric material of up to 176000 Da obtained.[114]

Recently, Herres-Pawlis and Strohmann *et al.* reported a range of air-stable zinc complexes with basic bidentate diamine ligands (Figure 1.51).[115]

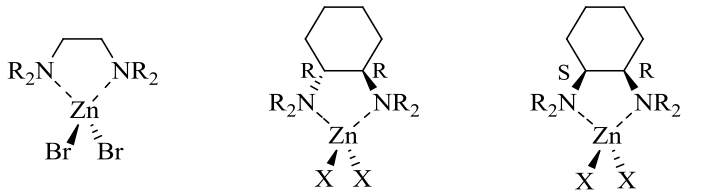

1; R = Me
2; R = Et

3; R = Me, X = Br
4; R = Et, X = Br
5; R = Me, X = Cl
6; R = Et, X = Cl

7; R = Me, X = Br
8; R = Me, X = Cl

Figure 1.51 Diamine zinc complexes reported by Herres-Pawlis and Strohman *et al.* and tested for ROP activity[115]

All eight tetrahedral complexes were tested for the ROP of *rac*-lactide with only **1** proving inactive and the nature of X having little effect on activity. Conditions used were solvent-free at 150 °C for 24 hours and it was reported that complexes **4** and **6** were most active, generating molecular weight in the region of 130000 Da. Yield was found to be high for **7** and **8** but with reduced molecular weight (M_n ~ 50000 – 70000 Da).[115] Reaction temperature was varied for **3** and **7** with activity being removed at 135 °C for **3** whilst **7** remained active, albeit reduced. Increasing the temperature to 165 °C increased yield but reduced the polymer molecular weight. Activity was understandably related to reaction temperature but as was transesterification, with PDI varying with temperature (higher at 165 °C). Polymer tacticity was also measured for all active complexes with microstructure identified to be in line with atactic PLA.[115]

Work previously undertaken by Jones *et al.* successfully complexed zinc (II) with Schiff base ligands; these polymerised unsublimed *rac*-lactide in solvent-free conditions with slight

heterotactic enrichment.[49] Subsequent grafting of the initiator to silica to create a heterogeneous analogue showed reduced activity and little selectivity.[49]

Bulky tridentate (OOO)-type bis(phenolate) complexes with magnesium and zinc (**2** and **3**) were isolated by Mountford *et al.* (Figure 1.48). It was also reported that whilst the Mg and Zn complexes were dimeric, the same cumyl-substituted ligand formed a monomeric species when coordinated to potassium. Synthesis of **1** in THF generated an analogue with a THF adduct. Analysis of **2** and **3** in the solid state found the metal centres to be tetra-coordinated, binding to three oxygens of one ligand and forming a bridge with one oxygen of the other.[116]

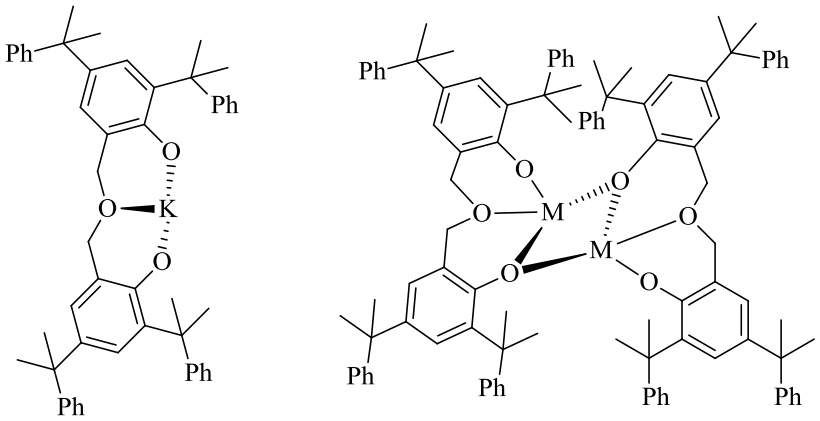

1

2; M = Zn
3; M = Mg

Figure 1.52 Complexes of K, Mg and Zn with bulky cumyl-substituted tridentate bis(phenolate) ligands[116]

Complexes **1**, **2** and **3** were found to be active for the ROP of *rac*-lactide and ε-caprolactone. Compound **1** was found to be active with and without benzyl alcohol, however, in the absence of the coinitiator, the polymerisation was slower and less well controlled. The polymer produced was atactic. Activity of **2** and **3** for the ROP of L-lactide and ε-caprolactone is reported as slower but still effective. Significant kinetic experiments were carried out for the ROP of ε-caprolactone using the dimeric zinc complex **2**. At 50 °C in toluene the ROP of ε-caprolactone was found to be order of one-half with respect to [**2**], this was attributed to a monomer-dimer equilibrium generated by the benzyl alcohol.[116]

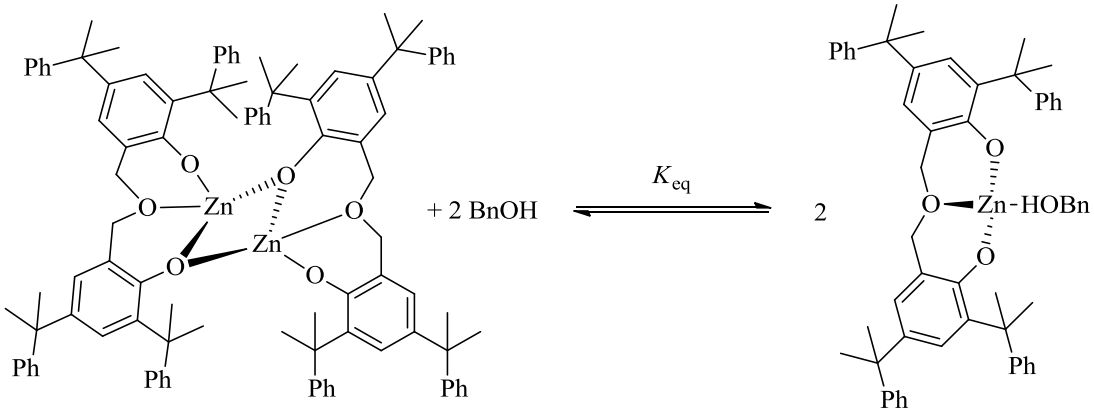

2 **2_BnOH**

Figure 1.53 Dimer-monomer equilibrium of **2** with benzyl alcohol adduct as explored by Mountford *et al.*

With **2_BnOH** assumed to be the ROP-active species the concentration of the active species was stated by the following relationship: $[\mathbf{2\_BnOH}] = {K_{eq}}^{0.5}[BnOH]_0{[\mathbf{2}]_0}^{0.5}$. Mountford *et al.* then went on to model the reaction under saturated conditions and use the Michaelis-Menten equation to generate the rate equation: $-\frac{d[CL]}{dt} = k_p[BnOH]_0{[\mathbf{3}]_0}^{0.5}$. This required that the [CL] was considerably greater than the Michaelis constant (K_M) and saw that the rate limiting step was that of the formation of the active **2_BnOH** species.[116] Similar studies had been reported by Hillmyer and Tolman for the polymerisation of ε-caprolactone where monomer binding potential was explored with respect to electronic effects of a ligand coordinated to an aluminium alkoxide species.[117]

In 2013, Mountford *et al.* presented a series of simple complexes incorporating calcium and strontium with monodentate 2,4-di-*tert*-butylphenolates (DPB) and bidentate 1,2-dimethoxyethane (DME).[118] The reaction of freshly filed calcium metal with DBP in THF yielded a monomeric six-coordinate complex with four THF adducts (Figure 1.54, **1**). The corresponding reaction with strontium metal gave a trinuclear species in the solid-state with bridging between strontium metal centres being facilitated by three DPB ligands (Figure 1.54, **3**). However, **3** was found to be fluxional in solution when analysed by NMR spectroscopy. When the reactions were carried out in DME instead of THF the calcium species was found to be dimeric in the solid-state with each calcium seven-coordinate with the calcium metal centres bridged through a bidentate DME (Figure 1.54, **2**). The solid-state structure of the strontium equivalent was dimeric with bridging *via* three phenolate ligands (Figure 1.54, **4**). Only one phenolate environment was obsereved in solution, suggesting rapid exchange of phenolate ligands between terminal and bridging positions.[118]

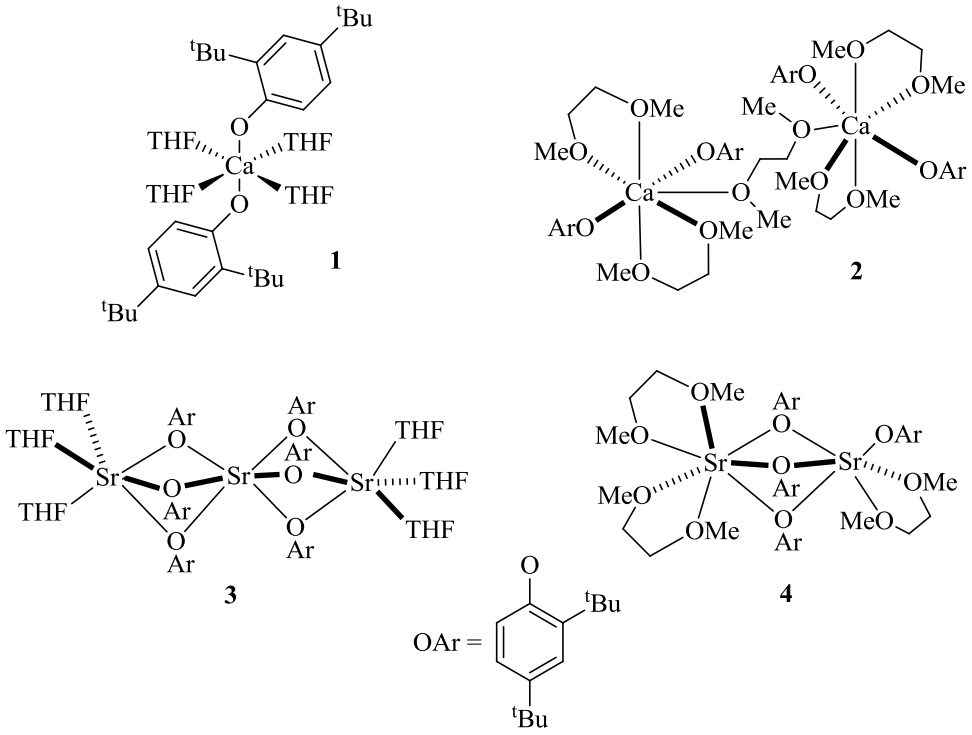

Figure 1.54 Complexes of calcium and strontium with 2,4-di-*tert*-butylphenol, prepared in THF or 1,2-diaminoethane, as isolated by Mountford *et al.* [118]

Trials of complexes **2** and **4** as potential initiators for the ROP of *rac*-lactide were carried out in THF at room temperature. In the absence of coinitiator, **2** was found to be more active than **4** with conversions in 30 minutes of 73 % and 51 % respectively. However, analysis *via* GPC of polymer molecular weight after 150 minutes, indicated that **2** produced one polymer chain per Ca-DBP moiety, whilst **4** remained a dimer with only one polymer chain per molecule. The addition of BnOH and $BnNH_2$ as a coinitiator saw significant increase in activity with > 90 % conversion achieved in 10 minutes, with molecular weight control indicating that there was one polymer chain per molecule of coinitiator.[118] The lack of replacement of DBP ligands by propagating polymer chains suggested that the polymerisation was taking place *via* an activated monomer mechanism rather than a coordination insertion mechanism. Kinetic studies concluded that the overall rate law was: $-\frac{d[LA]}{dt} = k_p[\mathbf{2}\ or\ \mathbf{4}]_0[rac-LA]^2[BnNH_2]^{2.5}$. This was different to the activated monomer rate law published by Carpentier *et al.*, in which rate was found to be first order with respect to complex, L-LA and coinitiator.[119] However work by Carpentier *et al.* utilised a better defined coordination environment with aza-crown ethers and thus Mountford *et al.* proposed that the more complex nature of the rate law was due to the fluxional and unstable nature of the supporting ligand system.[118]

1.5.4.3 Other initiators

Steric bulk of spectator ligands has been shown to have an effect on both activity and selectivity for polymerisation of lactide using yttrium and scandium alkoxide initiators.[120] Increasing the size of amidinate ligand substituents of the yttrium alkoxide initiators lowered activity whilst providing no effect on selectivity. A range of scandium bis(phenolate) ligands have been synthesised and shown to give increased heterotactic selectivity with increased ligand size; P_r was seen to increase from 0.78 to 0.90 due to a single CH_2 insertion into the bis(phenolate) bridge.[121] Coates *et al.* successfully complexed a tetradentate binap-salen ligand to a yttrium alkoxide to create a single site initiator; whilst analogues with other metals showed selectivity, none was seen for this species.[27] Over more recent years group III and lanthanide complexes have received continued interest with respect to activity and stereoselectivity.

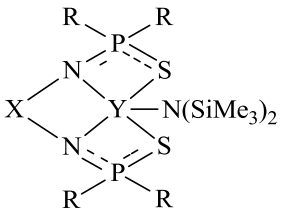

Williams *et al.*, 2008 [122]

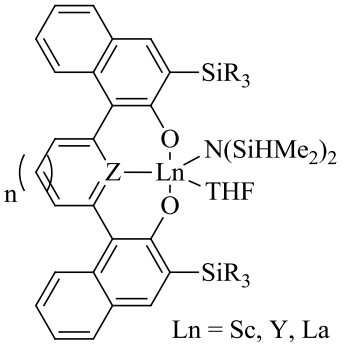

Carpentier *et al.*, 2010 [123]

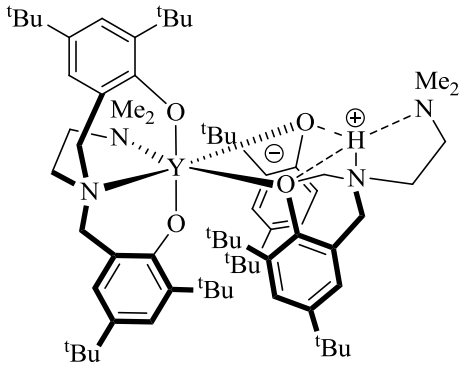

Mountford *et al.*, 2010 [124]

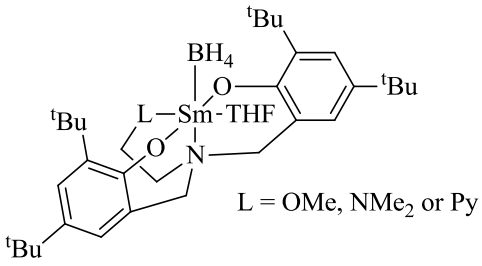

Mountford *et al.*, 2010 [125]

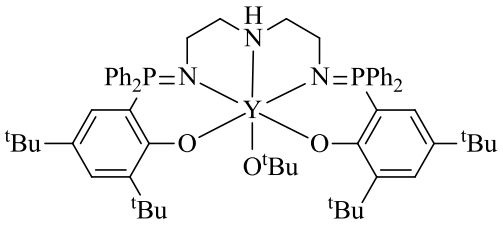

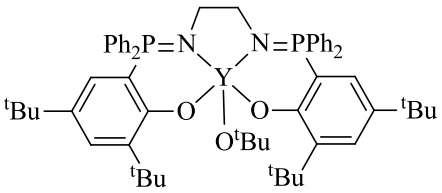

Williams *et al.*, 2012 [126]

Figure 1.55 Recently published group III and lanthanide complexes utilised for the ROP of lactide

In 2008, Williams *et al.* reported a series of yittrium amido complexes with bis(thiophosphinic amido) ligands to be active for the ROP of *rac*-lactide. The complexes were made *in-situ* due to their instability but polymeric material was found to have a heterotactic bias ($P_r \sim 0.7$).[122] Work followed by Carpentier *et al.* with scandium, yttrium and lanthanum amido complexes supported with tridentate naphthoxy-based ligands.[123] The complexes were reported as active for ROP in THF and toluene at room temperature, however significant solvent effects were observed with a $P_r = 0.93$ being achieved in THF whilst polymerisations carried out in toluene yielded atactic PLA.[123] Mountford *et al.* isolated a zwitterionic complex of yttrium with an amine bis(phenolate) encorporating a pendant amine donor ligand. This was reported as being

highly active for the ROP of *rac*-lactide yielding high conversion in 20 minutes at 70 °C in THF.[124] Mountford *et al.* also presented complexes of samarium borohydride with the same amine bis(phenolate) ligand that proved highly active yielding PLA at 80 % conversion in THF at room temperature in 30 minutes. Unlike the zwitterionic complex, stereoselectivity towards heterotactic PLA was observed.[125] Other examples of lanthanide complexes for the ROP of lactide followed, with Carpentier *et al.* publishing a heterobimetallic borohydrido neodymium complex supported by a diamino-bis(phenolate) ligand akin to that previously coordinated to Al(III), and a second with the amine bis(phenolate) ligand utilised above by Mountford generating a similar heterobimetallic bis(phenoxide) complex.[127] These were found to be active single-site initiators under mild conditions (20 °C) with the borohyride group acting as an initiator in the absence of such a group, through lactide insertion into a Nb–O bond.[127]

More recently Williams *et al.* have provided an exceptional range of stereoselectivity for a series of yttrium phosphasalen complexes that incorporated a new iminophosphorane derivative of the popular salen ligand.[128] Alteration of the ligand back bone that also altered the chelating effect of the ligand from pentadentate to tetradentate saw a shift from isotactic selectivity (P_r = 0.24) to high heterotactic selectivity (P_r = 0.90). Activity was high at ambient temperature in THF with the relative activity of the tetradentate complex significantly higher than the yttrium complex with the pentadentate phosphasalen ligand.[128]

1.6 Polylactide copolymers

1.6.1 Overview

Whilst polylactide is an attractive renewable alternative to traditional polymers, its application in both commodity and biomedical applications is limited due to its physical and chemical properties.[4] Its crystallinity, brittleness and instability at high temperatures make it unsuitable as an engineering plastic replacement; whilst being an unfunctionalised polymer chain and inherently hydrophobic leads to reduced biodegradation and little scope for use in targeted therapies.[4] Copolymerisation of lactide with other monomers is an essential route to widening its use in all applications. This route can alter both mechanical properties and add novel functionality to the resulting polymer.[129] For example, the alteration of drug permeability and *in vivo* degradation rate through the copolymerisation with ε-caprolactone,[130, 131] and the reduction of brittleness and improving tensile strength of poly(hydroxybutyrate) *via* block copolymerisation.[132]

1.6.2 Usage in Biomedical Applications

Tissue engineering aims to develop biological substitutes for living tissue and facilitate the restoration, maintenance and improvement of tissue function.[133] One approach to this sees the use of biomaterials as scaffold or matrix to introduce new cells into the body. The material used can be multi-purpose in that it can provide mechanical strength to the new tissue whilst acting as a barrier against large anti-bodies and letting through vital nutrients that encourage the new tissue to establish.[134] Polylactide is an attractive candidate for tissue engineering applications due to biocompatibility and minimal immunological response when introduced to a host. The biodegradation of PLA provides the opportunity for reduced post-operation treatment as implants breakdown over time and do not require removal. For biomedical applications lactide is often copolymerised with glycolide to give the copolymer poly(lactide-*co*-glycolide). Initial breakdown occurs *via* hydrolysis to give lactic and glycolic acid, which can both be metabolised in the body.[130] Controlled copolymerisation of lactide and glycolide can provide copolymers with a varying rates of degradation.[135] Lactide can also be copolymerised with other cyclic esters, such as ε-caprolactone, and biodegradable poly(ethylene glycol)s to provide other routes to tuning the properties of the material essential for biomedical applications.[56, 68, 69, 136]

1.6.3 Copolymers of lactide and other lactones

The copolymerisation of lactide with cyclic esters such as ε-caprolactone and δ-valerolactone provides an effective way of combining the properties of the two separate homopolymers (Figure 1.56). Polycaprolactone (PCL) has higher drug permeability than that of PLA, as well as elasticity and thermal properties that can be adopted by the resulting copolymer with lactide.[69] The macrostructure of the copolymer produced is also important, with the polymeric material behaving differently depending on whether the copolymers are random or block-like in nature. A random copolymer would provide continuity in behaviour whilst adopting a block structure would provide the polymer with properties more akin to the separate homopolymers. For example, early work presented that a block copolymer of polylactide and polycaprolactone can yield a material with the permability of PCL and the faster degradation of PLA.[137]

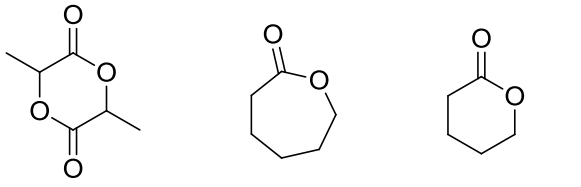

Figure 1.56 lactide, ε-caprolactone and δ-valerolactone

As with the homopolymerisation of lactide, a wide range of metal-based complexes have been used as copolymerisation initiators. Often those reported as active for lactide also have potential for the ROP of other lactones and subsequent copolymerisation. Early work by Jerome *et al.* displayed that $Al(O^iPr)_3$ could be used for the copolymerisation of both *rac*-lactide and L-lactide with ε-caprolactone.[56] Analysis of the resulting copolymer was carried out by $^{13}C\{^1H\}$ NMR spectroscopy and showed tapering of the copolymer macrostructure. Reactivity ratios (see section 1.8 for details) were calculated and clearly showed a bias towards the ROP of LA over CL; to the extent that insertion of lactide was still preferential even proceeding insertion of caprolactone.[56] Kasperczyk *et al.* carried out copolymerisaiton of lactide and ε-caprolatone using $Al(acac)_3$, $AlEt_3$ and $Zn(Et)_3$ as initiators.[138] As with work by Jerome, copolymer microstructure was analysed using $^{13}C\{^1H\}$ NMR spectroscopy with full assignment of the carbonyl signals to monomer triads in the microstructure for the copolymerisaiton of both *rac*-lactide and L-lactide with ε-caprolactone. This technique also allowed for identification of transesterificaiton due to the presence of a single lactyl ester between two caproyl units.[138]

Nakayama *et. al.* used a tin based initiator to carry out a number of copolymerisation of L-lacide and δ-valerolactone (VL) with variation of the monomer ratio.[139] Monomer incorporation was found to be more comparable and thus the polymers produced had compositions that corresponded to the monomer feeds. A range of melting points (T_m) were observed with the highest for copolymers predominantly of PLLA. No T_m was observed for copolymers of approximately 50:50 composition; which suggested an amorphous structure due to random copolymerisation. ^1H NMR spectroscopy allowed identification of homo and hetero diads for PVL and equivalent triads for the methine of the lactidyl units. Equal appearance of these in the spectra confirmed random polymerisation of L-lactide and δ-valerolactone.[139]

Achieving true block copolymers of L-lactide and ε-caprolactone can be achieved by sequential ROP of the monomers. A zirconium bis(phenolate) was used to initiate the homopolymerisation of ε-caprolactone before the addition of the L-lactide monomer.[83] The PCL chain acted as a macroinitiator and resulted in a PCL/PLA block copolymer. Thermal analysis of the polymeric

material showed two discreet melting points (46 °C and 146°C) that were assigned to blocks of PCL and PLA respectively; depressed slightly due to their copolymer nature. It should be noted that a PCL-PLA-PCL triblock was not obtainable due to the inactivity of the Zr-PLA-PCL-OR as a macroinitiator for the further ROP of ε-caprolactone.[83]

Jerome *et al.* took the approach of carrying out the one-pot copolymerisation of L-lactide and ε-caprolactone in super-critical CO_2 as a route to altering the copolymer microstructure.[140] In toluene, analysis of copolymer produced using a dibutyltin dimethoxide initiator found reactivity ratios of $r_1 = 0.7$ and $r_2 = 0.15$, indicative of an preference for alternate monomer insertion. In super-critical CO_2 copolymers with a tapered block structure were identified, according to experimentally acquired reactivity ratios of $r_1 = 0.7$ and $r_2 = 0.15$.[140]

Another approach to controlling the resulting macrostructure of a copolymer is through initiator design. Recently, Nomura *et. al.* have successfully polymerised truly random copolymers of L-lactide and ε-caprolactone by addressing the differences in the activity of CL and LLA[68] Reativity ratios for lactide and ε-caprolactone are often considerably different ($r_{CL} < 1 \ll r_{LA}$) leading to the preferential insertion of lactide into the copolymer chain. Despite the steric hindrance of the methyl groups on the lactide ring, its higher activity is deemed to be due to higher coordination ability.[68] For a truly random copolymerisation reactivity ratios need to comparable with $r_{CL} = r_{LA} = 1$ (Figure 1.57).

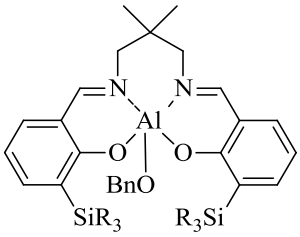

1; $R_3Si = tBuMe_2Si$
2; $R_3Si = iPr_3Si$

Complex	r_{CL}	r_{LA}	L_{CL}	L_{LA}	Notes
(Ideal random)	1	1	2	2	
1	-	-	1.5	2.9	low CL conversion
2	1.0	0.73	1.7	1.9	

Figure 1.57 Homo-salen aluminium complexes as initiators for tapered-block copolymers (**1**) or randomly sequenced copolymers (**2**) of lactide and caprolactone[68]

The bulky groups on a homosalen ligand coordinated to an aluminium metal centre were finely tuned to lower the activity of lactide whilst having a lesser effect on the caprolactone. It was found that the when R= ^{t}BuMe$_2$Si (**1**) a tapered block copolymer was formed. However, the presence of bulkier ^{i}Pr$_3$Si groups (**2**) on the ligand gave a practically random copolymer due to increased disturbance of coordination of the lactide monomer to the metal centre caused by the larger substituents; this reduced the preference to insert lactide units into the polymer chain.[68]

Meanwhile, Duda *et al.* have presented that utilising the chirality of an aluminium alkoxide initiator with a BINAP Schiff base ligand can reverse the net activities of L-lactide and ε-caprolactone in a one-pot copolymerisation.[141]

1.7 Polymerisation Kinetics

Polymerisation activity of potential initiators can be best assessed by determining the rate constant of polymerisation (k_p). The ring-opening polymerisation of lactide obeys the overall rate law:

$$\frac{-d[LA]}{dt} = k_p[I]^x[LA]$$

The rate of polymerisation is typically first order with respect to the initiator concentration and first order with respect to monomer concentration. Potential impurities can destroy or cause aggregation of the initiator, thus affecting its true activity.[26] For living polymerisations, such as the ROP of lactide, rate of initiation is significantly faster than the rate of propagation. Under this presumption, concentration of initiator can be deemed independent of the rate of polymerisation and a pseudo-first order rate law used:

$$\frac{-d[LA]}{dt} = k_{app}[LA]$$

Integration of the above rate law and rearrangement leads to the following:

$$\ln[A]_t = -k_{app}t + ln[A]_0$$

$$ln\left(\frac{[A]_0}{[A]_t}\right) = k_{app}t$$

Thus, a semi-logarithmic plot can be drawn with the gradient equal to k_{app}. To find k_p numerous experiments should be carried out at different initiator concentrations allowing the following relationship to be plotted:

$$k_{app} = k_p[I]_0^x$$

Whilst k_{app} can provide a useful indication of activity when compared to other initiators carried out under the same reaction conditions and initiator concentration, it is important to acknowledge that k_{app} can provide a distorted value due to unknown behaviour of the active species in solution.[120] To further understand the dependence between the initiator and rate of propagation, $[I]_0$ can be varied and then a ln-ln relationship plotted as follows:

$$\ln(k_{app}) = \ln(k_p[I]_0^x)$$

$$\ln(k_{app}) = \ln(k_p) + x\ln[I]_0$$

In the above, a plot of $\ln(k_{app})$ versus $\ln([I]_0)$ provides a straight line relationship where the gradient is equal to the order with respect to initiator. The intercept with the *y*-axis provides $\ln(k_p)$.

1.8 Copolymerisation reactivity ratios

1.8.1 Definitions and Derivation

When considering the copolymerisation of two monomers in a one-pot synthesis the relative rates of polymerisation can dictate the copolymer microstructure achieved. The rates of polymerisation cannot be modelled independently due to the presence of multiple propagation steps during the polymerisation. Mayo and Lewis generated a copolymerisation equation that was initially applied to the copolymerisation of styrene and methyl methacrylate.[142] The polymerisation takes place via a chain-end radical polymerisation with a steady state assumption with respect to the concentration of active species. Such a model is also appropriate for the ROP of lactide, which also exhibits a steady state condition with respect to initiator concentration. The Mayo-Lewis equation has been successfully applied to the copolymerisation of lactide and ε-caprolactone.[68]

In order to generate the copolymerisation equation it is necessary to consider all possible propagation reactions of the copolymerisations. For the copolymerisation of monomer A and B there are four potential reactions each with its own rate constant (k_{XX}):

$$A* + A \rightarrow AA* \; k_{AA}$$

$$A* + B \rightarrow AB* \; k_{AB}$$

$$B* + A \rightarrow BA* \; k_{BA}$$

$$B* + B \rightarrow BB* \; k_{BB}$$

In the case of ROP, A* indicates that monomer A was the last inserted into the polymer chain and is currently adjacent to the active metal centre. With each propagation step having a separate rate law the overall rate of polymerisation of each monomer is a combination of two of the propagation rate laws:

$$-\frac{d[A]}{dt} = k_{AA}[A]\sum[A*] + k_{BA}[A]\sum[B*]$$

$$-\frac{d[B]}{dt} = k_{BB}[B]\sum[B*] + k_{AB}[B]\sum[A*]$$

Under the steady state presumption, rate of change of $\sum[A*]$and $\sum[B*]$ is equal to zero and thus $k_{BA}[A]\sum[B*] = k_{AB}[B]\sum[A*]$. The two equations can be combined through division and rearranged to give the Mayo-Lewis or Copolymerisation Equation:[142]

$$\frac{d[A]}{d[B]} = \frac{[A](r_1[A] + [B])}{[B]([A] + r_2[B])}$$

Where $r_1 = \frac{k_{AA}}{k_{AB}}$ and $r_2 = \frac{k_{BB}}{k_{BA}}$ and can be referred to as the reactivity ratios for the copolymerisation of monomer A and B respectively. For ROP these reactivity ratios indicate the likelihood of insertion of A into an M-A* bond (M = metal centre) over the insertion of B into an M-A* bond, or vice-versa for the second reactivity ratio. Comparison of the reactivity ratios (r_1 and r_2) can provide insight into the expected macrostructure of the resulting copolymer.

$r_1 = r_2 \gg 1$ - would result in a mixture of two homopolymers and very little copolymerisation. Both reactivity ratios having a high value indicates overwhelming preference for homo-monomer insertion into the active site (ie. A into M-A*, B into M-B*).

$r_1 = r_2 > 1$ - with both monomers showing a preference for homopolymerisation on the rare insertion of A into B or vice versa leads that newly inserted monomer takes preference leading to a block-copolymer.

$r_1 = r_2 \approx 1$ – an equal probability of either monomer inserting into any active centre would provide conditions to generate a truly random copolymer.

$r_1 = r_2 \approx 0$ – with both reactivity ratios equal to zero it suggests that insertion of monomer A has to be followed by insertion of monomer B.

$r_1 \gg 1 \gg r_2$ – when the ratios lie either side of 1, a tapered block-copolymer is most likely to be produced. Macrostructure would be affected by the initial concentrations of each monomer and the rate of incorporation would change with the monomer ratio over time. For example, for the copolymerisation of A and B the copolymer produced would initially have a high weighting of A and very little B; the amount of B incorporated into the copolymer would increase over time as the relative concentration of B increases due to the preferential insertion of A. The copolymer would end with a block of essentially pure B.

1.8.2 Experimentally measured reactivity ratios

Reactivity ratios for copolymerisation systems can be found experimentally.[67-69, 143-145] Utilisation in the first instance by Mayo and Lewis used multiple linear plot with an expression of one reactivity ratio as a function of the other.[142] This required the rearrangement of the copolymerisation equation into the following form:

$$r_2 = \frac{f_A(1 + r_1 f_A)}{F_A} - f_A$$

Where f_A = the monomer ratio of monomer A in the initial feed, with F_1 equal to the corresponding copolymer composition after low conversion (< 15 %). A initial ‘guess’ for a value of r_1 is required and then an intersection method is used which will roughly define the actual values of r_1 and r_2.

Other methods that include the linearization of the copolymerisation equation include the Fineman-Ross plot and Kelen- Tűdōs plot.[146, 147] Fineman and Ross used a more conventional plot in which funtions of monomer ratio and copolymer composition were plotted against each other for various different initial monomer compositions. The resulting linear plot provided a

gradient equal to r_1 and an intercept of $-r_2$.[146] Kelen and Tűdōs acknowledged the limitations and inhenrent errors of linearization of the copolymerisaiton equation and thus used complex substitutions to better distribute the experimental data.[147]

A widely accepted approach is through a non-linear least square (NLLS) analysis of multiple copolymerisations at varying monomer ratios to find optimum values for r_1 and r_2 that satisfy a solution to the copolymerisation equation. The form of the copolymerisation equation used is as follows:[145]

$$F_A = \frac{r_1 f_A^2 + f_A f_B}{r_1 f_A^2 + 2 f_A f_B + r_2 f_B^2}$$

Where F_A equals the mole fraction of A in the copolymer and f_A and f_B equal the mole fractions of monomer in the feed for the A and B respectively.

f_A and f_B can be varied and the copolymerisation halted at low conversion (< 15%) to minimise all mass transfer effects and allow a steady state presumption. In the case of ROP of lactide and other lactones, the copolymer composition (F_A) can be quantified via ^{1}H or ^{13}C{^{1}H} NMR spectroscopy. The data can then be weighted and values found for r_1 and r_2 that provide the smallest sum total of the squared differences between theoretical and experimentally acquired values of F_A. The NLLS approach is outlined in the equation below:

$$\sum \left(w \times \left(F_A - \frac{r_1 f_A^2 + f_A f_B}{r_1 f_A^2 + 2 f_A f_B + r_2 f_B^2} \right)^2 \right)$$

Where w = relative weighting scheme, = $\frac{1}{F_A^2}$; F_A = experimentally acquired copolymer composition; f_A = composition of A in the monomer feed; and f_B = composition of B in the monomer feed.[68, 145]

1.9 Reflection and research aims

The controlled polymerisation of lactide had received considerable attention in the last 10-15 years due to attractive properties that can be attributed to stereoregular polymeric material, enhancing the potential application of this renewable and biodegradable material in the both high value biomedical applications and numerous commodity products and packaging. With a focus on initiator stereoselectivity, enhancement towards isotactic and heterotactic enchainment

has been achieved with, often minor, changes in the following aspects of ancillary ligand structure appearing to influence overall catalytic stereoselectivity: steric bulk, chirality, nature of heteroatom donor, ligand/backbone flexibility. In general, due to the preferential Lewis acidity required for ROP of lactide to take place *via* a coordinative mechanism, anionic ligand systems consisting of *N*- and *O*-type donor atoms providing metals centres in their high oxidation state are used. Substituted phenols have provided extensive variation in steric bulk of ligands with backbones and linking groups being widely used to influence coordination geometry. Due to limitations of polylactide, particularly with respect to biomedically relevant properties such as hydrophilicity and degradation rate, research has also focused on the copolymerisation of lactide with other polymers; both through macroinitiation to yield block copolymers, but also one-pot polymerisation with other lactones to yield copolymers with varying microstructure that is dependent on both monomer reactivity and initiator selectivity. As with stereoselectivity, it is difficult to predict copolymer structure with desirable stereoselectivities and copolymer microstructure often being obtained serendipitously. With this unpredictability in mind, the aims of the research reported in this thesis can be described in two major parts:

i. Following the unprecedentedly high stereoselectivity of a C_3-symmetrical zirconium alkoxide amine tris(phenolate) complex towards heterotactic PLA, research was also published to discern the importance of the chiral axial flipping in driving such high selectivity.[91, 92] To hopefully further understand the influence of sterics and chirality on both activity and stereoselectivity, a series of unsymmetrical amine tris(phenolate) ligands will be targeted and coordinated to Zr(IV) and Hf(IV) and trialled for the ROP of lactide. To date, disruption to these tripodal amine tris(phenolate) ligands has only be achieved through the alteration/removal of a methylene bridge or complete replacement of a phenolate arm with an alkoxide donor.[89, 94, 98]
ii. The series of group IV unsymmetrical amine tris(phenolate) complexes, coupled with the previous reported C_3-symmetric analogue, will hopefully also provide insight into the limitation of highly active and stereoselective initiators for the production of random copolymers of lactide and ε-caprolactone. Traditionally the incorporation of lactide is preferential to ε-caprolactone but small changes to ligand steric bulk has seen significant change to copolymer microstructure.[68] Copolymer microstructure, produced using sterically different group IV amine trisphenolate complexes, will be analysed through a variety of techniques to determine block length and reactivity ratios; for which it is hoped that relationships to initiator activity and selectivity can be drawn.

1.10 References

1. R. E. Drumright, P. R. Gruber and D. E. Henton, *Adv. Mater. (Weinheim, Ger.)*, 2000, **12**, 1841-1846.
2. P. Hormnirun, E. L. Marshall, V. C. Gibson, A. J. P. White and D. J. Williams, *J. Am. Chem. Soc.*, 2004, **126**, 2688-2689.
3. A.-C. Albertsson and I. K. Varma, *Biomacromolecules*, 2003, **4**, 1466-1486.
4. C. K. Williams, *Chem. Soc. Rev.*, 2007, **36**, 1573-1580.
5. D. Garlotta, *J. Polym. Environ.*, 2001, **9**, 63-84.
6. R. M. West, M. S. Holm, S. Saravanamurugan, J. M. Xiong, Z. Beversdorf, E. Taarning and C. H. Christensen, *J. Catal.*, 2010, **269**, 122-130.
7. R. Datta and M. Henry, *J. Chem. Technol. Biotechnol.*, 2006, **81**, 1119-1129.
8. M. S. Holm, S. Saravanamurugan and E. Taarning, *Science*, 2010, **328**, 602-605.
9. F. de Clippel, M. Dusselier, R. Van Rompaey, P. Vanelderen, J. Dijkmans, E. Makshina, L. Giebeler, S. Oswald, G. V. Baron, J. F. M. Denayer, P. P. Pescarmona, P. A. Jacobs and B. F. Sels, *J. Am. Chem. Soc.*, 2012, **134**, 10089-10101.
10. P. Van Wouwe, M. Dusselier, A. Basic and B. F. Sels, *Green Chemistry*, 2013, **15**, 2817-2824.
11. E. T. H. Vink, K. R. Rabago, D. A. Glassner, B. Springs, R. P. O'Connor, J. Kolstad and P. R. Gruber, *Macromol. Biosci.*, 2004, **4**, 551-564.
12. K. Hirao, Y. Nakatsuchi and H. Ohara, *Polym. Degrad. Stab.*, 2010, **95**, 925-928.
13. F. Nederberg, E. F. Connor, T. Glausser and J. L. Hedrick, *Chem. Commun.*, 2001, 2066-2067.
14. E. L. Whitelaw, M. G. Davidson and M. D. Jones, *Chem. Commun.*, 2011.
15. K. Odelius, A. Hoglund, S. Kumar, M. Hakkarainen, A. K. Ghosh, N. Bhatnagar and A. C. Albertsson, *Biomacromolecules*, 2011, **12**, 1250-1258.
16. O. Dechy-Cabaret, B. Martin-Vaca and D. Bourissou, *Chem. Rev.*, 2004, **104**, 6147-6176.
17. B. J. O'Keefe, M. A. Hillmyer and W. B. Tolman, *Dalton Trans.*, 2001, 2215-2224.
18. G. W. Nyce, S. Csihony, R. M. Waymouth and J. L. Hedrick, *Chemistry – A European Journal*, 2004, **10**, 4073-4079.
19. T. R. Jensen, L. E. Breyfogle, M. A. Hillmyer and W. B. Tolman, *Chem. Commun.*, 2004, 2504-2505.
20. A. P. Dove, H. Li, R. C. Pratt, B. G. G. Lohmeijer, D. A. Culkin, R. M. Waymouth and J. L. Hedrick, *Chem. Commun.*, 2006, 2881-2883.
21. O. Coulembier, B. G. G. Lohmeijer, A. P. Dove, R. C. Pratt, L. Mespouille, D. A. Culkin, S. J. Benight, P. Dubois, R. M. Waymouth and J. L. Hedrick, *Macromolecules*, 2006, **39**, 5617-5628.
22. L. Zhang, F. Nederberg, J. M. Messman, R. C. Pratt, J. L. Hedrick and C. G. Wade, *J. Am. Chem. Soc.*, 2007, **129**, 12610-12611.
23. S. Koeller, J. Kadota, F. Peruch, A. Deffieux, N. Pinaud, I. Pianet, S. Massip, J.-M. Léger, J.-P. Desvergne and B. Bibal, *Chemistry – A European Journal*, 2010, **16**, 4196-4205.

24. J. M. Becker, S. Tempelaar, M. J. Stanford, R. J. Pounder, J. A. Covington and A. P. Dove, *Chem. Eur. J.*, 2010, **16**, 6099-6105.

25. E. Brule, V. Guerineau, P. Vermaut, F. Prima, J. Balogh, L. Maron, A. M. Z. Slawin, S. P. Nolan and C. M. Thomas, *Polymer Chemistry*, 2013, **4**, 2414-2423.

26. R. H. Platel, L. M. Hodgson and C. K. Williams, *Polymer Reviews*, 2008, **48**, 11 - 63.

27. T. M. Ovitt and G. W. Coates, *J. Am. Chem. Soc.*, 2002, **124**, 1316-1327.

28. Y. Ikada, K. Jamshidi, H. Tsuji and S. H. Hyon, *Macromolecules*, 1987, **20**, 904-906.

29. J. R. Sarasua, N. L. Rodriguez, A. L. Arraiza and E. Meaurio, *Macromolecules*, 2005, **38**, 8362-8371.

30. H. Tsuji, *Macromol. Biosci.*, 2005, **5**, 569-597.

31. N. Yui, P. J. Dijkstra and J. Feijen, *Makromolekulare Chemie-Macromolecular Chemistry and Physics*, 1990, **191**, 481-488.

32. C. P. Radano, G. L. Baker and M. R. Smith, *J. Am. Chem. Soc.*, 2000, **122**, 1552-1553.

33. J. Wahlberg, P. V. Persson, T. Olsson, E. Hedenström and T. Iversen, *Biomacromolecules*, 2003, **4**, 1068-1071.

34. A. Richez, J. Belleney, L. Bouteiller and S. Pensec, *Journal of Polymer Science Part A: Polymer Chemistry*, 2006, **44**, 6782-6789.

35. B. Miksa, M. Sochacki, J. Libiszowski, A. Duda, W. Ciesielski and M. J. Potrzebowski, *Analytical Methods*, 2012, **4**, 377-383.

36. H. R. Kricheldorf, C. Boettcher and K.-U. Tönnes, *Polymer*, 1992, **33**, 2817-2824.

37. B. M. Chamberlain, M. Cheng, D. R. Moore, T. M. Ovitt, E. B. Lobkovsky and G. W. Coates, *J. Am. Chem. Soc.*, 2001, **123**, 3229-3238.

38. K. A. M. Thakur, R. T. Kean, E. S. Hall, J. J. Kolstad, T. A. Lindgren, M. A. Doscotch, J. I. Siepmann and E. J. Munson, *Macromolecules*, 1997, **30**, 2422-2428.

39. M. H. Chisholm, S. S. Iyer and M. E. Matison, *Chem. Commun.*, 1997, 1999-2000.

40. K. A. M. Thakur, R. T. Kean, M. T. Zell, B. E. Padden and E. J. Munson, *Chem. Commun.*, 1998, 1913-1914.

41. J. E. Kasperczyk, *Polymer*, 1999, **40**, 5455-5458.

42. M. W. F. Nielen, *Mass Spectrom. Rev.*, 1999, **18**, 309-344.

43. M. Mann, R. C. Hendrickson and A. Pandey, *Annu. Rev. Biochem.*, 2001, **70**, 437-473.

44. T. Hatakeyama and H. Hatakeyama, *Thermal Properties of Green Polymers and Biocomposites*, Kluwer Academic, 2004.

45. J. F. Carpentier, V. Poirier, T. Roisnel and Y. Sarazin, *Dalton Trans.*, 2011, **40**, 523-534.

46. A. Kowalski, A. Duda and S. Penczek, *Macromolecules*, 1998, **31**, 2114-2122.

47. A. J. Nijenhuis, D. W. Grijpma and A. J. Pennings, *Macromolecules*, 1992, **25**, 6419-6424.

48. A. Duda, A. Kowalski, J. Libiszowski, T. Biela, M. Cypryk and S. Penczek, *Macromolecules*, 2005, **38**, 8170-8176.

49. M. D. Jones, M. G. Davidson, C. G. Keir, L. M. Hughes, M. F. Mahon and D. C. Apperley, *Eur. J. Inorg. Chem.*, 2009, **2009**, 635-642.

50. A. P. Dove, V. C. Gibson, E. L. Marshall, A. J. P. White and D. J. Williams, *Chem. Commun.*, 2001, 283-284.

51. A. P. Dove, V. C. Gibson, E. L. Marshall, H. S. Rzepa, A. J. P. White and D. J. Williams, *J. Am. Chem. Soc.*, 2006, **128**, 9834-9843.

52. N. Nimitsiriwat, V. C. Gibson, E. L. Marshall, A. J. P. White, S. H. Dale and M. R. J. Elsegood, *Dalton Trans.*, 2007, 4464-4471.

53. N. Nimitsiriwat, E. L. Marshall, V. C. Gibson, M. R. J. Elsegood and S. H. Dale, *J. Am. Chem. Soc.*, 2004, **126**, 13598-13599.

54. M. H. Chisholm and E. E. Delbridge, *New J. Chem.*, 2003, **27**, 1177-1183.

55. L. Trofimoff, T. Aida and S. Inoue, *Chem. Lett.*, 1987, 991-994.

56. P. Vanhoorne, P. Dubois, R. Jerome and P. Teyssie, *Macromolecules*, 1992, **25**, 37-44.

57. N. Spassky, M. Wisniewski, C. Pluta and A. Le Borgne, *Macromol. Chem. Phys.*, 1996, **197**, 2627-2637.

58. N. Nomura, R. Ishii, M. Akakura and K. Aoi, *J. Am. Chem. Soc.*, 2002, **124**, 5938-5939.

59. Z. Zhong, P. J. Dijkstra and J. Feijen, *J. Am. Chem. Soc.*, 2003, **125**, 11291-11298.

60. Z. Zhong, P. J. Dijkstra and J. Feijen, *Angewandte Chemie International Edition*, 2002, **41**, 4510-4513.

61. H. Du, A. H. Velders, P. J. Dijkstra, J. Sun, Z. Zhong, X. Chen and J. Feijen, *Chem.--Eur. J.*, 2009, **15**, 9836-9845.

62. M. H. Chisholm, J. C. Gallucci, K. T. Quisenberry and Z. P. Zhou, *Inorg. Chem.*, 2008, **47**, 2613-2624.

63. Z. H. Tang and V. C. Gibson, *Eur. Polym. J.*, 2007, **43**, 150-155.

64. E. L. Whitelaw, G. Loraine, M. F. Mahon and M. D. Jones, *Dalton Trans.*, 2011, **40**, 11469-11473.

65. S. L. Hancock, M. D. Jones, C. J. Langridge and M. F. Mahon, *New J. Chem.*, 2012, **36**, 1891-1896.

66. S. L. Hancock, M. F. Mahon and M. D. Jones, *New J. Chem.*, 2013, **37**, 1996-2001.

67. D. J. Darensbourg, O. Karroonnirun and S. J. Wilson, *Inorg. Chem.*, 2011, **50**, 6775-6787.

68. N. Nomura, A. Akita, R. Ishii and M. Mizuno, *Journal of the American Chemical Society*, 2010, **132**, 1750-1751.

69. D. Pappalardo, L. Annunziata and C. Pellecchia, *Macromolecules*, 2009, **42**, 6056-6062.

70. C. Bakewell, R. H. Platel, S. K. Cary, S. M. Hubbard, J. M. Roaf, A. C. Levine, A. J. P. White, N. J. Long, M. Haaf and C. K. Williams, *Organometallics*, 2012, **31**, 4729-4736.

71. S. Tabthong, T. Nanok, P. Kongsaeree, S. Prabpai and P. Hormnirun, *Dalton Trans.*, 2014, **43**, 1348-1359.

72. A. F. Douglas, B. O. Patrick and P. Mehrkhodavandi, *Angewandte Chemie International Edition*, 2008, **47**, 2290-2293.

73. I. Yu, A. Acosta-Ramírez and P. Mehrkhodavandi, *J. Am. Chem. Soc.*, 2012, **134**, 12758-12773.

74. H. R. Kricheldorf, J. M. Jonte and M. Berl, *Makromol. Chem., Suppl.*, 1985, **12**, 25-38.

75. J. Baran, A. Duda, A. Kowalski, R. Szymanski and S. Penczek, *Macromol. Symp.*, 1997, **123**, 93-101.

76. C. K. Williams and M. A. Hillmyer, *Polymer Reviews*, 2008, **48**, 1 - 10.

77. A. Sauer, A. Kapelski, C. Fliedel, S. Dagorne, M. Kol and J. Okuda, *Dalton Trans.*, 2013, **42**, 9007-9023.

78. V. C. Gibson, C. K. A. Gregson, I. J. Blackmore, N. J. Long, E. L. Marshall and A. J. P. White, *Dalton Trans.*, 2006, 3134-3140.

79. E. Sergeeva, J. Kopilov, I. Goldberg and M. Kol, *Inorg. Chem.*, 2009, **48**, 8075-8077.

80. A. L. Zelikoff, J. Kopilov, I. Goldberg, G. W. Coates and M. Kol, *Chem. Commun.*, 2009, 6804-6806.

81. T. K. Saha, V. Ramkumar and D. Chakraborty, *Inorg. Chem.*, 2011, **50**, 2720-2722.

82. T. Aida, D. Takeuchi and T. Nakamura, *Macromolecules*, 2000, **33**, 725-729.

83. A. J. Chmura, M. G. Davidson, M. D. Jones, M. D. Lunn, M. F. Mahon, A. F. Johnson, P. Khunkamchoo, S. L. Roberts and S. S. F. Wong, *Macromolecules*, 2006, **39**, 7250-7257.

84. A. J. Chmura, M. G. Davidson, M. D. Jones, M. D. Lunn and M. F. Mahon, *Dalton Trans.*, 2006, 887-889.

85. Y. Kim and J. G. Verkade, *Macromol. Rapid Commun.*, 2002, **23**, 917-921.

86. Y. Kim and J. Verkade, *Phosphorus Sulfur and Silicon and the Related Elements*, 2004, **179**, 729-732.

87. Y. Kim and J. G. Verkade, *Organometallics*, 2002, **21**, 2395-2399.

88. Y. Kim, P. N. Kapoor and J. G. Verkade, *Inorg. Chem.*, 2002, **41**, 4834-4838.

89. Y. Kim, G. K. Jnaneshwara and J. G. Verkade, *Inorg. Chem.*, 2003, **42**, 1437-1447.

90. M. Kol, M. Shamis, I. Goldberg, Z. Goldschmidt, S. Alfi and E. Hayut-Salant, *Inorg. Chem. Commun.*, 2001, **4**, 177-179.

91. A. J. Chmura, M. G. Davidson, C. J. Frankis, M. D. Jones and M. D. Lunn, *Chem. Commun.*, 2008, 1293-1295.

92. A. J. Chmura, C. J. Chuck, M. G. Davidson, M. D. Jones, M. D. Lunn, S. D. Bull and M. F. Mahon, *Angew. Chem., Int. Ed.*, 2007, **46**, 2280-2283.

93. M. J. Stanford and A. P. Dove, *Chem. Soc. Rev.*, 2010, **39**, 486-494.

94. P. Axe, S. D. Bull, M. G. Davidson, C. J. Gilfillan, M. D. Jones, D. E. J. E. Robinson, L. E. Turner and W. L. Mitchell, *Org. Lett.*, 2007, **9**, 223-226.

95. A. J. Chmura, University of Bath, 2008.

96. A. J. Chmura, D. M. Cousins, M. G. Davidson, M. D. Jones, M. D. Lunn and M. F. Mahon, *Dalton Trans.*, 2008, 1437-1443.

97. C. J. Frankis, University of Bath, 2010.

98. E. L. Whitelaw, M. D. Jones, M. F. Mahon and G. Kociok-Kohn, *Dalton Trans.*, 2009, 9020-9025.

99. M. D. Jones, E. L. Whitelaw and M. F. Mahon, *Inorg. Chem.*, 2010, **49**, 7176-7181.

100. J. Okuda and J. C. Buffet, *Chem. Commun.*, 2011, **47**, 4796-4798.

101. A. Stopper, J. Okuda and M. Kol, *Macromolecules*, 2012, **45**, 698-704.

102. F. Marchetti, G. Pampaloni, C. Pinzino, F. Renili, T. Repo and S. Vuorinen, *Dalton Trans.*, 2013, **42**, 2792-2802.

103. J. E. Kasperczyk, *Macromolecules*, 1995, **28**, 3937-3939.

104. M. Bero, P. Dobrzynski and J. Kasperczyk, *J. Polym. Sci., Part A: Polym. Chem.*, 1999, **37**, 4038-4042.

105. S.-C. Rosca, D.-A. Rosca, V. Dorcet, C. M. Kozak, F. M. Kerton, J.-F. Carpentier and Y. Sarazin, *Dalton Trans.*, 2013, **42**, 9361-9375.

106. M. Cheng, A. B. Attygalle, E. B. Lobkovsky and G. W. Coates, *J. Am. Chem. Soc.*, 1999, **121**, 11583-11584.

107. C. N. Ayala, M. H. Chisholm, J. C. Gallucci and C. Krempner, *Dalton Trans.*, 2009, 9237-9245.

108. M. H. Chisholm, J. C. Gallucci and K. Phomphrai, *Inorg. Chem.*, 2005, **44**, 8004-8010.

109. M. H. Chisholm, J. Gallucci and K. Phomphrai, *Inorg. Chem.*, 2002, **41**, 2785-2794.

110. C. K. Williams, L. E. Breyfogle, S. K. Choi, W. Nam, V. G. Young, M. A. Hillmyer and W. B. Tolman, *J. Am. Chem. Soc.*, 2003, **125**, 11350-11359.

111. A. P. Dove, V. C. Gibson, E. L. Marshall, A. J. P. White and D. J. Williams, *Dalton Trans.*, 2004, 570-578.

112. L. M. Edward, C. G. Vernon and S. R. Henry, *J. Am. Chem. Soc.*, 2005, **127**, 6048-6051.

113. J. Börner, S. Herres-Pawlis, U. Flörke and K. Huber, *Eur. J. Inorg. Chem.*, 2007, **2007**, 5645-5651.

114. J. Börner, U. Flörke, K. Huber, A. Döring, D. Kuckling and S. Herres-Pawlis, *Chemistry – A European Journal*, 2009, **15**, 2362-2376.

115. P. K. Eckert, I. d. S. Vieira, V. H. Gessner, J. Börner, C. Strohmann and S. Herres-Pawlis, *Polyhedron*, 2013, **49**, 151-157.

116. Y. Huang, W. Wang, C.-C. Lin, M. P. Blake, L. Clark, A. D. Schwarz and P. Mountford, *Dalton Trans.*, 2013, **42**, 9313-9324.

117. K. Ding, M. O. Miranda, B. Moscato-Goodpaster, N. Ajellal, L. E. Breyfogle, E. D. Hermes, C. P. Schaller, S. E. Roe, C. J. Cramer, M. A. Hillmyer and W. B. Tolman, *Macromolecules*, 2012, **45**, 5387-5396.

118. L. Clark, G. B. Deacon, C. M. Forsyth, P. C. Junk, P. Mountford, J. P. Townley and J. Wang, *Dalton Trans.*, 2013, **42**, 9294-9312.

119. Y. Sarazin, B. Liu, T. Roisnel, L. Maron and J. F. Carpentier, *J. Am. Chem. Soc.*, 2011, **133**, 9069-9087.

120. K. B. Aubrecht, K. Chang, M. A. Hillmyer and W. B. Tolman, *J. Polym. Sci., Part A: Polym. Chem.*, 2001, **39**, 284-293.

121. H. Ma, T. P. Spaniol and J. Okuda, *Angew. Chem., Int. Ed.*, 2006, **45**, 7818-7821.

122. L. M. Hodgson, R. H. Platel, A. J. P. White and C. K. Williams, *Macromolecules*, 2008, **41**, 8603-8607.

123. E. Grunova, E. Kirillov, T. Roisnel and J.-F. Carpentier, *Dalton Trans.*, 2010, **39**, 6739-6752.

124. L. Clark, M. G. Cushion, H. E. Dyer, A. D. Schwarz, R. Duchateau and P. Mountford, *Chem. Commun.*, 2010, **46**, 273-275.

125. H. E. Dyer, S. Huijser, N. Susperregui, F. Bonnet, A. D. Schwarz, R. Duchateau, L. Maron and P. Mountford, *Organometallics*, 2010, **29**, 3602-3621.

126. C. Bakewell, T.-P.-A. Cao, N. Long, X. F. Le Goff, A. Auffrant and C. K. Williams, *J. Am. Chem. Soc.*, 2012, **134**, 20577-20580.

127. M. A. Sinenkov, G. K. Fukin, A. V. Cherkasov, N. Ajellal, T. Roisnel, F. M. Kerton, J.-F. Carpentier and A. A. Trifonov, *New J. Chem.*, 2011, **35**, 204-212.

128. C. Bakewell, T. P. A. Cao, N. Long, X. F. Le Goff, A. Auffrant and C. K. Williams, *J. Am. Chem. Soc.*, 2012, **134**, 20577-20580.

129. R. J. Pounder and A. P. Dove, *Polymer Chemistry*, 2010, **1**, 260-271.

130. Shalaby, *Biomedical polymers designed-to-degrade systems*, Hanser, Munich, 1994.

131. E. Chiellini and R. Solaro, *Adv Mater*, 1996, **8**, 305-313.

132. N. Othman, C. L. Xu, P. Mehrkhodavandi and S. G. Hatzikiriakos, *Polymer*, 2012, **53**, 2443-2452.

133. R. Langer and J. P. Vacanti, *Science*, 1993, **260**, 920-926.

134. W. M. Saltzman, *Tissue Engineering: Engineering Principles for the Design of Replacement Organs and Tissues*, Oxford University Press, USA, 2004.

135. M. J. Ellis and J. B. Chaudhuri, *Biotechnol. Bioeng.*, 2007, **96**, 177-187.

136. A. Gupta, D. S. Vara, G. Punshon, K. M. Sales, M. C. Winslet and A. M. Seifalian, *Biotechnol. Appl. Biochem.*, 2009, **54**, 221-229.

137. C. X. Song, H. F. Sun and X. D. Feng, *Polymer Journal*, 1987, **19**, 485-491.

138. M. Bero and J. Kasperczyk, *Macromol. Chem. Phys.*, 1996, **197**, 3251-3258.

139. A. Nakayama, N. Kawasaki, Y. Maeda, I. Arvanitoyannis, S. Aiba and N. Yamamoto, *J. Appl. Polym. Sci.*, 1997, **66**, 741-748.

140. F. Stassin and R. Jerome, *J Polym Sci Pol Chem*, 2005, **43**, 2777-2789.

141. M. Florczak and A. Duda, *Angewandte Chemie International Edition*, 2008, **47**, 9088-9091.

142. F. R. Mayo and F. M. Lewis, *J. Am. Chem. Soc.*, 1944, **66**, 1594-1601.

143. P. C. Painter and M. M. Coleman, *Essentials of polymer science and engineering*, DEStech Publications, Inc, 2008.

144. Y. Chen and A. Sen, *Macromolecules*, 2009, **42**, 3951-3957.

145. A. M. V. Herk and T. Dröge, *Macromol. Theory Simul.*, 1997, **6**, 1263-1276.

146. M. Fineman and S. D. Ross, *J Polym Sci*, 1950, **5**, 259-262.

147. T. Kelen and F. Tudos, *J Macromol Sci Chem*, 1975, **A 9**, 1-27.

CHAPTER 2

ALUMINIUM (III) AND TITANIUM (IV) IMINE BIS(PHENOLATE) COMPLEXES AS INITIATORS FOR THE RING-OPENING POLYMERISATION OF *RAC*-LACTIDE

2 Aluminium (III) and Titanium (IV) imine bis(phenolate) complexes as initiators for the ring-opening polymerisation of *racemic*-lactide

2.1 Preamble

In order to access unsymmetrical amine tris(phenolate) ligands a step-wise synthetic methodology must be employed. This will be discussed in detail in Chapter 3 but one route includes synthesis of an imine bis(phenolate) intermediate. Tridentate {ONO} systems with phenolate, amine or imine functionality have been widely reported in the literature with varying activity and stereoselectivity for the polymerisation of *rac*-lactide.[1-3] The cheap availability of substituted anilines leads to most ligand architectures lacking a methylene bridge on the nitrogen side of the imine. In order to vary the target amine tris(phenolate) in phenyl substituent alone, a source of 2-hydroxybenylamine needed to be used. This provided access to a range of previously unreported imine bis(phenolate) compounds that could be coordinated to a metal and trialled for the catalytic ROP of lactide.

2.2 Synthesis of imine bis(phenolate) ligands

The imine bis(phenolate) ligands (H_2**1-7**) were synthesised *via* an imine condensation reaction between a 3,5-substituted salicyaldehyde and salicylamine, that was generated *in-situ* from a salicylammonium acetate. To achieve substitution on both arms of the bis(phenolate) structure, a di-*tert*-butyl-substituted salicylammonium acetate species was generated from the corresponding aldehyde. The salicylammonium acetate was synthesised from salicylaldoximine; this required the dissolution of the salicylaldoximine in glacial acetic acid in the presence of zinc dust at room temperature to facilitate a coordinative reduction to the acetate salt. This followed a standard literature procedure.[4] The dimethyl-substituted salicyaldehyde had to be prepared from the 2,4-dimethylphenol according to a literature-based procedure.[5]

Purification of the ligands could be achieved by washing with hexane (H_2**1-2**) or recrystallisation in methanol (H_2**3-7**).

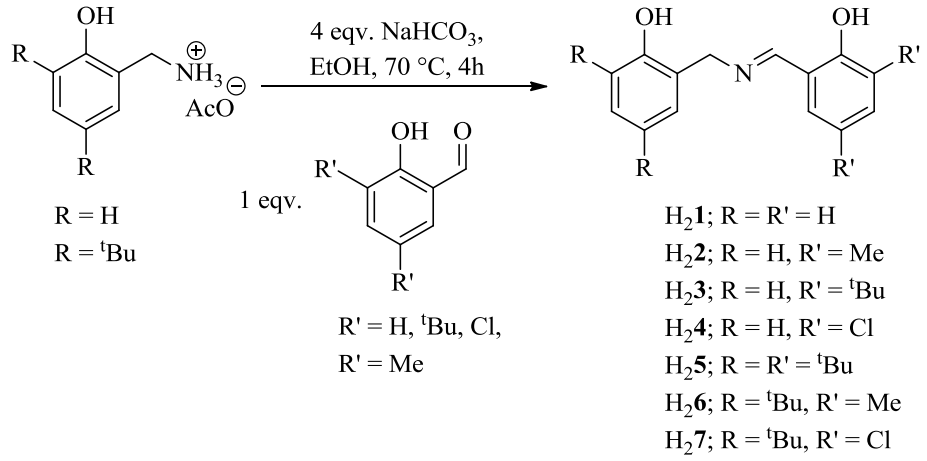

Scheme 2.1 Synthesis of substituted imine bis(phenolate) ligands H_2**1-7**

^{1}H and $^{13}C\{^{1}H\}$ NMR spectroscopy both confirmed the formation of the imine along with accurate mass spectrometry, providing sufficient characterisation of the ligands prior to coordination. Analysis in the solid-state by single crystal X-ray crystallography of H_2**1, 2, 4** and **5** highlighted the shorter C=N bond of the imine and a C-N=C bond angle ~120° as expected for a sp^2 hybridised nitrogen.

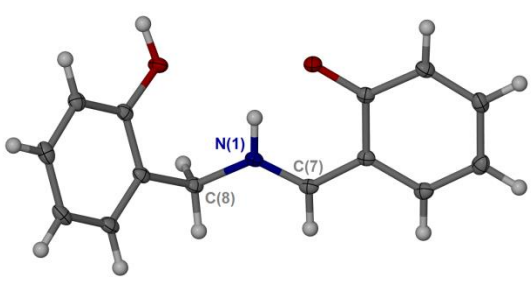

H_2**1**

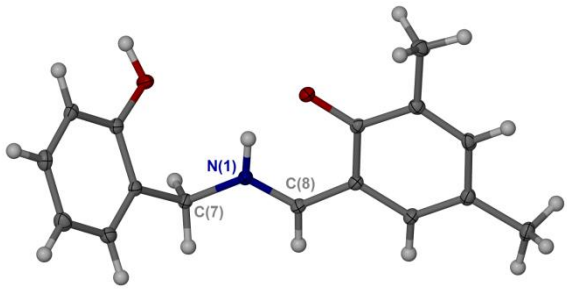

H_2**2**

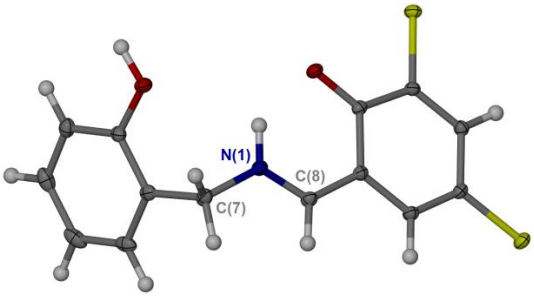

H_2**4**

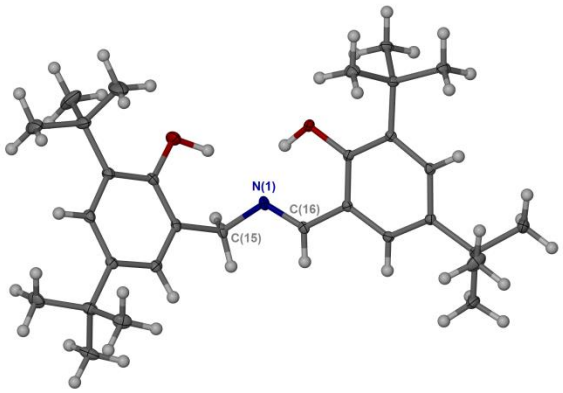

H_2**5**

Figure 2.1 Structures of ligands H_2**1**, H_2**2**, H_2**4** and H_2**5** as determined by single-crystal X-ray diffraction

The hydrogen atoms associated with the nitrogen and oxygen atoms of the ligands were located in the final difference Fourier map of the X-ray diffraction data (Figure 2.1). Whilst the imine nitrogen was protonated on three of the four imine ligands, H_2**5** had the hydrogen atom located on the imine-phenolate oxygen. This suggested that the ligands existed as zwitterions, in the solid state.

	H_2**1**	H_2**2**	H_2**4**	H_2**5**
N(1) – C(8)	1.2915(18)	1.2994(18)	1.294(2)	-
N(1) – C(7)	1.4710(16)	1.4685(18)	1.473(2)	-
C(7) – N(1) – C(8)	125.18(12)	124.66(12)	123.46(14)	-
N(1) – C(16)	-	-	-	1.2765(17)
N(1) – C(15)	-	-	-	1.4705(15)
C(15) – N(1) – C(16)	-	-	-	117.54(11)

Table 2.1 Selected bond length (Å) and bond angles (°) for H_2**1**, H_2**2**, H_2**4** and H_2**5** as determined by single-crystal X-ray diffraction

2.3 Coordination of imine bis(phenolate) ligands to Al(III)Me_3

Coordination of the imine bis(phenolate) ligands to trimethyl aluminium was carried out in toluene at room temperature. Initial analysis by ^{1}H NMR spectroscopy proved inconclusive as to the nature of the metal-ligand species, whether monomeric or dimeric. However, the presence of doublets with a high coupling constants (J ≈ 17 Hz) was indicative of an AX spin system caused by diastereotopic protons of the CH_2 methylene bridge when coordinated to a metal centre. Single-crystal X-ray diffraction provided further insight into the structural motif for some complexes and coupled with NMR spectroscopy it was concluded that all ligands formed an $Al_2(Me)_2$(**X**)$_2$ dimer structure, however the nature of the ligand affected which structural motif was adopted, with a number of complexes exhibiting more than one motif.

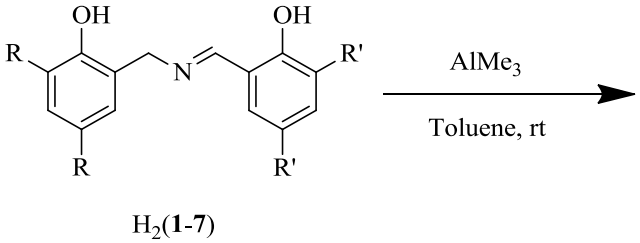

H_2(**1**-**7**)

$Al_2(Me)_2$(**1**)$_2$; R = R' = H
$Al_2(Me)_2$(**2**)$_2$; R = H, R' = Me
$Al_2(Me)_2$(**3**)$_2$ R = H, R' = ^{t}Bu
$Al_2(Me)_2$(**4**)$_2$; R = H, R' = Cl
$Al_2(Me)_2$(**5**)$_2$; R = R' = ^{t}Bu
$Al_2(Me)_2$(**6**)$_2$; R = ^{t}Bu, R' = Me
$Al_2(Me)_2$(**7**)$_2$; R = ^{t}Bu, R' = Cl

Scheme 2.2 Synthesis of Aluminium(III) imine bis(phenolate) complexes.

2.3.1 Single crystal X-ray crystallography

Two structural motifs were obtained from single crystal X-ray crystallographic data. This provided an insight into the different structures that formed during ligand coordination. An X-ray crystal structure was acquired of dimeric species: $Al_2(Me)_2(\mathbf{2})_2$, $Al_2(Me)_2(\mathbf{4})_2$ and $Al_2(Me)_2(\mathbf{5})_2$. $Al_2(Me)_2(\mathbf{2})_2$ and $Al_2(Me)_2(\mathbf{5})_2$ adopted one structural motif, whilst $Al_2(Me)_2(\mathbf{4})_2$ adopted another. The evidence of multiple isomers could explain the complex ^{1}H NMR spectra obtained and difficulties encountered during purification. The formation of dimers when using less sterically demanding tridentate ligands was akin to work recently published by Darensbourg *et. al.*[1] Bridging was also facilitated by a phenoxy donor and as with previous reports, where an unsubstituted ring is present in the ligand, it adopted the bridging position.[1] Crystal structure data acquired for the $Al_2(Me)_2(\mathbf{2})_2$ and $Al_2(Me)_2(\mathbf{5})_2$ suggested the presence of aluminium in both a pseudo-octahedral six-coordinate and pseudo-tetrahedral four-coordinate geometry. The dimer has a C_2-axis of symmetry passing through the two aluminium metal centres (Figure 2.2 and Figure 2.3).

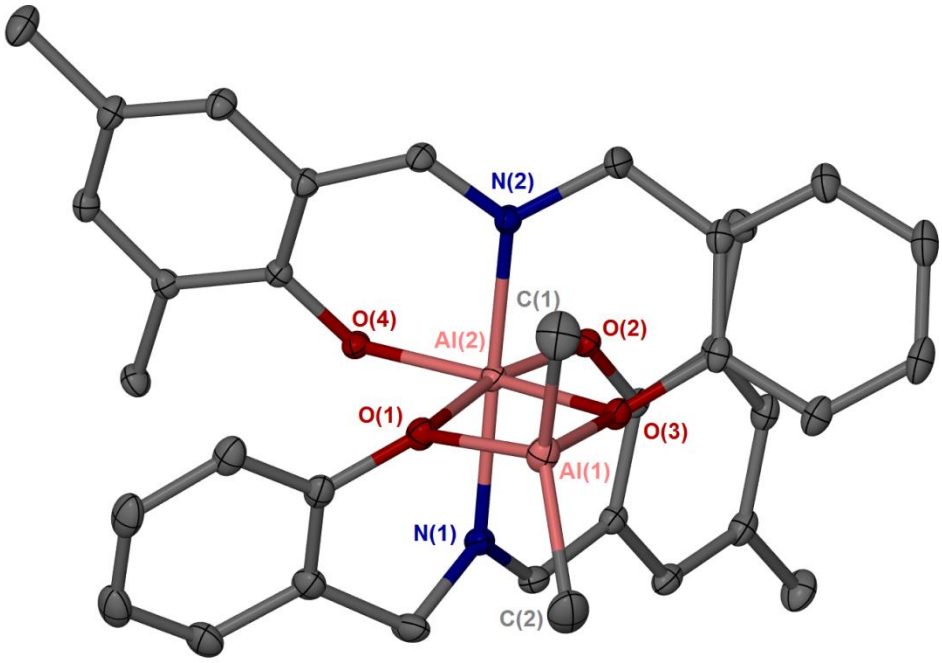

Figure 2.2 Solid-state structure of $Al_2(Me)_2(\mathbf{2})_2$ as determined by single-crystal X-ray diffraction. Ellipsoids are shown at the 30% probability level. All disorder and hydrogen atoms have been removed for clarity

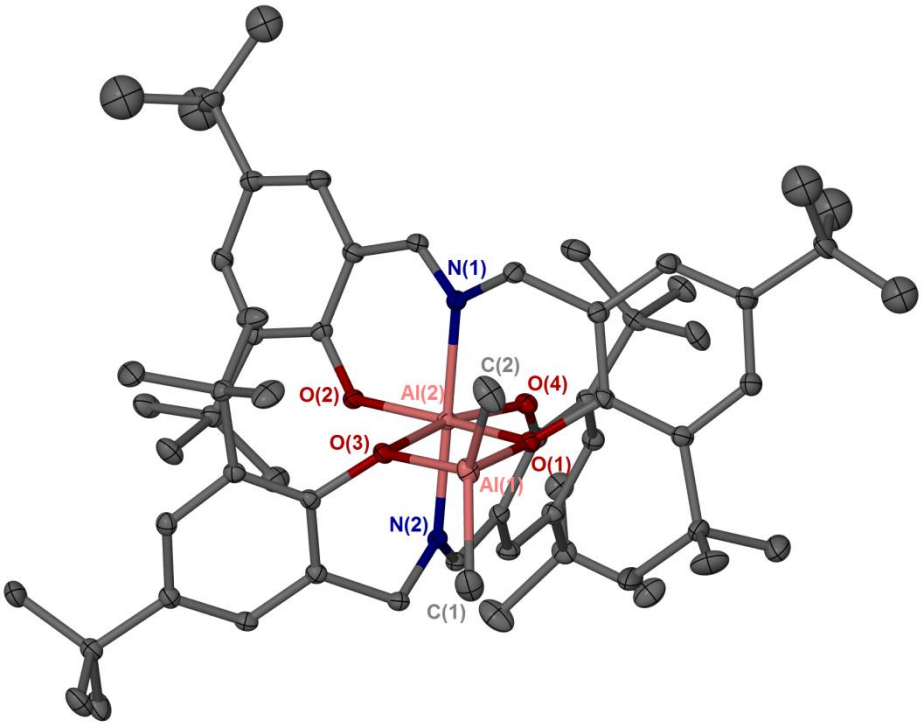

Figure 2.3 Solid-state structure of $Al_2(Me)_2(\mathbf{5})_2$ as determined by single-crystal X-ray diffraction. Ellipsoids are shown at the 30% probability level. All disorder and hydrogen atoms have been removed for clarity

	$Al_2(Me)_2(\mathbf{2})_2$	$Al_2(Me)_2(\mathbf{5})_2$
Al(1) – O(1)	1.8226(10)	1.842(2)
Al(1) – O(3)	1.8387(10)	1.843(2)
Al(1) – C(1)	1.9560(19)	1.964(4)
Al(1) – C(2)	1.9560(19)	1.964(4)
Al(2) – O(1)	1.9858(10)	1.973(2)
Al(2) – O(3)	1.9480(10)	2.029(2)
Al(2) – O(2)	1.8101(100	1.817(2)
Al(2) – O(4)	1.8011(9)	1.820(2)
Al(2) – N(1)	2.0427(12)	2.008(3)
Al(2) – N(2)	2.0043(11)	2.007(3)
Al(1) – O(1) – Al(2)	101.91(5)	103.74(10)
Al(1) – O(3) – Al(2)	102.77(5)	101.54(10)
C(1) – Al(1) – C(2)	118.40(10)	109.73(19)
O(1) – Al(1) – O(3)	80.81(4)	81.16(10)
O(1) – Al(2) – O(3)	74.21(4)	73.55(9)
O(2) – Al(2) – O(4)	101.97(4)	101.64(10)
O(2) – Al(2) – N(2)	90.05(4)	88.34(10)
O(2) – Al(2) – O(3)	93.55(4)	92.93(10)
O(1) – Al(2) – O(4)	90.55(4)	92.14(10)
N(1) – Al(2) – N(2)	178.00(5)	177.74(11)

Table 2.2 Selected bond lengths (Å) and bond angles (°) for $Al_2(Me)_2(\mathbf{2})_2$ and $Al_2(Me)_2(\mathbf{5})_2$ as determined by single-crystal X-ray diffraction

All metal-oxygen bonds to O(1) and O(3) were slightly longer than metal-oxygen bonds to O(2) and O(4), indicative of their bridging nature (Table 2.1). Repulsion between the two aluminium centres and the formation of a four-membered ring caused significant distortion to both the octahedral and tetrahedral geometry; O(1) – Al(1) – O(3) and O(1) – Al(2) – O(3) bond angles were both decreased from 109° and 90° respectively. As expected with an pseudo octahedral-type geometry, the N(1) – Al(2) – N(2) angle was close to 180°.

Metal-oxygen bonds for the solid-state structure of $Al_2(Me)_2(\mathbf{5})_2$ were of comparable length to $Al_2(Me)_2(\mathbf{2})_2$ with similar distortion caused to the octahedral and tetrahedral geometries by the bi-metallic bonding motif. A significant difference was seen in the C(1) – Al(1) – C(2) bond angles for the two isolated structures. For $Al_2(Me)_2(\mathbf{2})_2$ the bond angle between the two methyl groups and the four-coordinate aluminium was enlarged to ~118° whilst for $Al_2(Me)_2(\mathbf{5})_2$ it remained at ~109°. Whilst both structures exhibited similar distortion due to the presence of a di-metallic four-membered ring, this lack of change in the C(1) – Al(1) – C(2) bond angle for $Al_2(Me)_2(\mathbf{5})_2$ could be attributed to the increased steric bulk of the ligand and thus the methyl groups remaining orientated closer to the C_2-axis of the dimer. It should be noted that in the case of $Al_2(Me)_2(\mathbf{5})_2$ both phenyl rings were di-substituted in the 3,5-position. In the solid-state, the dimer formed with the more flexible methylene-connected phenolate {N-CH_2-Ph} occupying the bridging position, which better facilitated the formation of the oxy-bridged di-aluminium four-membered ring.

For the isolated solid-state structure of $Al_2(Me)_2(\mathbf{4})_2$, both aluminium metal centres are five-coordinate and have a pseudo-trigonal bipyramidal geometry; analogous to that seen with aluminium complexes with tridentate half-salen ligands.[1] The two bridging oxygens O(2) and O(4) are axial donors for the aluminium they bridge to whilst bind in an equatorial fashion to the other aluminium centre (Figure 2.4).

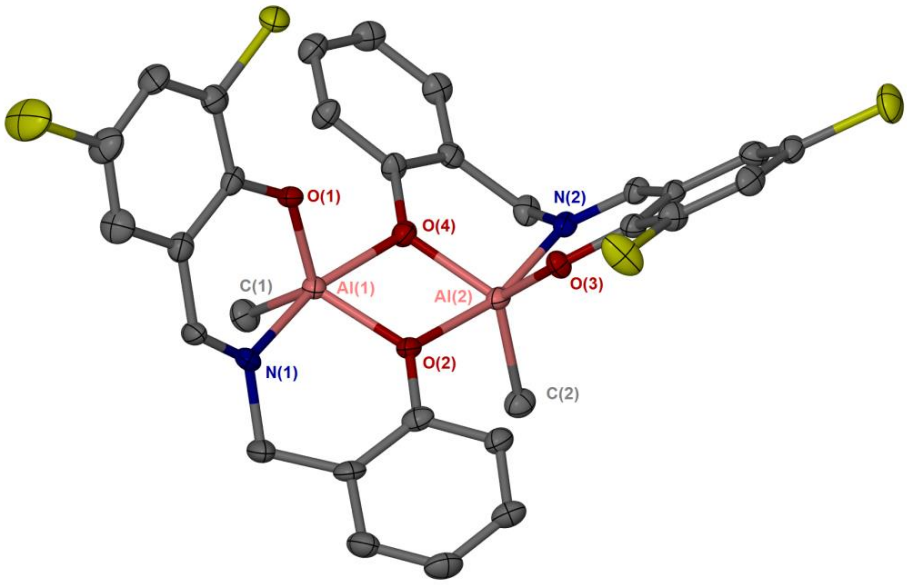

Figure 2.4 Solid-state structure of $Al_2(Me)_2$(**4**)$_2$ as determined by single-crystal X-ray diffraction. Ellipsoids are shown at the 30% probability level. All disorder and hydrogen atoms have been removed for clarity

	$Al_2(Me)_2$(**4**)$_2$
Al(1) – O(1)	1.784(4)
Al(1) – O(2)	1.855(5)
Al(1) – O(4)	1.948(5)
Al(1) – N(1)	2.006(6)
Al(1) – C(1)	1.977(7)
Al(2) – O(2)	1.974(5)
Al(2) – O(3)	1.777(4)
Al(2) – O(4)	1.855(5)
Al(2) – N(2)	1.988(6)
Al(2) – C(2)	1.953(7)
C(1) – Al(1) – O(1)	120.3(3)
C(1) – Al(1) – O(2)	123.6(3)
O(1) – Al(1) – O(2)	116.0(2)
N(1) – Al(1) – O(1)	89.9(2)
N(1) – Al(1) – O(4)	164.3(2)
C(2) – Al(2) – O(3)	123.2(3)
C(2) – Al(2) – O(4)	120.6(3)
O(3) – Al(2) – O(4)	115.8(2)
N(2) – Al(2) – O(3)	90.2(2)
N(2) – Al(2) – O(2)	164.6(2)
Al(1) – O(2) – Al(2)	102.9(2)

Table 2.3 Selected bond lengths (Å) and bond angles (°) for $Al_2(Me)_2$(**4**)$_2$ as determined by single-crystal X-ray diffraction

Distortion was caused to the bipyramidal structure due to repulsion between the metal centres, causing a decrease in the axial-metal-axial bond angle; whilst the non-bridging axial-metal-equtorial bond angle remained at approximately 90° (Table 2.3). Both methyl groups were found to be orientated on the same side of the Al-O-Al-O four-membered ring, giving rise to a C_2 axis of symmetry through the centre of the complex perpendicular to the plane of the four-membered ring. The presence of the methyl groups on the same side of the complex required the two ligands to be on the same side of the dimer, however due to the ligand geometry this facilitated minimal steric interaction between the chloro-substituted phenolate and the unsubstituted phenolate of the other ligand.

2.3.2 ^{1}H NMR Spectroscopy

^{1}H NMR spectra were recorded in C_6D_6 for the crystalline bulk material from which a solid-state structure was obtained. The ^{1}H NMR spectrum of $Al_2(Me)_2(\mathbf{2})_2$, showed the methylene protons {N-CH_2-Ph} to be discretely diastereotopic, appearing as two doublets of an AX spin system (J = 17.3 Hz) and confirming that the solid-state structure is maintained in solution (Figure 2.5). The presence of only one singlet at 7.70 ppm due to the imine and one singlet at -0.49 ppm (Al-CH_3) further confirmed the C_2-symmetry of the dimer and that both ligands were equivalent. This retention of C_2-symmetery in solution (C_6D_6) was also observed for $Al_2(Me)_2(\mathbf{5})_2$ with the diastereotopic methylene bridge protons appearing as doublets (J = 14.3 Hz). The doublets appeared at significantly different chemical shifts and analysis of the solid-state structures showed that the orientation of the bridging phenolate, and thus one proton of the methylene bridge, was closer to the bimetallic aluminium core for $Al_2(Me)_2(\mathbf{5})_2$ compared to $Al_2(Me)_2(\mathbf{2})_2$; 4.258 Å for $Al_2(Me)_2(\mathbf{2})_2$ whilst only 2.981 Å for $Al_2(Me)_2(\mathbf{5})_2$. This closer proximity would lead to increased deshielding and a higher chemical shift for that proton. This orientation of the methylene bridge was attributed to the greater steric demand of the di-*tert*-butyl-substituted phenolate that was acting as the bridging group for $Al_2(Me)_2(\mathbf{5})_2$.

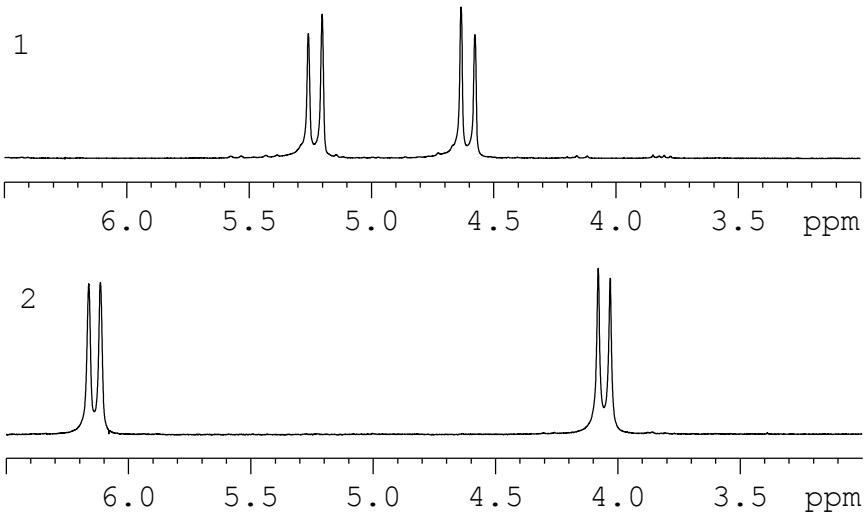

Figure 2.5 Parts of the ^{1}H NMR (C_6D_6) spectra for 1. $Al_2(Me)_2$(**2**)$_2$ and 2. $Al_2(Me)_2$(**5**)$_2$ showing the AX spin system for the methylene bridge proton.

The pseudo-C_2-symmetrical nature of the $Al_2(Me)_2$(**4**)$_2$ dimer was also maintained in solution with only one methyl signal appearing at -0.30 ppm. The methylene CH_2 protons also appeared as discreet doublets of an AX spin system (J = 13.0 Hz), indicating that they were diastereotopic (Figure 2.6). Whilst the splitting and integration of the methylene bridge protons indicated that the ligands were equivalent, the imine proton (8.6 ppm) appeared as a doublet. The solution ^{1}H NMR spectroscopy for this complex also showed smaller signals with slightly different chemical shifts and may be indicative of other isomers present, for example, a dimeric species in which both aluminium metals are still five-coordinate (5°) but with the methyl groups orientated on opposite sides of the Al-O-Al-O four-membered ring (5°-5° 'trans' species).

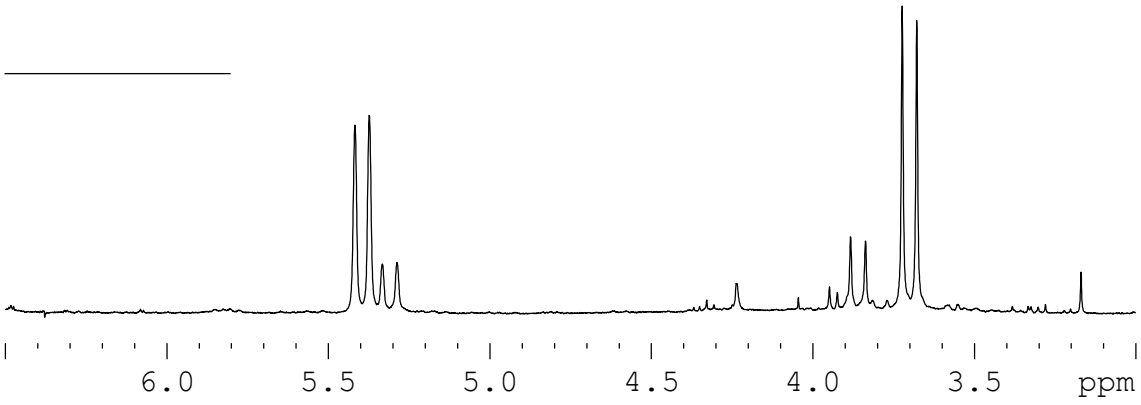

Figure 2.6 Extract of ^{1}H NMR (C_6D_6) spectrum for $Al_2(Me)_2$(**4**)$_2$ showing AX spin system for the methylene bridge protons.

Pairing of this spectroscopic data with the solid-state structural data provided insight into two possible structural motifs for these Aluminium (III) imine bis(phenolate) complexes. This information was used to attempt identification of structural motifs for other complexes where crystallographic data could not be obtained or multiple sets of doublets were observed in the methylene bridge region of the ^{1}H NMR spectrum (3.0-6.0 ppm). This indicated the possibility of multiple isomers in the crude material, two of which have been isolated thus far, and provided a reason for why straightforward purification *via* recrystallization proved difficult.

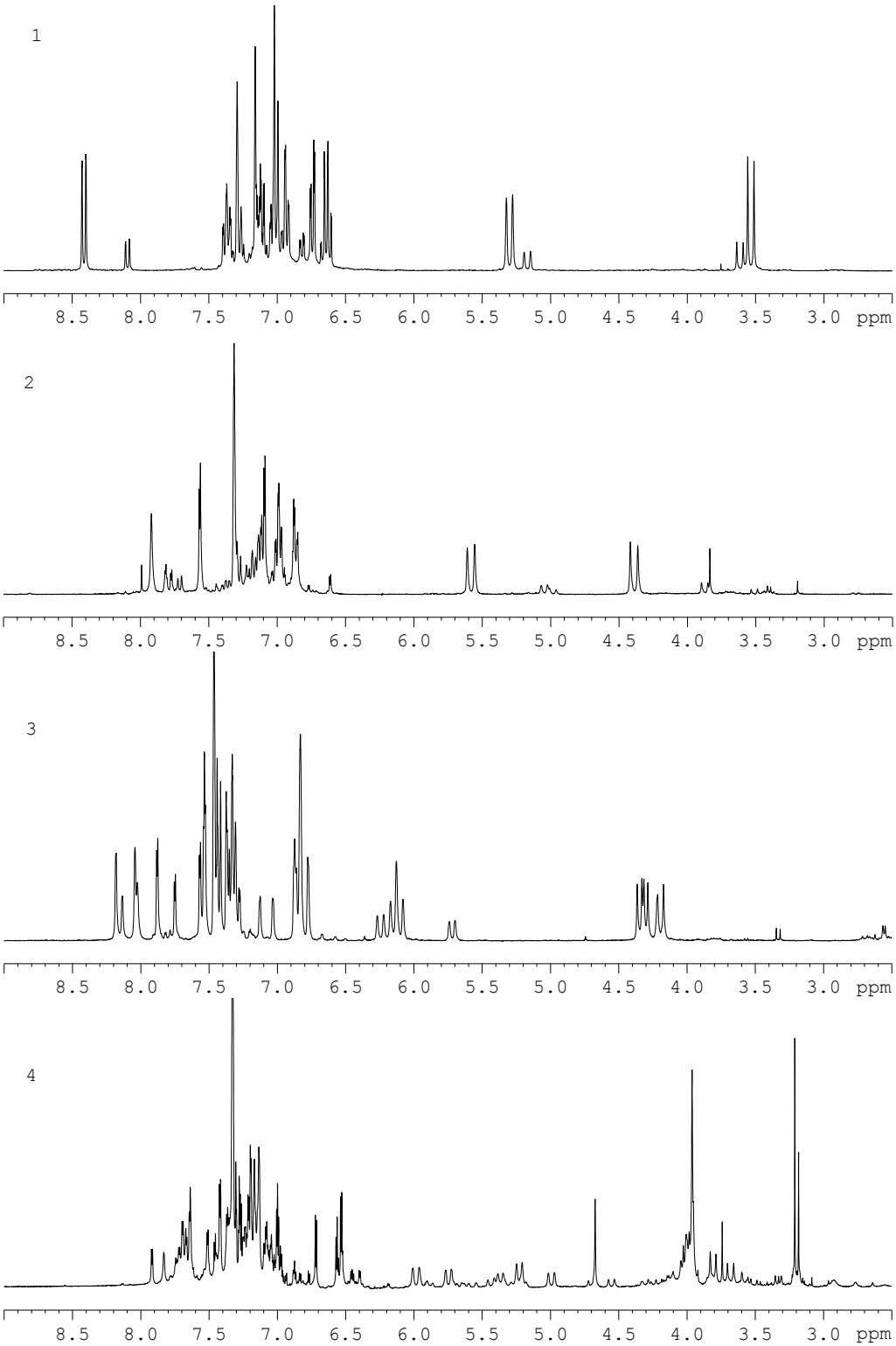

Figure 2.7 ^{1}H NMR spectra (C_6D_6) for 1. $Al_2(Me)_2$(**1**)$_2$, 2. $Al_2(Me)_2$(**3**)$_2$, 3. $Al_2(Me)_2$(**6**)$_2$ and 4. $Al_2(Me)_2$(**7**)$_2$

2.3.3 Summary and further discussion

Characterisation of these Aluminium (III) imine bis(phenolate) complexes identified two structural motifs. Whilst both were dimeric they afforded Aluminium metal centres in different coordination environments (Scheme 2.3).

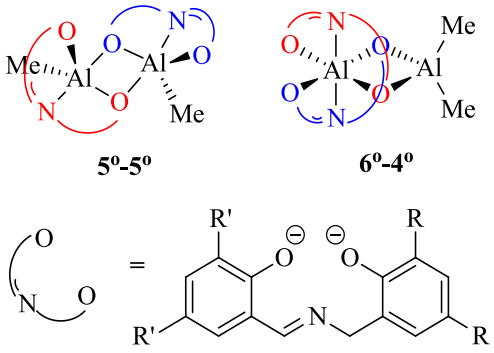

Scheme 2.3 Schematic representation of two identified structural motifs for $Al_2(Me)_2(\mathbf{X})_2$.

From the ligands investigated it was concluded that the steric requirements of the ligand dictated the structural motif adopted. The least sterically demanding fully unsubstituted imine (H_2**1**) yielded a complex with the 5°-5° structural geometry: Figure 2.7 (1). Substitution on the 'imine-side' of the ligand in the 3,5- position with chloro-substituents did not increase the stereic demands of the ligand enough and purely the 5°-5° geometry is observed. However, in the presence of methyl-substituents in the 3,5-position the both the 5°-5° and 6°-4° geometries were observed in the bulk ^{1}H NMR spectrum (Figure 2.8) and the 6°-4° geometry was isolated *via* recrystallisation.

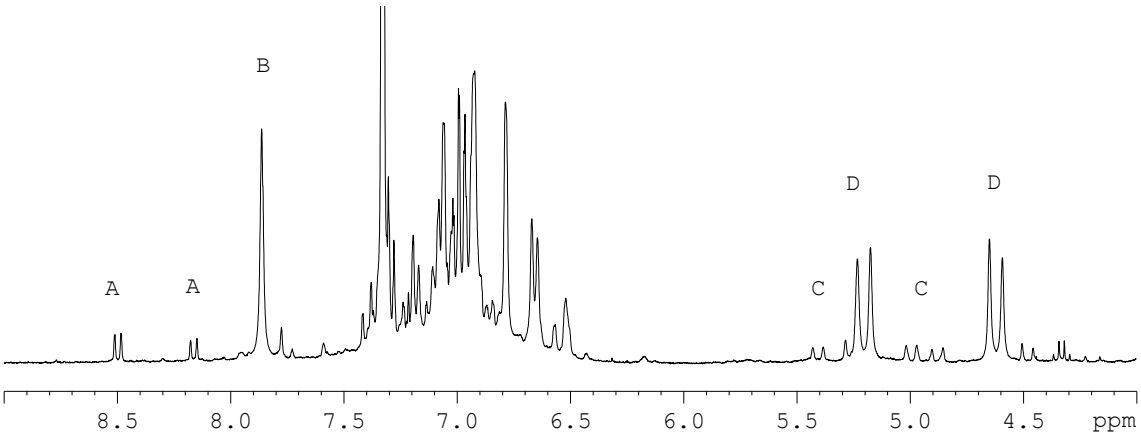

Figure 2.8 Extract of the ^{1}H NMR spectrum (C_6D_6) for non-recrystallised $Al_2(Me)_2(\mathbf{2})_2$ exhibiting signals for the 5°-5° structural geometry: A (imine), C (methylene bridge) and the predominant 6°-4° structural geometry: B (imine) and D (methylene bridge).

Replacing the substituents with *tert*-butyl groups increased the steric demand of the ligand and whilst purification *via* recrystallisation proved unsuccessful, analysis of the ^{1}H NMR spectrum of the bulk material, Figure 2.7 (2), led to the conclusion that $Al_2(Me)_2(\mathbf{3})_2$ is predominately of the 6°-4° geometry. The ligand with greatest steric-demand was the doubly di-*tert*-butyl-substituted imine ($H_2\mathbf{5}$). This purified easily *via* recrystallisation and was deemed to be wholly of the 6°-4° structural geometry. Comparison of the two structural geometries highlighted that in the 5°-5° geometry the substituent in the 3-position is directed towards the phenyl ring of the other ligand. Whereas the 6°-4° allowed each ligand to occupy one side of the dimer, orientated at 90° to one another and provided maximum space for the bulkier substituents.

In an attempt to further understand the factors controlling structural geometry the synthesis of $Al_2(Me)_2(\mathbf{2})_2$, which had been shown to form both the 5°-5° and 6°-4° geometry, solutions of $H_2\mathbf{2}$ were prepared at 0.1 M and 0.2 M in toluene before the addition of equal amounts of $AlMe_3$. After stirring for one hour at room temperature the solvent was removed and the yellow solid dried further under *vacu*. Crude material was analysed *via* ^{1}H NMR spectroscopy and the relative amounts of each motif quantified by integration of the imine {N=CH} proton signals.

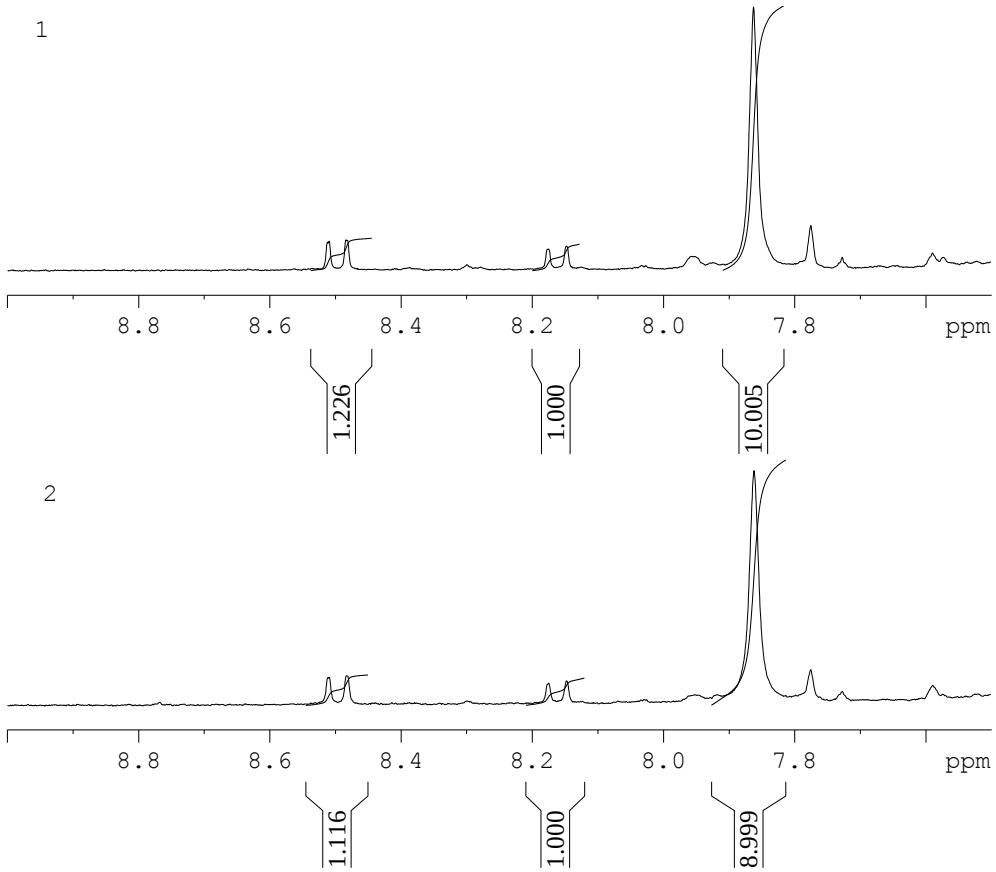

Figure 2.9 Extracts of the ^{1}H NMR spectra (C_6D_6) for the synthesis of $Al_2(Me)_2(\mathbf{2})_2$ at: 1. 0.2 M ligand concentration and 2. 0.1 M ligand concentration

With consideration of the broad nature of the imine signal at 7.86 ppm and other impurities in the spectrum it was concluded that changing the ligand solution concentration, at this level, did not alter the preference to structural motif. Therefore, it is postulated that formation of one motif over the other is kinetically driven rather than by the thermodynamics and the availability of another ligand when forming the dimer.

In the analysis of $Al_2(Me)_2(\mathbf{4})_2$ by single-crystal X-ray diffraction (Figure 2.4) the 5°-5° structural motif was identified with the methyl groups bonded to the Aluminium centre orientated 'cis' with respect to the plane of the dimer. Analysis of the material *via* ^{1}H NMR spectroscopy showed a second set of signals that was deemed a potential second isomer. This second set of signals was also observed for $Al_2(Me)_2(\mathbf{1})_2$ {Figure 2.7 (1)} and for $Al_2(Me)_2(\mathbf{2})_2$ (Figure 2.8). One potential isomer is that which has the methyl groups of the aluminium metal centre orientated 'trans' with respect to the plane of the dimer.

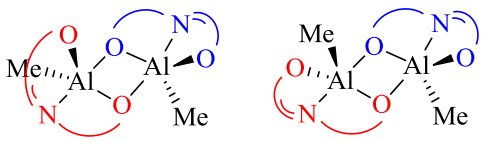

5°-5° 'cis' (found) **5°-5° 'trans' (proposed)**

Scheme 2.4 Representation for the proposed 5°-5° 'trans' isomer for $Al_2(Me)_2(\mathbf{1}\text{-}\mathbf{3})_2$ alongside the 5°-5° 'cis' isomer that was determined by single-crystal X-ray crystallography of $Al_2(Me)_2(\mathbf{3})_2$

As this second set of signals was present in a number of the complexes that exhibit the 5°-5° structural motif the relative integrals of the two potential isomers were quantified to elucidate if the steric bulk of the ligand has an effect on that formed (Figure 2.10).

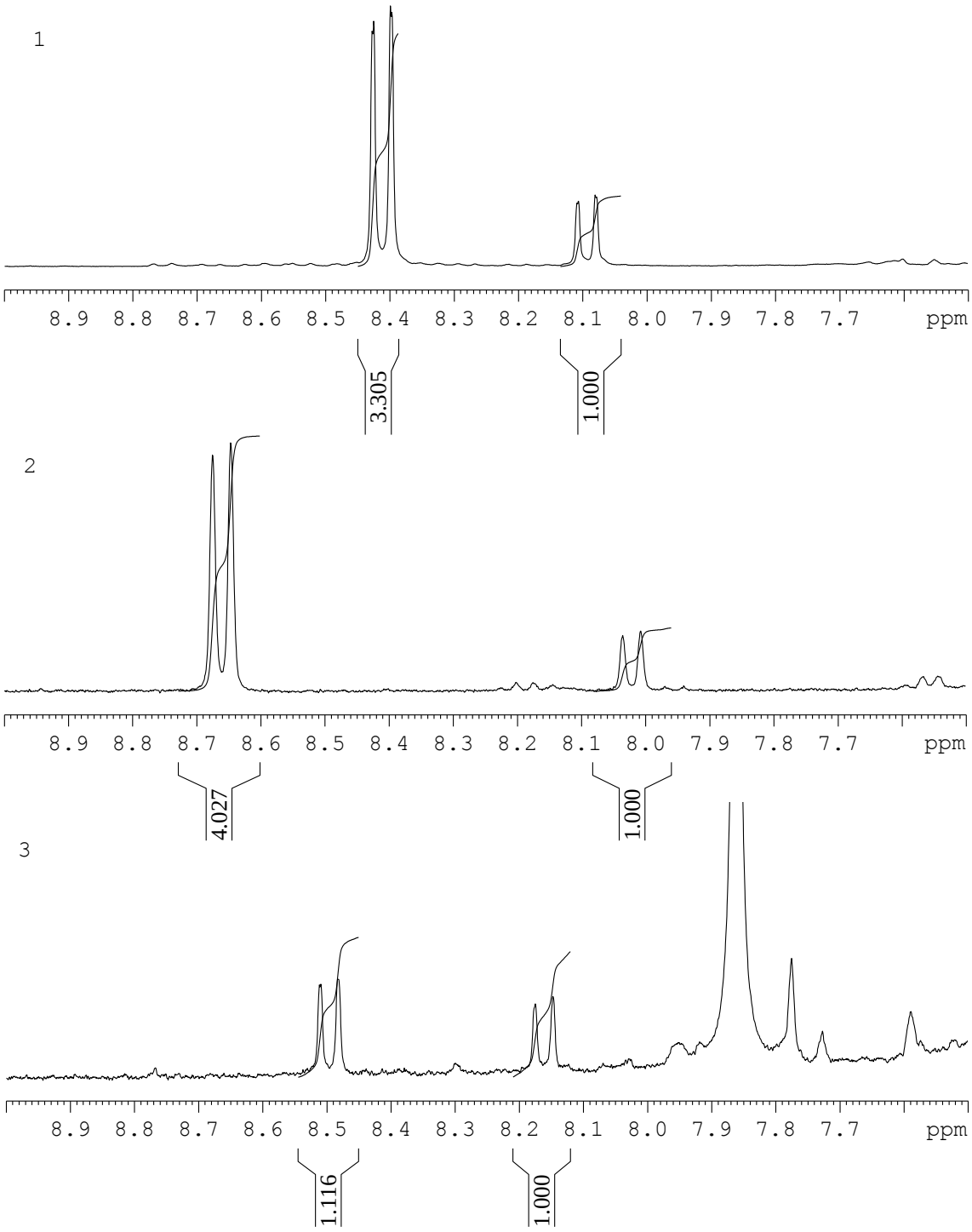

Figure 2.10 Extracts of the ^{1}H NMR spectra (C_6D_6) for: 1. $Al_2(Me)_2(\mathbf{1})_2$, 2. $Al_2(Me)_2(\mathbf{4})_2$ and 3. $Al_2(Me)_2(\mathbf{2})_2$ showing the relative peaks for the imine signals of two possible isomers with increasing ligand steric bulk

Combining the above information with the structural information derived from single crystal X-ray diffraction of $Al_2(Me)_2(\mathbf{4})_2$ it was concluded that the major product was the 'cis' orientated 5°-5° dimer. With the presumption that the second set of signals was due to a second 'trans'

isomer then the imine signal at 8.67 ppm for $Al_2(Me)_2(\mathbf{4})_2$ was assigned to the major 'cis' isomer that had been confirmed in the solid state. Relative abundance of the two isomers was less biased for $Al_2(Me)_2(\mathbf{1})_2$ for which the ligand was unsubstituted and less sterically demanding. However the trend was not confirmed by $Al_2(Me)_2(\mathbf{2})_2$, with the di-methyl-substituted ligand, but the formation of the 6°-4° motif also occurred for that ligand system.

To further investigate the cause of the two sets of signals in the ^{1}H NMR spectrum. $Al_2(Me)_2(\mathbf{4})_2$, which is shown to take only the 5°-5° structural motif, was synthesised by both a high dilution (ligand-to-metal) and low dilution (metal-to-ligand) method in an attempt to influence the relative intensity of the two sets of signals (Figure 2.11).

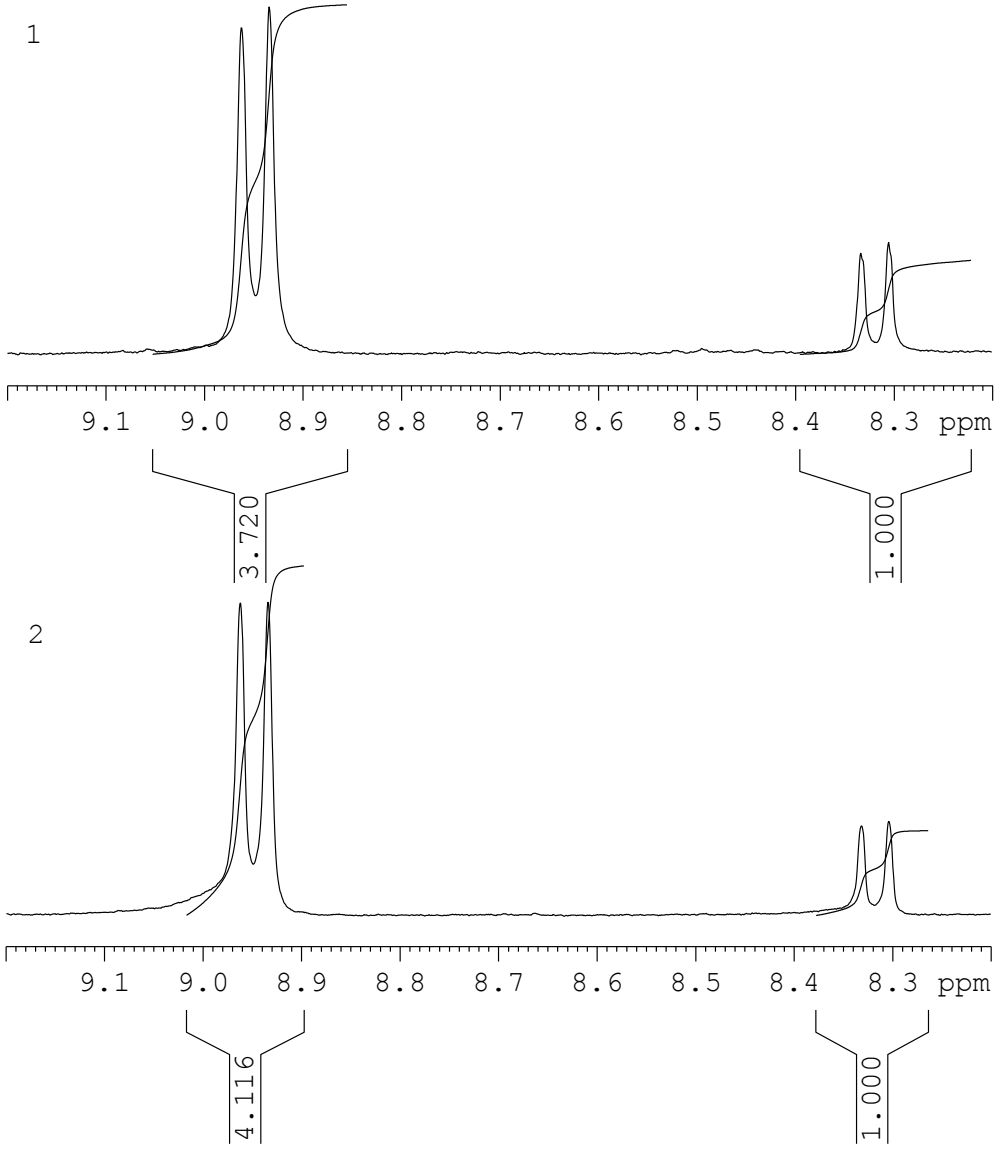

Figure 2.11 Extracts of the ^{1}H NMR spectra ($CDCl_3$) of $Al_2(Me)_2(\mathbf{4})_2$ synthesised by: 1. High dilution method and 2. Low dilution method. Showing the imine signals of the proposed major (8.95 ppm) and minor (8.32 ppm) isomers of the 5°-5° structural motif

Comparison of the ^{1}H NMR spectra ($CDCl_3$) for $Al_2(Me)_2(\mathbf{4})_2$ generated by both high dilution and low dilution methods led to the conclusion that ligand availability had little effect on the relative intensities of the two sets of signals. This provided greater evidence that the ligand architecture had overwhelming influence on the structural motif of the Aluminium imine bis(phenolate) complex.

In an attempt to probe the possibility of a 'trans' isomer being present, DFT calculations were carried out to determine the free energies of the 'cis' and 'trans' isomers of $Al_2(Me)_2(\mathbf{4})_2$. Crystallographic data provided the input coordinates for the 'cis' isomer and this was manipulated to swap the position of C(2) and O(3) as labelled in Figure 2.4. Optimisation was carried out using the following protocol: rwb97xd / 6-13g(d,p) / scrf= (cpcm,solvent=toluene). Free energies for the optimised 5°-5° 'cis' isomer and 5°-5° 'trans' isomer were found with the 'cis' isomer more favourable by 0.51 kcal mol^{-1}. Such an energy difference is not significant and based on this initial calculation, using the basis set stated, the 'cis' and 'trans' isomers are not thermodynamically distinguishable and both possible. The different intensities of the two sets of signals could possibly have been attributed to differing energies in intermediates during the coordination process but such modelling was outside the scope of this investigation.

Further consideration should also be given to the potential structural motifs of $Al_2(Me)_2(\mathbf{6})_2$ and $Al_2(Me)_2(\mathbf{7})_2$. Whilst purification proved difficult and single-crystal X-ray crystallography data could not be obtained, analysis of the ^{1}H NMR spectra of the crude material with comparison to the behaviour of the other ligands in this series provided insight into possible species present. Firstly, it was noted that for $H_2\mathbf{6}$ and $H_2\mathbf{7}$ the greater steric bulk was present on the methylene-side of the tridentate ligand. For all three solid-state structures determined, the phenolate on the methylene-side of the ligand acted as the bridge between the two metal centres with the greater flexibility in the CH_2 allowing accommodation of the bimetallic 4-membered ring. In the case of $Al_2(Me)_2(\mathbf{6})_2$ and $Al_2(Me)_2(\mathbf{7})_2$ it was possible that bridging *via* the methylene phenolate was not guaranteed, due to the greater steric bulk, and that structural motifs may have formed in which the bridging phenolate is in fact on the imine-side. Further to this it is possible that the two ligands may orientate differently – one providing a methylene-side bridging phenolate and the other a imine-side bridiging phenolate – which provided access to a multitude of possible motifs / isomers (Scheme 2.5).

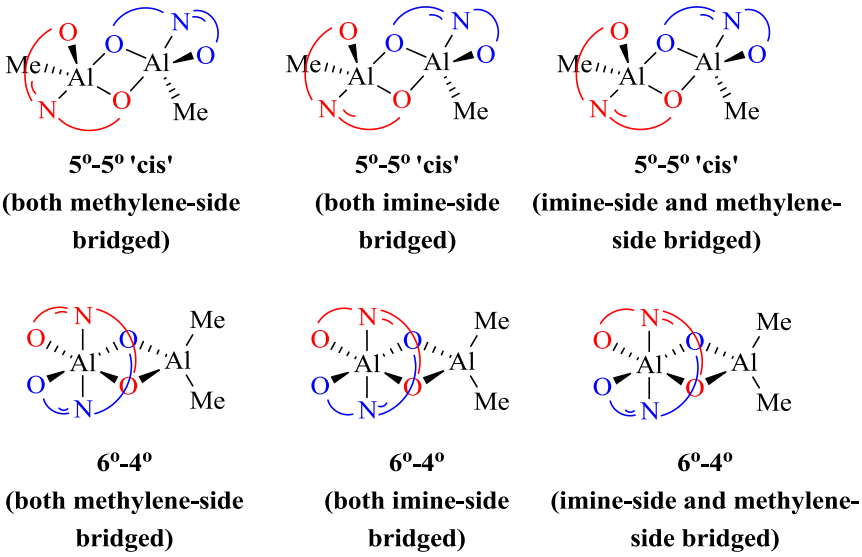

Scheme 2.5 Possible structural motifs / isomers when bridging is not restricted to the methylene-side phenolate for Aluminum (III) imine bis(phenolate) complexes, $Al_2(Me)_2(\mathbf{X})_2$

The presence of multiple doublets in the methylene bridge region of the ^{1}H NMR spectra and also multiple signals in the Aluminium-methyl region (-0.5 – 0.5 ppm) suggested that at least some of these motifs / isomers may also be possible for these types of ligand (Figure 2.12). The multiple products would explain the increased difficulty in recrystallisation and could explain why full characterisation was not possible.

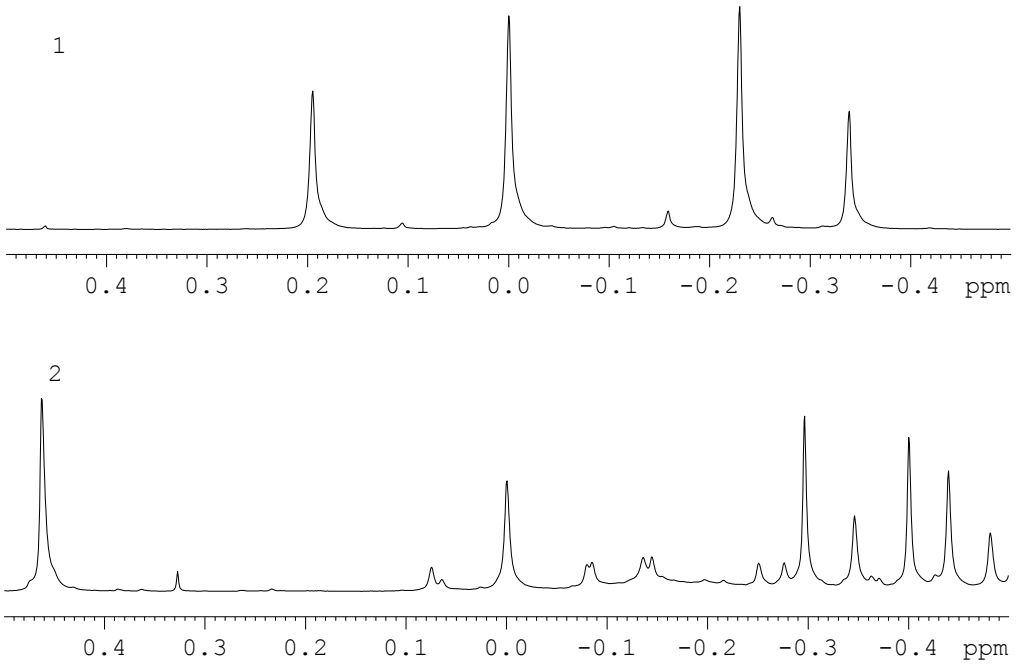

Figure 2.12 Extracts of the ^{1}H NMR spectra (C_6D_6) for: 1. $Al_2(Me)_2(\mathbf{6})_2$ and 2. $Al_2(Me)_2(\mathbf{7})_2$ showing the Aluminium-methyl proton region and the multiple environments present

Finally, as these Aluminium (III) imine bis(phenolate) complexes were synthesised as potential new catalytic initiators for the ROP of *rac*-lactide, $Al_2(Me)_2(\mathbf{1})_2$ was studied by ^{1}H NMR spectroscopy in a coordinative solvent (THF-d_8) in an attempt to understand if the dimer would persist as the active species in the presence of lactide (presuming a coordination-insertions mechanism propagates) (Figure 2.13).

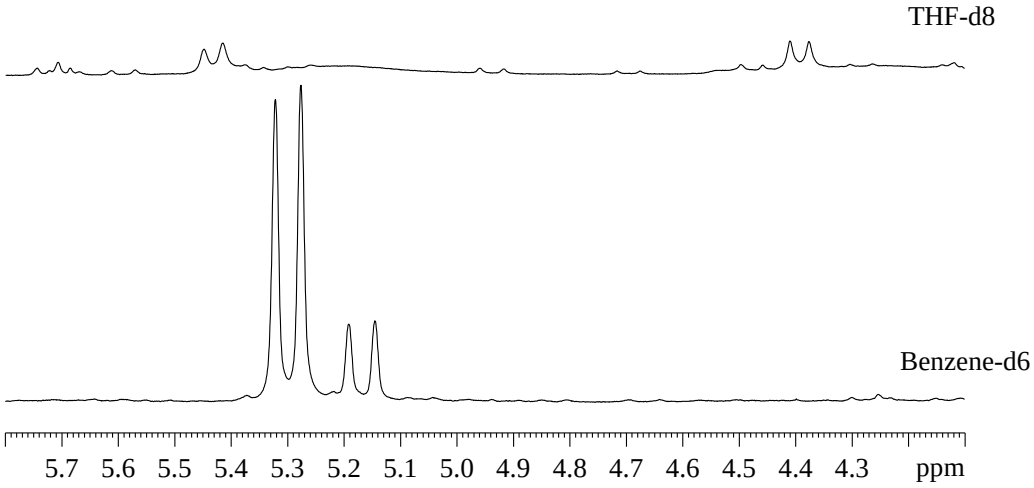

Figure 2.13 Extracts of the ^{1}H NMR spectrum for $Al_2(Me)_2(\mathbf{1})_2$ in C_6D_6 and THF-d_8

Under the presumption that the two sets of signals in the ^{1}H NMR spectrum were indeed due to two possible isomers then the comparison between a spectrum acquired in C_6D_6 and coordinative THF-d_8 suggested that one isomer is susceptible to coordination and breakdown of the dimer whilst the other isomer is not. This is signified by the loss of one set of diastereotopic doublets in the ^{1}H NMR spectrum (THF-d_8) and its appearance as a broad singlet. It has been identified that the methylene-side phenolate acts as the bridge in the dimer so in the dissociation of the dimer this would appear labile and the diastereotopic nature of the CH_2 protons would be lost. $Al_2(Me)_2(\mathbf{1})_2$ in THF-d_8 was also analysed *via* variable temperature NMR (VT-NMR) spectroscopy to alter the rate of any dynamic coordination of THF (Figure 2.14).

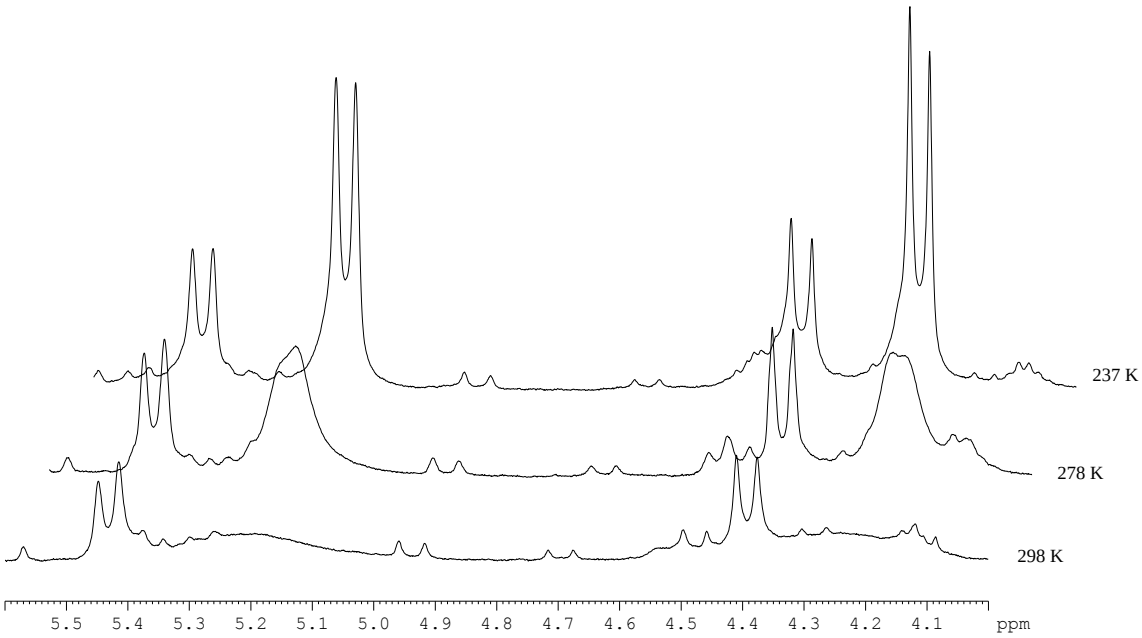

Figure 2.14 Extracts of the ^{1}H NMR spectra for $Al_2(Me)_2(\mathbf{1})_2$ acquired *via* VT-NMR spectroscopy in THF-d_8.

Decreasing the temperature from 298 K to 237 K induced the resolution of the second pair of doublets attributed to diastereotopic protons of the CH_2 methylene bridge. This further affirmed that the 5°-5° dimer structural motif was disrupted by a coordinative solvent and that if active for the ROP of lactide the active species was unlikely to be the dimer. However, it was noted that one set of doublets remained unchanged in THF-d_8 and under variable temperature conditions suggesting that it may be an isomer of the 5°-5° motif that is not disrupted in the presence of lactide. This would therefore be inactive which would in turn affect the molecular weight control achieved by the initiator. This was considered when evaluating the trials of these complexes as initiators for the ROP of lactide.

2.4 Coordination of imine bis(phenolate) ligands to Ti(IV)($O^{i}Pr$)$_4$

Titanium (IV) complexes have been shown to be active for the ROP of lactide both as the simple four-coordinate alkoxides [6] and as coordination compounds encoroporating polydentate ligands.[7-10] Titanium alkoxides, and indeed group IV alkoxides in general, are of particular interest as potential initiators for the ROP of lactide due to their Lewis acidity which provides the possibility for lactide to coordinate readily to the metal centre. Group IV complexes have a similar coordination sphere to that of Tin (II), which is widely used for the ROP of lactide in

industry, and the potential for the alkoxide to act as a readily available initiating group is also attractive.

In this study imine bis(phenolate) ligands H_2**1** and H_2**3**, as introduced in section 2.2, were complexed to titanium (IV). This was provided as the precursor $Ti(O^iPr)_4$ with the intention that as tridentate ligands the resulting titanium (IV) imine bis(phenolate) complexes would retain at least one isoproxide per metal centre. In fact it was found that with the larger titanium (IV) coordination sphere, compared to Al(III), it was possible for different complexes to form with a metal-to-ligand ratio of either 1:1 or 1:2 and, further to this, that it was affected by synthetic procedure followed. For this reason, the following two procedures were used and the compounds isolated outlined below (Scheme 2.6).

Procedure A (low dilution method): under air-sensitive conditions the ligand (H_2**X**) was dissolved in dry toluene before the addition of $Ti(O^iPr)_4$.

Procedure B (high dilution method): under air sensitive conditions the ligand (H_2**X**) was dissolved in dry toluene before adding dropwise to a solution of $Ti(O^iPr)_4$ in dry toluene.

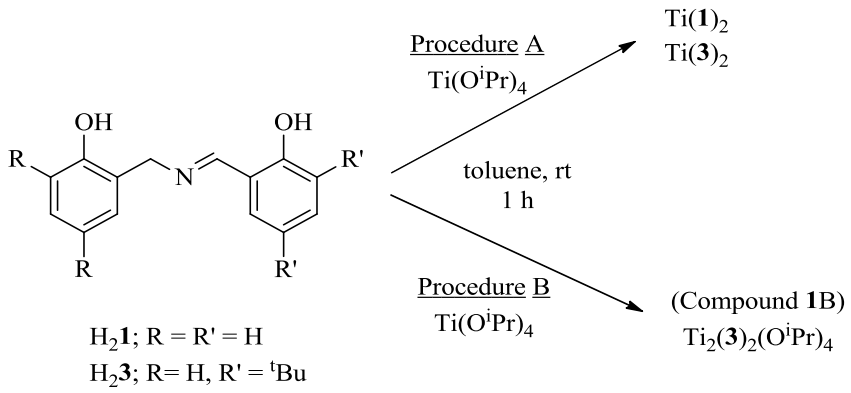

Scheme 2.6 Coordination of H_2**1** and H_2**3** to $Ti(O^iPr)_4$ *via* A (low dilution) and B (high dilution) to yield titanium (IV) imine bis(phenolate) complexes with different metal-to-ligand ratios.

Whilst $Ti(\mathbf{1})_2$ and $Ti_2(\mathbf{3})_2(O^iPr)_4$ were successfully isolated and analysed in the solid state by single-crystal X-ray diffraction and in solution ($CDCl_3$) by NMR spectroscopy, $Ti(\mathbf{3})_2$ could not be recrystallised. Yet ^{1}H NMR spectroscopic analysis provided effective insight into the structure of the complex. It should be noted that the structure of Compound **1**B (i.e. ligand H_2**1** coordinated *via* procedure B) could not be determined yet the ^{1}H NMR spectrum acquired will be discussed in this section along with its activity as an initiator for the ROP of lactide in section 2.5.

2.4.1 Single-crystal X-ray crystallography

The structure as determined by single-crystal X-ray crystallography for Ti(**1**)$_2$ was that of a coordinatively saturated six-coordinate complex. The complex had a pseudo-octahedral geometry with the tridentate ligands occupying opposite hemispheres of the metal centre, binding in the *mer* arrangement and orientated at 90° to one another, as to minimise steric interaction between the phenyl rings of each ligand (Figure 2.15).

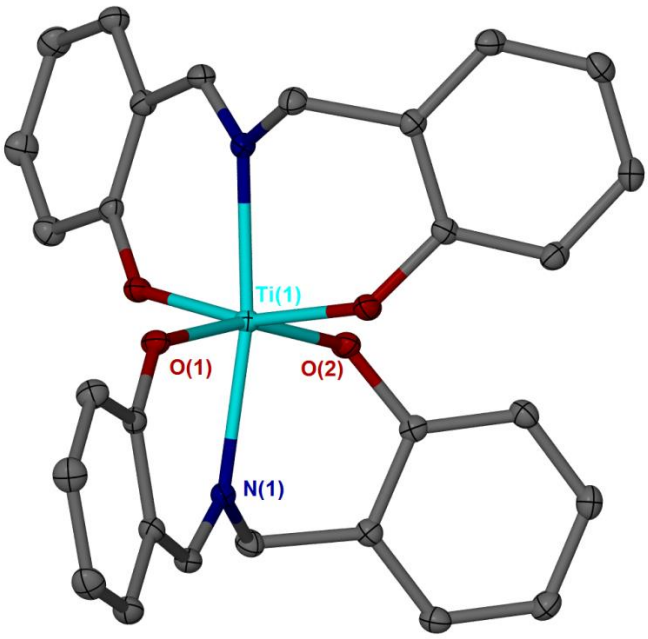

Figure 2.15 Solid-state structure of Ti(**1**)$_2$ as determined *via* single-crystal X-ray diffraction. Ellipsoids are shown at the 30 % probability level. All disorder and hydrogen atoms have been removed for clarity

	Ti(**1**)$_2$
Ti(1) – O(1)	1.8848(14)
Ti(1) – O(2)	1.8988(14)
Ti(1) – N(1)	2.1791(15)
O(1) – Ti(1) – O(1)’	97.14(9)
O(1) – Ti(1) – O(2)	162.43(5)
N(1) – Ti(1) – N(1)’	170.91(8)

Table 2.4 Selected bond lengths (Å) and bond angles (°) for Ti(**1**)$_2$ as determined by single-crystal X-ray diffraction

Distorted axial bond angles between coordinated nitrogen atoms and the Ti metal centre, 170.91° instead of 180°, along with distortion in the arrangement of the equatorial groups was attributed to the steric requirements of the phenyl rings and the reduction in movement of the imine-side of the ligand due to the sp^2-hybridised nature of the imino carbon (Table 2.4).

Ti(**1**)$_2$ was isolated from material generated using procedure A. This was a low dilution method that led to higher concentration of ligand with respect to the Ti(O^{i}Pr)$_4$ precursor. Conversely, *via* procedure B, which provided a greater concentration of Ti(O^{i}Pr)$_4$ with respect to the ligand, the species Ti$_2$(**3**)$_2$(O^{i}Pr)$_4$ was isolated from the coordination of H$_2$**3** with Ti(O^{i}Pr)$_4$. This crystalline material was analysed *via* single-crystal X-ray crystallography and allowed the solid state structure to be determined (Figure 2.16).

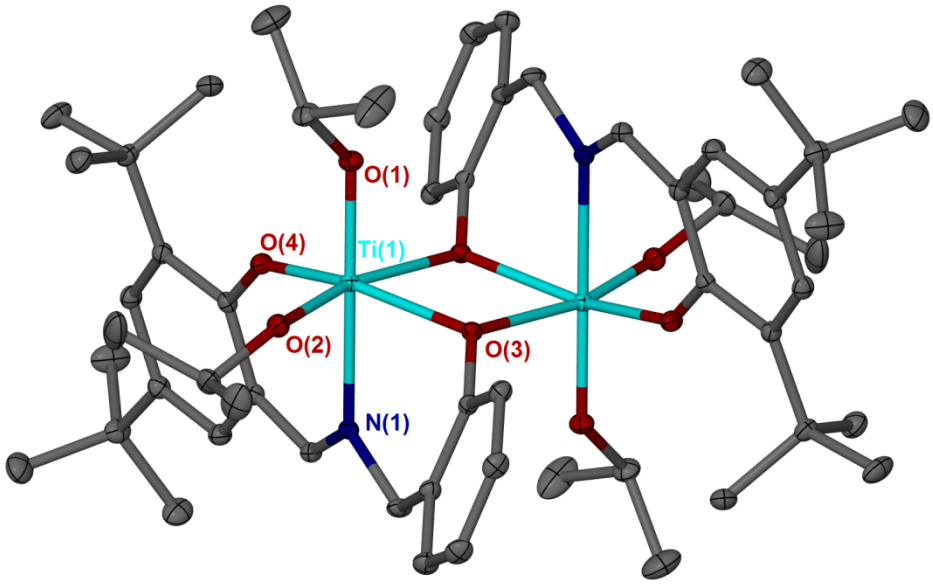

Figure 2.16 Solid-state structure of Ti$_2$(**3**)$_2$(O^{i}Pr)$_4$ as determined by X-ray diffraction. Ellipsoids are shown at the 30 % probability level. All disorder and hydrogen atoms have been removed for clarity

	Ti$_2$(**3**)$_2$(O^{i}Pr)$_4$
Ti(1) – O(1)	1.8258(10)
Ti(1) – O(2)	1.7772(10)
Ti(1) – O(3)	2.0220(9)
Ti(1) – O(4)	1.8877(10)
Ti(1) – N(1)	2.2607(12)
O(1) – Ti(1) – O(2)	95.67(5)
O(1) – Ti(1) – O(3)	101.65(4)
O(1) – Ti(1) – O(4)	95.80(4)
N(1) – Ti(1) – O(1)	176.42(4)
N(1) – Ti(1) – O(2)	87.27(4)
N(1) – Ti(1) – O(3)	80.05(4)
N(1) – Ti(1) – O(4)	81.57(4)
O(2) – Ti(1) – O(3)	95.58(4)
O(3) – Ti(1) – O(4)	153.94(4)

Table 2.5 Selected bond lengths (Å) and bond angles (°) for Ti$_2$(**3**)$_2$(O^{i}Pr)$_4$ as determined by single-crystal X-ray crystallography.

In the solid-state $Ti_2(\mathbf{3})_2(O^iPr)_4$ existed as a dimer with a metal-to-ligand ratio of 1:1. With both metals adopting a six-coordinate pseudo-octahedral geometry each titanium metal centre also retained two isopropoxide groups. The dimeric structure contains a crystollographic inversion centre with the titanium metal centres being bound through two oxy-bridges provided, akin to the Aluminium analogues, by the methylene-side phenolate group. The axial bond angle N(1) – Ti(1) – O(1) was slightly reduced due to the dimeric nature of the complex whilst the bond angles between the axial isopropoxide group {O(1)} and the equatorial donors {O(2-3)} were found to be above 90° due to the steric requirements of the tridentate imine bis(phenolate) ligand and the limitation in movement of the sp^2 hybridised imino carbon. Octahedral distortion is also apparent due to the trans {ONO} angle, O(3) – Ti(1) – O(4), of the ligand being reduced below 180° to 153.94°. Correspondingly, the angles between the coordinated nitrogen of the ligand and the equatorial oxygen-donors were reduced below 90°, with least reduction observed for the isopropoxide group, N(1) – Ti(1) – O(2) = 87.27(4)°, as it was not restricted by the ligand architecture (Table 2.5).

2.4.2 ^{1}H NMR Spectroscopy

The bulk crystalline material that provided the solid-state structure for $Ti(\mathbf{1})_2$ was also analysed by ^{1}H NMR spectroscopy ($CDCl_3$). As with the Aluminium imine bis(phenoloate) complexes characterised previously, the strongly bound phenolate groups gave rise to the methylene bridge protons to appear diastereotopic, appearing as two doublets of an AX spin system with a large coupling constant (J = 13.1 Hz). A similar geminal coupling constant was also observed for the diastereotopic protons of the Ti(salalen)$(O^iPr)_2$ complexes published by Jones et. al.[11] The relative small difference in chemical shift for the two proton signals (0.23 ppm) gave rise to a slight roofing effect that caused the peak intensities to be distorted (Figure 2.17).

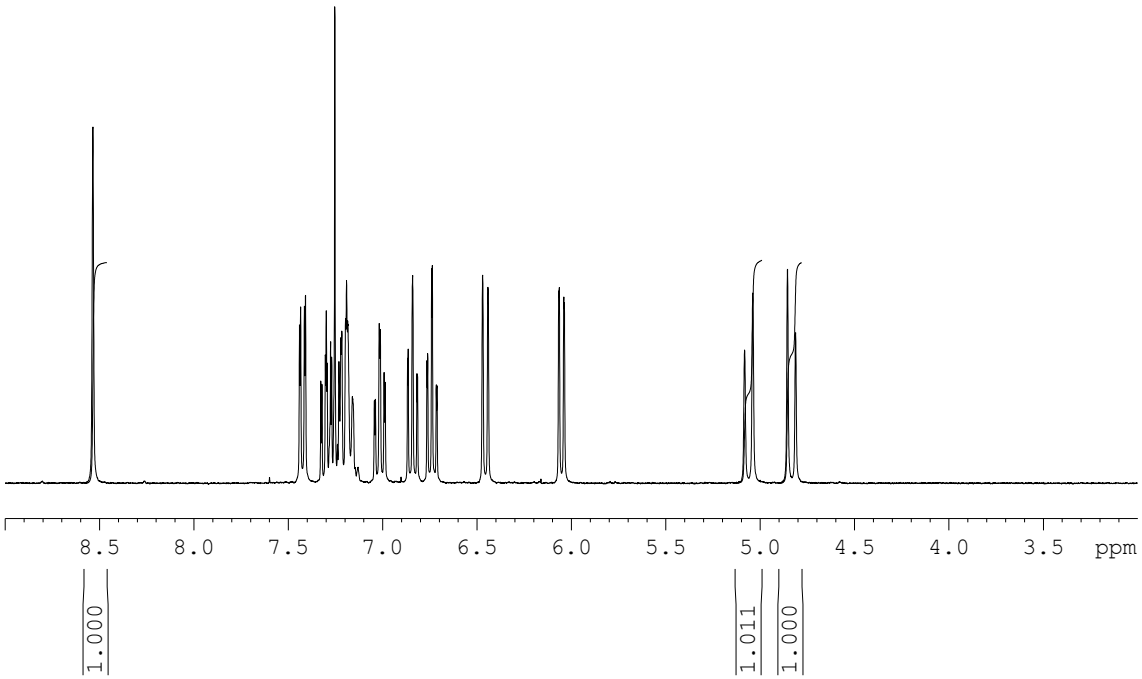

Figure 2.17 Extract of the ^{1}H NMR spectrum ($CDCl_3$) for Ti(**1**)$_2$ showing the doublets for the diastereotopic protons of the methylene bridge (4.80 – 5.10 ppm) and the single imino protio-environment (8.54 ppm).

The presence of only two doublets in the methylene bridge region and only one singlet resonance in the imine region (~8.5 ppm) suggested that there was only one ligand environment present. Along with the absence of a isopropoxide septet (~4.0 ppm) it was concluded that the metal-to-ligand ratio of 1:2 was maintained in solution.

Analysis of material isolated for Compound **1**B *via* ^{1}H NMR spectroscopy produced a spectrum with features similar to that obtained for Ti(**1**)$_2$. A single imine resonance was observed (8.53 ppm) and an AX spin system of two doublets at 4.85 ppm and 5.07 ppm suggesting the presence of the 1:2 metal-to-ligand complex (Figure 2.18).

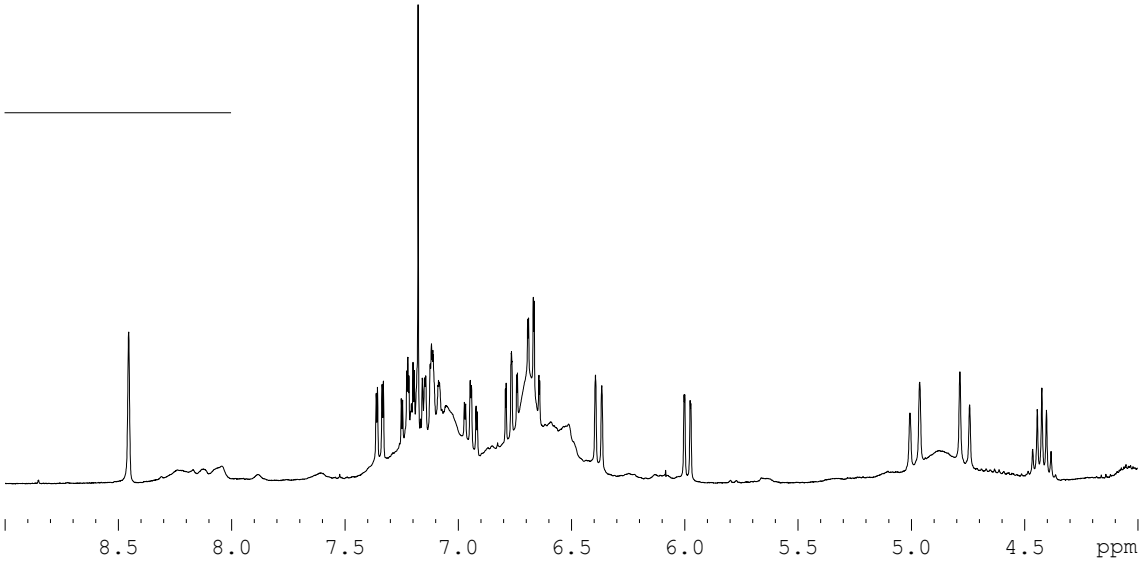

Figure 2.18 Extract of ^{1}H NMR spectrum for Compound **1**B, synthesised *via* Procedure B. Showing a single strong imine resonance (8.53 ppm) and diastereotopic doublets (4.85 ppm, 5.07 ppm) similar to that observed for Ti(**1**)$_2$.

However, unlike Ti(**1**)$_2$, the spectra also contained a septet at 4.51 ppm which was attributed to the presence of isopropoxide {OC**H**$(CH_3)_2$}. It should be noted that the chemical shift observed for this resonance was significantly lower than that for complex Ti_2(**3**)$_2(O^iPr)_4$ (4.93 ppm, see below) where solid-state analysis confirmed the isopropoxide was bound to the titanium of the metal-imine bis(phenolate) complex. With the lack of crystallographic data, it was possible that unreacted $Ti(O^iPr)_4$ is also present in the sample. This was supported by the presence of only a single resonance for the OCH(C**H**$_3)_2$ of the isopropoxide, differing to that observed for Ti_2(**3**)$_2(O^iPr)_4$. The ^{1}H NMR spectrum displayed the presence of toluene, despite purification by recrystallisation and subsequent drying under reduced pressure. A broad signal was observed under the diastereotopic doublets (4.70 – 5.00 ppm) suggesting the presence of other species, potentially Ti_2(**1**)$_2(O^iPr)_4$, that could not be separated and hindered full characterisation.

Complex Ti(**3**)$_2$, synthesised by the low dilution Procedure A, was recrystallised and analysed by ^{1}H NMR spectroscopy. As with Ti(**1**)$_2$, a 1:2 metal-to-ligand ratio has been proposed due to the single imine resonance and lack of a quantifiable isopropoxide OC**H(**$CH_3)_2$ signal. In the case of Ti(**3**)$_2$ the doublets assigned to the diastereotopic protons of the methylene bridge had a very small difference in chemical shift (0.06 ppm) and therefore there was considerably greater roofing effect on the signals and significant distortion to the relative peak intensities (Figure 2.19).

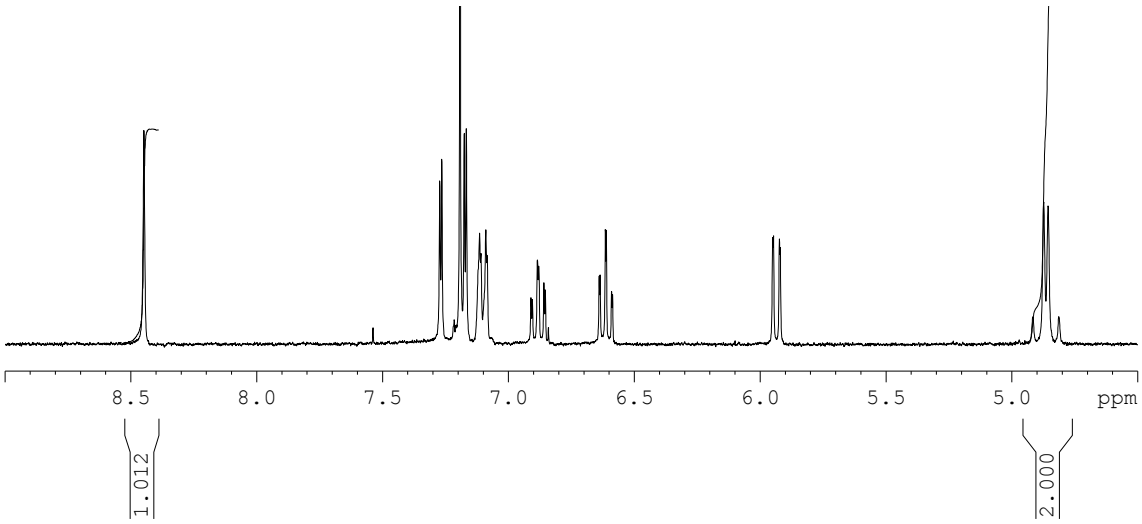

Figure 2.19 Extract of the ^{1}H NMR spectrum ($CDCl_3$) for Ti(**3**)$_2$ showing a single imine resonance (8.45 ppm) and methylene bridge doublets (4.85 ppm) with relative integrals.

The solid-state structure of Ti_2(**3**)$_2$(O^iPr)$_4$ was confirmed in solution ($CDCl_3$) by ^{1}H NMR spectroscopy. At first glance the spectrum appeared lacking the characteristic AX spin-system doublets for the methylene bridge dimer; however analysis of the relative peak intensities suggested the PhC**H**$_2$N signal to be at the same chemical shift as the isopropoxide septet signal (Figure 2.20).

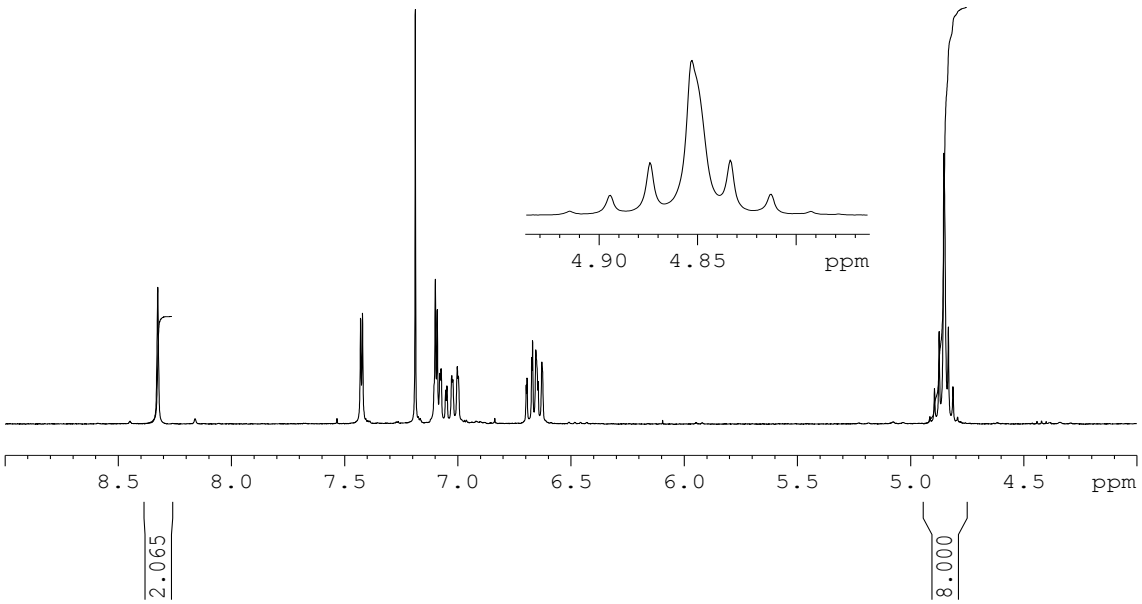

Figure 2.20 Extract of the ^{1}H NMR spectrum ($CDCl_3$) of Ti_2(**3**)$_2$(O^iPr)$_4$ with relative integrals corresponding to ligand-to-isopropoxide group of 1:2. Insert shows distortion to the isopropoxide septet due to overlap with signal for methylene bridge protons.

When the solid-state structure was compared with the ^{1}H NMR spectrum acquired, it was anticipated that two septets may be observed due to the two environments of the isopropoxides; *trans* to the imine nitrogen and *trans* to a bridging oxygen. To further elucidate the nature of the structure in solution and confirm the 1:1 metal-to-ligand ratio, $Ti_2(\mathbf{3})_2(O^iPr)_4$ was analysed *via* ^{1}H NMR spectroscopy in a coordinative solvent (THF-d_8). Changing the solvent caused different chemical shifts and separated the isopropoxide and methylene bridge signals. It also, as a coordinative solvent, had potential to disrupt the dimer structure if it does persist in solution (Figure 2.21).

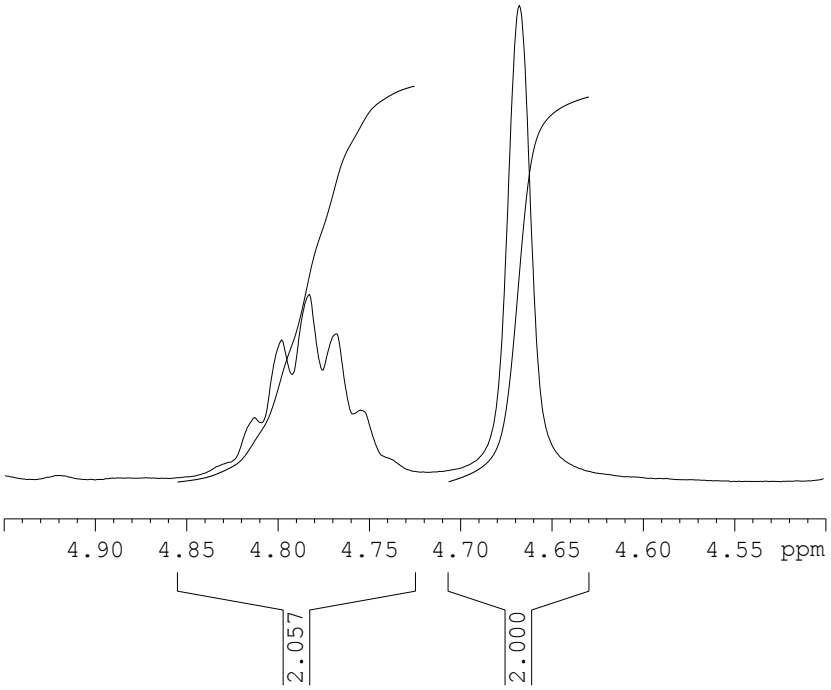

Figure 2.21 Extract of the ^{1}H NMR spectrum (THF-d_8) for $Ti_2(\mathbf{3})_2(O^iPr)_4$. Whilst the resonances appear separate this corresponds to a metal-to-ligand ratio of 1:1 with two isopropoxide groups per metal centre.

^{1}H NMR spectroscopy in THF-d_8 separated the isopropoxide and methylene bridge signals. The appearance of the methylene bridge as a singlet (4.67 ppm) suggests that the ligand is not strongly bound as observed in the solid-state but more labile, the CH_2 protons appearing both chemically and magnetically equivalent. Spectroscopy was carried out over a temperature range (298 K to 218 K) however no further splitting was observed preventing the determination of any monomer-dimer equilibrium.

2.5 Trialling of Al (III) and Ti (IV) complexes as initiators for the ROP of *rac*-lactide

Aluminum (III) imine bis(phenolate) complexes $Al_2(Me)_2(\mathbf{1}\text{-}\mathbf{5})_2$ were trialled as initiators for the ring-opening polymerisation of *rac*-lactide in the presence of one equivalent of benzyl alcohol as a co-initiator. Titanium (IV) imine bis(phenolate) complexes $Ti(\mathbf{1})_2$, Compound **1**B, $Ti(\mathbf{3})_2$ and $Ti_2(\mathbf{3})_2(O^iPr)_4$ were also trialled as initiators for the ROP of lactide (Figure 2.22). Monomer conversion was calculated *via* ^{1}H NMR spectroscopy, hense an expected polymer molecular weight (M_n) based on monomer-to-initiator ratio ([M]:[I]) and conversion could be determined. Polymer molecular weight and polydispersity were measured by gel permeation chromatography (GPC) and polymer tacticity quantified as a P_r value as calculated by tetrad intensity from homonuclear decoupled ^{1}H NMR spectroscopy.

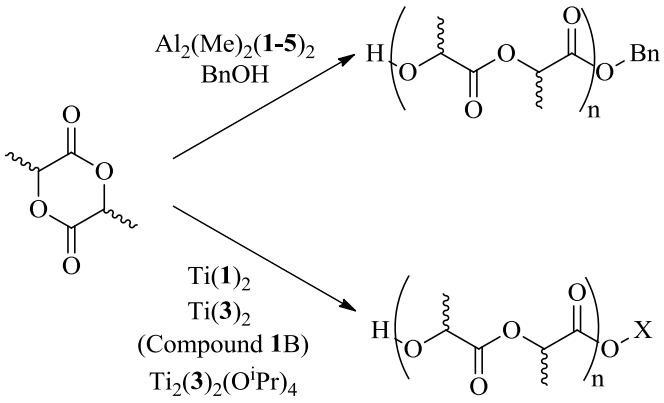

Figure 2.22 Trialling of aluminium and titanium imine bis(phenolate) complexes as initiators for the ROP of *rac*-lactide.

2.5.1 Al (III) imine bis(phenolate) initiators

$Al_2(Me)_2(\mathbf{1}\text{-}\mathbf{5})_2$ provided complexes with only the 5°-5° structural motif, $Al_2(Me)_2(\mathbf{1})_2$, and the 6°-4° motif, $Al_2(Me)_2(\mathbf{5})_2$. Along with ligands with a 'mid-range' steric requirement and the electronic effect of the di-chloro-substituents of $Al_2(Me)_2(\mathbf{4})_2$, the selection provided a broad range of the initiators that were fully characterised. Polymerisations were carried out in toluene at a lactide concentration, [LA], of 0.8 M and a monomer-to-initiator ratio, [LA]:[I], of 100:1. Ratios were calculated "per metal centre" due to the dimer dissociation observed in a coordinative solvent.

Entry	Initiator	Time /h	Conv. /% [a]	M_n^{calc}	M_n [b]	PDI[b]	P_r [c]
1	$Al_2(Me)_2(\mathbf{1})_2$	24	97	14100	24250	1.41	0.53
2	$Al_2(Me)_2(\mathbf{2})_2$	24	97	14100	11800	1.19	0.47
3	$Al_2(Me)_2(\mathbf{3})_2$	24	95	13800	10300	1.22	0.56
4	$Al_2(Me)_2(\mathbf{4})_2$	24	99	14350	13050	1.32	0.45
5	$Al_2(Me)_2(\mathbf{5})_2$	24	90	13050	21125	1.07	0.55

[a] As determined *via* ^{1}H NMR, [b] Determined from GPC (in THF) referenced to polystyrene standards. It is noted that a Mark-Houwink correction is not applied; this is discussed in section 5.1.2. [c] Calculated from the ^{1}H homonuclear decoupled NMR ($CDCl_3$) analysis. The calculated molecular weights were determined by the following (144 ×conversion) + 108 {where 108 is the mass of the end groups (H/OCH_2Ph)}

Table 2.6 Solution polymerisation studies for the ROP of *rac*-lactide by $Al_2(Me)_2(\mathbf{1}\text{-}\mathbf{5})_2$ in the presence of benzyl alcohol. [LA] = 0.8 M, [I]:[BnOH] = 1:1, 253 K, toluene.

Entries 1-5 of Table 2.6 provided initial screening of $Al_2(Me)_2(\mathbf{1}\text{-}\mathbf{5})_2$ for the ROP of *rac*-lactide. All initiators proved active with high conversion achieved in each case. High molecular weights were achieved with molecular weights close to that expected being obtained for initiators $Al_2(Me)_2(\mathbf{2}\text{-}\mathbf{4})_2$. In the case of $Al_2(Me)_2(\mathbf{1})_2$ and $Al_2(Me)_2(\mathbf{5})_2$ (Entries 1 & 5) molecular weights, as determined by GPC, were considerably higher than expected for high conversion and a [LA]:[I] of 100:1. Studies of $Al_2(Me)_2(\mathbf{1})_2$ in THF-d_8 (Figure 2.13) showed that potentially one form of the 5°-5° structural motif was undisturbed by a coordinative solvent. This could explain the higher molecular weight (M_n) observed due to catalyst inactivity *via* a coordination-insertion mechanism. A similar inherent inactivity may be present in the 6°-4° structural motif due to the lack of methyl groups on the six-coordinate aluminium. Due to the high reactivity of the Aluminium-methyl bond, it is likely that a metal alkoxide species is formed *in-situ* between the metal complex and benzyl alcohol before further initiation and propagation *via* a coordination-insertion mechanism. This process would not be straight forward for the six-coordinate Aluminium, where all methyl groups have been removed. PDI was higher for the less-sterically hindered $Al_2(Me)_2(\mathbf{1})_2$ compared to $Al_2(Me)_2(\mathbf{5})_2$ which had significant steric bulk due to the *t*-butyl groups. This increased steric bulk would lower the rate of undesirable transesterification reactions that would increase the polydispersity. With respect to polymer tacticity, all polymeric material was found to be essentially atactic suggesting $Al_2(Me)_2(\mathbf{1}\text{-}\mathbf{5})_2$ had no stereoselectivity.

Entry	Initiator	[M]:[I]	Conv. /% [a]	M_n^{calc}	M_n [b]	PDI[b]	P_r [c]
1	$Al_2(Me)_2(\mathbf{1})_2$	50:1	99	7250	11450	1.49	0.47
2	$Al_2(Me)_2(\mathbf{1})_2$	100:1	97	14100	24250	1.41	0.53
3	$Al_2(Me)_2(\mathbf{1})_2$	200:1	98	28350	51525	1.28	0.51
4	$Al_2(Me)_2(\mathbf{5})_2$	50:1	99	7250	9975	1.20	0.54
5	$Al_2(Me)_2(\mathbf{5})_2$	100:1	90	13050	21125	1.07	0.55
6	$Al_2(Me)_2(\mathbf{5})_2$	200:1	99	28600	19725	1.37	0.56

Table 2.7 Solution polymerisation studies for the ROP of *rac*-lactide by $Al_2(Me)_2(\mathbf{1})_2$ and $Al_2(Me)_2(\mathbf{5})_2$ at varying monomer-initiator ratios. [LA] = 0.8 M, [I]:[BnOH] = 1:1, 253 K, toluene.

To further investigate the discrepancy in expected versus measured polymer molecular weight, polymerisations with $Al_2(Me)_2(\mathbf{1})_2$ and $Al_2(Me)_2(\mathbf{5})_2$ were repeated with [LA]:[I] at 50:1 and 200:1. For $Al_2(Me)_2(\mathbf{1})_2$ all polymerisation provide a higher molecular weight than expected but the molecular weight does increase as expected, approximately doubling from entry 1 to entry 2 and then doubling again as the loading was halved from 100:1 to 200:1 (entry 2 and 3). This suggested that the inactivity was related to the nature of the complex rather than an artefact of the experimental procedure and that as expected with a living polymerisation, molecular weight could be controlled by the monomer-initiator ratio. Molecular weight was less controlled for $Al_2(Me)_2(\mathbf{5})_2$ with a lower molecular weight achieved for 200:1 compared to 100:1 suggesting other unknown factors were present.

Entry	Initiator	Time /h	Conv. /% [a]	M_n^{calc}	M_n [b]	PDI[b]	P_r [c]
1	$Al_2(Me)_2(\mathbf{1})_2$	6	97	14100	21325	1.10	0.55
2	$Al_2(Me)_2(\mathbf{1})_2$	24	97	14100	24250	1.41	0.53

Table 2.8 Solution polymerisation studies for the ROP of *rac*-lactide by $Al_2(Me)_2(\mathbf{1})_2$ at different reaction times. [LA] = 0.8 M, [I]:[BnOH] = 1:1, 253 K, toluene.

The high conversion achieved for all initiator loadings suggested that a reaction time of 24 hours was more than adequate for the activity of these catalytic initiators. Entry 1 reduced the reaction time to six hours and high conversion was still obtained. Molecular weight (M_n) was comparable at both 6 and 24 hour reaction times which suggested that initiation was rapid at the

start of the reaction, as expected and desired for a controlled living polymerisation. PDI was significantly lower at the shorter reaction time; it was therefore possible that the extended reaction time of 24 hours provided opportunity for transesterification to take place, widening the polydispersity. It should also be noted that polymer tacticity was comparable at both 6 and 24 hours further confirming the lack of stereoselectivity of this initiator; rather than it being caused by excessive transesterification post-polymerisation.

Kinetic studies of the ROP of *rac*-lactide were carried out for $Al_2(Me)_2(\mathbf{1})_2$ to further quantify the activity of this initiator. Studies were carried out 0.6 ml of toluene-d_8 at 253 K with conversion measured *in-situ* using ^{1}H NMR spectroscopy. Studies of both *rac*-lactide (Figure 2.23) and L-lactide (Figure 2.24) showed ROP to be pseudo-first order with respect to lactide concentration.

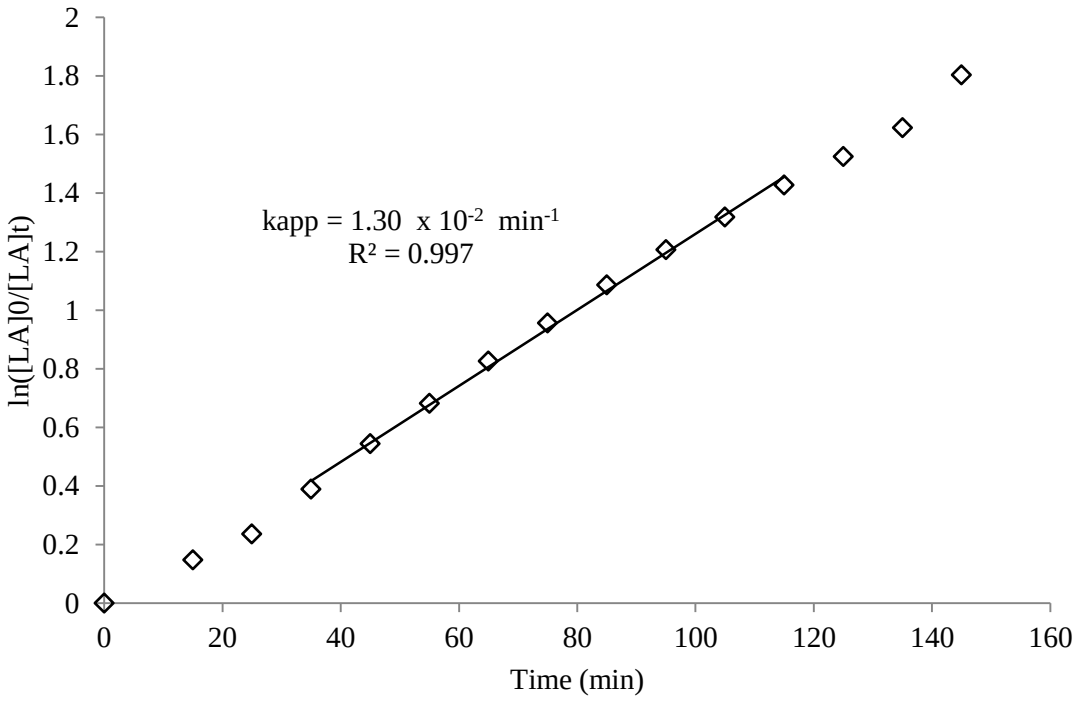

Figure 2.23 Semi-logarithmic plot for the ROP of *rac*-lactide by $Al_2(Me)_2(\mathbf{1})_2$ showing *pseudo*-first order kinetics. [LA] = 0.8 M, [LA]:[I]:[Bn] = 100:1:1, 253 K, toluene-d_8

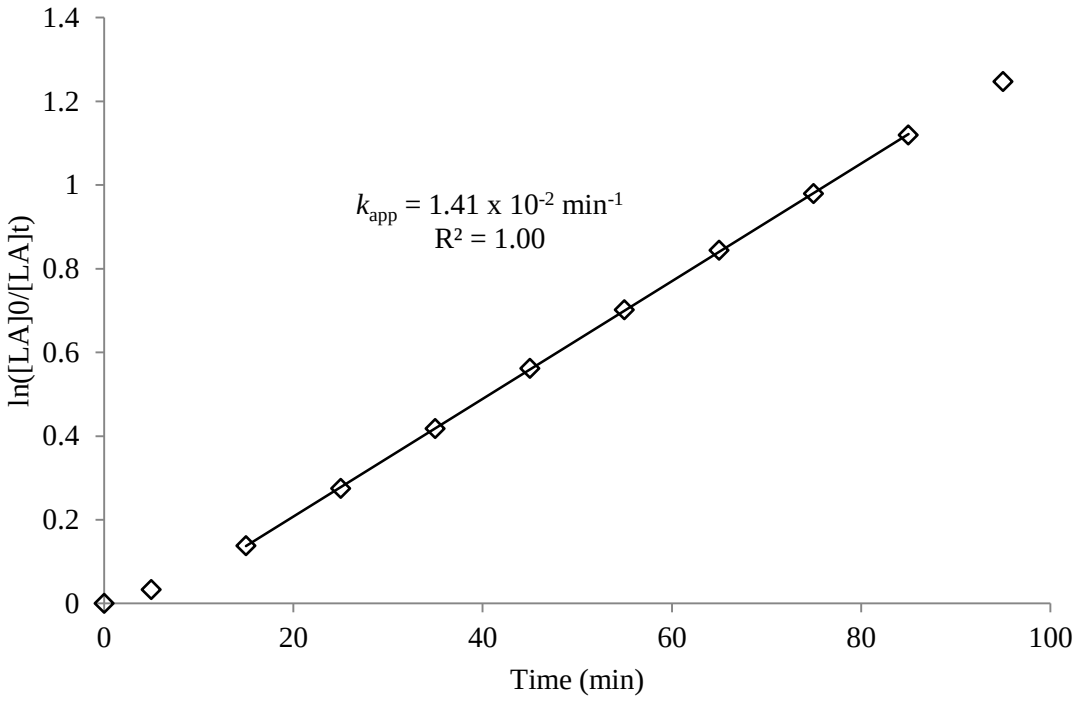

Figure 2.24 Semi-logarithmic plot for the ROP of L-lactide by $Al_2(Me)_2$(**1**)$_2$ showing *pseudo*-first order kinetics. [LA] = 0.8 M, [LA]:[I]:[Bn] = 100:1:1, 253 K, toluene-d_8

Apparent rate constants (k_{app}) were calculated and found comparable for both *rac*-lactide and L-lactide, 1.30 × 10^{-2} min^{-1} and 1.41 × 10^{-2} min^{-1} respectively. Similar rate constants for both racemic and enantiopure lactide further confirmed that $Al_2(Me)_2$(**1**)$_2$ was not stereoselective. Previous reports have used kinetic data to predict stereocontrol.[12] Where $k_{(rac)}$ is the rate constant for the ROP of *rac*-lactide and $k_{(L\text{-}L)}$ is the rate constant for the ROP of L-lactide, P_r can be calculated as follows:

$$P_r = 1 - \frac{1}{2}\left(\frac{k_{(L-L)}}{k_{(rac)}}\right)$$

Under the assumption that the concentration and order with respect to the initiator were constant for the ROP of lactide, rate constants was directly proportional to apparent rate constant (k_{app}) and thus for $Al_2(Me)_2$(**1**)$_2$: $\frac{k_{app(L-L)}}{k_{app(rac)}} = 1.08$ and therefore P_r = 0.46, which was comparable to that measured *via* homonuclear decoupled ^{1}H NMR of polymeric material.

2.5.2 Ti (IV) imine bis(phenolate) initiators

Titanium (IV) imine bis(phenolate) complexes Ti(**1**)$_2$, Compound **1**B, Ti(**3**)$_2$ and Ti$_2$(**3**)$_2$(O^{i}Pr)$_4$ were also trialled as initiators for the ROP of lactide. The presence of O^{i}Pr groups in Compound **1**B and Ti$_2$(**3**)$_2$(O^{i}Pr)$_4$ meant no co-initiator was required. Polymerisation were carried out under solvent-free conditions at 130 °C (403 K) and at a monomer-initiator ratio of 300:1 and calculated on a per-metal-centre basis.

Entry	Initiator	Time /h	Conv. /% [a]	M_n^{calc}	M_n [b]	PDI [b]	P_r [c]
1	Ti(**1**)$_2$	24	-	-	-	-	-
2	Compound **1**B	0.5	60	26200	29950	1.20	0.54
3	Ti(**3**)$_2$	4.7	46	19950	19750	1.51	0.53
4	Ti$_2$(**3**)$_2$(O^{i}Pr)$_4$	2.5	69	29900	22550	1.26	0.50

[a] As determined *via* ^{1}H NMR, [b] Determined from GPC (in THF) referenced to polystyrene standards. It is noted that a Mark-Houwink correction is not applied; this is discussed in section 5.1.2. [c] Calculated from the ^{1}H homonuclear decoupled NMR ($CDCl_3$) analysis. The calculated molecular weights were determined by the following (144 × 3 x conversion) + 60 {where 60 is the mass of the end groups (H/OCH(CH$_3$)$_2$)}

Table 2.9 Solvent-free polymerisation of *rac*-lactide initiated by titanium imine bis(phenolate) complexes. [LA]:[I] = 300:1, 403 K.

Ti(**1**)$_2$ (Table 2.9, entry 1) provided no polymeric material. This confirmed the lack of any initiating groups and the inactivity of this octahedral complex, with a 1:2 metal-to-ligand ratio, as an initiator for the ROP of lactide. Entries 2-4 highlight the polymeric material yielded in the presence of Compound **1**B, Ti(**3**)$_2$ and Ti$_2$(**3**)$_2$(O^{i}Pr)$_4$ respectively. All produced essentially atactic polymeric material ($P_r \approx 0.5$) as seen with previously reported titanium complexes.[9, 10, 13] Spectroscopic analysis of Compound **1**B and Ti(**3**)$_2$ suggested significant amounts of the ROP-inactive species with a metal-to-ligand ratio of 1:2 were present; in the case of Ti(**3**)$_2$ no quantifiable amount of isopropoxide was detected. However, entry 2 and 3 showed that polymer was generated leading to the conclusion that either initiating isopropoxide groups must be present or the phenolate of the ligand is able to act as an initiating group. In the case of Ti(**3**)$_2$, the higher PDI suggests there could be unreacted Ti(O^{i}Pr)$_4$, previously reported as producing polylactide with a broader polydispersity.[6] Polymer yielded through initiation using Ti$_2$(**3**)$_2$(O^{i}Pr)$_4$ had a lower PDI than that reported for other Ti (IV) based initiators but also significantly lower activity, achieving 69 % conversion in 2.5 hours.[11] Molecular weight (M_n)

was lower than expected based on conversion. This could be attributed to the possibility of two polymer chain growing per metal centre due to the presence of two isopropoxide groups per metal centre, however if so, it cannot be the case for all metals as molecular weight was not halved.

To further investigate the behaviour of $Ti_2(\mathbf{3})_2(O^iPr)_4$ as an initiator for the ROP of *rac*-lactide initiator loading was varied (Table 2.10).

Entry	Initiator	[LA]:[I]	Time /h	Conv. /% [a]	M_n^{calc}	M_n [b]	PDI[b]	P_r [c]
1	$Ti_2(\mathbf{3})_2(O^iPr)_4$	150:1	1.9	89	19300	16380	1.30	0.55
2	$Ti_2(\mathbf{3})_2(O^iPr)_4$	300:1	2.5	69	29900	22550	1.26	0.50
3	$Ti_2(\mathbf{3})_2(O^iPr)_4$	600:1	3.0	43	37250	29650	1.16	0.49

Table 2.10 Solvent-free polymerisation of *rac*-lactide with $Ti_2(\mathbf{3})_2(O^iPr)_4$ altering monomer-to-initiator ratio, [LA]:[I]. Reaction time as stated, 403 K

As expected, due to the living nature of the polymerisation, reducing the loading of initiator resulted in an increase in molecular weight. However, the increase observed was not representative of the change in initiator loading. These results suggested that for this titanium imine bis(phenolate) complex, where dimer dissociation is necessary and the potential for multiple polymer chains per metal centre are possible, impacting molecular weight control and, as with other titanium initiators reported in this work, no stereocontrol.

2.6 Conclusions and further work

Through the use of salicylammonium acetate, or the di-*tert*-butyl substituted derivative, a wide range of imine bis(phenolate) tridentate ligands were able to be synthesised. Unlike many previously published ligands and complexes, the utilisation of the acetate starting material gave access to species with a methylene bridge whilst still maintaining the unsymmetrical phenolate substitution where desired.

Coordination of ligands H_2**1**-**7** to trimethyl aluminium produced dimers with a ligand-to-metal ratio of 1:1. Two structural motifs were isolated in the solid-state, one consisting of two metal centres both with five-coordinate geometry (5°-5°) and the second offering a dimer with aluminium existing in both a six-coordinate and four-coordinate environment (6°-4°). ^{1}H NMR spectroscopic studies gave evidence of a potential second isomer for the 5°-5° geometry and it has been suggested that this was a 'trans' arrangement of the remaining methyl groups on the aluminium metal centres. Whilst structural data in the solid-state for all isolated complexes showed that the 'methylene-side' phenolate acted as a bridge in both dimer motifs, crude spectroscopic analysis of $Al_2(Me)_2$(**6**-**7**)$_2$ showed the presence of multiple species and this work has outlined possible motifs where dimer bridging is facilitated by the imine phenolate.

A narrower investigation was carried out for the behaviour of these tridentate ligands through the coordination of H_2**1** and H_2**3** to titanium (IV) isopropoxide. Two structural motifs were isolated in the solid-state and fully characterised in solution using NMR spectroscopy. These consisted of a monomeric species with a ligand-to-metal ratio of 2:1, Ti(**X**)$_2$, and a dimer species Ti_2(**X**)$_2$(O^iPr)$_4$. From a coordination chemistry point of interest it was noted that whilst the preferable motif for the $Al_2(Me)_2$(**X**)$_2$ appeared to be wholly dependent on the steric demands of the imine bis(phenolate) ligand, the motif formed for the titanium analogues could be influenced by the experimental procedure followed. The steric requirement of the ligand still had an affect with the Ti(**X**)$_2$ complex considerably more preferable for the unsubstituted Ti(**1**)$_2$. The greater available control in structural motif observed for the titanium analogues was attributed to the larger coordination sphere of the titanium metal centre relative to aluminium.

Complexes $Al_2(Me)_2$(**1**-**5**)$_2$, in the presence of one equivalent of benzyl alcohol per metal centre as a co-initiator, were found to be active for the ROP of *rac*-lactide. Higher PDIs were measured for the less sterically demanding complexes, $Al_2(Me)_2$(**1**)$_2$ and $Al_2(Me)_2$(**4**)$_2$, and this was attributed to a potential for higher rates of transesterification during polymer propagation. Studies in coordinative solvent indicated that one isomer of the 5°-5° motif appeared undistrupted and thus likely inactive as an initiator for ROP, this would limit the ability to

control molecular weight through monomer-initiator ratio. Initiator loading studies for both $Al_2(Me)_2(\mathbf{1})_2$ and $Al_2(Me)_2(\mathbf{5})_2$ highlighted that whilst polymer molecular weight was higher than expected it was controlled by initiator loading. This allowed for the conclusion that the discrepancy was due to initiator inactivity rather than experimental error. Despite the significant variation in steric bulk of the phenyl substituents, all initiators were found to be non-stereoselective for the ROP of *rac*-lactide.

This lack of stereoselectivity was in contrast to the early aluminium bis(salen) complexes reported by Nomura *et al.*.[14] The larger tetradentate ligands gave rise to monomeric species that, with *tert*-butyl groups in the ortho position of the donor phenolates, could yield highly isotactic PLA.[14] The dimeric nature of the aluminium complexes presented in this thesis can be compared to that reported by Darensbourg *et al.* for a range of chiral and achiral half-salen complexes with similarly tridentate ligands.[1] Polymeric material produced using these aluminium half-salen complexes generally had a narrower PDI than that produced using the initiators studied herein. However, Darensbourg *et al.* reported that kinetics studies suggested initiator aggregation during propagation and, that whilst potentially hindering transesterification due to increased steric bulk about the metal centres, also resulted in slower apparent rate constants (k_{app}). Pseudo first-order rate constants for $Al_2(Me)_2(\mathbf{1})_2$ are reported as an order of magnitude higher than for the dimers reported by Darensbourg *et al.*.[1]

Polymeric material was found to have similar molecular weights to that produced using monomeric aluminium salalen {ONNO} complexes, previously reported by the Jones research group.[15] However, these complexes with tetradentate ligands provided narrowly dispersed polymeric material even with sterically small ortho-phenolate substituents. Whereas for the smaller tridentate aluminium imine bis(phenolate) complexes a noticeable trend was seen as steric bulk of the substituents was increased. Compared to the tetradentate aluminium homopiperazine complexes presented by Jones *et al.*, complexes $Al_2(Me)_2(\mathbf{1\text{-}5})_2$ produced polymeric material of a narrower polydispersity and it proposed this is due to the fixed dimer motif rather than the fluxional form reported for the homopiperazine complexes.[16]

It is also prudent to compare these aluminium imine bis(phenolate) complexes to the recently reported mono- and di-methyl aluminium pyrrolylaldiminates by Hormnirun *et al.*.[17] In comparison to these smaller bidentate ligands, polydispersity is comparable whilst $Al_2(Me)_2(\mathbf{1})_2$ maintains an apparent rate constant (k_{app}) an order of magnitude larger than both the mono- and dimethyl pyrrolylaldiminate complex that incorporate an ortho-^{t}Bu-substitued ring, suggesting that changing to a "too-small-a-ligand" does not necessarily benefit activity.

As with the aluminium initiators trialled, all titanium-based initiators were found to be essentially non-stereoselective, as reported for the majority of titanium complexes.[18] As expected, Ti(**1**)$_2$ was found to be inactive for the ROP of *rac*-lactide due to the lack of initiating isoproxide groups. Conversely, Ti(**3**)$_2$ was active which suggested the presence of unidentified initiating groups. With the larger coordination sphere of titanium with respect to Aluminium a lower degree of molecular weight control was observed, with the initiator loading study providing a less predictable polymer molecular weight suggesting the ability for multiple growing chains per metal centre and the presence of other active species.

The imine bis(phenolate) ligand system has less control over the resulting complex motif, with the synthetic methodology and ligand steric bulk influencing the resulting structural motif. This is in contradiction to titanium (IV) complexes reported with larger tetradentate bis(salen) and amine bis(phenolate) complexes which were monomeric octahedral geometries.[10, 19]

The synthetic methodology used to create the imine bis(phenolate) ligands presented in this work can be expanded to provide a much wider range of ligands both in terms of steric bulk and electronic properties of the phenyl-substituents. In this work the methylene-side phenolate was unsubstituted or di-*tert*-butyl substituted. Readily available dimethyl-substituted and dichloro-substituted salicylaldehydes could provide access to the corresponding ammonium acetate expanding the range of ligands considerably (Figure 2.25).

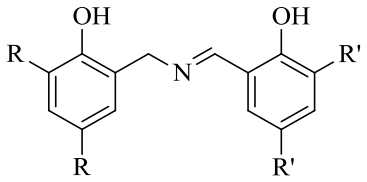

R = R' = Me
R = Me, R' = Cl
R = Me, R' = ^{t}Bu
R = Cl, R' = H
R = R' = Cl
R = Cl, R' = Me
R = Cl, R' = ^{t}Bu

Figure 2.25 Further imine bis(phenolate) ligands possible *via* other substituted salicylammonium actetates.

Expanding the ligand set would provide analogues that only varied in the placement of the substituents with respect to the imine bond. This would allow investigation into whether dimer bridging was always facilitated by the methylene-side phenolate or if in some cases the steric requirement of the phenolate substituents overrides this. This would provide insight into the other isomers that seem to be present in the crude ^{1}H NMR spectra of $Al_2(Me)_2$(**6-7**)$_2$.

Attempts could also be made to create substituted imine bis(phenolate) ligands with greater steric bulk, for example trityl substituents that may force the formation of monomeric aluminium species and remove the dilution control that was observed for the synthesis of the titanium analogues.

All of these potential new imine bis(phenolate) complexes could be studied in a coordinative solvent to ascertain if the susceptibility of the dimer to disruption is controlled by the steric demand of the phenolate substituents. Those active for the ROP of *rac*-lactide could undergo a kinetic study akin to that present herein for $Al_2(Me)_2(\mathbf{1})_2$ to further probe the role of ligand substituents on activity. With the increase in use of DFT as tool by synthetic chemists, this computational approach could be further used to understand the apparent stability of one dimeric motif/isomer over another.

However, it should be noted that all of the initiators presented in this work showed no stereoselectivity for the ROP of *rac*-lactide and in the case of the aluminium analogues a large range of substituents were screened. It is therefore unlikely that, whilst providing an interesting study of coordination behaviour and useful insight into the ongoing issue with identifying ROP-active species, the expansion of the ligand set would not yield any stereoselective initiators. They would therefore not provide any advantage over $Al(O^iPr)_3$ or any other aluminium complexes already presented in the literature. Placing the findings of this study within the literature, pseudo first-order rate constants for $Al_2(Me)_2(\mathbf{1})_2$ are reported at an order of magnitude higher than both the tridentate half-salen complexes and smaller bidentate pyrrolylaldiminates, however, with the loss of stereoselectivity. Initiators previously published by Darensbourg achieved isotactic stereoselectivity with aluminium half-salen complexes both with and without chirality in the more flexible alky-side of the donor; however these were slower due to initiator aggregation.[1] Whilst catalytic studies were not carried out to establish order with respect to initiator for the $Al_2(Me)_2(\mathbf{X})_2$ presented in this thesis, larger steric bulk of the phenyl ring on the methylene-side of the bis(phenolate) potentially creates a more discreet ROP-active species. It should be noted that enantiomorphic site control is proposed for both complexes with the chiral bis(salen)-type ligands and the half-salen ligands so the introduction of steric bulk and ligand chirality should be considered for future studies in this area. Further work of a less predictable outcome would entail the replacement of aluminium and titanium with other metals, such as scandium, yttrium and zinc which have been shown to be both active and selective with phenolate-type ligand systems.

2.7 References

1. D. J. Darensbourg, O. Karroonnirun and S. J. Wilson, *Inorg. Chem.*, 2011, **50**, 6775-6787.
2. Z. H. Tang and V. C. Gibson, *Eur. Polym. J.*, 2007, **43**, 150-155.
3. A. J. Chmura, M. G. Davidson, M. D. Jones, M. D. Lunn and M. F. Mahon, *Dalton Trans.*, 2006, 887-889.
4. I. Zagol-Ikapitte, V. Amarnath, M. Bala, L. J. Roberts, J. A. Oates and O. Boutaud, *Chem. Res. Toxicol.*, 2010, **23**, 240-250.
5. P. D. Knight, P. N. O'Shaughnessy, I. J. Munslow, B. S. Kimberley and P. Scott, *J. Organomet. Chem.*, 2003, **683**, 103-113.
6. Y. Kim, G. K. Jnaneshwara and J. G. Verkade, *Inorg. Chem.*, 2003, **42**, 1437-1447.
7. A. J. Chmura, D. M. Cousins, M. G. Davidson, M. D. Jones, M. D. Lunn and M. F. Mahon, *Dalton Trans.*, 2008, 1437-1443.
8. T. Aida, D. Takeuchi and T. Nakamura, *Macromolecules*, 2000, **33**, 725-729.
9. V. C. Gibson, C. K. A. Gregson, I. J. Blackmore, N. J. Long, E. L. Marshall and A. J. P. White, *Dalton Trans.*, 2006, 3134-3140.
10. A. J. Chmura, M. G. Davidson, M. D. Jones, M. D. Lunn, M. F. Mahon, A. F. Johnson, P. Khunkamchoo, S. L. Roberts and S. S. F. Wong, *Macromolecules*, 2006, **39**, 7250-7257.
11. M. D. Jones, E. L. Whitelaw and M. F. Mahon, *Inorg. Chem.*, 2010, **49**, 7176-7181.
12. N. Nomura, R. Ishii, Y. Yamamoto and T. Kondo, *Chem. Eur. J.*, 2007, **13**, 4433-4451.
13. E. L. Whitelaw, M. D. Jones, M. F. Mahon and G. Kociok-Kohn, *Dalton Trans.*, 2009, 9020-9025.
14. N. Nomura, R. Ishii, M. Akakura and K. Aoi, *J. Am. Chem. Soc.*, 2002, **124**, 5938-5939.
15. E. L. Whitelaw, G. Loraine, M. F. Mahon and M. D. Jones, *Dalton Trans.*, 2011, **40**, 11469-11473.
16. S. L. Hancock, M. D. Jones, C. J. Langridge and M. F. Mahon, *New J. Chem.*, 2012, **36**, 1891-1896.
17. S. Tabthong, T. Nanok, P. Kongsaeree, S. Prabpai and P. Hormnirun, *Dalton Trans.*, 2014, **43**, 1348-1359.
18. A. Sauer, A. Kapelski, C. Fliedel, S. Dagorne, M. Kol and J. Okuda, *Dalton Trans.*, 2013, **42**, 9007-9023.
19. E. Sergeeva, J. Kopilov, I. Goldberg and M. Kol, *Inorg. Chem.*, 2009, **48**, 8075-8077.

CHAPTER 3

UNSYMMETRICAL GROUP IV AMINE TRIS(PHENOLATE) COMPLEXES AS INITIATORS FOR THE ROP OF *RAC*-LACTIDE

3 Unsymmetrical Group IV amine tris(phenolate) complexes as initiators for the ROP of *racemic*-lactide

3.1 Preamble

Poly(phenolate) anionic ligands have been widely shown to be effective ligands for complexes that are active for the catalytic ROP of lactide.[1-5] Particular attention should be drawn to the symmetrical amine tris(phenolate) systems that have proved both highly active and heterotactically-selective for the polymerisation of *rac*-lactide.[6] A range of these tetradentate ligands can be easily synthesised *via* a one-pot modified Mannich reaction, due to the range of 2,4-disubsituted phenol derivatives that are available.[7] Small changes in ligand structure can have a significant effect on the selectivity of the initiator and there are scarce (if any) examples of amine tris(phenolate) ligands that are unsymmetrical with respect to phenolate substituents but maintain the strong anionic bonding offered by the three hydroxyl groups. The work herein presents a systematic study of the influence of symmetry and steric bulk on the catalytic activity and stereoselectivity of the zirconium alkoxide amine tris(phenolate) presented by Davidson *et. al.*[6] Hafnium analogues were also synthesised to provide insight into the effect of metal centre.

3.2 Synthesis of unsymmetrical amine tris(phenolate) ligands

Unlike the aforementioned C_3-symmetrical amine tris(phenolate) ligands,[7] unsymmetrical analogues had to be accessed *via* a step-wise synthesis. Starting material costs and availability led to the use of a salicylammonium acetate as a source of 2-hydroxybenzylamine, synthesised by the coordinative-reduction of salicyaldoxime by zinc in acetic acid, following literature procedures.[8] An amine tris(phenolate) with one unsubstituted phenolate arm (H_3**8**) was accessed by the double addition of a 3,5-di-*tert*-butyl-substituted salicylbromide[9] in the presence of sodium bicarbonate and triethylamine (Scheme 3.1).

Further removal of phenolate substituents and the synthesis of a fully unsymmetrical amine tris(phenolate) was predominately accessed *via* imine bis(phenolate) intermediates (H_2**1**-**2**); these have also been utilised as ligands and have been discussed in chapter 2. The imine bis(phenolate) was reduced to the respective amine bis(phenol) before the addition of a di-*tert*-butyl phenol *via* an S_N2 substitution reaction with the corresponding bromide.

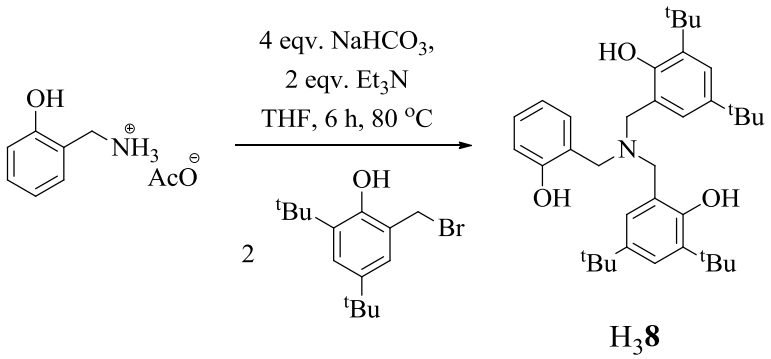

H_3**8**

Scheme 3.1 Synthesis of unsymmetrical amine tris(phenolate) ligand, H_3**8**

Initial attempts at the reduction of H_2**1-2** with sodium borohydride proved problematic with low yields in the subsequent reaction to generate the amine tris(phenolate) (Scheme 3.2). This synthetic result yielded significantly impure product with purification only being achieved through metal coordination.

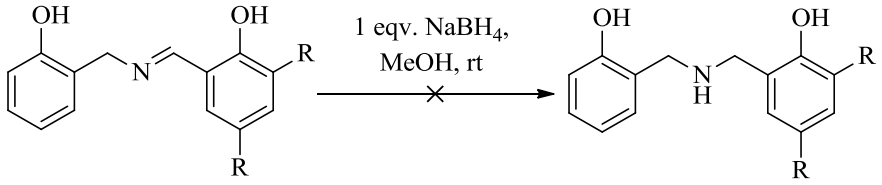

H_2**1**; R = H

H_2**2**; R = Me

Scheme 3.2 Unsuccessful synthetic route for the reduction of unsymmetrical imine bis(phenolate) (H_2**1-2**) using $NaBH_4$

^{1}H NMR spectra of the products from the reduction of H_2**1-2** showed complex splitting of the CH_2 protons (Figure 3.1, Figure 3.2). This was attributed to the diastereotopic nature of the methylene bridge protons due to intermolecular hydrolysis of the boron intermediate. A more complex splitting pattern was also observed for the aromatic protons. Intergrals of the signals were appropriate for an amine bis(phenolate) (H_2**1**) (approx. 8:4).

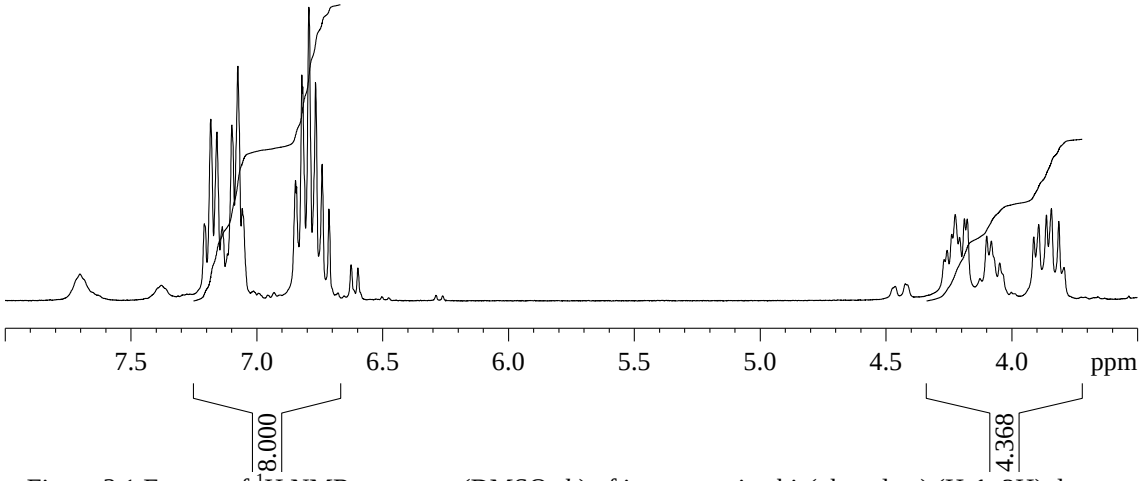

Figure 3.1 Extract of ^{1}H NMR spectrum (DMSO-d_6) of impure amine bis(phenolate) (H_2**1**+2H) due to intermolecular boranamine hydrolysis.

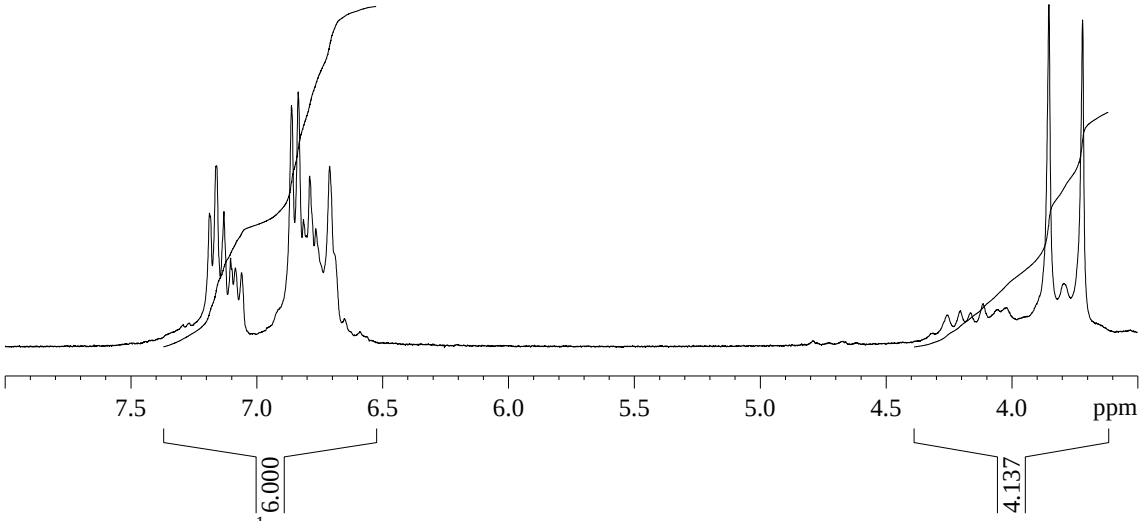

Figure 3.2 Extract of ^{1}H NMR spectrum (DMSO-d_6) of impure amine bis(phenolate) (H_2**2**+2H) due to intermolecular boranamine hydrolysis.

Crystals of an alkoxylated boron amine bis(phenolate) were serendipitously isolated after the crude amine (H_2**1**+2H) was reacted with the substituted bromide and subsequently attempted coordination to Zr(IV) isopropoxide with purification *via* recrystallization in toluene. Single-crystal X-ray diffraction data provided bond lengths similar to that published in the literature for analogous boron compounds with tertiary amines and alkoxides (Figure 3.1).[10, 11]

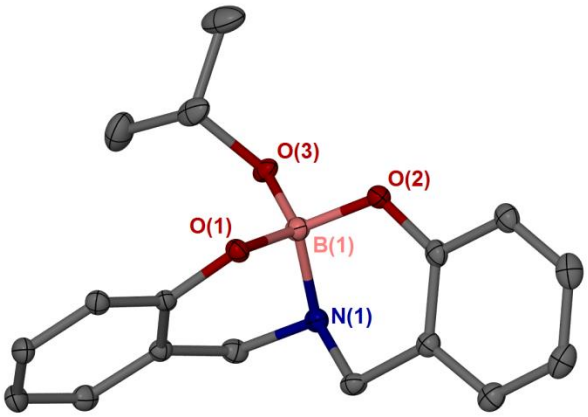

Figure 3.3 Solid-state structure of undesired boron bis(phenolate) isopropoxide as determined by single-crystal X-ray diffraction. Ellipsoids are shown at the 30% probability level. All disorder and hydrogen atoms have been removed for clarity.

	B(**1**)(O^iPr)
B(1) – O(1)	1.454(4)
B(1) – O(2)	1.444(4)
B(1) – O(3)	1.433(4)
B(1) – N(1)	1.620(4)
O(1) – B(1) – O(2)	110.6(3)
N(1) – B(1) – O(3)	106.2(2)

Table 3.1 Selected bond lengths (Å) and bond angles (°) for undesired boron bis(phenolate) isopropoxide as determined by single-crystal X-ray diffraction

In an attempt to reduce this undesired side reaction, the reduction was carried out under acidic conditions to avoid formation of the boranamine intermediate. Whilst this proved more successful for the reduction of H_2**1,** yields of the desired amine was still extremely low for reduction of H_2**2**. Other reductants were trialled in the attempt to achieve a clean synthesis, including the use of $LiAlH_4$ and H_2 over Pd/C, however products were still highly impure. Greatest success was achieved through the use of a benzyl-protected salicylaldehyde (TCI ltd), attributed to the unavailability of the phenolic group as strong anionic donor and the steric-hindrance of the aromatic ring. Synthesis of the mono-protected analogue of imine bis(phenolate) H_2**1** was intitially trialled from the aforementioned salicylammonium acetate and protected salicylaldehyde however, after reduction with $NaBH_4$, products of undesirable side reactions were identified by mass spectrometry (Figure 3.4).

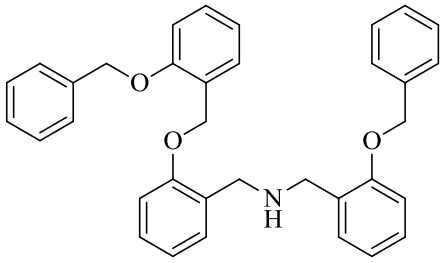

Figure 3.4 Structure of undesirable side products formed from reduction of the imine condensation product of salicylammonium acetate and a protected salicylaldehyde.

Synthesis was further refined by the transformation of the protected-salicylaldehyde into the corresponding ammonium acetate *via* an oxime intermediate. This provided a good yield of the desired imine and clean reduction to the amine. Formation of a mono-protected amine tris(phenolate) could then be synthesised by reaction with the di-substituted benzyl bromide before the removal of the benzyl protecting group under hydrogen with Pd/C to yield the tetradentate ligand suitable for metal coordination. This step-wise methodology is presented in Scheme 3.3.

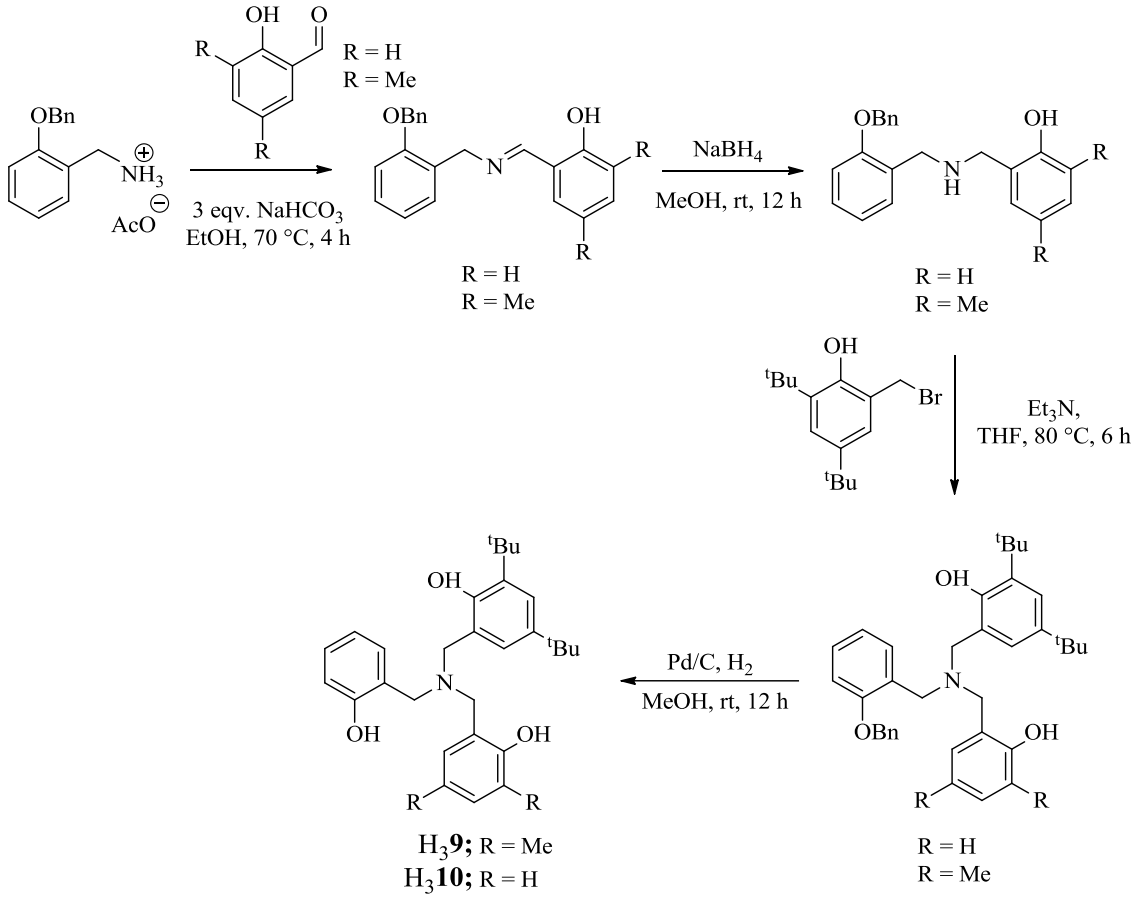

Scheme 3.3 Step-wise synthetic pathway for the formation of unsymmetrical amine tris(phenolate) ligands. Utilising benzyl-protection chemistry to avoid boron enclosure at the imine reduction step

3.3 Coordination of unsymmetrical amine tris(phenolate) ligands to group IV alkoxides

Ligands were coordinated to the group IV metal centres using a 1:1 stoichiometry of the appropriate ligand and metal alkoxide (Scheme 3.4). The reaction was carried out in toluene at room temperature. Basic purification of the complex was achieved by removal of the solvent and recrystallisation in hexane and toluene.

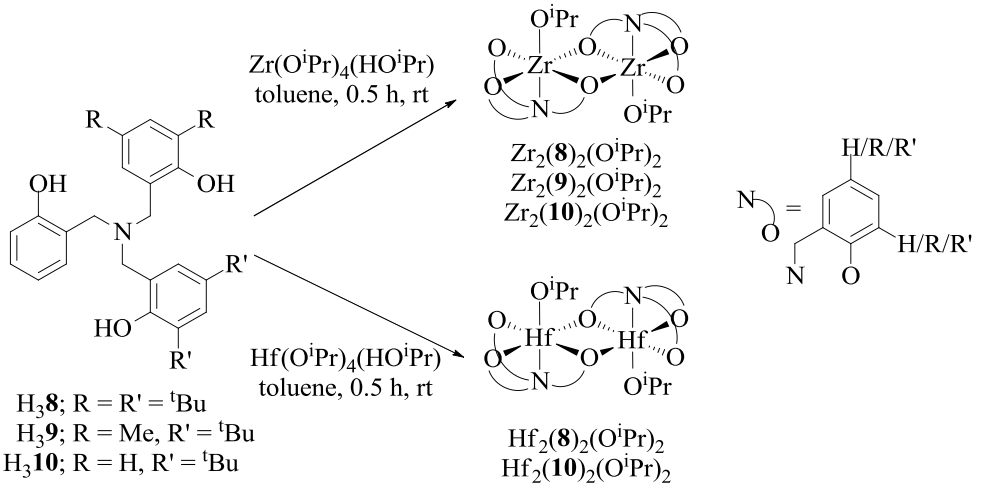

Scheme 3.4 Coordination of unsymmetrical amine tris(phenolate) ligands to group IV metal alkoxides

Due to only small quantities isolated, the coordination of H_3**9** was only carried out with $Zr(O^iPr)_4(HO^iPr)$. All zirconium and hafnium complexes were characterised *via* ^1H and $^{13}C\{^1H\}$ NMR spectroscopy with purity confirmed by element analysis. Structure in the solid-state was determined by single-crystal X-ray diffraction for Zr_2(**8**)$_2(O^iPr)_2$, Zr_2(**9**)$_2(O^iPr)_2$, Hf_2(**8**)$_2(O^iPr)_2$ and Hf_2(**10**)$_2(O^iPr)_2$. From the characterisation data available, all complexes appear to adopt a dimeric structure in both the solid state and solution. Metal centres are six-coordinate in an octahedral geometry. This is in contrast to the monomeric species formed when a C_3-symmetric amine tris(phenolate), where all phenols were 3,5-*tert*-butyl-substituted, was coordinated to Zr(IV): Zr-$C_3{}^tBu$.[6] Crystallographic and ^1H NMR spectroscopic data indicated that the less sterically demanding unsubstituted phenolate acted as the bridge, allowing the more sterically demanding *tert*-butyl substituted phenolate arms of the ligand to project away from the two-metal centres of the dimer. The disruption to C_3-symmetry of an amine tris(phenolate) ligand had previously been reported in the literature, however disruption included the removal of a methylene bridge.[12] Subsequent coordination to zirconium and hafnium isopropoxide also produced dimeric complexes with the non-methylene bridge phenolate acting as the bridging phenolate.

3.3.1 Solid-state single crystal X-ray diffraction

Zr_2(**8**)$_2$(O^iPr)$_2$, Zr_2(**9**)$_2$(O^iPr)$_2$, Hf_2(**8**)$_2$(O^iPr)$_2$ and Hf_2(**10**)$_2$(O^iPr)$_2$ were successfully recrystallised from toluene allowing the collection of single crystal X-ray diffraction data. Zr_2(**8**)$_2$(O^iPr)$_2$, Hf_2(**8**)$_2$(O^iPr)$_2$ and Hf_2(**10**)$_2$(O^iPr)$_2$ were triclinic and crystallised into the *P*-1 space group, whilst Zr_2(**9**)$_2$(O^iPr)$_2$ was trigonal and of the *R*-3 space group. All had inversion point symmetry about the centre of the dimeric complex with pseudo-octahedral geometry of the group IV metal centres. The nitrogen and isopropoxide donors maintained their axial orientation as seen in C_3-symmetrical group IV amine tris(phenolate) complexes.[6]

Whilst all complexes exhibited the same structural motif, closer examination of solid-state structure was carried out between Zr_2(**8**)$_2$(O^iPr)$_2$ (Figure 3.5) and Zr_2(**9**)$_2$(O^iPr)$_2$ (Figure 3.6) in an attempt to draw conclusions on the effect of ligand sterics on dimeric structure.

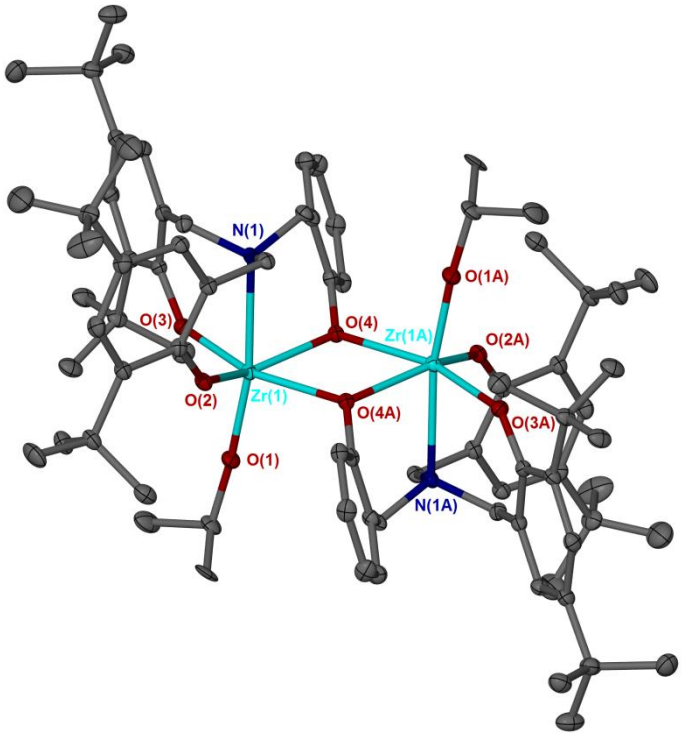

Figure 3.5 Solid-state structure of $Zr_2(\mathbf{8})_2(O^iPr)_2$ as determined by single-crystal X-ray diffraction. Ellipsoids are shown at the 30% probability level. All disorder and hydrogen atoms have been removed for clarity

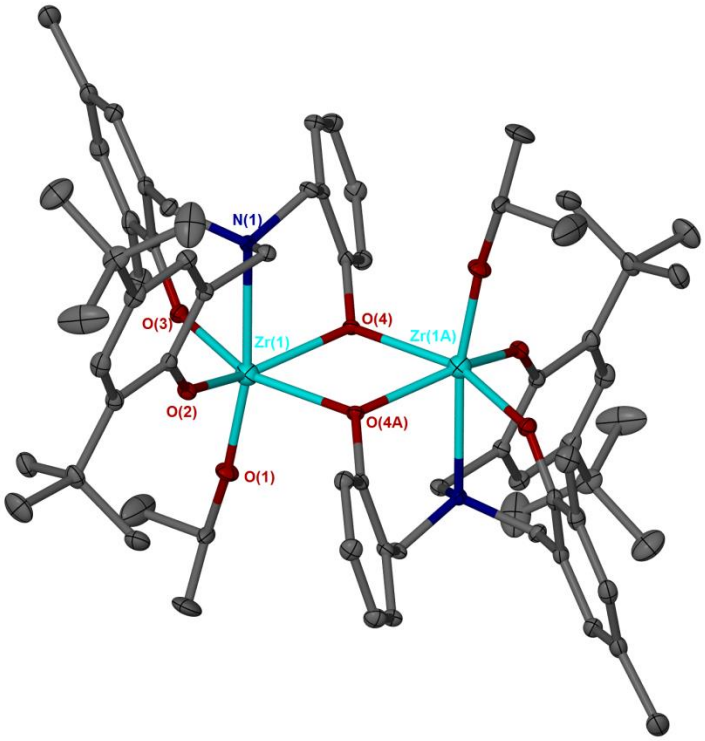

Figure 3.6 Solid-state structure of $Zr_2(\mathbf{9})_2(O^iPr)_2$ as determined by single-crystal X-ray diffraction. Ellipsoids are shown at the 30% probability level. All disorder and hydrogen atoms have been removed for clarity

	$Zr_2(\mathbf{8})_2(O^iPr)_2$	$Zr_2(\mathbf{9})_2(O^iPr)_2$
Zr(1) – O(1)	1.929(2)	1.923(3)
Zr(1) – O(2)	1.984(2)	1.988(3)
Zr(1) – O(3)	2.005(2)	1.985(3)
Zr(1) – O(4)	2.179(2)	2.163(3)
Zr(1) – O(4A)	2.250(2)	2.201(3)
Zr(1) – N(1)	2.450(3)	2.447(4)
O(1) – Zr(1) – N(1)	170.14(10)	169.59(15)
O(2) – Zr(1) – O(3)	105.93(10)	107.79(14)
O(3) – Zr(1) – O(4)	94.72(9)	91.20(13)
O(2) – Zr(1) – O(4A)	89.46(9)	90.71(13)
O(4) – Zr(1) – O(4A)	66.80(10)	67.04(14)
O(1) – Zr(1) – O(2)	98.39(11)	100.15(15)
O(1) – Zr(1) – O(3)	93.91(10)	93.12(15)
O(1) – Zr(1) – O(4)	106.69(10)	105.44(14)
O(1) – Zr(1) – O(4A)	94.28(10)	95.08(14)
N(1) – Zr(1) – O(2)	78.80(10)	77.93(13)
N(1) – Zr(1) – O(3)	77.95(10)	77.92(14)
N(1) – Zr(1) – O(4)	79.80(9)	80.29(12)
N(1) – Zr(1) – O(4A)	95.15(9)	95.18(12)
Zr(1) – O(4) – Zr(1A)	113.20(10)	112.96(14)

Table 3.2 Selected bond lengths (Å) and bond angles (°) for $Zr_2(\mathbf{8})_2(O^iPr)_2$ and $Zr_2(\mathbf{9})_2(O^iPr)_2$ as determined by single-crystal X-ray diffraction.

For both $Zr_2(\mathbf{8})_2(O^iPr)_2$ and $Zr_2(\mathbf{9})_2(O^iPr)_2$ the bridging phenolates exhibited slightly longer Zr-O bond distances. (Table 3.2) Non-bridging Zr-O^{Ph}, the Zr-O^iPr and the Zr-N bond lengths were found to be comparable to monomeric amine tris(phenolate) complexes previously published in the literature.[3] Distortion to the equatorial donors in the axial direction was caused by the formation of the six membered rings incorporating the metal, nitrogen and oxygen atoms. The bond angle between the non-bridging phenolates increased significantly due to the steric repulsion between the phenolate substituents. A further increase was seen for $Zr_2(\mathbf{9})_2(O^iPr)_2$ due to the reduction in steric bulk on one phenolate (^{t}Bu > Me > H) giving rise to a smaller bond angle with the bridging phenolate, O(3)-Zr(1)-O(4). Distortion to the axial bond angle to less than 180° was likely caused by the unfavourable proximity of the isopropoxide group to the opposing ligand. Bond angles of the four-membered ring created between the zirconium centres

and bridging oxygens were distorted due to repulsion between the two ligands. The metal-to-metal distance was slightly less for $Zr_2(\mathbf{9})_2(O^iPr)_2$ compared to $Zr_2(\mathbf{8})_2(O^iPr)_2$ which was attributed to the overall reduction in steric bulk of ligand $H_3\mathbf{9}$ with respect to $H_3\mathbf{8}$.

Similar distortion to the octahedral coordination geometry was seen for $Hf_2(\mathbf{8})_2(O^iPr)_2$ and $Hf_2(\mathbf{10})_2(O^iPr)_2$ due to the polydentate constraints of the amine tris(phenolate) ligand and, unlike the monomeric species, no significant reduction in the hafnium-nitrogen bond length is seen due to the increased oxophilicity of Hf over Zr.[3, 6] Comparison of $Hf_2(\mathbf{8})_2(O^iPr)_2$ (Figure 3.7) and $Hf_2(\mathbf{10})_2(O^iPr)_2$ (Figure 3.8) offered a greater reduction in ligand steric bulk due to the removal of di-*tert*-butyl substituents on two of the phenolate arms. As with the zirconium complexes characterised in the solid-state, removal of ligand steric bulk resulted in less distortion to the axial N(1)-Hf(1)-O(1) bond angle and shorter distance between the two metal centres, Hf(1)-Hf(1A)/(2). However the greater reduction in steric bulk of the phenolate substituents did not result in a larger shift in respective bond angles (Table 3.3). Whilst zirconium and hafnium have similar atomic radius, this was attributed to the more diffuse and flexible coordination sphere of hafnium.

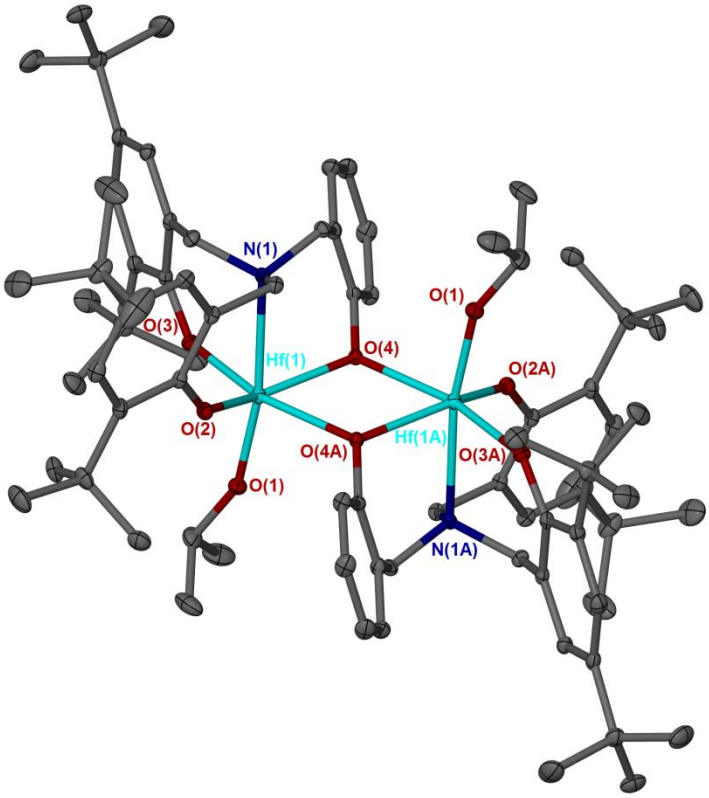

Figure 3.7 Solid-state structure of $Hf_2(\mathbf{9})_2(O^iPr)_2$ as determined by single-crystal X-ray diffraction. Ellipsoids are shown at the 30% probability level. All disorder and hydrogen atoms have been removed for clarity.

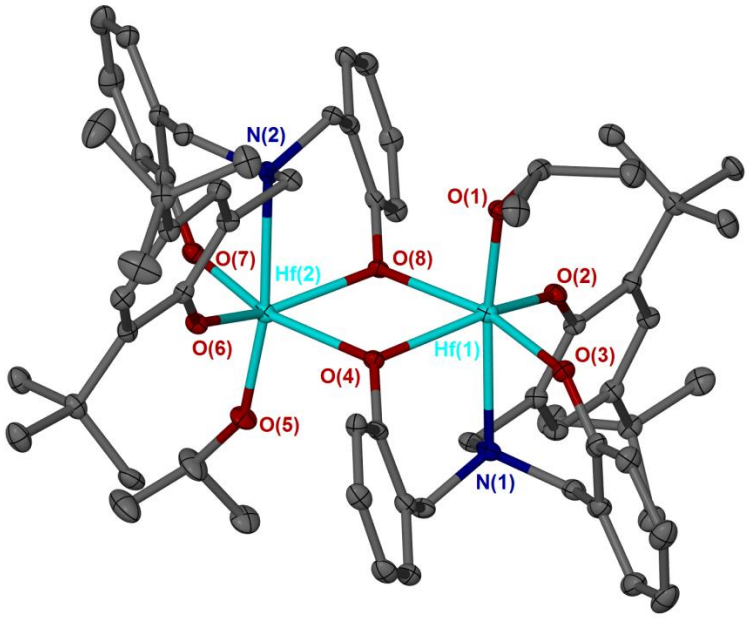

Figure 3.8 Solid-state structure of $Hf_2(\mathbf{10})_2(O^iPr)_2$ as determined by single-crystal X-ray diffraction. Ellipsoids are shown at the 30% probability level. All disorder and hydrogen atoms have been removed for clarity.

	Hf_2(**8**)$_2$(O^iPr)$_2$	Hf_2(**10**)$_2$(O^iPr)$_2$
Hf(1) – O(1)	1.930(2)	1.935(4)
Hf(1) – O(2)	1.977(2)	1.967(4)
Hf(1) – O(3)	1.991(2)	1.993(4)
Hf(1) – O(4)	2.147(2)	2.143(4)
Hf(1) – O(4A)/(8)	2.222(2)	2.207(4)
Hf(1) – N(1)	2.437(3)	2.431(5)
O(1) – Hf(1) – N(1)	169.72(9)	170.21(17)
O(2) – Hf(1) – O(3)	104.88(9)	103.91(17)
O(3) – Hf(1) – O(4)	96.61(8)	96.96(16)
O(2) – Hf(1) – O(4A)/(8)	89.16(8)	88.71(16)
O(4) – Hf(1) – O(4A)/(8)	67.82(9)	68.04(14)
O(1) – Hf(1) – O(2)	98.74(10)	103.65(17)
O(1) – Hf(1) – O(3)	92.45(10)	91.34(17)
O(1) – Hf(1) – O(4)	105.72(9)	101.17(16)
O(1) – Hf(1) – O(4A)/(8)	92.03(9)	93.87(16)
N(1) – Hf(1) – O(2)	78.58(9)	78.93(17)
N(1) – Hf(1) – O(3)	78.80(9)	78.87(17)
N(1) – Hf(1) – O(4)	80.88(8)	80.31(16)
N(1) – Hf(1) – O(4A)/(8)	97.83(8)	95.64(16)
Hf(1) – O(4) – Hf(1A)/(2)	112.18(9)	111.85(16)

Table 3.3 Selected bond lengths (Å) and bond angles (°) for Hf_2(**8**)$_2$(O^iPr)$_2$ and Hf_2(**10**)$_2$(O^iPr)$_2$ as determined by single-crystal X-ray diffraction.

3.3.2 Solution-state NMR spectroscopy

^{1}H and $^{13}C\{^{1}H\}$ NMR spectra were obtained in $CDCl_3$ for all complexes. The ^{1}H NMR spectrum exhibited an AX spin system with six doublets due to the six diastereotopic methylene CH_2 protons. This confirmed that the dimeric solid-state structure was maintained in solution using a non-coordinative solvent (Figure 3.9).

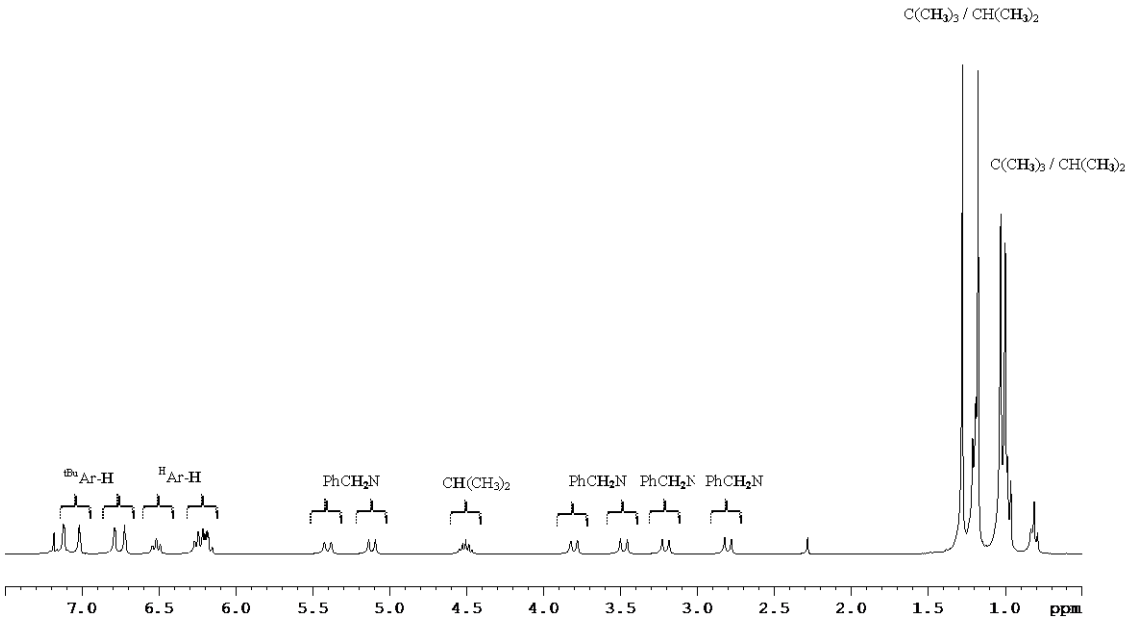

Figure 3.9 Assigned ^{1}H NMR spectrum ($CDCl_3$) for $Zr_2(\mathbf{8})_2(O^iPr)_2$. Four ^{tBu}Ar-**H** and four C(C**H**$_3$)$_3$ signals due to the inequivalence caused by phenolate-bridged dimer motif persisting in solution

Variable temperature NMR (VT-NMR) spectroscopy was carried out on $Zr_2(\mathbf{8})_2(O^iPr)_2$ in $CDCl_3$ and no change to the splitting or relative integrals was observed confirming the non-fluxtional nature of the dimeric complex; either as a monomer-dimer equilibrium or between *P* and *M* isomers as seen for the previously reported C_3-symmetric zirconium amine tris(phenolate).[6] This further highlighted a difference between unsymmetrical amine tris(phenolate) complexes and the previously reported C_3-symmetric complexes; which as fluxional five-coordinate species in solution displayed two broad singlets at room temperature.[6] NOSEY and COSY NMR spectra were also acquired for $Zr_2(\mathbf{8})_2(O^iPr)_2$ in order to fully assign the methylene bridge protons. The high shift resonances (5.40 and 5.12 ppm) were due to the equatorial protons ($H1_{(eq)}$ and $H2_{(eq)}$) orientated towards the centre of the complex causing them to be deshielded by the two zirconium metal centres. The lowest chemical shift was experience by $H3_{(eq)}$ due to its orientation between the two substituted phenol rings and thus shielded by the large *tert*-butyl groups (Figure 3.10) and (Figure 3.11).

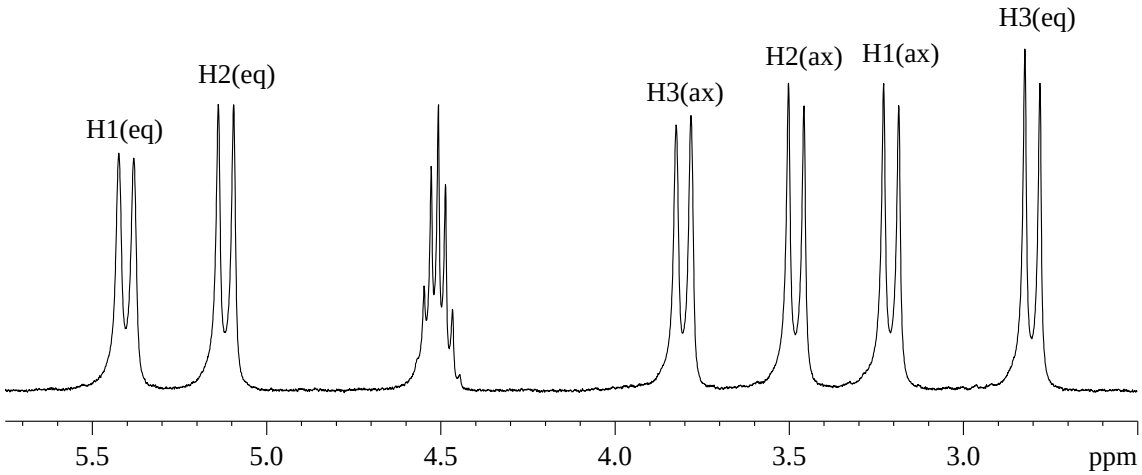

Figure 3.10 Extract of ^{1}H NMR spectrum ($CDCl_3$) for $Zr_2(\mathbf{8})_2(O^iPr)_2$ showing six doublets for the six diastereotopic CH_2 protons of the methylene bridges.

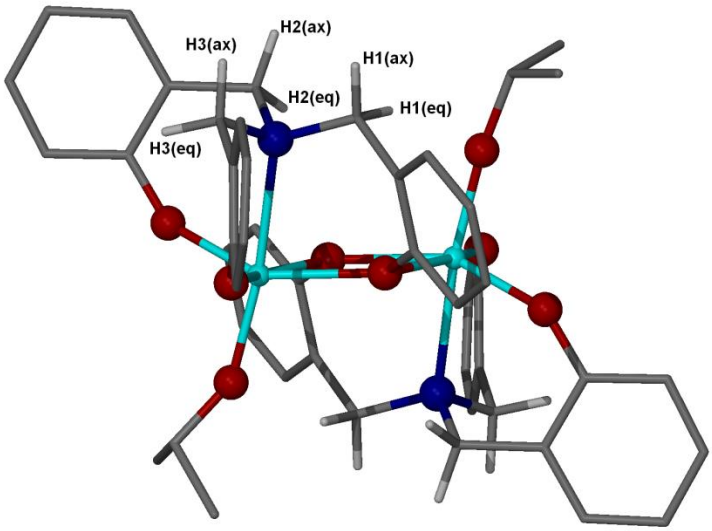

Figure 3.11 Structure of $Zr_2(\mathbf{8})_2(O^iPr)_2$ with labelled methylene bridge protons. All other protons and *tert*-butyl groups removed for clarity

NMR spectroscopy of $Hf_2(\mathbf{8})_2(O^iPr)_2$ also identified that the locked dimer motif was maintained in a non-coordinative solvent ($CDCl_3$) (Figure 3.12). As with $Zr_2(\mathbf{8})_2(O^iPr)_2$ six discreet doublets were observed and the presence of only one septet signal, due to the isopropoxide O**C**$\mathbf{H}(CH_3)_2$, implying the solid-state structure is maintained in solution. The aromatic protons of the *tert*-butyl phenolates appeared as four discrete singlets, as did the $C(C\mathbf{H_3})_3$ singlets for the *tert*-butyl groups; this would only occur if the two phenolate groups were inequivalent due to the dimer structure.

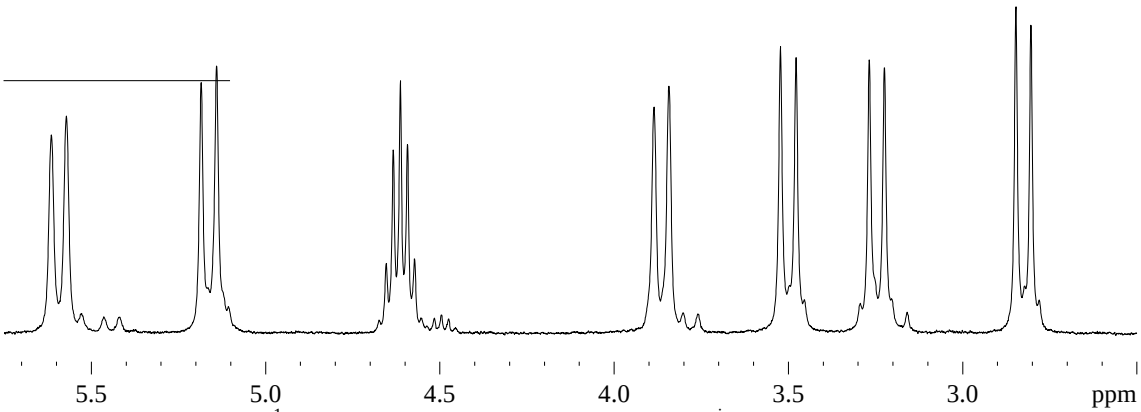

Figure 3.12 Extract of ^{1}H NMR spectrum ($CDCl_3$) for $Hf_2(\mathbf{8})_2(O^iPr)_2$ showing six doublets for the six diastereotopic CH_2 protons of the methylene bridges.

Spectroscopic analysis of $Zr_2(\mathbf{9}\text{-}\mathbf{10})_2(O^iPr)_2$ and $Hf_2(\mathbf{10})_2(O^iPr)_2$ confirmed that the locked dimer was maintained in solution ($CDCl_3$) with the presence of six doublets of an AX-spin system. However, unlike the ^{1}H NMR spectra of $Zr_2(\mathbf{8})_2(O^iPr)_2$ and $Hf_2(\mathbf{8})_2(O^iPr)_2$, there were clearly multiple sets of methylene resonances (Figure 3.13).

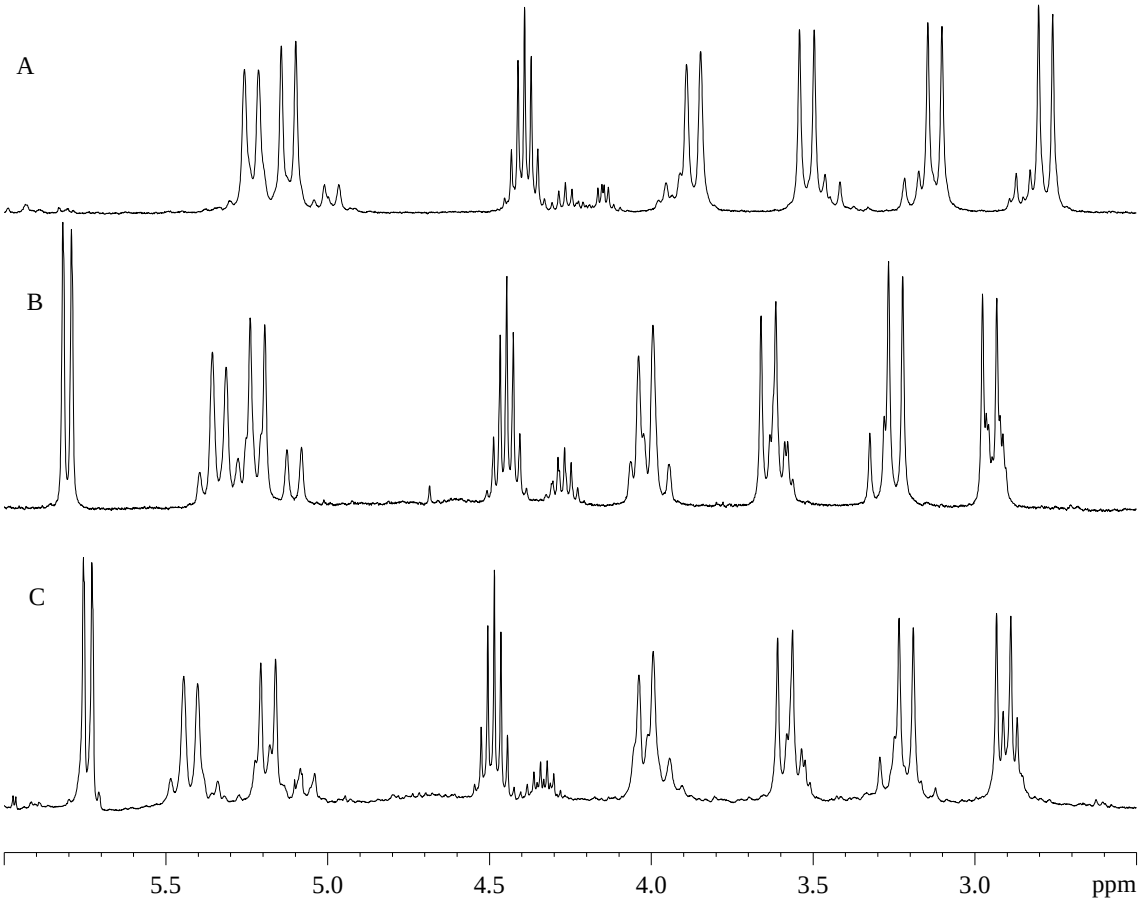

Figure 3.13 Extracts of ^{1}H NMR spectra ($CDCl_3$) for: **A** - $Zr_2(\mathbf{9})_2(O^iPr)_2$, **B** - $Zr_2(\mathbf{10})_2(O^iPr)_2$, **C** - $Hf_2(\mathbf{10})_2(O^iPr)_2$ showing multiple sets of six doublets for the six diastereotopic protons of the methylene bridges due to the presence of multiple dimeric isomers

These have been attributed to the possibility of multiple isomers of the dimer motif when zirconium and hafnium are coordinated to the unsymmetrical amine tris(phenolate) ligands, H_3**9** and H_3**10**. All crystallographic data for these unsymmetrical group IV amine tris(phenolate) complexes indicate that an unsubstituted phenolate occupied the bridging position. With the complexes of ligand H_3**8** both non-bridging phenolate arms were di-*tert*-butyl substituted and therefore only one arrangement was possible. However, for complexes with H_3**9** and H_3**10**, only one phenolate arm was di-*tert*-butyl substituted and therefore they can be orientated either "transoid" or "cisoid" across the dimer. In order to define stereochemistry to these potential isomers the chirality of each metal centre was judged as a discreet five-coordinate trigonal bipyramidal motif and assigned either Δ or Λ. The dimer could consist of an enantiomeric pair (Λ,Δ) that required the *tert*-butyl-substituted phenolate arms to adopt a "transoid" arrangement across the dimer (Figure 3.14 **a** and **b**). For the ^{t}Bu -substituted arms to be arranged "cisoid" the dimer had to consist of an Λ,Λ or Δ,Δ pairing (Figure 3.14 **c**).

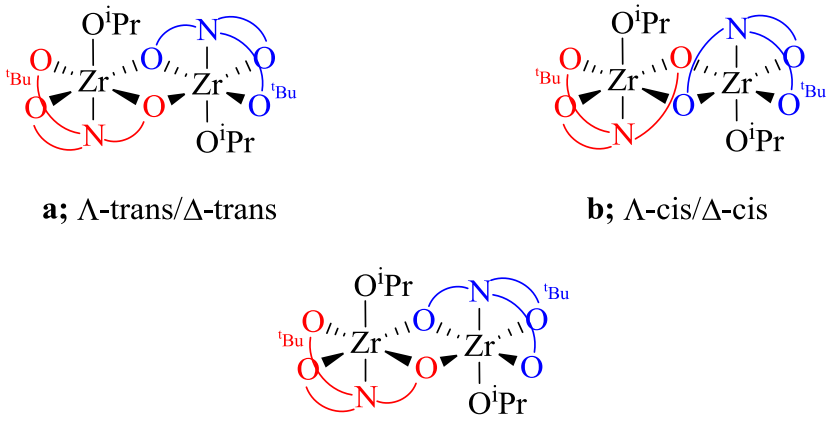

Figure 3.14 Possible isomers for the dimer Zr_2(**10**)$_2$(O^iPr)$_2$. Methylene bridges, phenolates and substituents have been graphically represented for clarity. ^{t}Bu annotation indicates which phenolate arm is di- ^{t}Bu-substituted.

Geometry was further distinguished by the arrangement of the *tert*-butyl-substituted phenolate arm with respect to the bridging phenolate arm of the same ligand. This led to the resolution of two forms of the transoid dimer (Figure 3.14, **a** and **b**) whereas the cisoid dimer arrangement required there to always be a trans/cis pairing.

To further ascertain the presence of different isomers of the dimer motif, Zr_2(**9**)$_2$(O^iPr)$_2$ was analysed *via* NMR (VT-NMR) spectroscopy in $CDCl_3$ (Figure 3.15). The ^{1}H NMR spectra

showed no change in relative peak intensity and peak broadening at lower temperatures was attributed to reduced solubility of the complex. The stability over a wide range of temperatures gave evidence that the multiple set of peaks were not due to a thermodynamic monomer/dimer equilibrium and further to that that the formation of the different isomers was kinetically driven rather than thermodynamic.

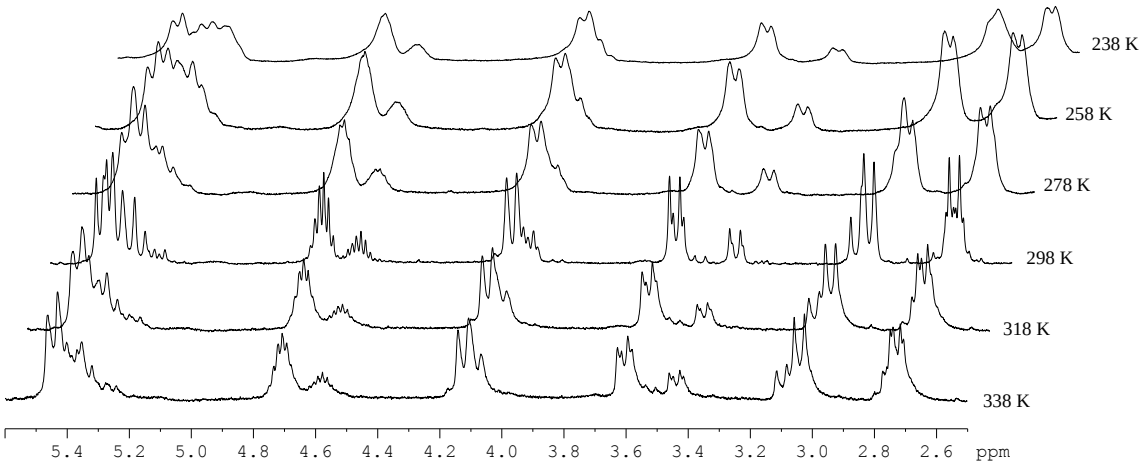

Figure 3.15 VT-NMR spectroscopy ($CDCl_3$) of $Zr_2(\mathbf{9})_2(O^iPr)_2$ over 238 – 338 K. ^1H NMR spectra shown for region of doublets assigned to diastereotopic protons of the methylene bridges (NC$\mathbf{H_2}$Ph)

These complexes were targeted as potential initiators for the ROP of lactide. The C_3-symmetric analogue is a monomeric species from which the polymerisation of lactide occurs *via* a coordination insertion mechanism.[6] Due to the similarities with this well-characterised initiator it was proposed that the ROP-active species for these unsymmetrical dimers would be a five-coordinate monomeric complex. To investigate, dimer $Zr_2(\mathbf{8})_2(O^iPr)_2$ was subjected to VT-NMR in d_8-THF with the aim of disrupting the dimer and identifying a monomeric species for the unsymmetrical analogues (Figure 3.16).

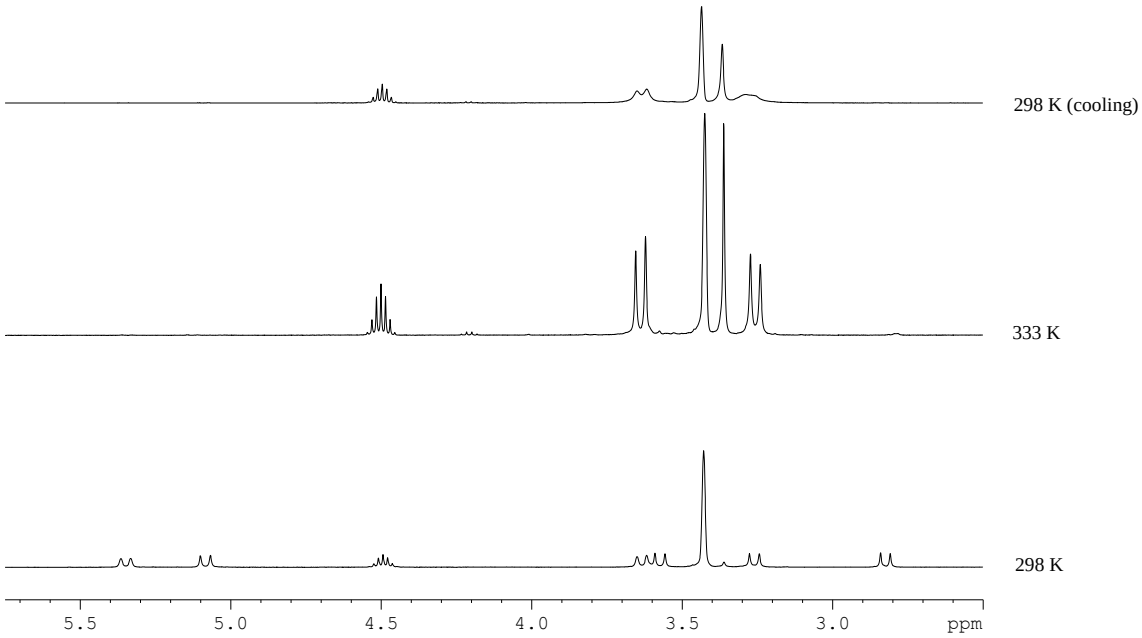

Figure 3.16 VT-NMR of $Zr_2(\mathbf{8})_2(O^iPr)_2$ in d_8-THF, sample was heated from 298 K to 333 K before cooling to 298 K. ^{1}H NMR spectra shown for the region assigned to doublets of diastereotopic protons of the methylene bridges (PhC$\mathbf{H}_2$N) with spectra relatively reference to the isopropoxide methane signal for comparison.

Initial solubility of $Zr_2(\mathbf{8})_2(O^iPr)_2$ was found to be low in d_8-THF. Analysis by ^{1}H NMR spectroscopy at 298 K before any heating provided a spectrum with six doublets attributed to the protons of the methylene bridge. As six discreet doublets it was concluded that the dimer was persisting in the presence of a coordinative solvent. Heating the sample to 333 K saw a gradual change, with the loss of the doublets and the appearance of two doublets and one singlet, suggesting a disruption to the dimer motif. On cooling back to 298 K there was no reformation of the discreet six-doublet system and it was concluded that the monomeric species, with coordinated d_8-THF, persisted. Signal broadening was attributed to reduced solubility or a dynamic exchange process with the solvent.

Further investigation of the ^{1}H NMR spectrum at 333 K in d_8-THF found that whilst in non-coordinative solvents the aromatic hydrogens of the di-*tert*-butyl-substituted phenolates appeared as four singlets, in d_8-THF there were only two. This was attributed to the inequivalence caused by the dimer motif in a non-coordinative solvent ($CDCl_3$) and dissociation into a monomeric species in d_8-THF that led to the two substituted phenolate arms appearing equivalent. A similar change was observed for the singlets assigned to the *tert*-butyl groups (C(C$\mathbf{H}_3$)$_3$) whilst the reduction to one doublet for the isopropoxide methyl groups was attributed to an increase in ease of rotation of the O-CH$(CH_3)_2$ bond for the monomeric form (Figure 3.17). The presence of two doublets with a total integral of four led to their assignment to the

methylene bridges of the two di-*tert*-butyl-substituted phenolate arms. A coupling constant of J = 13.0 Hz was measured which is typical of an AX spin system suggesting that they remain diastereotopic. With the aromatic (^{tBu}Ar-**H**) and *tert*-butyl (C(C**H**$_3$)$_3$) appearing equivalent, a monomeric species with a plane of symmetry dissecting between the two substituted arms was proposed with increased movement in the unsubstituted phenolate arm due to THF coordination and reduced steric bulk causing the appearance the methylene bridge protons as a singlet. Solubility issues at lower temperatures prevented investigation with a lower rate of THF exchange.

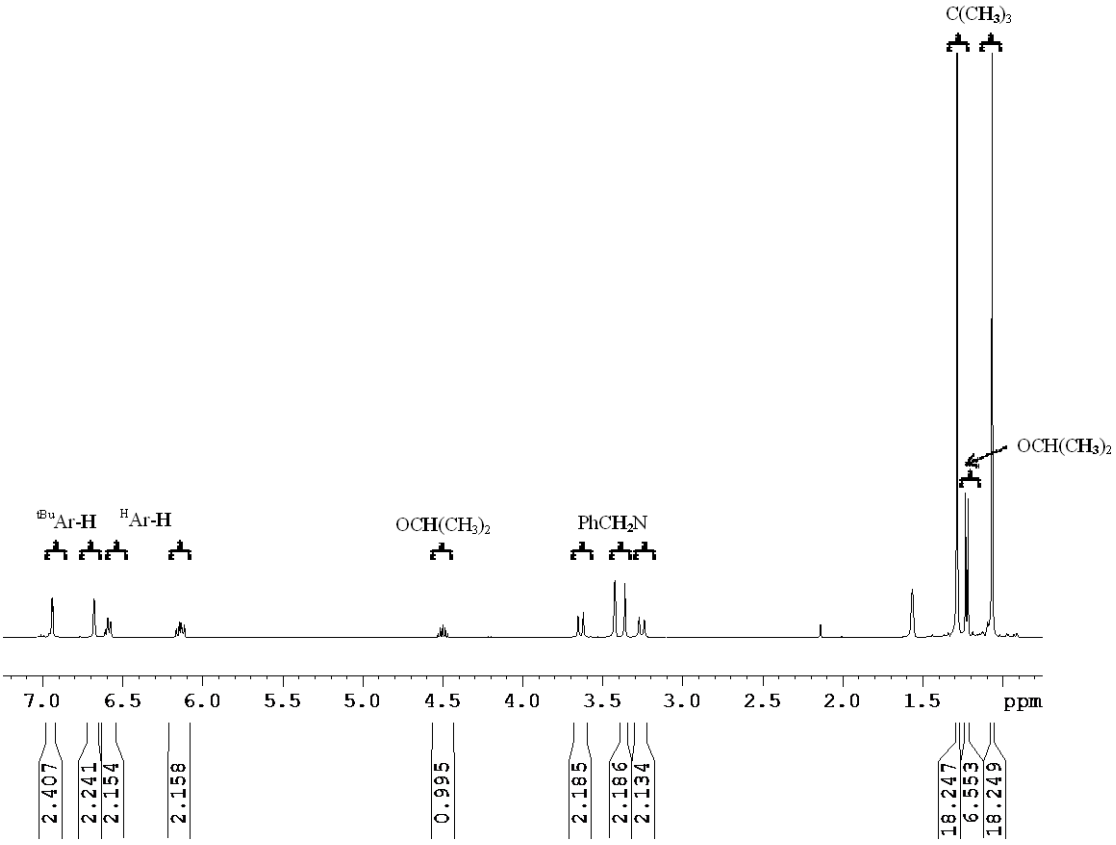

Figure 3.17 ^{1}H NMR spectrum of Zr_2(**8**)$_2$(O^iPr)$_2$ in coordinative d_8-THF at 333 K. Assignment of signals for a monomeric species Zr(**8**)(O^iPr)_(THF) with aromatic and *tert*-butyl signals appearing equivalent

3.4 Trialling of unsymmetrical group IV amine tris(phenolate) complexes and initiators for the ROP of *rac*-lactide

All unsymmetrical group IV amine tris(phenolates) complexes were trialled as initiators for the ROP of *rac*-lactide. Due to availability of pure complex, $Zr_2(\mathbf{9})_2(O^iPr)_2$ was only screened for selectivity in the melt and kinetic studies in solution. $Zr_2(\mathbf{8,10})_2(O^iPr)_2$ and $Hf_2(\mathbf{9,10})_2(O^iPr)_2$ were subjected to a full catalytic study including catalyst loading to establish further insight into the behaviour of the dimer in the presence of lactide and the nature of the active species. Analysis in both the solid-state and solution identified a labile isopropoxide group as an initiating group, akin to that of the C_3-symmetric analogue.[6] Therefore no co-initiator, such as benzyl alcohol, was used.

3.4.1 Preliminary Screening

Solution polymerisations were carried out in toluene at 80 °C and 0.5 M lactide concentration at a [M]:[I] of 100:1. More industrially relevant solvent-free reactions were carried out at 130 °C and a [M]:[I] ratio of 300:1. Conversion of monomer was calculated from the ^{1}H NMR spectrum of quenched reaction material with molecular weight data acquired using gel permeation chromatography (GPC) of purified polymeric material, through washing with methanol. Stereoselectivity of the initiators was quantified by a P_r value that was determined *via* homonuclear decoupled NMR spectroscopy and the Bernoullian statistics of potential monomer connectivity.[13]

Entry	Initiator	Time /h	Conv. /% [c]	M_n^{calc}	M_n^{d}	PDI[d]	P_r^{e}
1[a]	Zr_2(**8**)$_2$(O^iPr)$_2$	0.5	76	32900	66900	1.40	0.72
2[a]	Zr_2(**9**)$_2$(O^iPr)$_2$	0.5	80	37650	19100	1.54	0.71
3[a]	Zr_2(**10**)$_2$(O^iPr)$_2$	0.5	87	34600	41900	1.76	0.70
4[a]	Hf_2(**8**)$_2$(O^iPr)$_2$	0.5	56	24250	301100	1.19	0.70
5[a]	Hf_2(**10**)$_2$(O^iPr)$_2$	0.5	91	39350	30800	1.44	0.66
6[b]	Zr_2(**8**)$_2$(O^iPr)$_2$	1	94	13650	22500	1.54	0.64
7[b]	Zr_2(**10**)$_2$(O^iPr)$_2$	3	50	7300	9750	1.08	0.69
8[b]	Hf_2(**8**)$_2$(O^iPr)$_2$	1	90	13500	28200	1.39	0.67
9[b]	Hf_2(**10**)$_2$(O^iPr)$_2$	3	89	12900	16300	1.13	0.68

Conditions: [a] [M]/[I] = 300, solvent-free, 130 °C. [b] [M]/[I] = 100, [M] = 0.5 M, toluene, 80 °C. [c] As determined *via* ^{1}H NMR, [d] Determined from GPC (in THF) referenced to polystyrene standards. It is noted that a Mark-Houwink correction is not applied; this is discussed in section 5.1.2. [e] Calculated from the ^{1}H homonuclear decoupled NMR ($CDCl_3$) analysis. The calculated molecular weights were determined by the following $(144 \times ([M]/[I]) \times \frac{conv}{100}) + 60$ {where 60 is the mass of the end groups (H/OCH$(CH_3)_2$)}

Table 3.4 Polymerisation data for the trialling of unsymmetrical group IV amine tris(phenolate) complexes as initiators for the ROP of *rac*-lactide. Solvent-free (entries 1-5) and solution (entries 6-9)

All complexes were found to be active as initiators for the ROP of *rac*-lactide in both the melt and solution. Polymerisations carried out at 130 °C under solvent-free conditions (entries 1-5) showed good conversion of monomer for all but Hf_2(**8**)$_2$(O^iPr)$_2$ in a reaction time of 0.5 hours. This activity was comparable to the C_3-symmetrical analogue for which a conversion in the melt of 76 % in 0.1 hours has been reported.[6] Stereoselectivity was reduced with the removal of *tert*-butyl substituents on one phenolate arm; Zr_2(**8**)$_2$(O^iPr)$_2$ yielding polymeric material with a P_r value of 0.72 in comaparison to 0.96 for Zr-$C_3{}^tBu$.[6] Further removal of steric bulk, either through replacement of *tert*-butyl substituents with methyl substituents {Zr_2(**9**)$_2$(O^iPr)$_2$} or with an unsubstituted phenolate {Zr_2(**10**)$_2$(O^iPr)$_2$}, saw no significant reduction in the stereoselectivity. This suggested that the *P*/*M* isomerism offered by the C_3-symmetric nature of Zr-$C_3{}^tBu$ was more influential in the high stereoselectivity than the simple presence of bulky *tert*-butyl substituents. A similar step reduction in stereoselectivity was seen for the hafnium analogues with a reduction in P_r from 0.88 to 0.70 for Hf-$C_3{}^tBu$ to Hf_2(**8**)$_2$(O^iPr)$_2$. Molecular weight of polymeric material was less predictable, with higher molecular weights obtained for

Zr_2(**8**)$_2$(O^iPr)$_2$ and Zr_2(**10**)$_2$(O^iPr)$_2$ compared to that based on monomer-initiator ratio and conversion. This has been attributed to the presumed requirement for the dimer to dissociate to be active for the ROP of lactide and the relative stability of each dimer. This was studied further in solution-based kinetics. An extremely large difference between calculated molecular weight and measured molecular weight was observed for Hf_2(**8**)$_2$(O^iPr)$_2$. An M_n of over 300 kDa was measured (GPC) compared to an M_n of ~25 kDa that was calculated based on conversion. Suggesting that rate of propagation was much faster than the rate of initiation. This molecular weight disagreement could have been attributed to complex inactivity due to purity, however, recrystallisation and analysis suggested high complex purity. This further suggested that dimer dissociation may not be complete when introduced to lactide despite its coordinative potential. Comparison of polydispersity index values found an increase in PDI with removal of steric bulk. With less stereically hindered complexes the potential for transesterification post polymerisation was increased.

Polymerisations carried out in solution, compared to that in the melt, were found to have a lower stereoselectivity for all initiators tested, P_r ~ 0.65 (entries 6 – 9). As previously published for the C_3-symmetric initiator, longer reaction times were required to reach high conversion in solution. However, there was no associated increase in stereoselectivity for the unsymmetrical analogues. This further strengthened the argument for a *P*/*M* equilibrium, influenced by the stereochemistry of the previous monomer inserted, providing the high selectivity of Zr-$C_3{}^tBu$ and Hf-$C_3{}^tBu$. At lower temperatures the energy barrier to overcome the equilibrium would be larger leading to higher selectivity. However, for the unsymmetrical complexes presented in this work the *P*/*M* equilibrium was not present.

3.4.2 Polymerisation Kinetics

A catalytic activity study of this series of unsymmetrical group IV amine tris(phenolate) initiators was carried out in solution at 80 °C with a [M]:[I] ratio of 100:1 and [M] = 0.5 M. This was equivalent to 0.5g scale polymerisations carried out in solution, however, kinetic data was acquired *insitu* using ^{1}H NMR spectroscopy with the reaction volume of 0.6 ml toluene-d_8 in a Young's NMR tube. Integrals of the monomer and polymer unit methine signals were used to quantify conversion and under the presumption that the polymerisation was pseudo-first order with respect to lactide concentration, a value for k_{app} was calculated by plotting $ln\left(\frac{[LA]_0}{[LA]_t}\right)$ versus time, where the gradient was equal to k_{app} (Table 3.5).

Initiator	Monomer	k_{app} (min^{-1}) [a]	Standard Error [b]
Zr-$C_3{}^tBu$	*rac*-lactide	29.9×10^{-3}	0.0006
	L-lactide	13.8×10^{-3}	0.0001
Zr_2(**8**)$_2$(O^iPr)$_2$	*rac*-lactide	130×10^{-3}	0.005
	L-lactide	67.8×10^{-3}	0.001
Zr_2(**9**)$_2$(O^iPr)$_2$	*rac*-lactide	8.56×10^{-3}	0.00009
	L-lactide	7.88×10^{-3}	0.0005
Zr_2(**10**)$_2$(O^iPr)$_2$	*rac*-lactide	4.13×10^{-3}	0.00003
	L-lactide	8.02×10^{-3}	0.00006
Hf_2(**8**)$_2$(O^iPr)$_2$	*rac*-lactide	65.7×10^{-3}	0.002
	L-lactide	47.1×10^{-3}	0.001
Hf_2(**10**)$_2$(O^iPr)$_2$	*rac*-lactide	10.1×10^{-3}	0.0002
	L-lactide	9.61×10^{-3}	0.0001

Conditions: [M]/[I] = 100, [M] = 0.5 M, toluene, 80 °C. [a] k_{app} found from the slope of $ln\left(\frac{[M]_0}{[M]_t}\right)$ vs. time. [b] Standard error calculated using the following: $S.E. = \sqrt{\frac{\sum_{s=1}^{m}\sum_{i=1}^{n} y_{is}{}^2}{(n_y-1)(n_y)}}$, where s = series number, i = point number in series s, m = no. of series for point y in chart, n = no. of points in each series, y_{is} = data value of series s and the i^{th} point, n_y = total no. of data values in all series.

Table 3.5 Pseudo first-order rate constants, k_{app}, for the ROP of *rac*-lactide and L-lactide by: Zr-$C_3{}^tBu$, Zr_2(**8**-**10**)$_2$(O^iPr)$_2$ and Hf_2(**8,10**)$_2$(O^iPr)$_2$.

Kinetic studies were carried out for the previously published C_3-symmetrical zirconium amine tris(phenolate) to provide a direct comparison of activity under the same conditions. A rate constant of 4.2×10^{-3} min^{-1} had previously been reported for Zr-$C_3{}^tBu$, however this was in solution ($CDCl_3$) at room temperature.[6] As was expected, at 80°C a larger rate constant of 29.9×10^{-3} min^{-1} was calculated for the ROP of *rac*-lactide. Rate of ROP of *rac*-lactide was seen to increase over four-fold with Zr_2(**8**)$_2$(O^iPr)$_2$ and was attributed to the removal of steric bulk, in the form of *tert*-butyl substituents, about the metal centre. This would have provided less hindrance for the coordination of lactide to the metal centre in the coordination-insertion mechanism. However, if this had been the only factor involved in the rate determination of ROP

activity for this series of initiators then further removal of steric bulk, as with Zr_2(**9**-**10**)$_2$(O^iPr)$_2$, would have further increased rate. Conversely to this it was observed that, in solution, the first-order rate constant of Zr_2(**9**)$_2$(O^iPr)$_2$ was smaller than Zr-*C*$_3$^{t}*Bu* with Zr_2(**10**)$_2$(O^iPr)$_2$ providing yet further reduction. A similar retardation in solution-based rate was observed between Hf_2(**8**)$_2$(O^iPr)$_2$ and Hf_2(**10**)$_2$(O^iPr)$_2$ providing further evidence of a more complex process involved in determining ROP. Further kinetic studies were carried out to determine the rate of reaction with respect to initiator with a goal of establishing if dimer stability or potential aggregation of less hindered complexes during polymerisation caused an apparent drop in rate. This is discussed in detail in Section 3.4.3.

Rate constants were also calculated for the rate of ROP of enatiopure L-lactide at the same monomer concentration and initiator loading. Previous reports have used the relative rates of *rac*-lactide and L-lactide to estimate the resulting stereocontrol of the initiator.[14] The following relationships were reported, where $k_{(rac)}$ is the rate of ROP of *rac*-lactide and $k_{(L\text{-}L)}$ is the rate of inserting an L-lactide monomer into a metal – L-lactide bond:

$$P_r = 1 - \frac{1}{2}\left(\frac{k_{(L-L)}}{k_{(rac)}}\right)$$

Under the assumption that concentration and order of initiator are constant for the ROP of lactide, rate is directly proportional to rate constant and therefore:

$$\frac{k_{app(L-L)}}{k_{app(rac)}} = \frac{k_{(L-L)}}{k_{(rac)}}$$

$$P_r = 1 - \frac{1}{2}\left(\frac{k_{app(L-L)}}{k_{app(rac)}}\right)$$

Rate constants for the ROP of *rac*-lactide and L-lactide are graphically compared in Figure 3.18 through Figure 3.23 with rate-based P_r values summarised in Table 3.6.

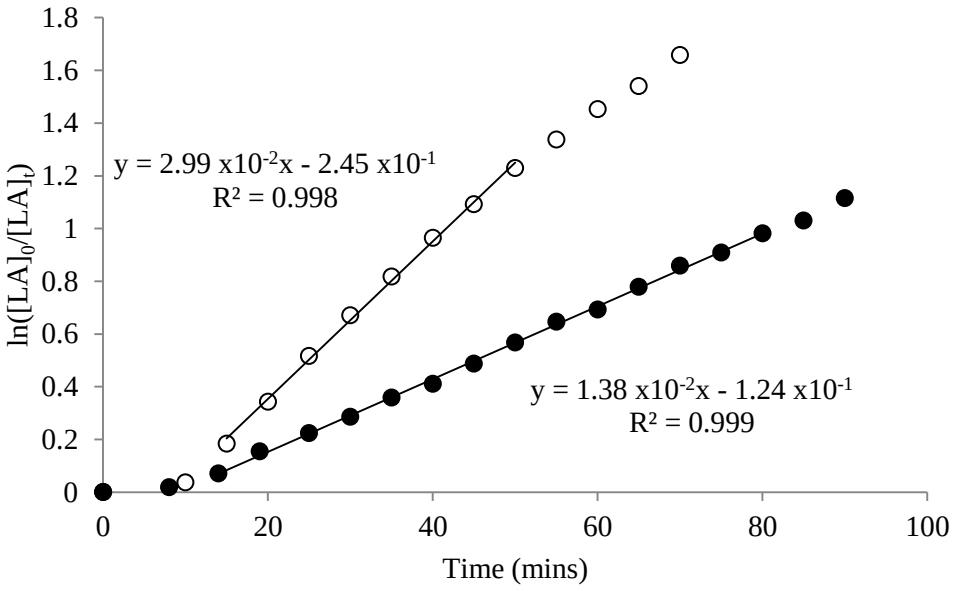

Figure 3.18 Semi-ln plot for the pseudo-first order kinetics of the ROP of *rac*-lactide (○) and L-lactide (●) by Zr-$C_3{}^tBu$

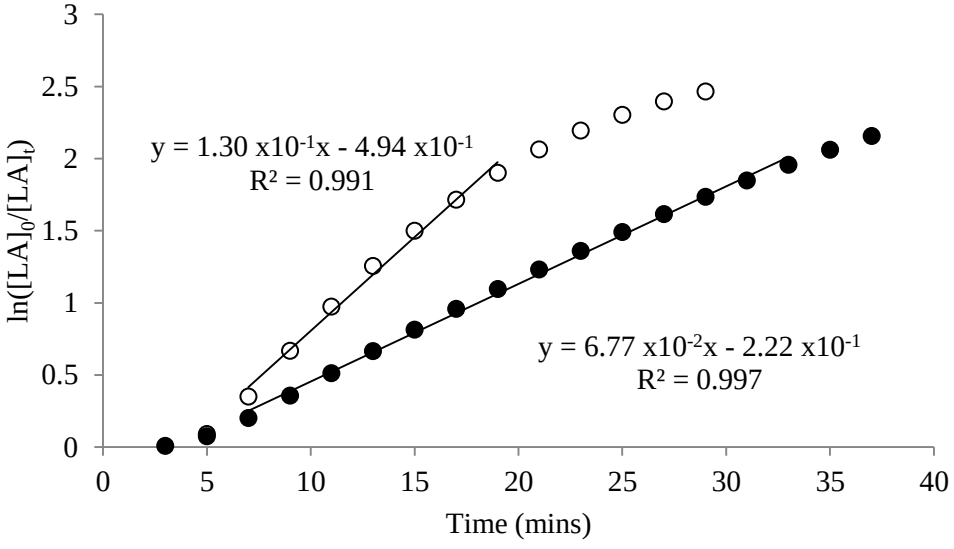

Figure 3.19 Semi-ln plot for the pseudo-first order kinetics of the ROP of *rac*-lactide (○) and L-lactide (●) by $Zr_2(\mathbf{8})_2(O^iPr)_2$

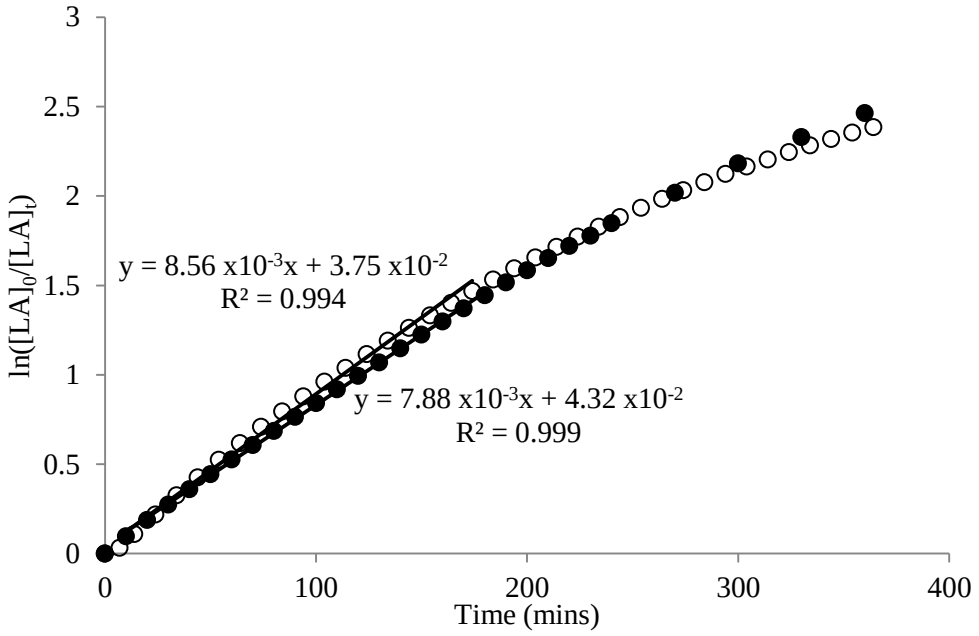

Figure 3.20 Semi-ln plot for the pseudo-first order kinetics of the ROP of *rac*-lactide (○) and L-lactide (●) by $Zr_2(\mathbf{9})_2(O^iPr)_2$

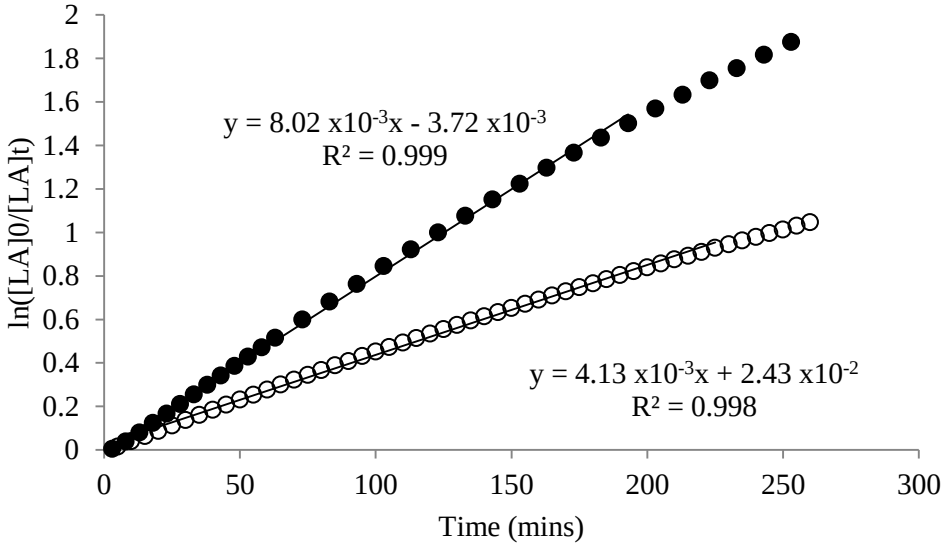

Figure 3.21 Semi-ln plot for the pseudo-first order kinetics of the ROP of *rac*-lactide (○) and L-lactide (●) by $Zr_2(\mathbf{10})_2(O^iPr)_2$

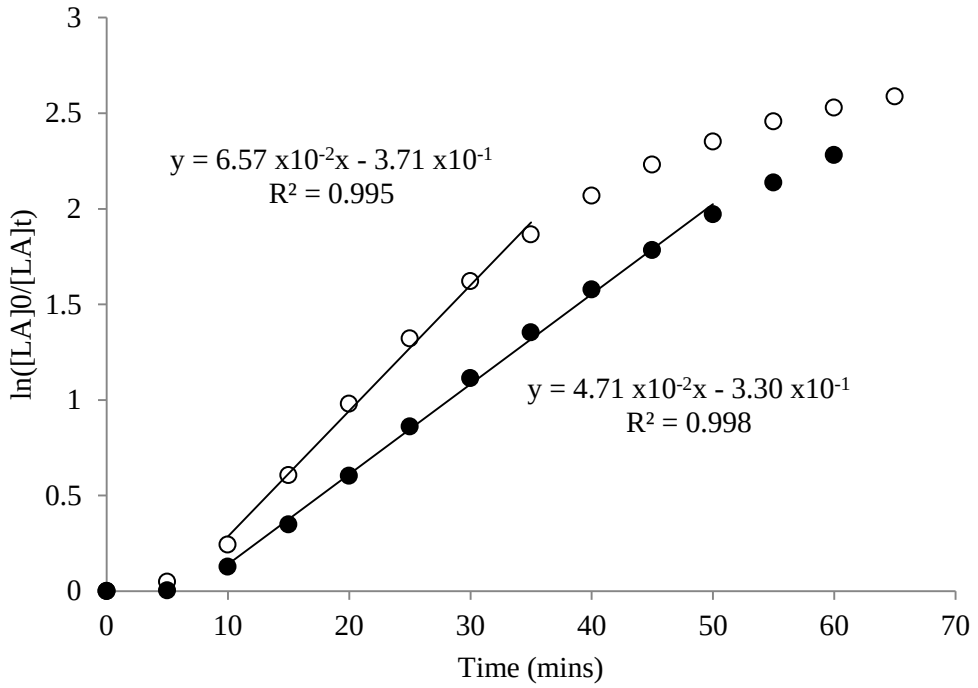

Figure 3.22 Semi-ln plot for the pseudo-first order kinetics of the ROP of *rac*-lactide (○) and L-lactide (●) by $Hf_2(\mathbf{8})_2(O^iPr)_2$

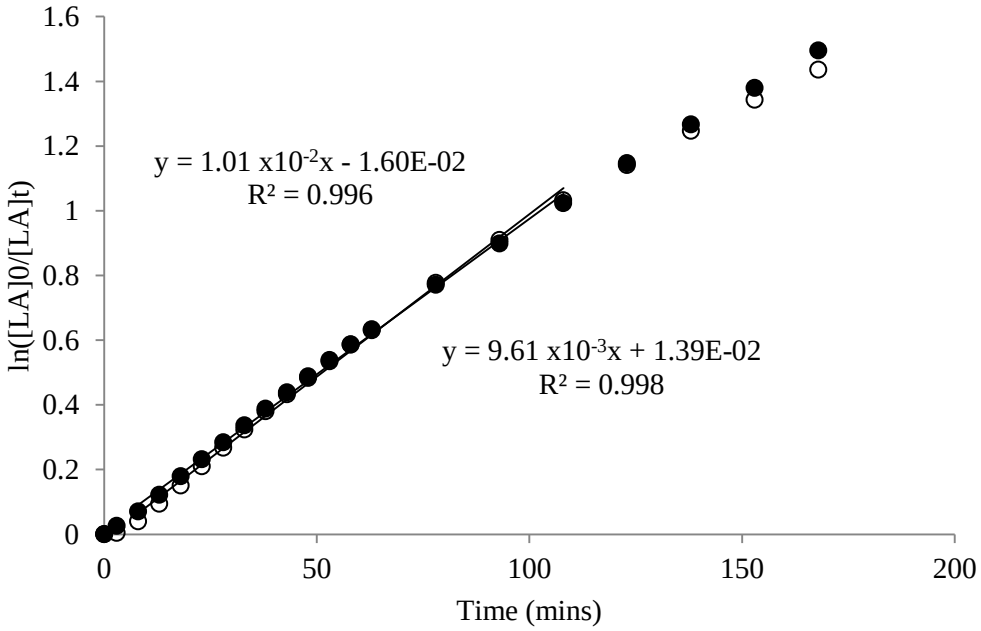

Figure 3.23 Semi-ln plot for the pseudo-first order kinetics of the ROP of *rac*-lactide (○) and L-lactide (●) by $Hf_2(\mathbf{10})_2(O^iPr)_2$

Initiator	P_r (kinetic-based)
Zr-$C_3{}^tBu$	0.77
Zr_2(**8**)$_2$(O^iPr)$_2$	0.73
Zr_2(**9**)$_2$(O^iPr)$_2$	0.54
Zr_2(**10**)$_2$(O^iPr)$_2$	0.03
Hf_2(**8**)$_2$(O^iPr)$_2$	0.64
Hf_2(**10**)$_2$(O^iPr)$_2$	0.52

Table 3.6 Quantification of initiator stereoselectivity through a P_r value, probability of racemic enchainment, that is calculated based on the ratio of pseudo first-order rate constants for the ROP of *rac*-lactide and L-lactide

Kinetic-based P_r values for Zr_2(**8**)$_2$(O^iPr)$_2$ and Hf_2(**8,10**)$_2$(O^iPr)$_2$ were found to be similar to that obtained by homonuclear decoupled ^{1}H NMR of polymeric material (Table 3.4, entries 6-9). Comparison of values provided insight into the extent of any undesirable transesterification taking place. If kinetic-based values had been much higher than that measured experimentally it would have suggested that heterotacticity was being reduced by scrambling of monomer connectivity through transesterification. As values were reasonably comparable it was concluded little transesterification was taking place. Apparent stereoselectivity of Zr-$C_3{}^tBu$ and Zr_2(**8**)$_2$(O^iPr)$_2$ was more comaparable however issues of mass transfer and monomer solubility were greater at the NMR-scale and likely influenced the kinetic-based P_r values. The kinetic-based P_r value for Zr_2(**10**)$_2$(O^iPr)$_2$ was judged to be vastly different to that obtained for polymeric material. It is possible that this is due to the simplication of reaction order with respect to initiator that is required for the P_r to be calculated from kinetic data, as presented by Nomura *et al*.[14] The behaviour of the dimeric initiator and subsequent reaction order is discussed in Section 3.4.3.

3.4.3 Investigation Reaction Order

Kinetic studies presented and discussed in section 3.4.2 suggested that relative rate is not just determined by steric hindrance of the coordination of lactide. Catalyst loading studies allowed the order of reaction with respected to initiator to be determined. Under the presumption that the reaction was first-order with respect to monomer, kinetic data was collected for polymerisations

carried out at the following values of [M]/[I]: 50, 100, 200, 400. Initial monomer concentration was 0.5 M and all polymerisations were carried out at 80 °C. Under a pseudo first-order presumption the following rate law applies:

$$-\frac{d[M]}{dt} = k_{app}[M]_0$$

$$where: k_{app} = k_p[I]_0{}^x$$

$$and\ thus: \ln k_{app} = \ln k_p + x \ln[I]_0$$

$$where\ k_p = rate\ constant\ of\ propagation, x = order\ wrt\ [I]$$

Therefore, a plot of $\ln k_{app}$ versus $\ln[I]_0$ provided a linear line of best fit with gradient equal to the order with respect to initiator (x). With a known value of x a plot of k_{app} versus $[I]^x$ a linear line of best fit gave a gradient equal to the rate constant of propagation (k_p). Reaction order with respect to initiator and true rate constants of propagation are summarised in Table 3.7 with the associated plots presented in Figure 3.24 through Figure 3.33.

Initiator	$[I]^x$ [a]	Standard Error [c]	k_p $(min^{-1}(mol^{-1}dm^3)^x)$ [b]	Standard Error [c]
Zr-$C_3{}^tBu$	1.05	0.11	7.68	0.47
Zr_2(**1**)$_2$(O^iPr)$_2$	1.22	0.15	68.5	10.3
Zr_2(**3**)$_2$(O^iPr)$_2$	0.43	0.06	0.038	0.004
Hf_2(**1**)$_2$(O^iPr)$_2$	0.65	0.04	2.03	0.15
Hf_2(**3**)$_2$(O^iPr)$_2$	0.91	0.12	1.04	0.10

Conditions: [M]/[I] = 50, 100, 200, 400, [M] = 0.5 M, toluene, 80 °C. [a] x found from the slope of ln(k_{app}) vs. ln([I]). [b] k_p found from the slope of k_{app} vs. $[I]^x$. [c] Standard error calculated using the following: $S.E. = \sqrt{\frac{\sum_{s=1}^{m}\sum_{i=1}^{n} y_{is}{}^2}{(n_y-1)(n_y)}}$, where s = series number, i = point number in series s, m = no. of series for point y in chart, n = no. of points in each series, y_{is} = data value of series s and the i^{th} point, n_y = total no. of data values in all series.

Table 3.7 Summary of reaction order with resepct to intiator ($[I]^x$) and true rate constant of propagation (k_p) for the ROP of *rac*-lactide as initiated by: Zr-$C_3{}^tBu$, Zr_2(**8,10**)$_2$(O^iPr)$_2$ and Hf_2(**8,10**)$_2$(O^iPr)$_2$

As expected for the well characterised and previously published C_3-symmetrical initiator (Zr-$C_3{}^tBu$), reaction order with respect to initiator was found to be unitary. Order with $Zr_2(\mathbf{8})_2(O^iPr)_2$ was also deemed to be essentially first order, when standard error is applied to the experimentally found value of 1.22. However, studies showed the ROP of *rac*-lactide to be to the order of ~0.5 with respect to $Zr_2(\mathbf{10})_2(O^iPr)_2$. Half-order dependence has previously been reported for the polymerisation of ε-caprolactone *via* an activated monomer mechanism using a zinc bis(phenolate) complex.[15] Isolated as a $(Zn(\mathbf{L}))_2$ dimer species in the solid-state, Mountford *et.al.* proposed this to be due to only partial dissociation of the dimer in to a catalytically active species and the presence of an equilibrium during the polymerisation process. It is not unreasonable to make a similar suggestion for the behaviour of $Zr_2(\mathbf{10})_2(O^iPr)_2$. NMR spectroscopy studies in THF have shown dimer dissociation in a coordinative environment and MALDI-ToF mass spectrometry has shown the isopropoxide present as an end group suggesting a coordination-insertion mechanism. Therefore both $Zr_2(\mathbf{8})_2(O^iPr)_2$ and $Zr_2(\mathbf{10})_2(O^iPr)_2$ are deemed to at least partially dissociate in solution in the presence of lactide. In the case of the active growing species $Zr(\mathbf{8})((LA)_nO^iPr)$, steric bulk of the ligand prevented aggregation to an inactive species whereas the further unsubstituted species $Zr(\mathbf{10})((LA)_nO^iPr)$ could recombine to an inactive $Zr_2(\mathbf{10})_2((LA)_nO^iPr)_2$.

It was possible to find k_p from the intercept of the ln-ln plot however plotting k_{app} versus $[I]_0{}^x$ provided a more accurate value. As expected with the relationship: $k_{app} = k_p[I]_0{}^x$, values for k_p were found to be significantly higher than k_{app}. $Zr_2(\mathbf{8})_2(O^iPr)_2$ exhibited the largest k_p and thus rate of propagation. However, the value of 68.5 $min^{-1}(mol^{-1}dm^3)^x$ was almost nine times faster than that calculated for the highly active Zr-$C_3{}^tBu$ complex. With a dependency of less than one with respect to initiator, k_p values for $Zr_2(\mathbf{10})_2(O^iPr)_2$ and $Hf_2(\mathbf{8,10})_2(O^iPr)_2$ had less of an increase; $Hf_2(\mathbf{8})_2(O^iPr)_2$ exhibited a k_p value smaller than that for Zr-$C_3{}^tBu$, unlike the respective k_{app} values. If recombination of the active species to an inactive dimer is present this would complicate the kinetics further and will be discussed shortly.

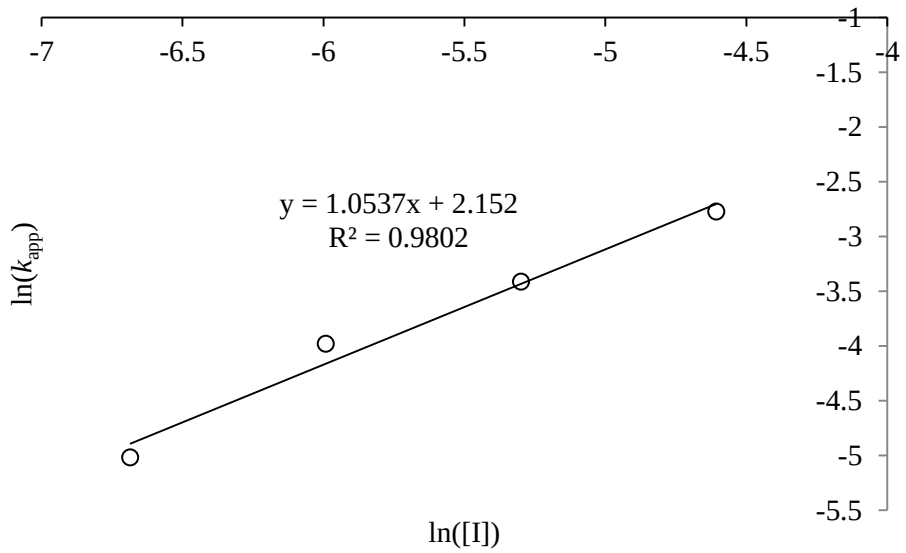

Figure 3.24 ln-ln plot for the initiator loading study of the ROP of *rac*-lactide by Zr-C_3^tBu. Gradient is equal to the order of reaction with respect to initiator: $\ln(k_{app}) = \ln k_p + x \ln([I])$

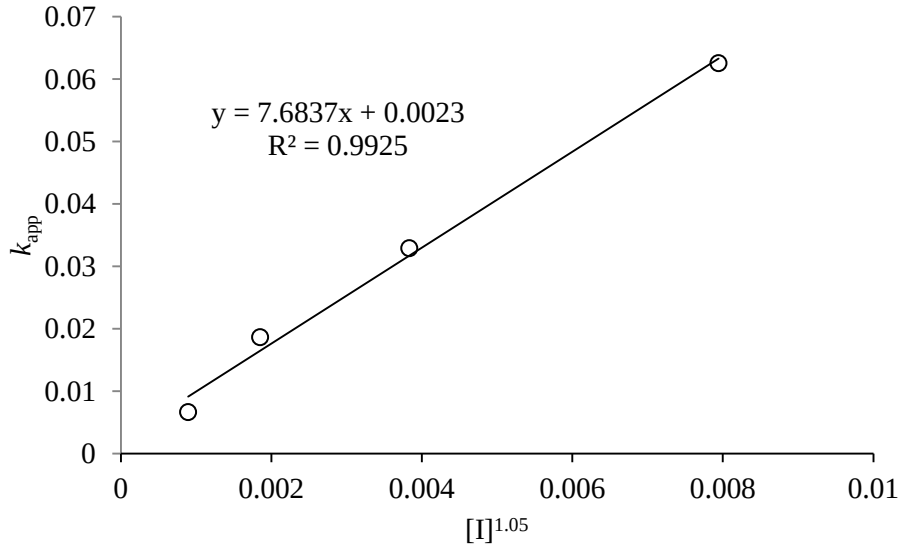

Figure 3.25 Plot providing a gradient equal to the true rate constant of propagation (k_p) for the ROP of *rac*-lactide by Zr-C_3^tBu. $k_{app} = k_p[I]^{1.05}$

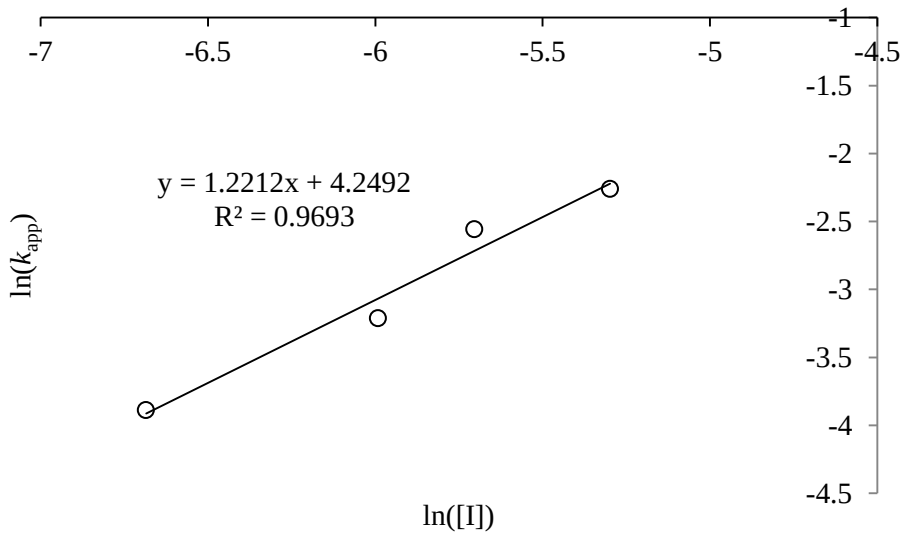

Figure 3.26 ln-ln plot for the initiator loading study of the ROP of *rac*-lactide by Zr_2(**8**)$_2$(O^iPr)$_2$. Gradient is equal to the order of reaction with respect to initiator: $\ln(k_{app}) = \ln k_p + x \ln([I])$

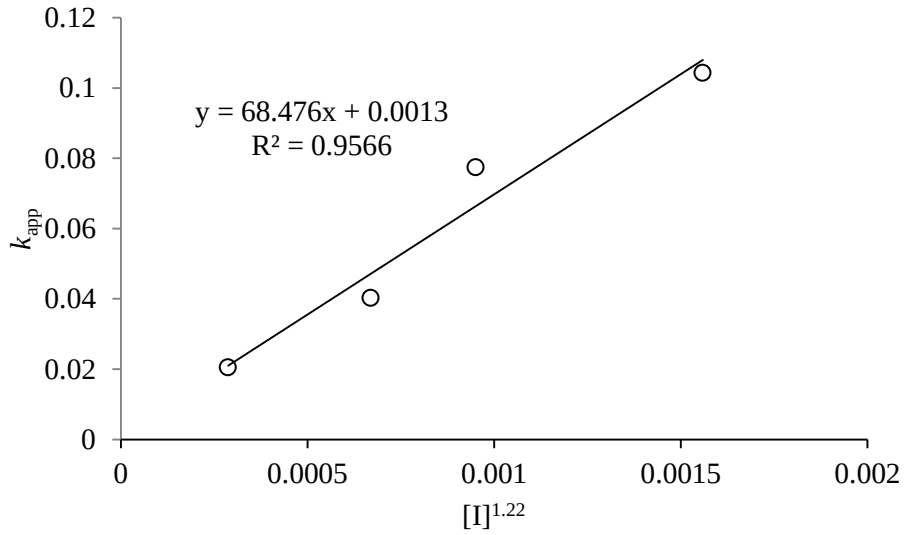

Figure 3.27 Plot providing a gradient equal to the true rate constant of propagation (k_p) for the ROP of *rac*-lactide by Zr_2(**8**)$_2$(O^iPr)$_2$. $k_{app} = k_p[I]^{1.22}$

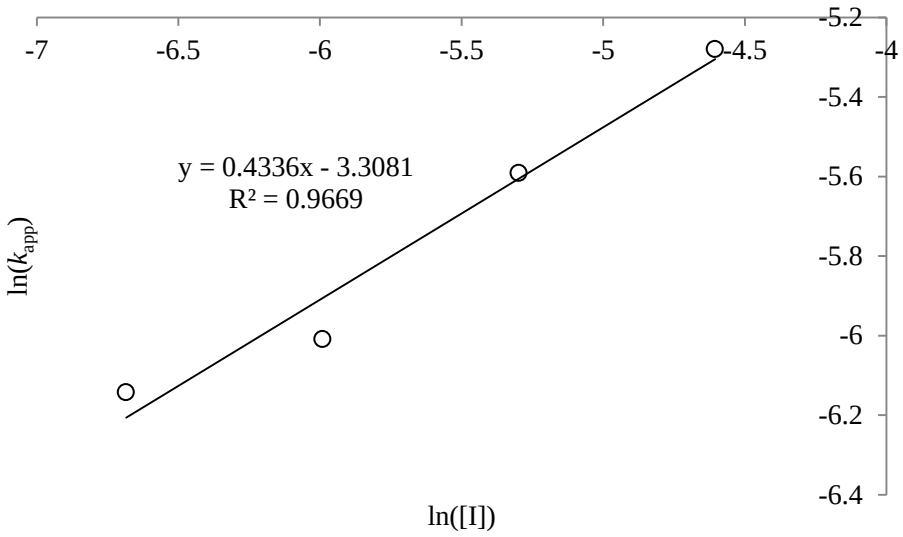

Figure 3.28 ln-ln plot for the initiator loading study of the ROP of *rac*-lactide by Zr_2(**10**)$_2$(O^iPr)$_2$. Gradient is equal to the order of reaction with respect to initiator: $\ln(k_{app}) = \ln k_p + x \ln([I])$

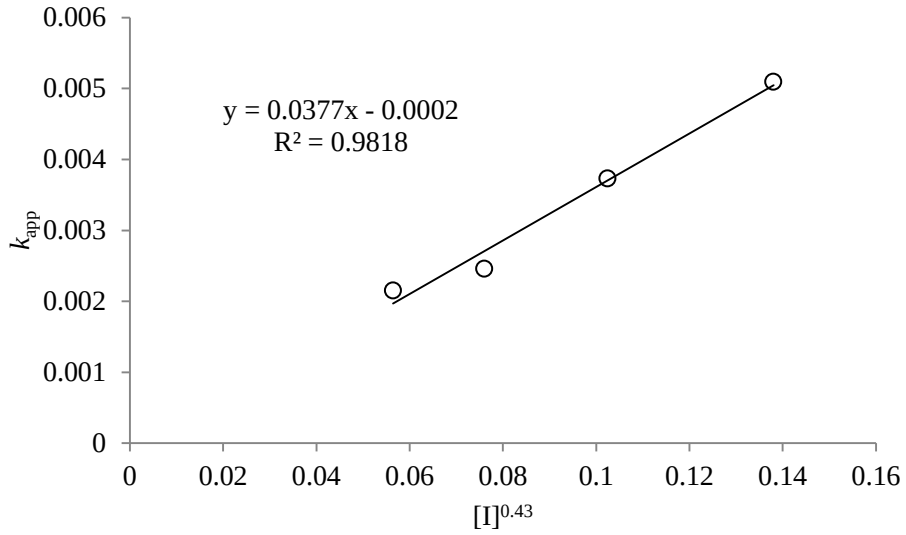

Figure 3.29 Plot providing a gradient equal to the true rate constant of propagation (k_p) for the ROP of *rac*-lactide by Zr_2(**10**)$_2$(O^iPr)$_2$. $k_{app} = k_p[I]^{0.43}$

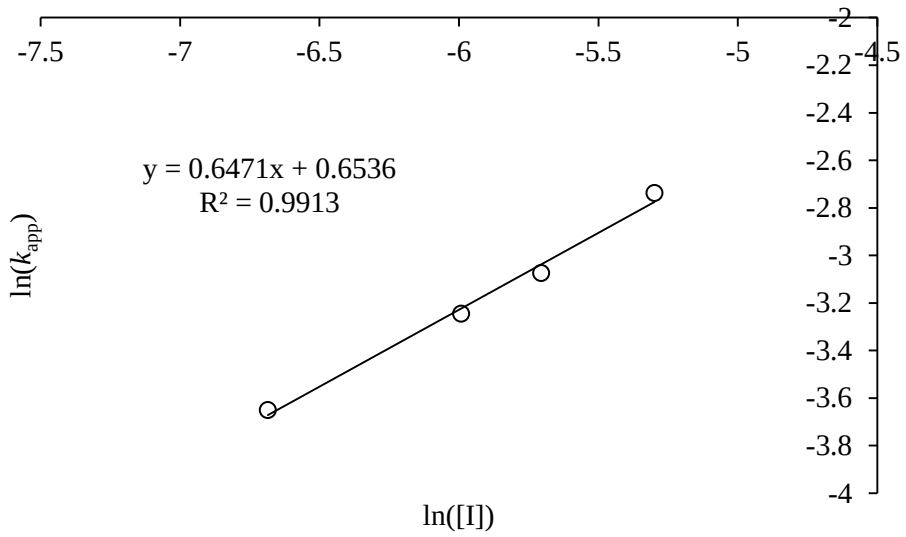

Figure 3.30 ln-ln plot for the initiator loading study of the ROP of *rac*-lactide by $Hf_2(\mathbf{8})_2(O^iPr)_2$. Gradient is equal to the order of reaction with respect to initiator: $\ln(k_{app}) = \ln k_p + x \ln([I])$

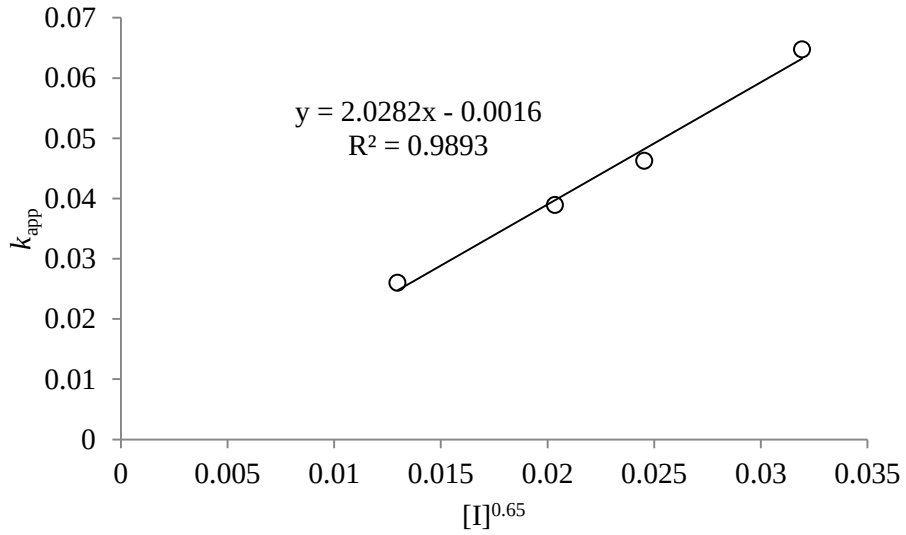

Figure 3.31 Plot providing a gradient equal to the true rate constant of propagation (k_p) for the ROP of *rac*-lactide by $Hf_2(\mathbf{8})_2(O^iPr)_2$. $k_{app} = k_p[I]^{0.65}$

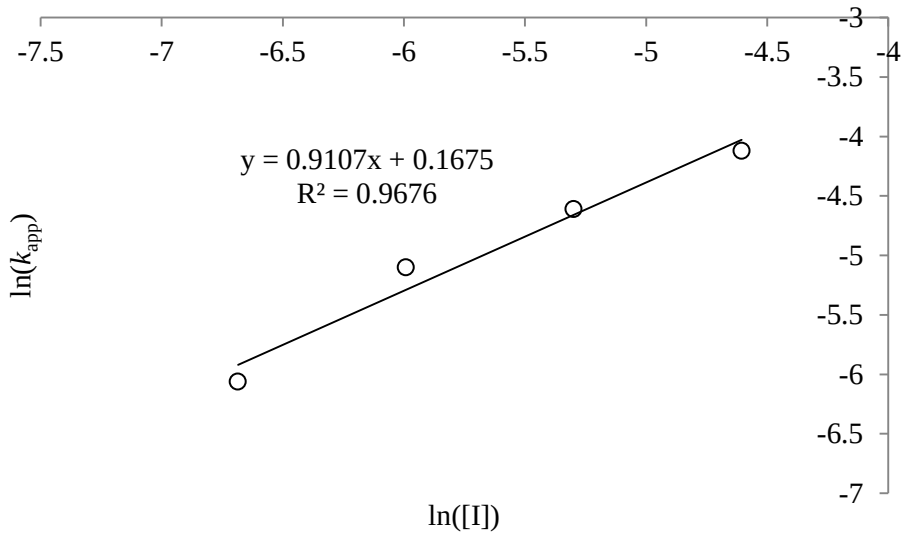

Figure 3.32 ln-ln plot for the initiator loading study of the ROP of *rac*-lactide by Hf_2(**10**)$_2$(O^iPr)$_2$. Gradient is equal to the order of reaction with respect to initiator: $\ln(k_{app}) = \ln k_p + x \ln([I])$

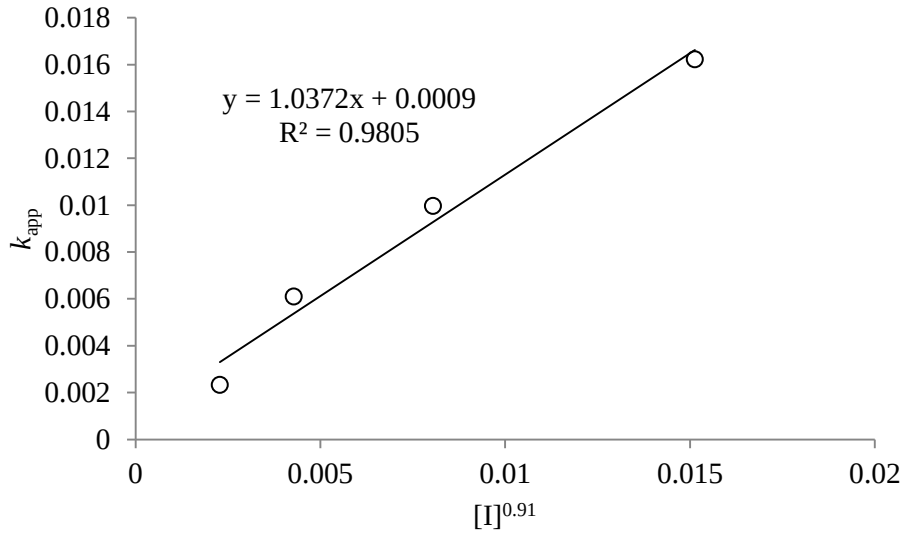

Figure 3.33 Plot providing a gradient equal to the true rate constant of propagation (k_p) for the ROP of *rac*-lactide by Hf_2(**10**)$_2$(O^iPr)$_2$. $k_{app} = k_p[I]^{0.91}$

In-depth studies of the aggregation of a growing species were carried out by Duda *et. al.* for the ROP of ε-caprolactone by a dialkylaluminium alkoxide.[16]

$$(Al(OR))_n \overset{K_{eq}}{\rightleftharpoons} n\ Al(OR)$$

With the above equilibrium and a steady state assumption that all initiator ($[I]_0$) was either in an active or inactive aggregate form, a linear method was used plotting $(k_{app})^{n-1}$ versus $[I]_0/(k_{app})^n$ wherein the gradient was equal to k_p and the intercept was equal to a function of k_p and K_{eq}. However, such a method is a linearization of a complex multi-variable system in which a dependent variable (k_{app}) is plotted on both axis and therefore is limited. There is also the assumption that aggregation/disaggregation occurs spontaneously without the influence of any other species. VT-NMR of these usymmetrical zirconium amine tris(phenolate) complexes found that dissociation was not favourable and thus must be driven by the presence of a coordinative species, i.e. lactide. Leading to the following equilibrium:

$$Zr_2(\mathbf{X})_2(O^iPr)_2 \ +\ 2\ LA \overset{K_{eq(init)}}{\rightleftharpoons} 2\ Zr(\mathbf{X})(O^iPr)\_(LA)$$

An analogous equilibrium was proposed by Mountford for the aforementioned zinc bis(phenolate) complex, however it propagated *via* an activated monomer mechanism and the zinc dimer dissociated in the presence of a benzyl alcohol co-initiator.[15] Herein aggregation of a growing species is theorised for propagation occurring *via* a coordination-insertion method with dissociation caused by lactide coordination. Therefore, for $Zr_2(\mathbf{10})_2(O^iPr)_2$ at least, the following equilibrium is also possible:

$$Zr_2(\mathbf{10})_2((LA)_nO^iPr)_2 \ +\ 2\ LA \overset{K_{eq(prop)}}{\rightleftharpoons} 2\ Zr(\mathbf{10})((LA)_nO^iPr)\_(LA)$$

Further to the above equilibrium, the monomeric species with coordinated lactide: $Zr(\mathbf{10})((LA)_nO^iPr)\_(LA)$, can undergo ring-opening adding one monomer unit to the chain:

$$Zr_2(\mathbf{10})_2((LA)_nO^iPr)_2 \ +\ 2\ LA \underset{k_{-1}}{\overset{k_1}{\rightleftharpoons}} 2\ Zr(\mathbf{10})((LA)_nO^iPr)\_(LA)$$

$$Zr(\mathbf{10})((LA)_nO^iPr)\_(LA) \xrightarrow{k_2} Zr(\mathbf{10})((LA)_{n+1}O^iPr)$$

Where: $K_{eq(prop)} = \frac{k_1}{k_{-1}}$ and k_2 = rate of monomer insertion. This new species would still be susceptible to aggregation to the inactive dimer.

Where rapid reversible coordination of a monomer is taking place saturation kinetics can be applied. Tolman, Hillmyer[17] and Mountford[15] have represented the rate of ROP of ε-caprolactone by the Michaelis-Menten equation; adapted below for lactide (LA) and the active form of an initiator (*I**):

$$-\frac{d[LA]}{dt} = \frac{k_2[I^*][LA]}{K_M + [LA]}$$

$$K_M = \frac{k_{-1} + k_2}{k_1}$$

The Michaelis constant, K_M, is the [LA] at which half maximum rate of polymerisation is achieved based on saturating concentration. For systems as discussed here, it is reasonable to assume that $K_M \ll$ [LA] in line with examples in the literature.[15, 17] Therefore:

$$-\frac{d[LA]}{dt} = \frac{k_2[I^*][LA]}{[LA]}$$

$$-\frac{d[LA]}{dt} = k_2[I^*]$$

For this system [*I**] is the monomeric [Zr(**10**)((LA)$_n$O^{i}Pr)_(LA)] and the steady-state equilibrium can be expressed in terms of $K_{eq(prop)}$, $[LA]_0$ and $[Zr_2(\mathbf{10})_2(O^iPr)_2]_0$; due to the living polymerisation conditions and steady-state assumption that [I] is constant, where:

$$K_{eq(prop)} = \frac{\left[Zr(\mathbf{10})\left(O^iPr\right)\_(LA)\right]^2}{[Zr_2(\mathbf{10})_2(O^iPr)_2]_0[LA]_0{}^2}$$

$$\left[Zr(\mathbf{10})\left(O^iPr\right)\_(LA)\right] = K_{eq(prop)}{}^{0.5}\left[Zr_2(\mathbf{10})_2\left(O^iPr\right)_2\right]_0^{0.5}[LA]_0$$

This can be substituted into rate equation derived from the Michaelis-Menton equation above to give the following revised rate equation:

$$-\frac{d[LA]}{dt} = k_p\left[Zr_2(\mathbf{10})_2\left(O^iPr\right)_2\right]_0^{0.5}[LA]_0$$

$$k_p = k_2 K_{eq(prop)}{}^{0.5}$$

This further confirms that a dependency of a half with respect to initiator can be attributed to an aggregation of the initiator back to an inactive dimer. Unlike the system presented by Mountford, where the rate is zero-order with respect to monomer, lactide is present due to the role played in dissociating the dimer. The rate of propagation, k_p, is also dependent on the equilibrium constant, $K_{eq(prop)}$. For $Zr_2(\mathbf{8})_2(O^iPr)_2$ and $Zr_2(\mathbf{10})_2(O^iPr)_2$, where the metal centre was the same and ligand alteration was predominately steric rather than electronic, it can be fair to assume that rate of monomer insertion, k_2, will be similar. Therefore the cause of the large

differences in k_p (Table 3.7) can be attributed to active-inactive equilibrium. The catalysts loading studies for $Zr_2(\mathbf{8})_2(O^iPr)_2$ found a rate law dependency of one, akin to Zr-C_3^tBu initiator for a which a dimer has never been identified.[6, 18] If there is no deactivation of the active propagating species then $K_{eq(prop)}$ will be very large potentially leading to initiator appearing to have a first-order dependency. In work presented by Hillmyer and Tolman,[17] an iterative program was used to fit the Michaelis-Menten based differential equation to experimental data and in the process find values for rate of insertion, k_2, and equilibrium constant, K_{eq}.

In summary, the kinetic experiments carried out on this system, in comparison with similar studies in the literature, highlight that initiator behaviour cannot be classified as a single-site initiator with first-order dependency on the rate law. The following equilibriums are proposed to be present, with the position of each dependent on the architecture of the ligand:

- Initial dissociation of the unsymmetrical dimer $M_2(\mathbf{X})_2(O^iPr)_2$ into a ROP-active species, $M(\mathbf{X})(O^iPr)\_(LA)$. Based on VT-NMR this requires the presence of a coordinative species and has equilibrium constant, $K_{eq(init)}$
- Ring-opening insertion of the coordinated lactide into the M-O^iPr bond generating the propagating ROP-active species: $M(\mathbf{X})((LA)_nO^iPr)$. Whilst theoretically reversible, the favourable entropic change associated with ring-opening means the process can be given rate constant, k_2. With little change in electronic properties of the ligands in this system and the comparable oxophillicity of zirconium and hafnium, k_2 can be assumed to be comparable for Zr-C_3^tBu, $Zr_2(\mathbf{X})_2(O^iPr)_2$ and $Hf_2(\mathbf{X})_2(O^iPr)_2$.
- Recombination of the propagating ROP-active species $M(\mathbf{X})((LA)_nO^iPr)$ into an inactive $M_2(\mathbf{X})_2((LA)_nO^iPr)_2$ dimer or coordination of a new lactide monomer to give $M(\mathbf{X})((LA)_nO^iPr)\_(LA)$. These two species exist in equilibrium with constant $K_{eq(prop)}$
- Further ring-opening insertion of coordinated lactide, for this study presumed to be the same as initial insertion rate constant, k_2.

Other than k_2, it is proposed that these rate and equilibrium constants are dependent on the steric bulk of the unsymmetrical amine tris(phenolate) ligand. The above mentioned constants with relative sizes and weighting are schematically represented for the largely di-*tert*-butyl substituted $Zr_2(\mathbf{8})_2(O^iPr)_2$ and less substituted $Zr_2(\mathbf{10})_2(O^iPr)_2$ in Table 3.8 and Scheme 3.5.

Reaction Step	Constant	$Zr_2(\mathbf{8})_2(O^iPr)_2$	$Zr_2(\mathbf{10})_2(O^iPr)_2$
Initial dissociation of dimer in the presence of lactide	$K_{eq(init)}$ (k_1/k_{-1})	Large, but k_1 and k_{-1} both small	Small, but k_1 and k_{-1} both large
Ring-opening insertion of lactide	k_2	Similar	Similar
Aggregation of ROP-active into inactive dimer	k_3	Smaller	Larger
Stabilisation of ROP by coordination of lactide	k_4	Larger	Smaller
Dissociation / aggregation of the dimer of propagating species	$K_{eq(prop)}$ (k_5/k_{-5})	Large, but k_5 and k_{-5} both small	Small, but k_5 and k_{-5} both large
Further ring-opening insertion coordinated lactide	k_2	Similar	Similar

Table 3.8 Comparison of proposed relative sizes of rate constants and equilibrium constants for the ROP of lactide by $Zr_2(\mathbf{8,10})_2(O^iPr)_2$

Scheme 3.5 proposes that the rate of initiation (k_i) of the polymerisation consisted of both a dimer dissociation step (k_1/k_{-1}) and initial lactide ring-opening step (k_2). The rate of propagation (k_p) consisted of a dimer dissociation / aggregation (k_3, k_4, k_5/k_{-5}) and subsequent lactide ring opening (k_2) step. It is typical for living polymerisations, such as the ROP of lactide, for the rate of initiation to be significantly faster that the rate of propagation. However, here it is proposed that $Zr_2(\mathbf{8})_2(O^iPr)_2$ has a slower rate of initiation of than $Zr_2(\mathbf{10})_2(O^iPr)_2$ due to dimer stability. This is also apparent in the higher M_n (GPC) obtained for $Zr_2(\mathbf{8})_2(O^iPr)_2$ relative to that expected based on monomer-initiator ratio and conversion (Table 3.4). Propagation is proposed to be slower for $Zr_2(\mathbf{10})_2(O^iPr)_2$ due to aggregation of the ROP-active species into an active dimer. Catalytic loading studies removed the initiation step (k_i) and thus any rate impedance caused by the dissociation of $Zr_2(\mathbf{8})_2(O^iPr)_2$ and exaggerating the difference in rate.

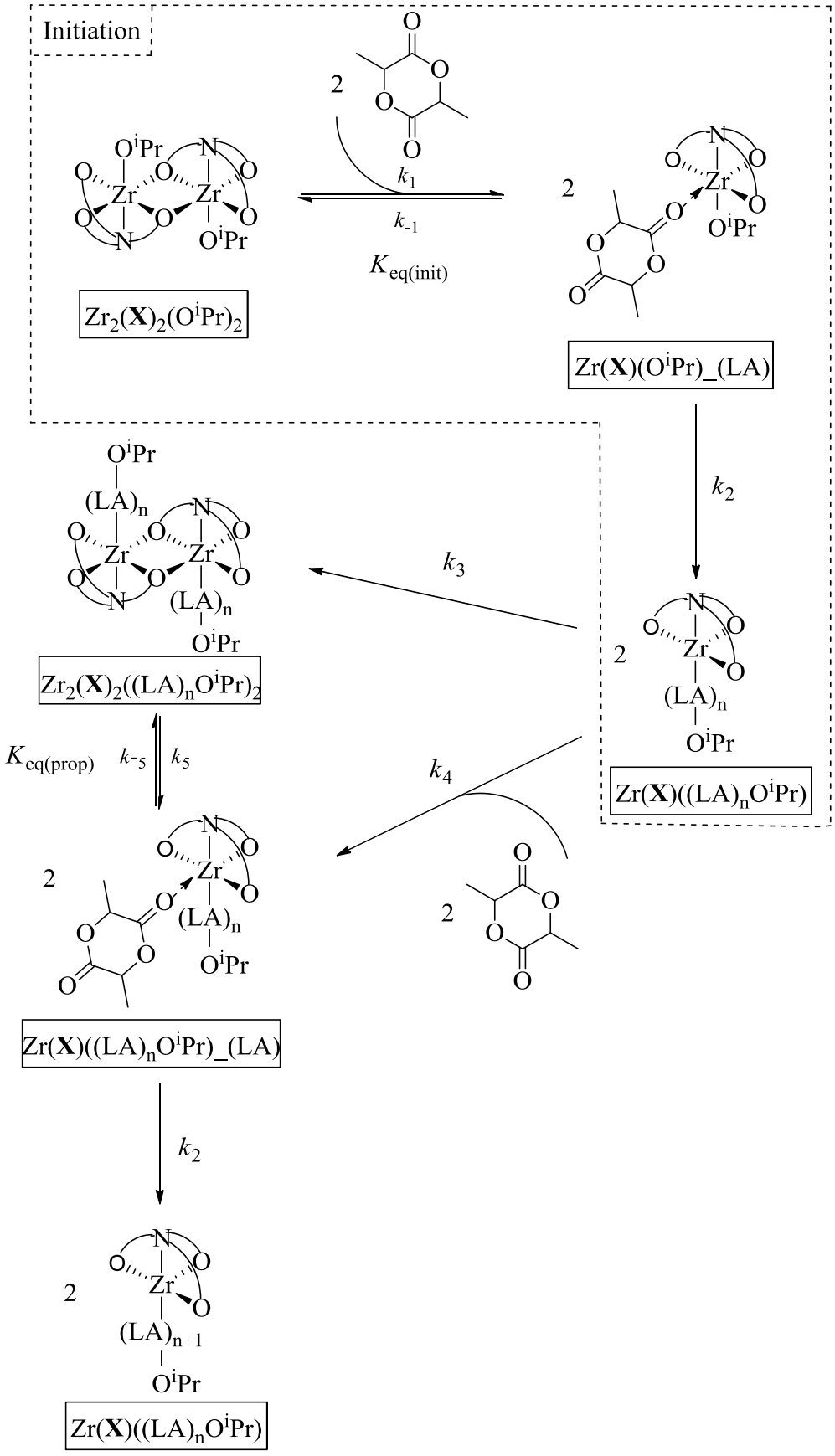

Scheme 3.5 Proposed reaction pathway for dissociation of $Zr_2(\mathbf{X})_2(O^iPr)_2$ and ROP of lactide with aggregation causing initiator inactivity. Initiation step (k_i) inside dashed box

3.4.4 *In-situ* FT-IR monitoring of *rac*-lactide polymerisation in the melt

Studies using ^{1}H NMR spectroscopy provided kinetic data for solution-based polymerisations on a small scale. Whilst this provided a comparison between initiators and an idea of relative activity, it has only limited use with respect to more industrially relevant conditions. Purac are a commercial manufacturer of PLA and carry out ROP under solvent-free conditions at temperatures anywhere between 165 – 200 °C. Catalyst loading is usually as low as 15000:1 and never more than 5000:1 to avoid plastic discolouration. Monomer used is usually unrecrystallised and can have as high as 5% w/w lactic acid.[19]

As part of research carried out to trial group IV unsymmetrial amine tris(phenolate) complexes as suitable initiators for industrial application, polymerisations of unrecrystallized *rac*-lactide were carried out on a 35g scale using Zr_2(**8**)$_2$(O^iPr)$_2$, Zr_2(**10**)$_2$(O^iPr)$_2$ and Hf_2(**8**)$_2$(O^iPr)$_2$. A monomer/initiator ratio of 5000:1 was used under solvent-free conditions at 165 °C. Zr-C_3^tBu, first published by Davidson *et. al.*,[6] was also tested under the same conditions to provide more insight into the phenyl substituents effect on activity. Lactide conversion was monitored *in situ* using a FT-IR probe with an integration established for the carbonyl-acyl oxygen asymmetric stretch; occurring at ~1250 cm^{-1} (Figure 3.34).

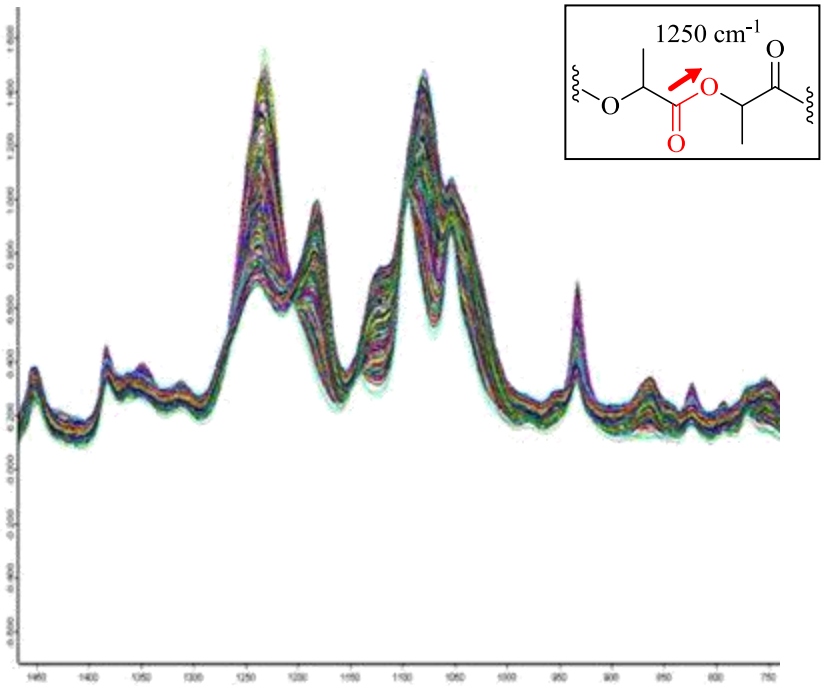

Figure 3.34 Example FT-IR spectra for the ROP of lactide; showing the shift in the asymmetric stretch (see insert) over time due to ROP

Resulting polymeric material, all with >95 % conversion, was characterised by gel permeation chromatography (GPC) for number-average molecular weight (M_n) and polydispersity index

(PDI). Homonuclear decoupled ^{1}H $\{^{1}H\}$ NMR spectroscopy was used to quantify polymer tacticity due to any stereoselectivity of the initiator (Table 3.9).

Initiator	M_n	PDI	P_r
Zr(8)(O^{i}Pr)	21200	1.19	0.62
Zr(9)(O^{i}Pr)	15300	1.21	0.64
Hf(8)(O^{i}Pr)	8900	1.14	0.57
Zr-*C*$_3$^{t}*Bu*	83300	1.65	0.60

Table 3.9 Characterisation for polymer produced on 35g scale whilst monitoring *via in situ* FT-IR. M_n and PDI acquired through size exclusion chromatography (GPC), referenced to polystyrene standards. > 95 % conversion for all samples.

All initiators had similar stereoselectivity (P_r ~ 0.6) which resulted in a significant reduction in selectivity for Zr-*C*$_3$^{t}*Bu* compared to that observed at higher catalyst loading (300:1) and lower melt temperatures (130 °C). At higher temperature the energy barriers associated with the *P*/*M* equilibrium of the *C*$_3$-symmetrical initiator would be more easily overcome. This has been proposed as a key factor in providing high selectivity.[18] Molecular weight was much lower than expected for such a high [M]:[I] however the use of non-recrystallised *rac*-lactide would introduce lactic acid to the polymerisation system. Lactic acid is capable of acting as a chain transfer agent and cooinitiator, causing a significantly lower polymer molecular weight.

As with ^{1}H NMR spectroscopy-based experiments, with the presumption that the ROP is pseudo-first order with respect to monomer, k_{app} can be calculated by plotting $ln\left(\frac{[LA]_0}{[LA]_t}\right)$ versus time (Figure 3.35 and Table 3.10).

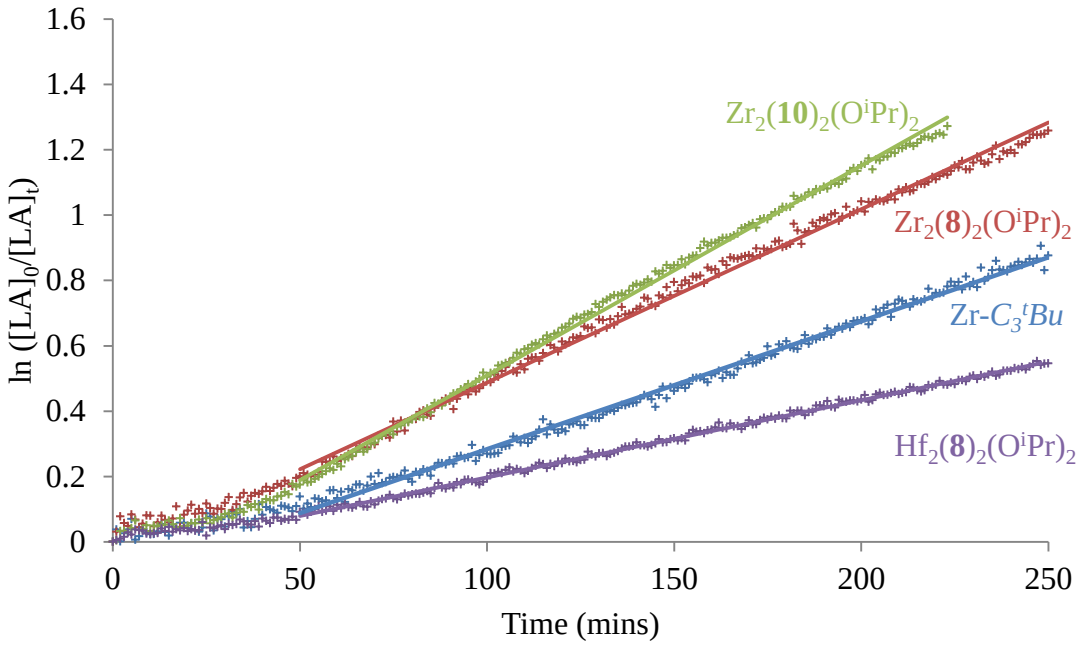

Figure 3.35 Semi-ln plot for the ROP of rac-lactide initiated by Zr_2(**8,10**)$_2$(O^iPr)$_2$, Hf_2(**8**)$_2$(O^iPr)$_2$ and Zr-$C_3{}^tBu$; gradient is the apparent rate constant (k_{app})

Initiator	k_{app} (mins^{-1})
Zr-$C_3{}^tBu$	3.92 ×10^{-3}
Zr_2(8)$_2$(O^iPr)$_2$	5.31 ×10^{-3}
Zr_2(10)$_2$(O^iPr)$_2$	6.41 ×10^{-3}
Hf_2(8)$_2$(O^iPr)$_2$	2.36 ×10^{-3}

Table 3.10 Apparent rate constants (k_{app}) for Zr_2(**8,10**)$_2$(O^iPr)$_2$, Hf_2(**8**)$_2$(O^iPr)$_2$ and Zr-$C_3{}^tBu$. Calculated from the gradient of $\ln\left(\frac{[LA]_0}{[LA]_t}\right)$ versus *time* as generated from *in situ* monitoring of the shift in (C=O)-O stretch from monomer to polymer using FT-IR spectroscopy

In contrast to kinetic studies carried out in solution (toluene-d_8), there was an increase in rate of ROP of *rac*-lactide when Zr_2(**8**)$_2$(O^iPr)$_2$ was used over Zr-$C_3{}^tBu$ under solvent-free conditions. A further increase was seen for Zr_2(**10**)$_2$(O^iPr)$_2$ as the steric bulk about the metal centre was reduced further by the removal of a second pair of *tert*-butyl substituents (R = H *vs* R = ^{t}Bu). This trend corresponds to that previously reported in which increased steric bulk resulted in overall lower activity.[20] Under melt conditions, whilst described as solvent-free, the lactide was acting as a solvent for the catalyst. With its coordinative ability and ^{1}H NMR spectroscopy studies in THF-d_8 suggesting the breakdown of the dimer into a monomeric species, it is

reasonable to assume a similar dissociation takes place in the melt. Therefore the dimer was more effectively disrupted than in dilute conditions in toluene or chloroform. If this was the case then the limiting step became the coordination of lactide to the metal centre rather than the recombination of the ROP-active species into an inactive dimer. The slower rate observed for t < 50 minutes can be attributed to the formation of the monomeric active species of initiator and reaction with impurities in the lactide.

3.5 Conclusions and further work

This research has developed a stepwise method for the synthesis of amine tris(phenolate) ligands that can have different substituents, including unsubstituted, on each phenolate arm. Whilst this work was limited to a set of three ligands: H_3**8** (H/^{t}Bu/^{t}Bu), H_3**9** (H/Me/^{t}Bu) and H_3**10** (H/H/^{t}Bu), the range of widely available 2,4-di-substituted phenols offers the ability to create a wide range of unsymmetrical tetradentate ligands. 3,5-dimethyl-2-hydroxybenzaldehyde was synthesised from the corresponding phenol and this could be done for other phenols. Of particular interest is the aldehyde of 2-trityl-4-methyphenol which would offer the synthesis of an amine tris(phenolate) with at least one arm substituted with groups larger than *tert*-butyl. Whilst in this work there was always one unsubstituted phenolate arm, imine bis(phenolate) ligands synthesised in chapter 2 utilised a di-*tert*-butyl-substituted salicylammonium acetate as a starting material; accessed from the aldehyde *via* the oxime. This would allow all phenolate arms to remain substituted and, with the increased steric bulk of the substituents, less boron enclosure may occur during the reduction of the imine to the corresponding amine, removing the need for benzyl protection chemistry. However, if protection of the hydroxyl group of the phenol was required then the protection of an aromatic –OH group is widely achieved using benzyl bromide.

Coordination of ligand H_3**8**-H_3**10** to M(O^iPr)$_4$(HO^iPr) (where M = Zr, Hf) produced a range of dimer complexes with general formula M_2(**X**)$_2$(O^iPr)$_2$ with each metal occupying the centre of a pseudo-octahedral geometry and one remaining isoproxide group in the axial position *trans* to the amine of the ligand. Structural analysis in the solid-state by single-crystal X-ray diffraction suggested that the less hindered unsubstituted phenolate occupied the bridging position. Solution NMR spectroscopy in non-coordinative solvents showed that the dimer bonding motif persisted.

Trialling of these complexes as initiators for the ROP of lactide found them to be active without the presence of a co-initiator. This suggested polymerisation by the expected coordination-

insertion method utilising the labile ispropoxide group, that was also identified as a polymer end group *via* MALDI-ToF mass spectrometry. Spectroscopic studies in a coordinative solvent, plus previous understanding of the coordination geometry behaviour of group IV metals suggested that the ROP-active species would be a five-coordinated monomeric species. This set of complexes therefore provided an interesting comparison to the previously reported C_3-symmetrical zirconium amine tris(phenolate) that exhibited high activity and heterotactic selectivity in the melt.[6] Stereoselectivity of Zr_2(**8-10**)$_2$(O^iPr)$_2$ were found to be comparable with a step reduction to $P_r \sim 0.7$ compared to 0.96 for the C_3 analogue for polymeric material produced in the melt. This provided evidence that the axial flipping exhibited by Zr-$C_3{}^tBu$ coupled with the presence of *tert*-butyl groups on each phenolate arm was central to the high selectivity. Previous work has suggested a weighted equilibrium in which the coordination of one diasteromer of lactide is preferential for the *P* isomer of the complex over *M* isomer. Whilst the presence of the *tert*-butyl substituents is presumably essential to restrict lactide approach to the coordination site the fact that little change is observed as further substituents are removed / reduced in size suggests that the symmetrical nature and subsequent symmetrical flipping is paramount to the high activity for these systems. A similar step-reduction in selectivity from the monomeric species was observed for the hafnium analogues.

The unsymmetrical group IV amine tris(phenolate) complexes previously reported by Jones *et al.* also had reduced selectivity compared to the highly selective C_3-symmetric zirconium based initiator (Zr-$C_3{}^tBu$).[6, 21] The series presented by Jones *et al.* produced wholly atactic polymeric material with a slightly narrower PDI and, whilst the complexes were also dimeric with one ortho-phenolate substituent absent, this may be due to faster initiation and the lack of any aggregation of the propagating species. However, no kinetic studies were reported. [21]

The aim of generating this series of unsymmetrical amine tris(phenolate) complexes was to provide further insight into the highly-selective Zr-$C_3{}^tBu$ initiator.[6] Varying the steric bulk of the phenolate substituents was not found to tune the selectivity, rather "switch-off" the enhanced chain-end control that is coupled with preferential *tert*-butyl steric bulk at the ortho position of the phenolates. This is contrary to that by Okuda *et al.* who reported a series of more flexible tetradentate {ONSO}-type ligands coordinated to zirconium as discreet octahedral complexes.[22] It is important to recognise the increase in both rigidity and flexibility through the incorporation of imine functionality and an ethyl linker to the thio group, and the use of sterically bulky adamantly substituents to influence the fluxional nature of the *fac-mer* isomerisation process.[22]

Further comparison to linear tetradentate salalen ligands coordinated to zirconium (IV), as reported by Jones *et al.* finds that the unsymmetrical initiators reported herein have significantly higher activity with a slightly higher degree of stereoselectivity towards heterotactic enchainment.[23] The monomeric octahedral complexes offered reduced steric bulk about the metal centre but comparable kinetic studies (80 °C, toluene-d_8) found the pseudo first-order rate constant for $Zr_2(\mathbf{8})_2(O^iPr)_2$ to be 400 times larger than for a *tert*-butyl substituted salalen complex.[23] It should also be noted that $Zr_2(\mathbf{8})_2(O^iPr)_2$ has been found to be more active that the C_3-symmetric analogue and the tuneable complexes presented be Okuda *et al.*, although under slightly different conditions.[6, 22]

Molecular weight control based on monomer/initiator ratio was not as well defined as seen for the monomeric Zr-$C_3{}^tBu$ initiator. It has been discussed that this is potentially due to the requirement for the dimer to break apart before becoming active for ROP. This dimer dissociation was found not to be favourable and required the presence of lactide (or other coordinating species). Further to this, the trends observed in solution-based kinetics lead to the conclusion that ligand bulk was influential in both the dissociation of the dimer in the initiation step of the polymerisation and aggregation to an inactive dimer species during propagation. Kinetic studies in the melt, where lactide acts as a coordinative solvent prevented the reformation of a dimer and thus relative rate was seen to increase with the removal of the steric bulk of the ligand substituents. This highlights the limitations of using solution-based kinetics for applications in more industrially relevant conditions and that whilst complexes can be characterised in the solid state and solution it should not be presumed that they relate to the ROP-active species.

Considerable further work can be carried out to investigate the behaviour of the dimer complexes as initiators for the ROP of lactide. The coordination behaviour of lactide compared to THF is undoubtedly different and thus VT-NMR of the dimer complexes in the presence of lactide would provide insight into the presumed dissociation into the monomeric species. An initial study was carried out with $Zr_2(\mathbf{8})_2(O^iPr)_2$ being subjected to VT-NMR ($CDCl_3$) in the presence of ~1.1 equivalents of lactide (Figure 3.36). The AX spin system persisted with six doublets corresponding to the six diatereotopic protons of the methylene bridges and the four singlets assigned to the aromatic protons of the substituted phenolate arms due to the inequivalence imposed by the dimer motif.

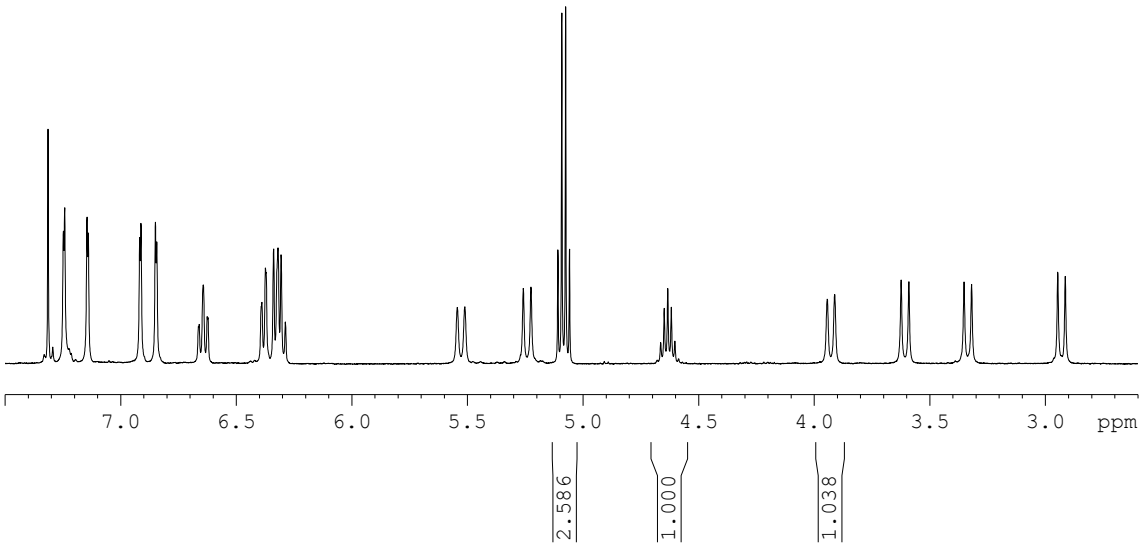

Figure 3.36 ^{1}H NMR spectrum ($CDCl_3$) for $Zr_2(\mathbf{8})_2(O^iPr)_2$ in the presence of ~1.1 equivalents of lactide. Region shown is that of aromatic protons and doublets assigned to the diastereotopic protons of the methylene bridges (PhC$\mathbf{H_2}$N). Integrals shown for the lactide methine (5.09 ppm), isopropoxide methine (4.64 ppm) and one methylene bridge proton (3.94 ppm).

This provided evidence of the stability of the dimer motif of $Zr_2(\mathbf{8})_2(O^iPr)_2$, suggested as a reason for higher polymer molecular weight due to some initiator inactivity. Hillmyer and Tolman effectively used ^{1}H NMR spectroscopy to calculate a K_{eq} for the coordination equilibrium of caprolactone to an aluminium alkoxide bis(phenolate) species independent of the traditional kinetic data.[17] Signals observed for the aromatic protons of the phenolate ring drifted over the reaction time as caprolactone monomer was consumed. For the fast association/dissociation of caprolactone to the aluminium centre the ^{1}H NMR spectrum at a given moment provided an average of both the coordinated and uncoordinated complex. With the presumption that the complex finished as an uncoordinated species, due to full conversion of caprolactone, the average and thus the chemical shift drifted as a function of caprolactone concentration and thus reaction time (Figure 3.37). Such a study should be carried out on the least hindered $Zr_2(\mathbf{10})_2(O^iPr)_2$ which is believed to recombine to an uncoordinated inactive dimer. This would be need to be a carried out at higher catalyst loading and at lower monomer concentration in order to distinguish the initiator signals from the spectrum baseline. Issues may also arise with the rapid nature of these polymerisations preventing a greater number of scans that in turn would provide increased resolution.

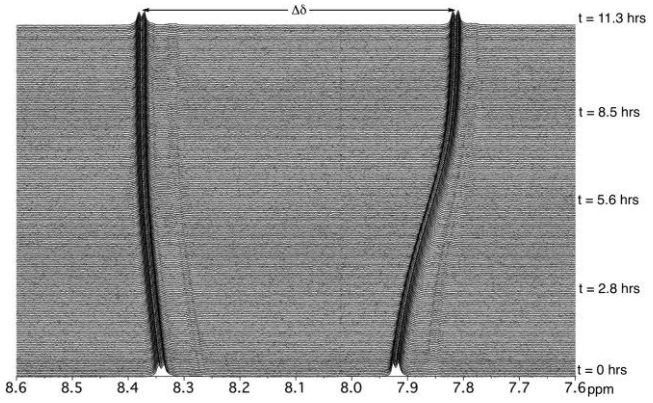

Figure 3.37 Time-resolved ^{1}H NMR spectroscopy of the ROP of caprolactone initiated by an aluminium alkoxide amine bis(phenolate) complex. Spectra show the drift in chemical shift (Δδ) of the aromatic protons of the phenolate rings with a function of time and decreasing [CL]. Image take from the literature[17]

Consideration of saturation kinetics proposed that $[LA]_0$ had influence on the dissociation of the dimer in the initiation of the polymerisation. Carrying out polymerisations at different concentrations of lactide would therefore alter the amount of active initiator at $t \approx 0$ and a more comparable molecular weight to that calculated from [M]:[I] and conversion. However, the discrepancy in molecular weight that was also observed in the melt, where full saturation is assumed suggests that a thermodynamic barrier is in place that would be better studied through reaction temperature variation. Further kinetic study of these systems could be carried out in THF-d_8 in an attempt to ensure all initiator is in the monomeric form. However, this would then introduce a potential competitive coordination environment that would have an effect on rate of ROP.

With respect to the synthesis of new unsymmetrical group IV amine tris(phenolate) complexes as potential initiators, results directed towards targeting an unsymmetrical complex with increased steric bulk of the substituents. As mentioned previously, the use of a phenol with a considerably more bulky trityl group in the 2-position would offer one route to this type to complex. An increased ligand steric bulk would potentially prevent the formation of a dimer; if not, then molecular weights would be expected to be higher if lactide coordination was further hindered or alternatively the dimer may become thermodynamically fluxional with a monomeric species without the presence of a coordinative species. With respect to selectivity an unsymmetrical monomeric species with increased steric bulk on one if not two arms is an attractive target. Selectivity of Zr-$C_3{}^tBu$ initiator suggests that *tert*-butyl substituents are of an adequate size to influence which diastereomer of lacide is inserted into the growing chain.[18] Larger steric bulk may drive the prefence further and with the lack of symmetry and *P*/*M*

isomerism one diastereomer may always be inserted over the other leading to isotactic stereoselectivity. The higher activity with respect to previously reported tetradentate salalen ligands and even the {OSNO}-type ligands with tunable selectivity, suggests that the tripodal structure of these amine tris(phenolate) ligands provides active species with high Lewis acidity and ease of lactide coordination.

Finally, the study of ROP kinetics of lactide in the melt is an area little discussed in the literature, however, offers vital insight into the behaviour of catalytic initiators under relevant conditions for industrial applications. Practical limitations for new catalytic initiator systems for the set-up used in this work include the large amounts of material required (> 20 g of monomer). With less active initiators reactions could be monitored by freezing and quenching the reaction, however this would introduce considerable experimental error in timing and potential depolymerisation / transesterification during work-up.

3.6 References

1. Y. Kim and J. G. Verkade, *Organometallics*, 2002, **21**, 2395-2399.
2. Y. Kim, G. K. Jnaneshwara and J. G. Verkade, *Inorg. Chem.*, 2003, **42**, 1437-1447.
3. S. Gendler, S. Segal and I. Goldberg, *Inorg. Chem.*, 2006, **45**, 4783-4791.
4. S. D. Bull, M. G. Davidson, A. L. Johnson, D. E. J. E. Robinson and M. F. Mahon, *Chem. Commun.*, 2003, 1750-1751.
5. M. G. Davidson, C. L. Doherty, A. L. Johnson and M. F. Mahon, *Chem. Commun.*, 2003, 1832-1833.
6. A. J. Chmura, M. G. Davidson, C. J. Frankis, M. D. Jones and M. D. Lunn, *Chem. Commun.*, 2008, 1293-1295.
7. M. Kol, M. Shamis, I. Goldberg, Z. Goldschmidt, S. Alfi and E. Hayut-Salant, *Inorg. Chem. Commun.*, 2001, **4**, 177-179.
8. I. Zagol-Ikapitte, V. Amarnath, M. Bala, L. J. Roberts, J. A. Oates and O. Boutaud, *Chem. Res. Toxicol.*, 2010, **23**, 240-250.
9. A. Sokolowski, J. Muller, T. Weyhermuller, R. Schnepf, P. Hildebrandt, K. Hildenbrand, E. Bothe and K. Wieghardt, *J. Am. Chem. Soc.*, 1997, **119**, 8889-8900.
10. Y. Geng and W. Wu, *Acta Crystallographica Section E*, 2011, **67**, o1380.
11. P. D. Woodgate, G. M. Horner, N. P. Maynard and C. E. F. Rickard, *J. Organomet. Chem.*, 1999, **592**, 180-193.
12. B. J. Jeffery, E. L. Whitelaw, D. Garcia-Vivo, J. A. Stewart, M. F. Mahon, M. G. Davidson and M. D. Jones, *Chem. Commun.*, 2011, **47**, 12328-12330.
13. B. M. Chamberlain, M. Cheng, D. R. Moore, T. M. Ovitt, E. B. Lobkovsky and G. W. Coates, *J. Am. Chem. Soc.*, 2001, **123**, 3229-3238.
14. N. Nomura, R. Ishii, Y. Yamamoto and T. Kondo, *Chem. Eur. J.*, 2007, **13**, 4433-4451.
15. Y. Huang, W. Wang, C.-C. Lin, M. P. Blake, L. Clark, A. D. Schwarz and P. Mountford, *Dalton Trans.*, 2013, **42**, 9313-9324.
16. A. Duda and S. Penczek, *Makromolekulare Chemie. Macromolecular Symposia*, 1991, **47**, 127-140.
17. K. Ding, M. O. Miranda, B. Moscato-Goodpaster, N. Ajellal, L. E. Breyfogle, E. D. Hermes, C. P. Schaller, S. E. Roe, C. J. Cramer, M. A. Hillmyer and W. B. Tolman, *Macromolecules*, 2012, **45**, 5387-5396.
18. A. J. Chmura, C. J. Chuck, M. G. Davidson, M. D. Jones, M. D. Lunn, S. D. Bull and M. F. Mahon, *Angew. Chem., Int. Ed.*, 2007, **46**, 2280-2283.
19. C. J. Chuck, Editon edn., 2011.
20. A. P. Dove, V. C. Gibson, E. L. Marshall, A. J. P. White and D. J. Williams, *Dalton Trans.*, 2004, 570-578.
21. E. L. Whitelaw, M. D. Jones, M. F. Mahon and G. Kociok-Kohn, *Dalton Trans.*, 2009, 9020-9025.
22. A. Stopper, J. Okuda and M. Kol, *Macromolecules*, 2012, **45**, 698-704.
23. M. D. Jones, E. L. Whitelaw and M. F. Mahon, *Inorg. Chem.*, 2010, **49**, 7176-7181.

CHAPTER 4

COPOLYMERISATION STUDIES

4 Copolymerisation studies

4.1 Preamble

Copolymerisation offers an attractive route to tuning the properties of polymeric material. The controlled copolymerisation of lactide and ε-caprolactone has received considerable attention due to the complementary properties of the respective homopolymers (polylactide, PLA, polycaprolactone, PCL), especially with respect to biomedical applications.[1-6] Poly(lactide-*co*-ε-caprolactone) can be more permeable to drugs than PLA alone due to the high hydrophilicity of PLA.[1] However, the *in vivo* lifetime of PLA is relatively short (weeks) compared to PCL (1 year).[2] Whilst block copolymers of PLA and PCL can be achieved through the sequential addition of the respective monomers, a random copolymer with even distribution of both monomers cannot be achieved through this method. Studies of the one-pot copolymerisation of lactide and ε-caprolactone have shown the preferential incorporation of lactide over ε-caprolactone, creating tapered block copolymers.[3, 5] Recently, Nomura *et al* have reported the copolymerisation of lactide and ε-caprolactone with practically random (Bernoullian) distributions using a homosalen aluminium complex.[6] Control was achieved through ligand variation with an increase in the phenol substituent bulk in close proximity to the metal centre promoting random insertion over the tapering seen with smaller phenol substituents.[6]

Ligand influence on both the polymerisation and copolymerisation of lactide is difficult to predict, with the desired selectively often obtained serendipitously. Herein, the previously presented series of zirconium amine tris(phenolate) alkoxide initiators (Chapter 3) are studied as initiators for the copolymerisation of lactide and ε-caprolactone. With only small changes to the ligand substituents, compolymer composition will be analysed for each initiator to ascertain if such changes influence monomer incorporation into the copolymer. This series of initiators present differences in stereoselectivity and activity; the C_3-symmetrical zirconium initator offers unprecedented heterotactic selectivity for the ROP of *rac*-lactide and subsequent much lower activity for the ROP of the enantiopure L-lacitde.[7] The study will therefore also investigate if high stereoselectivity impedes the potential of a random copolymerisation for this type of intiator.

4.2 Copolymerisation of L-lactide and ε-caprolactone using zirconium amine tris(phenolate) alkoxides

Copolymerisation trials were carried out with the previously published C_3-symmetrical zirconium amine tris(phenolate) (Zr-$C_3{}^tBu$)[7] and Zr_2(**8,10**)$_2$(O^iPr)$_2$, as presented in chapter 3. The aims were to establish if: (a) they were capable of producing copolymers with the monomers lactide and ε-caprolactone, and (b) if so, what types of copolymer were produced and if copolymer microstructure varied depending on the initiator. The investigation was limited to L-lactide for larger-scale polymerisations to provide more straight forward ^{1}H and ^{13}C{^{1}H} NMR spectroscopic analysis of polymeric material due to the lack of stereochemical influence on the methine and carbonyl resonances.

Copolymerisation trials were carried out with ~1.0 g of monomer in dry toluene under air-sensitive conditions. [M] = 0.66 M with [M]/[I] = 100. Monomer conversion was calculated through ^{1}H NMR spectroscopy with relative integration of the signals assigned to the methine signal of the lactide/polylactide and the methylene protons adjacent to the acyl oxygen of the caprolactone/polycaprolactone (Figure 4.1). Polymeric material, after washing with methanol to remove unreacted monomer, was analysed *via* GPC (THF) for number-average molecular weight (M_n) and polydispersity index (PDI). Due to the presumed living nature of the polymerisations taking place, an expected polymer molecular weight was calculated based on monomer-initiator ratio and conversion (Table 4.1). Reaction time was initially 24 hours with a repetition carried out if reaction completion (> 99% monomer conversion) seemed apparent.

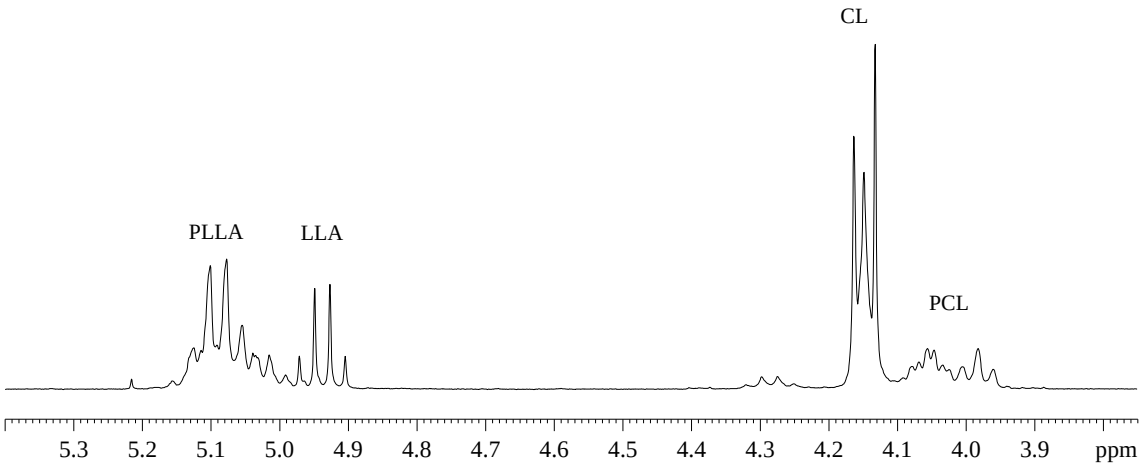

Figure 4.1 Extract of ^{1}H NMR spectrum of unwashed poly(L-lactide-*co*-ε-caprolactone). Region shown with labelled lactide/polylactide methine signals (4.90-5.15 ppm) and methylene adjacent to the acyl-oxygen signals of caprolactone/polycaprolactone (3.93-4.19 ppm)

Entry	Initiator	Time /h	L-LA conv. /% [a]	ε-CL conv. /% [a]	M_n [calc]	M_n [b]	PDI [b]
1	Zr-C_3^tBu	24	>99	>99	13000	11400	1.4
2	Zr-C_3^tBu	6	80	41	8150	9500	1.1
3	Zr_2(**8**)$_2$(O^iPr)$_2$	24	>99	>99	13000	19800	1.6
4	Zr_2(**8**)$_2$(O^iPr)$_2$	2	74	83	10100	16200	1.5
5	Zr_2(**10**)$_2$(O^iPr)$_2$	24	71	68	9050	11000	1.7

Conditions: [LA]/[Cl] = 1, [M]/[I] = 100, [M] = 0.66 M, toluene, 80 °C. [a] As determined *via* ^{1}H NMR, [b] Determined from GPC (in THF) referenced to polystyrene standards. It is noted that a Mark-Houwink correction is not applied; this is discussed in section 5.1.2. The calculated molecular weights were determined by the following (7200 x $\frac{LA\ conv}{100}$) + (5700 × $\frac{CL\ conv}{100}$) + 60 {where 60 is the mass of the end groups (H/OCH(CH$_3$)$_2$)}

Table 4.1 Polymerisation data for the trailing of zirconium amine tris(phenolate) complexes as initiator for the one-pot copolymerisation of L-lactide and ε-caprolactone

On this ~1.0 g scale, all initiators exhibited activity for the one-pot polymerisation of L-lactide and ε-caprolactone. Molecular weights generally showed good correlation to weights calculated from conversion and monomer-initiator ratio. Measured polymer molecular weights (GPC) were slightly higher for Zr_2(**8**)$_2$(O^iPr)$_2$, in line with that observed in the, previously discussed, full polymerisation study (chapter 3). Based on the conversion to high molecular weight and preliminary analysis of the ^{1}H NMR spectra it can be concluded that copolymerisation, whether block, tapered or random, is taking place. A reduction in reaction time for Zr-C_3^tBu and Zr_2(**8**)$_2$(O^iPr)$_2$ to six and two hours respectively saw lower monomer conversion and whilst this cannot be used as an indication of rate, a significantly higher conversion of lactide to polylactide was observed for Zr-C_3^tBu suggesting a preference for lactide incorporation into the growing polymer chain. A shorted reaction time also gave a narrower PDI for the polymeric material produced using the Zr-C_3^tBu which is an attribute of a polymerisation with a rapid initiation step, akin to that reported for homopolymerisation of lactide with this initiator.[7] The wider PDI for material isolated from the 24 hour reactions could be due to increased transesterification either during the polymerisation of the less-hindered ε-caprolactone or the unnecessary extended reaction time. Higher PDI values for Zr_2(**8**)$_2$(O^iPr)$_2$ and Zr_2(**10**)$_2$(O^iPr)$_2$ compared to Zr-C_3^tBu were observed and could be attributed to the reduced steric bulk about the metal centre allowing greater ease of transesterification and/or a slower rate of initiation due to the dimer nature of the complexes.

4.2.1 ^{1}H NMR Spectroscopy for average block length and reactivity ratios

Further analysis of the ^{1}H NMR spectra of polymeric materials can identify the extent of block and copolymerisation (Scheme 4.1). Both the methine signals of the lactidyl and α-methylene (carbonyl) / ε-methylene (acyl) signals of the caproyl repeat units appear at slightly different chemical shifts depending on the nature of the adjacent repeat unit (Figure 4.2).

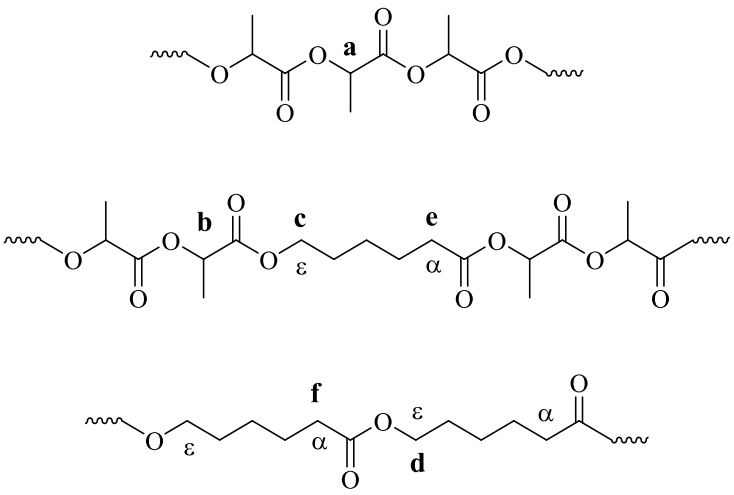

Scheme 4.1 Chemical structure of poly(L-lactide-*co*-caprolactone) with annotation for: **a** – LA-LA methine, **b** – LA-CL methine, **c** – CL-LA (acyl) ε-methylene, **d** – CL-CL (acyl) ε-methylene, **e** – CL-LA (carbonyl) α-methylene, **f** – CL-CL (carbonyl) α-methylene

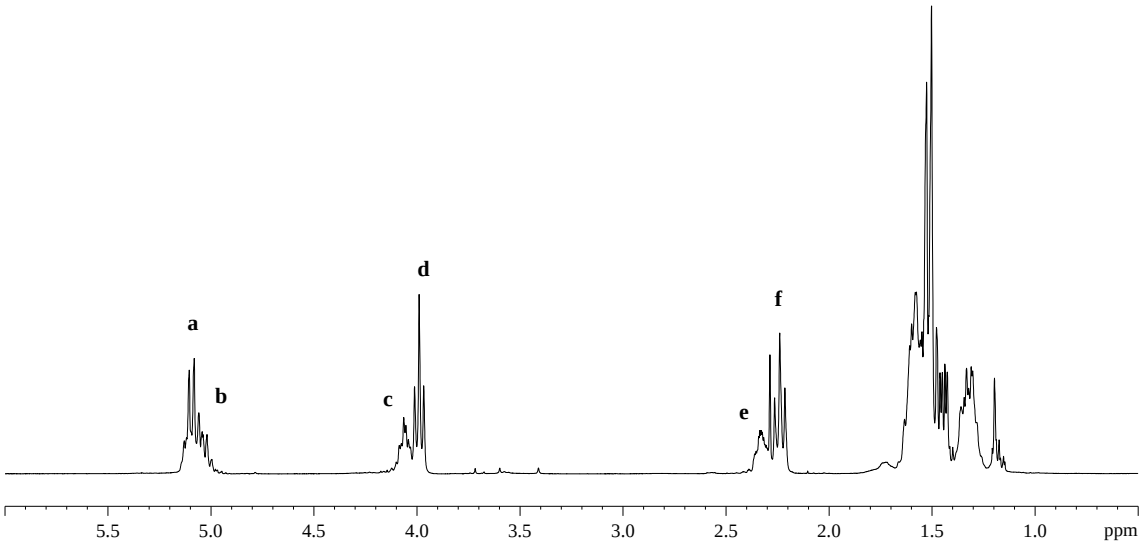

Figure 4.2 Extract of ^{1}H NMR ($CDCl_3$) spectrum of poly(l-lactide-*co*-lactide). Annotation for: **a** – LA-LA methine, **b** – LA-CL methine, **c** – CL-LA (acyl) ε-methylene, **d** – CL-CL (acyl) ε-methylene, **e** – CL-LA (carbonyl) α-methylene, **f** – CL-CL (carbonyl) α-methylene

Relative integration of the full lactidyl methine signal (**a**+**b**) and the ε-methylene (**c**+**d**) provided a ratio of LA/CL in the polymer; noting that the lactide monomer contributes two lactidyl unit to the polymer chain, and thus two methine protons. With the hetero-diad CL-LA and homo-diad CL-CL more easily integrated separately it was reasonably approximated that the relative intensity of hetero-methine (LA-CL) and hetero-methylene (CL-LA) signals should be equivalent and thus: **b** = **c**, **a** = (**a**+**b**) – **c** or [LA-LA] = [PLLA] – [CL-LA]. Deconvolution of the PLA methine signal (**a** + **b**) was also carried out to approximate the intensity of the homo-diad LA-LA, exhibiting good correlation to that calculated by the difference (Table 4.2).

Entry	Initiator	L-LA : εCL	Relative polymeric molar fractions [a]						$\frac{[LA-LA]}{[PLA]}$	$\frac{[CL-CL]}{[PCL]}$
			[PLLA] (**a**+**b**)	[PCL] (**c**+**d**)	[LA-LA] [**a**] [b]	[LA-CL] [**b**]	[CL-LA] [**c**]	[CL-CL] [**d**]		
1	Zr-C_3^tBu	1:2	0.33	0.67	0.17	0.16	0.16	0.51	0.52	0.76
2	Zr-C_3^tBu	1:1	0.49	0.51	0.32	0.18	0.18	0.33	0.63	0.65
3	Zr-C_3^tBu	2:1	0.66	0.34	0.61	0.16	0.16	0.18	0.76	0.53
4	Zr_2(**8**)$_2$(O^iPr)$_2$	1:3	0.24	0.76	0.10	0.16	0.16	0.6	0.33	0.79
5	Zr_2(**8**)$_2$(O^iPr)$_2$	1:1	0.42	0.58	0.23	0.19	0.19	0.39	0.55	0.67
6	Zr_2(**8**)$_2$(O^iPr)$_2$	2:1	0.67	0.33	0.56	0.18	0.18	0.15	0.73	0.45
7	Zr_2(**10**)$_2$(O^iPr)$_2$	1:3	0.28	0.72	0.14	0.23	0.23	0.49	0.18	0.68
8	Zr_2(**10**)$_2$(O^iPr)$_2$	1:1	0.52	0.48	0.39	0.2	0.20	0.28	0.62	0.58
9	Zr_2(**10**)$_2$(O^iPr)$_2$	3:1	0.82	0.18	0.71	0.12	0.12	0.06	0.85	0.33

Conditions: [LA]/[Cl] = 1, [M]/[I] = 100, [M] = 0.66 M, toluene, 80 °C. [a] As determined *via* ^{1}H NMR. [b] **b** = **c**, **a** = (**a**+**b**) – **c** or [LA-LA] = [PLLA] – [CL-LA]

Table 4.2 Selected diads, as determined by ^{1}H NMR spectroscopy, for poly(L-lactide-*co*-caprolactone) from the one-pot polymerisation of L-lactide and ε-caprolactone initiated by zirconium amine tris(phenolate) complexes: Zr-C_3^tBu and Zr_2(**8,10**)$_2$(O^iPr)$_2$

Entries 1-6 of Table 4.2 had all reached > 99% conversion and thus the monomer ratio correlated to the repeat unit ratio in the polymeric material. Increasing the mole fraction of either monomer resulted in an increase in the proportion of homo-diad for that monomer. Both monomers appeared to have equal weighting in this effect. However, it should be noted that whilst the fraction of 'homo-polymerised' monomer increased with monomer feed fraction, the mole fraction of 'hetero-polymerised' caprolactone (**[c]**) exhibited no trend with respect to either monomer feed ratio or initiator. The signal, **c**, at ~4.10 ppm was attributed to the methylene protons next to the acyl oxygen in the caproyl repeat unit. In a coordination-insertion mechanism, this would be adjacent to the metal centre immediately after insertion into the growing polymer chain. For it to become a (CL-LA) diad lactide would have to be the next monomer inserted into the polymer chain. This apparent lack of dependence on initiator or monomer feed ratio for the incorporation of lactide into a growing polymer chain would suggest that for this system alteration of the steric bulk of the initiator has little effect on insertion of lactide into a growing chain at the range of feed ratios studied. The increase in homo-polymerisation with increased monomer feed could be attributed to the excess of caprolactone polymerising after all lactide is converted or a lactide/caprolactone monomer ratio is reached that is weighted enough to influence the insertion preference of lactide.

Whilst ^{13}C $\{^{1}H\}$ NMR has widely been used to probe the microstructure of polymers, the information provided by the diads of the ^{1}H NMR spectra of poly(lacide-*co*-caprolactone) has also been used.[8] The use of relative diad intensity only considers the effect of the previously inserted monomer and, whilst penultimate unit chain end control is influential in radical polymerisation, there is little effect for ROP *via* a coordination insertion mechanism. The chemical nature of an adjacent unit to a propagating lactidyl or caproyl alkoxide will have little effect on selectivity. With relative quantification of the comonomer fractions, [PLLA], [PCL] and the hetero-diad [LA-CL] it is possible to calculate the average block length ($\bar{L}_m$), where *m* is either the monomer L-lactide or ε-caprolactone, using the following equations:

$$\bar{L}_{LA} = \frac{2[PLLA]}{[LA-CL]}$$

$$\bar{L}_{CL} = \frac{2[PCL]}{[LA-CL]}$$

These can be compared to the average block length expected for a true random copolymer ($(\bar{L}_m)_{random}$) based on Bernoullian statistics as follows:

$$(\bar{L}_{LA})_{random} = \frac{1}{f_{CL}} \quad , \quad (\bar{L}_{CL})_{random} = \frac{1}{f_{LA}}$$

Where f_{CL} and f_{LA} are the monomer mole fraction of ε-caprolactone and lactide respectively. Further to this, a randomness factor (R) can be calculated:

$$R = \frac{[LA - CL]}{2[PLLA][PCL]}$$

For a block copolymer $R \to 0$ whilst for a truly random copolymer $R \to 1$. These values were calculated for entries 1-9 of Table 4.2 and are tabulated below (Table 4.3) with the relationship between lactide monomer mole fraction (f_{LA}) and average block length graphically represented in Figure 4.3 and Figure 4.4.

Entry	Initiator	L-LA : εCL	Average block length ($\bar{L}_m$) [a]				R
			$(\bar{L}_{LA})_{random}$ [b]	$(\bar{L}_{CL})_{random}$ [b]	$\bar{L}_{LA}$	$\bar{L}_{CL}$	
1	Zr-C_3^tBu	1:2	1.5	3.0	4.1	8.4	0.36
2	Zr-C_3^tBu	1:1	2.0	2.0	5.4	5.6	0.36
3	Zr-C_3^tBu	2:1	2.9	1.5	8.3	4.3	0.10
4	Zr_2(**8**)$_2$(O^iPr)$_2$	1:3	1.3	4.2	3.0	9.5	0.43
5	Zr_2(**8**)$_2$(O^iPr)$_2$	1:1	2.4	2.1	4.4	6.1	0.39
6	Zr_2(**8**)$_2$(O^iPr)$_2$	2:1	3.0	1.5	7.4	3.7	0.41
7	Zr_2(**10**)$_2$(O^iPr)$_2$	1:3	1.3	4.0	2.4	6.3	0.57
8	Zr_2(**10**)$_2$(O^iPr)$_2$	1:1	2.0	2.0	5.2	4.8	0.40
9	Zr_2(**10**)$_2$(O^iPr)$_2$	3:1	4.0	1.3	13.7	3.0	0.41

Conditions: [LA]/[Cl] = 1, [M]/[I] = 100, [M] = 0.66 M, toluene, 80 °C. [a] As determined *via* ^{1}H NMR. [b] $(\bar{L}_M)_{random}$ = average block length based on Bernoullian statistics. $(\bar{L}_{M_1})_{random} = \frac{1}{f_{M_2}}$. Conversion > 99 % for all except 7-9

Table 4.3 Average block length ($\bar{L}_m$) and randomness factor (R), as determined by ^{1}H NMR spectroscopy, for poly(L-lactide-*co*-caprolactone) from the one-pot polymerisation of L-lactide and ε-caprolactone initiated by zirconium amine tris(phenolate) complexes: Zr-C_3^tBu and Zr_2(**8,10**)$_2$(O^iPr)$_2$

Comparison of average block length, as determined by ^{1}H NMR spectroscopy, with that predicted for a random copolymer using Bernoullian statistics highlights that for all initiators and monomer feed ratios the average block length is larger than expected for a truly random copolymer. As this value is an average over the whole polymer microstructure an increase

would be caused by the block segments of poly(L-lactide) and poly(ε-capolactone) at each end of the polymer chain. Average block length is relatively larger for lactide with respect to the increase in average block length for caprolactone, providing further evidence that there is a preference for the polymerisation of lactide with these initiators. Graphical comparison of the effect of monomer mole fraction on average block length for each initiator (Figure 4.3 and Figure 4.4) showed there to be no apparent relationship between initiator steric bulk and average block length for this copolymer system using this method of analysis. However, it is important to note that full conversion (> 99 %) was not achieved for entries 7-9 (Table 4.3) and thus the blocky-natured part of the copolymer is presumably reduced.

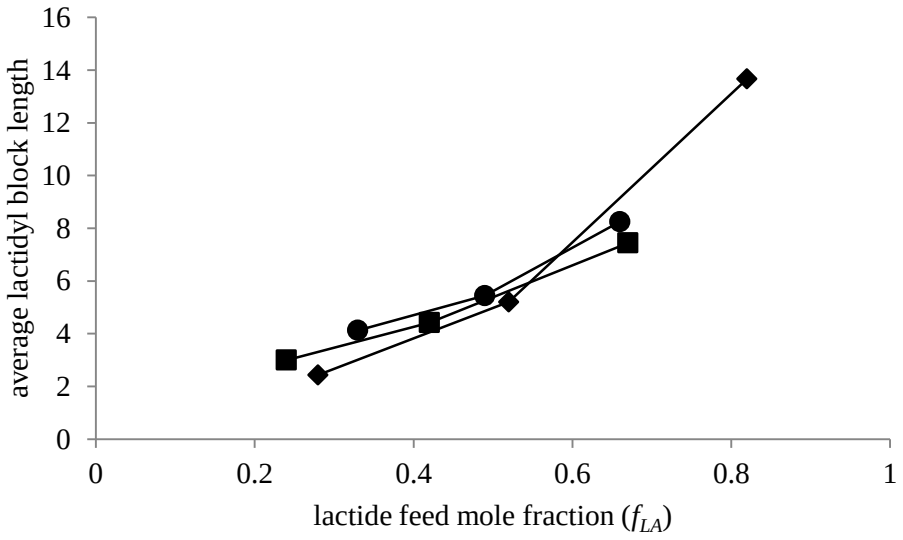

Figure 4.3 Average lactidyl block length ($\bar{L}_{LA}$) with respect to lactide monomer mole fraction (f_1) for poly(L-lactide-*co*-caprolactone) from the one-pot polymerisation of L-lactide and ε-caprolactone initiated by zirconium amine tris(phenolate) complexes: Zr-$C_3{}^tBu$ (●), Zr_2(**8**)$_2$(O^iPr)$_2$ (■) and Zr_2(**10**)$_2$(O^iPr)$_2$ (♦). Line joining points is for ease of comparison only.

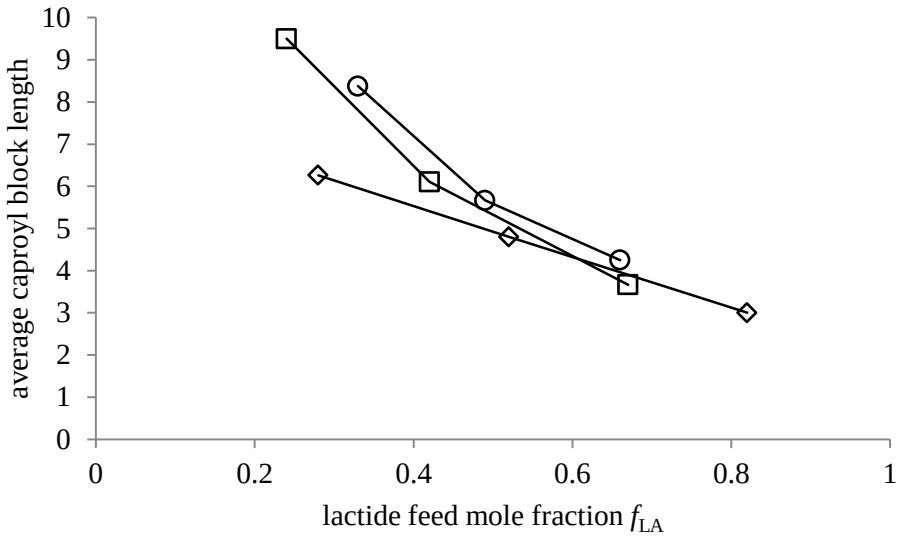

Figure 4.4 Average caproyl block length ($\bar{L}_{CL}$) with respect to lactide monomer mole fraction (f_1) for poly(L-lactide-*co*-caprolactone) from the one-pot polymerisation of L-lactide and ε-caprolactone initiated by zirconium amine tris(phenolate) complexes: Zr-C_3^tBu (○), Zr_2(**8**)$_2$(O^iPr)$_2$ (□) and Zr_2(**10**)$_2$(O^iPr)$_2$ (◊). Line joining points is for ease of comparison only.

Entries 2, 5 and 8 of Table 4.3 do provide insight into the effect of removing steric bulk from the catalytic initiating metal centre. Each of the entries had monomer ratio of 1:1 and thus in a truly random copolymer should have an average block length equal to 2. For the initiator Zr-C_3^tBu (entry 2) the average block length is approximately equivalent for each monomer indicating a tapered block copolymer with equal molar proportions in the blocks at each end of the copolymer chain. Replacing the initiator with Zr_2(**8**)$_2$(O^iPr)$_2$ removes steric bulk in the form of *tert*-butyl groups from one of the phenolate arms of the ligand. The average block length for lactide reduces from 5.4 to 4.4 whilst the average block length for caprolactone increases slightly to 6.1, corresponding to a reduction in the block-nature of the poly(L-lactide) component of the copolymer. This can be attributed to a slight increase in the preference of caprolactone insertion relative to lactide; also leading to an increase in average block length of caprolactone due to increase in the probability of caprolactone inserting into a growing caprolactone chain. This is also indicated by the slight increase in randomness factor. Continuing to remove steric bulk from the initiator with Zr_2(**10**)$_2$(O^iPr)$_2$ (entry 8) can be interpreted to provide insight into monomer preference for this copolymerisation. Whilst high conversion was not achieved, conversion for the 1:1 monomer ratio of L-lactide and ε-caprolactone was comparable (68 % and 71 % respectively). Compared to entry Zr-C_3^tBu (entry 2) and Zr_2(**8**)$_2$(O^iPr)$_2$ (entry 5), the relative average block lengths invert with $\bar{L}_{LA}$ increasing to 5.2 and $\bar{L}_{CL}$ decreasing to 4.8. The decrease in $\bar{L}_{CL}$ could be caused by the lack of a block polycaprolactone that is polymerised after the conversion of the lactide. However, with

conversion for each monomer at a comparable level, and thus the monomer mole fraction still ~1:1, the preference of insertion of each monomer must be more comparable. This is also apparent with the comparable values for average block length.

The comparable intensity of the ε-methylene protons, **[c]**, and α-methylene protons, **[e]**, signals in the ^{1}H NMR spectra can provide further evidence of copolymerisation (Table 4.4). With the polymerisation likely taking place *via* a coordination insertion mechanism the acyl oxygen of the previously inserted monomer is always located adjacent to zirconium metal centre; the acyl-carbonyl carbon bond breaks with the metal alkoxide of the monomer forming. In this mechanism the formation of the hetero-diad **c** is only formed on the insertion of lactide into a growing chain where caprolactone was the last monomer inserted. Likewise, the heterodiad **e** only occurs when a caprolactone chain is inserted into a growing chain where the previous monomer inserted was lactide. The signal equivalence, whilst not providing insight into block length, shows that insertion of lactide into caprolactone and *vice versa* are both possible in the one-pot copolymerisation of L-lactide and ε-caprolactone, graphically represented in Scheme 4.2. If this is not the case then, on the insertion of one monomer into the growing chain, only homo polymerisation would occur.

Entry	Initiator	L-LA:εCL	$\frac{\varepsilon[CL-LA]}{\varepsilon[PCL]}$ [a]	$\frac{\alpha[CL-LA]}{\alpha[PCL]}$ [a]
1	Zr-C_3^tBu	1:2	0.24	0.24
2	Zr-C_3^tBu	1:1	0.36	0.36
3	Zr-C_3^tBu	2:1	0.46	0.46
4	Zr_2(**8**)$_2$(O^iPr)$_2$	1:3	0.21	0.21
5	Zr_2(**8**)$_2$(O^iPr)$_2$	1:1	0.33	0.33
6	Zr_2(**8**)$_2$(O^iPr)$_2$	2:1	0.53	0.53
7	Zr_2(**10**)$_2$(O^iPr)$_2$	1:3	0.32	0.32
8	Zr_2(**10**)$_2$(O^iPr)$_2$	1:1	0.41	0.41
9	Zr_2(**10**)$_2$(O^iPr)$_2$	3:1	0.67	0.65

Conditions: [LA]/[Cl] = 1, [M]/[I] = 100, [M] = 0.66 M, toluene, 80 °C. [a] As determined *via* ^{1}H NMR

Table 4.4 Mole fraction of lactide and ε-caprolactone repeat units appearing as the homo-diad [LA-LA] and hetero-diad [CL-LA] respectively, for poly(L-lactide-*co*-caprolactone) from the one-pot polymerisation of L-lactide and ε-caprolactone initiated by zirconium amine tris(phenolate) complexes: Zr-C_3^tBu and Zr_2(**8,10**)$_2$(O^iPr)$_2$

LA-(CL)$_n$-LA	**c : d : e : f**
1 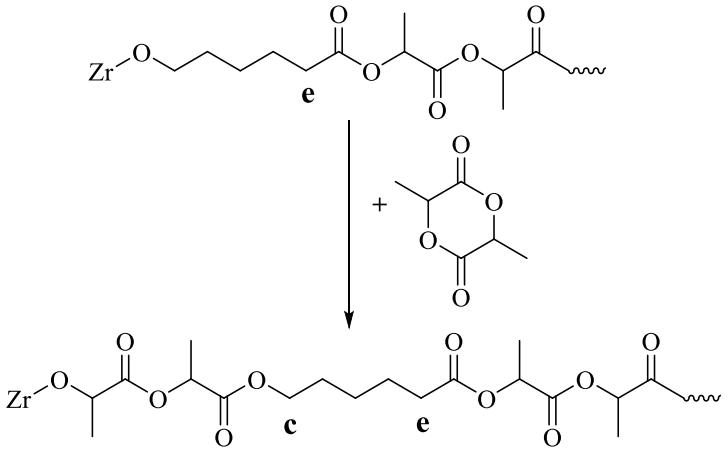	**0 : 0 : 1 : 0** **1 : 0 : 1 : 0**
2 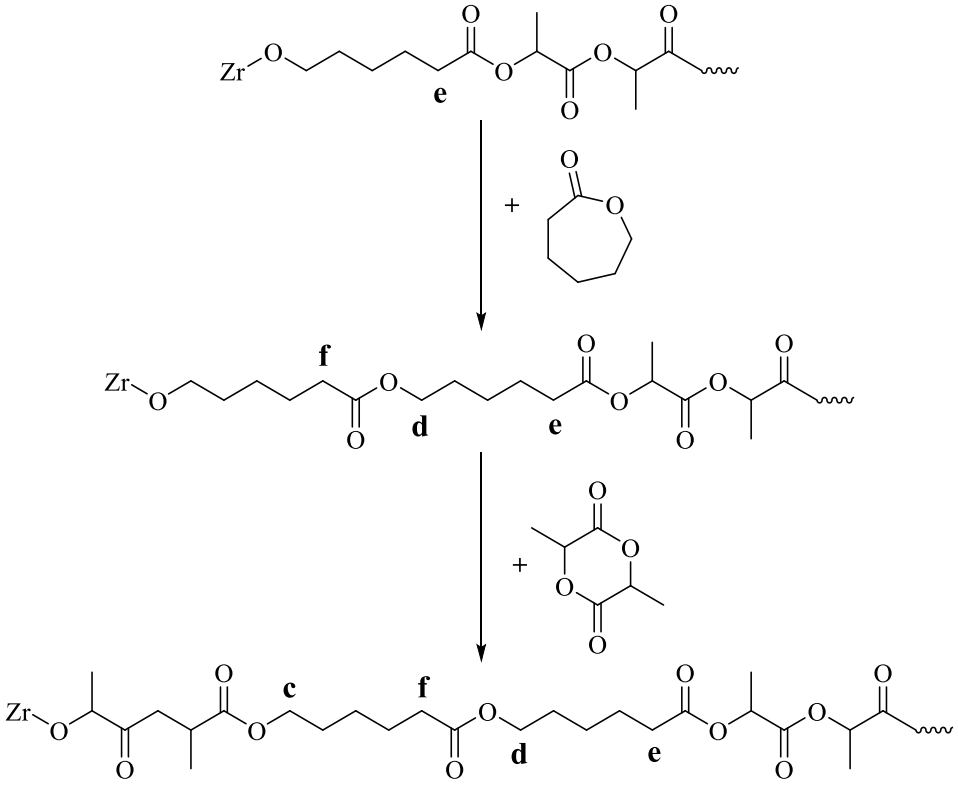	**0 : 0 : 1 : 0** **0 : 1 : 1 : 1** **1 : 1 : 1 : 1**

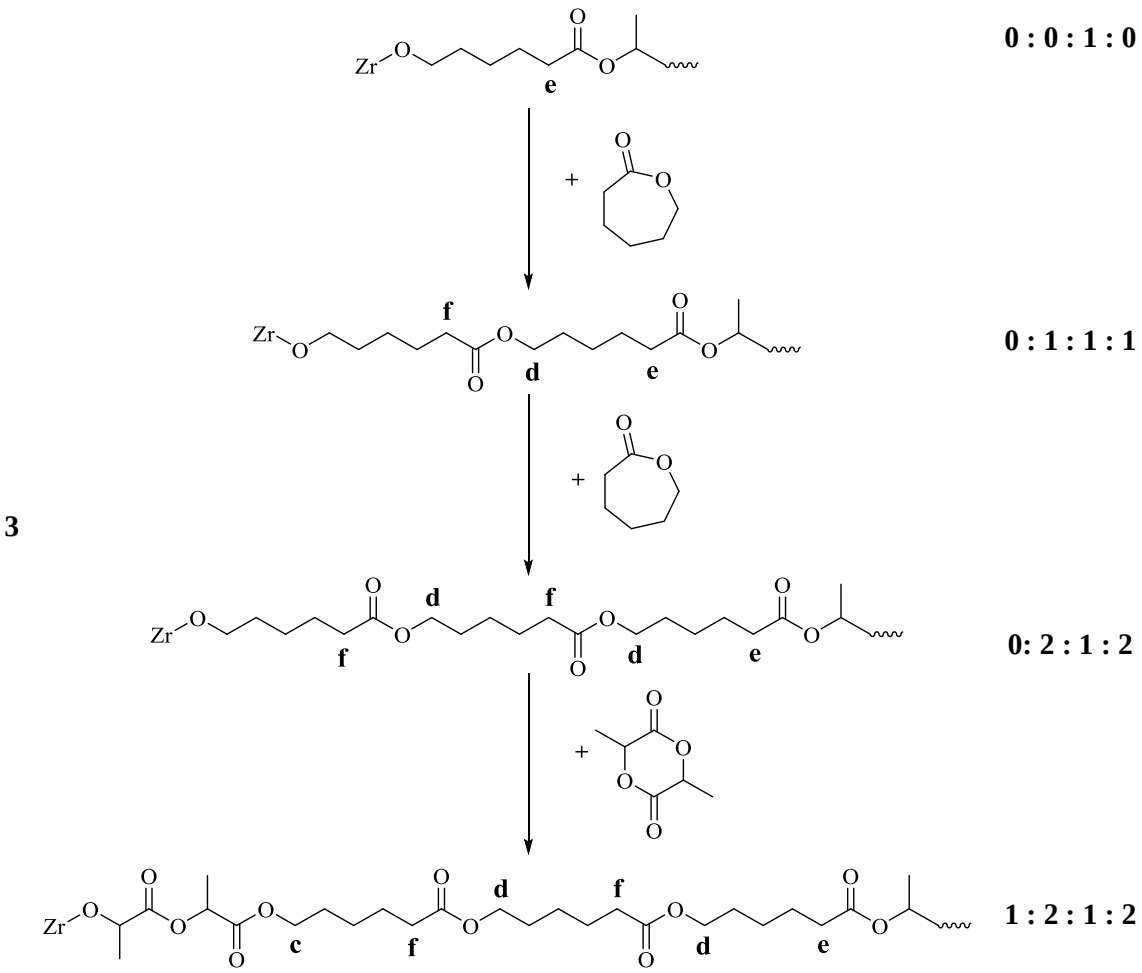

Scheme 4.2 Relative quantification of ^{1}H NMR spectroscopy signal intensities for the hetero-diad acyl-methylene (**c**), homo-diad acyl-methylene (**d**), hetero-diad carbonyl-methylene (**e**) and homo-diad carbonyl-methylene (**f**) caused by the insertion of **1**, **2**, or **3** caproyl units into a growing polymer chain with a lactidyl unit adjacent to the zirconium metal centre

Finally, it is also possible to use the relative quantification of the hetero- and homo-diads to calculate reactivity ratios for the copolymerisation of L-lactide and ε-caprolactone. With an assumption that propagation of the polymerisation obeys a first-order rate equation, reactivity ratios provide insight into the relationship between the rate constant of homo-polymerisation and copolymerisation. In line with the literature reaction ratios were calculated using the following equations:[8, 9]

$$r_1\left(\frac{1}{f}\right) = \frac{2[LA-LA]}{[LA-CL]}$$

$$r_2(f) = \frac{2[CL-CL]}{[CL-LA]}$$

$$f = \frac{[CL]}{[LA]}$$

Entry	Initiator	L-LA : εCL	reactivity ratios [a]		
			r_1	r_2	$r_1 \cdot r_2$
1	Zr-C_3^tBu	1:2	4.31	3.14	13.55
2	Zr-C_3^tBu	1:1	3.59	3.52	12.63
3	Zr-C_3^tBu	2:1	3.22	4.37	14.06
4	Zr_2(**8**)$_2$(O^iPr)$_2$	1:3	3.17	2.37	7.50
5	Zr_2(**8**)$_2$(O^iPr)$_2$	1:1	3.34	2.97	9.94
6	Zr_2(**8**)$_2$(O^iPr)$_2$	2:1	2.68	3.38	9.07
7	Zr_2(**10**)$_2$(O^iPr)$_2$	1:3	1.30	1.42	1.85
8	Zr_2(**10**)$_2$(O^iPr)$_2$	1:1	3.20	2.80	8.96
9	Zr_2(**10**)$_2$(O^iPr)$_2$	3:1	3.89	3.00	11.67

Conditions: [LA]/[Cl] = 1, [M]/[I] = 100, [M] = 0.66 M, toluene, 80 °C. [a] As determined *via* ^{1}H NMR. $r_1 = \frac{k_{LALA}}{k_{LACL}}$, $r_2 = \frac{k_{CLCL}}{k_{CLLA}}$. Conversion > 99 % for all except 7-9

Table 4.5 Reactivity ratios and $r_1 \cdot r_2$ as determined by relative intensities of homo- and hetero-diads of ^{1}H NMR spectrum of poly(L-lactide-*co*-ε-caprolactone) produced through the one-pot polymerisation of L-lactide and ε-caprolactone initiated by a zirconium amine tris(phenolate) alkoxide

With . $r_1 = \frac{k_{LALA}}{k_{LACL}}$ and $r_2 = \frac{k_{CLCL}}{k_{CLLA}}$, values suggest that all the copolymers produced, regardless of initiator are significantly block-like. $r_1 \cdot r_2$ values are all > 1 indicating a block copolymer rather than alternating or random (Table 4.5). The values of r_1 and r_2 are all > 1 which indicates that the rate of insertion of lactide into a growing polymer chain with a previously inserted lactide is preferred over the insertion of caprolactone into the chain. The same is true for the corresponding insertion of caprolactone into a growing polycaprolactone chain. However, it is important to note that the use of ^{1}H NMR diads provides an average of the entire copolymer microstructure and thus the reactivity ratios do not provide insight into the instantaneous incorporation of the two monomers into the polymer chain.

4.2.2 $^{13}C\{^{1}H\}$ NMR spectroscopy for average block length and reactivity ratios

The chemical shift of signals in $^{13}C\{^{1}H\}$ NMR spectroscopy is highly sensitive to the chemical and stereochemical environment of the atom in question. The higher sensitivity to the carbon atoms chemical environment has made it a useful tool in the study of the copolymerisation of traditional monomers in the production of aliphatic polymers, such as the poly(methyl methacrylate-*co*-1-hexene).[10] In such copolymer systems sensitivity is sufficient to distinguish between triads, where groupings of three monomer units can be identified. This can allow the the calculation of more complex reactivity ratios, in which the last but one monomer added to the copolymer chain has an induction effect on the rate of incorporation of a monomer.

Whilst it has already been highlighted that for these copolymerisation systems the triad resolution is not required, the use of $^{13}C\{^{1}H\}$ NMR spectroscopy has been widely documented in the literature for the copolymerisation of lactide and ε-caprolactone.[3, 6, 11, 12] For the analysis of poly(lactide-*co*-caprolactone) the carbonyl region of the $^{13}C\ \{^{1}H\}$ spectrum was utilised (169 – 175 ppm) with the signals assigned according to the literature (Figure 4.6).[11] Annotation has the assumption that the –OH group is on the left of the copolymer chain, implying that monomers were inserted into the chain in order from right to left. It is also important to note that the addition of lactidyl unit to the polymer chain results in the incorporation of two new ester carbonyls; the lactidyl unit is therefore represented as LL in the annotation with each "L" representing an ester carbonyl, with caproyl unit represented as either Cap (Figure 4.6) or C (Table 4.6). Underlining indicates the carbonyl to which the resonance is assigned. For example, the assignment LLL<u>L</u>Cap is for the carbon of the lactidyl ester highlighted in red in Figure 4.5.

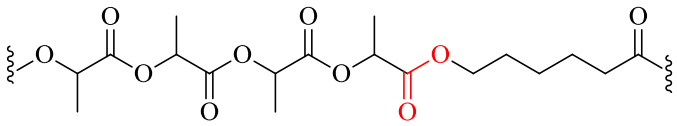

Figure 4.5 Identification of the carbonyl ester for which the $^{13}C\{^{1}H\}$ NMR spectroscopy resonance is indicated by the annotation LLL<u>L</u>Cap

With the 'growing end' of the chain located on the left, the highlighted carbonyl is that of a lactidyl unit that was inserted into a growing chain with a previously inserted caproyl unit. The highlighted lactidyl unit was followed by the insertion of a lactide.

Whilst visual inspection of the spectra provides limited information on the microstructure of the copolymer, it should be noted that there is a significantly more prominent Cap<u>L</u>Cap triad for the copolymer produced using $Zr_2(\mathbf{10})_2(O^iPr)_2$ (Figure 4.6-C). This triad is only possible due to

post-polymerisation transesterification, causing the separation of the diester lactidyl unit. Analysis of polymeric material *via* GPC showed polymer produced using $Zr_2(\mathbf{8})_2(O^iPr)_2$ and $Zr_2(\mathbf{10})_2(O^iPr)_2$ had similar PDI (1.6 and 1.7 respectively). This provided further evidence that the less sterically hindered $Zr_2(\mathbf{10})_2(O^iPr)_2$ initiator yielded polymeric material with a wider PDI due to the increased ease of transesterification due to the removal of *tert*-butyl substituents from the amine tris(phenolate) ligand. The increased PDI for material produced using $Zr_2(\mathbf{8})_2(O^iPr)_2$, due to less evidence of transesterification, can be attributed to a slower initiation step (k_{init}) due to the stability of the dimer; this is in line with previous discussion of theses initiators (Chapter 3). Within the monomer ratios investigated for $Zr_2(\mathbf{10})_2(O^iPr)_2$ the highest intensity of the transesterification triad [Cap<u>L</u>Cap] was observed for a L-lactide : ε-caprolactone ratio of 1:3, with the lowest for that with the inverse 3:1. This suggest that despite lactidyl repeat units offering two sites for transesterification per monomer incorporated, the less sterically hindered caprolactone aliphatic chain has greater influence in the rate of transesterification.

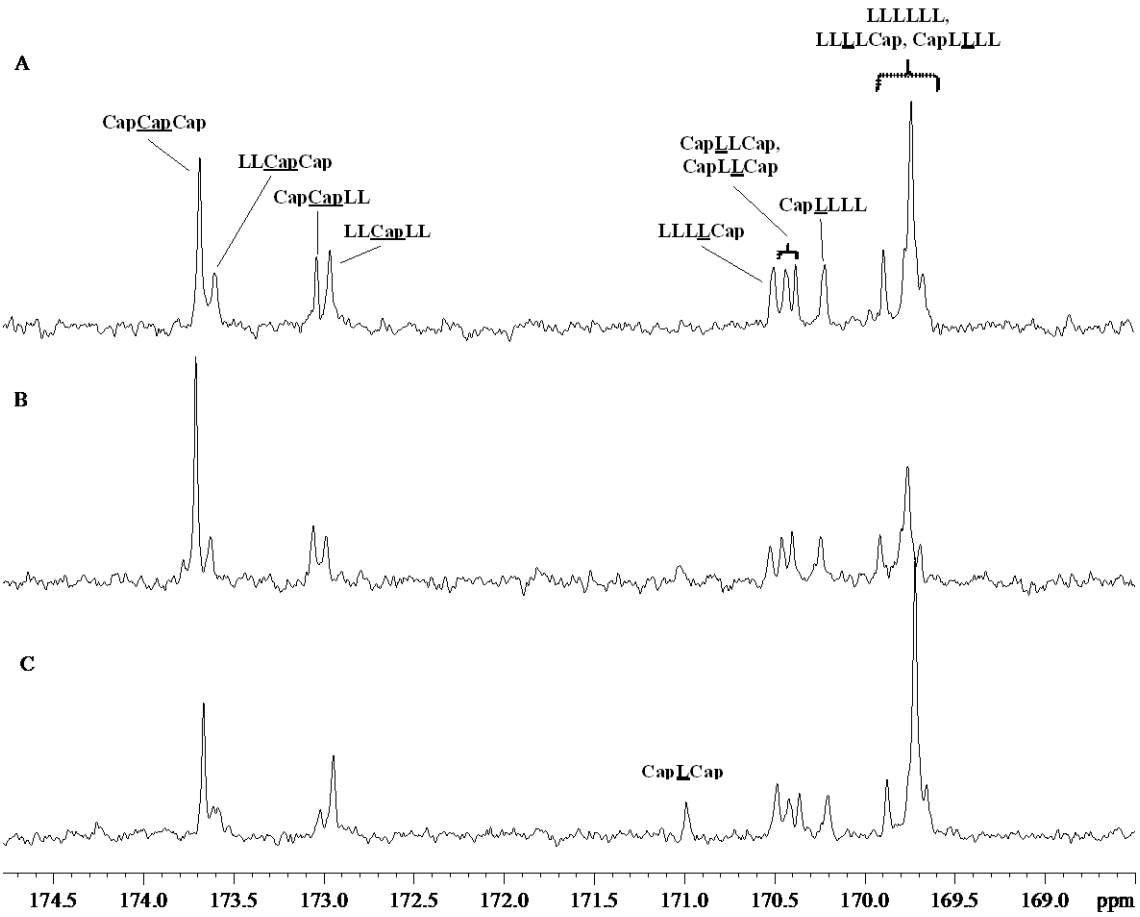

Figure 4.6 Extract of the carbonyl region of the ^{13}C {^1H} NMR spectra for poly(l-lactide-*co*-ε-caprolactone) produced *via* the one-pot copolymerisation of L-lactide and ε-caprolactone by: A – Zr-$C_3{}^tBu$, B – $Zr_2(\mathbf{8})_2(O^iPr)_2$ and C – $Zr_2(\mathbf{10})_2(O^iPr)_2$ with an initial monomer ratio of 1:1. Triad assignment according to the literature.[3, 6, 11]

Entry	Initiator	L-LA : εCL	Relative triad intensities of carbonyl signals [a]				
			[CC<u>C</u>] + [LLC<u>C</u>]	[CC<u>L</u>LL] + [LL<u>C</u>LL]	[C<u>L</u>C]	[LLL<u>L</u>C],[C<u>L</u>LLL] + [CL<u>L</u>C],[C<u>L</u>LLL]	[LL<u>L</u>LLL],[LLL<u>L</u>LL] + [LL<u>L</u>LC],[CL<u>L</u>LL]
1	Zr-C_3^tBu	1:2	0.383	0.125	0.007	0.309	0.276
2	Zr-C_3^tBu	1:1	0.206	0.149	0.003	0.237	0.405
3	Zr-C_3^tBu	2:1	0.113	0.101	0.014	0.177	0.596
4	Zr_2(**8**)$_2$(O^iPr)$_2$	1:3	0.560	0.145	0.022	0.154	0.119
6	Zr_2(**8**)$_2$(O^iPr)$_2$	1:1	0.290	0.128	0.025	0.228	0.329
5	Zr_2(**8**)$_2$(O^iPr)$_2$	2:1	0.089	0.107	0.016	0.202	0.586
6	Zr_2(**10**)$_2$(O^iPr)$_2$	1:3	0.403	0.162	0.058	0.193	0.186
7	Zr_2(**10**)$_2$(O^iPr)$_2$	1:1	0.175	0.123	0.027	0.211	0.464
8	Zr_2(**10**)$_2$(O^iPr)$_2$	3:1	0.026	0.079	0.012	0.123	0.760

Conditions: [LA]/[Cl] = 1, [M]/[I] = 100, [M] = 0.66 M, toluene, 80 °C. [a] As determined *via* $^{13}C\{^1H\}$ NMR spectroscopy. Conversion > 99 % for all except 7-9

Table 4.6 Selected traids, as determined by $^{13}C\{^1H\}$ NMR spectroscopy, for poly(L-lactide-*co*-caprolactone) from the one-pot polymerisation of L-lactide and ε-caprolactone initiated by zirconium amine tris(phenolate) complexes: Zr-C_3^tBu and Zr_2(**8,10**)$_2$(O^iPr)$_2$

Triads of the $^{13}C\{^1H\}$ NMR spectra were grouped and relatively quantified (Table 4.6) allowing for the average block length ($\bar{L}_m$) and reactivity ratios using the following equations and according to the literature.[3]

$$\bar{L}_{LA} = \left(\frac{[LLLLLL] + \frac{1}{2}[LLLLC + CLLLL]}{\frac{1}{2}[LLLLC + CLLLL] + [CLLC]} + 1 \right) \frac{1}{2} \quad , \quad \bar{L}_{CL} = \left(\frac{[CCC + LLCC]}{[CCLL + LLCLL]} \right)$$

$$r_1 \left(\frac{1}{f} \right) = \left(\frac{[LLLLLL] + \frac{1}{2}[LLLLC + CLLLL]}{[CCLL + LLCLL] + \frac{1}{2}[LLLLC + CLLLL]} \right)$$

$$r_2(f) = \left(\frac{[CCC + LLCC] + \frac{1}{2}[CCLL + LLCLL]}{[LLLLC + CLLLL] + \frac{1}{2}[CCLL + LLCLL]} \right)$$

$$where: \; f = \frac{[CL]}{[LA]}$$

Entry	Initiator	L-LA : εCL	Average block length ($\bar{L}_m$) and reactivity ratios [a]				
			$\bar{L}_{LA}$	$\bar{L}_{CL}$	r_1	r_2	$r_1 \cdot r_2$
1	Zr-C_3^tBu	1:2	1.8	4.1	1.79	1.53	2.70
2	Zr-C_3^tBu	1:1	2.7	2.4	1.71	1.38	2.36
3	Zr-C_3^tBu	2:1	3.8	2.1	1.68	2.24	3.77
4	Zr_2(**8**)$_2$(O^iPr)$_2$	1:3	1.5	4.9	2.32	1.29	2.98
5	Zr_2(**8**)$_2$(O^iPr)$_2$	1:1	2.1	3.3	1.44	2.27	3.27
6	Zr_2(**8**)$_2$(O^iPr)$_2$	2:1	3.4	1.8	1.45	1.66	2.41
7	Zr_2(**10**)$_2$(O^iPr)$_2$	1:3	1.4	3.5	2.89	0.83	2.40
8	Zr_2(**10**)$_2$(O^iPr)$_2$	1:1	2.6	2.4	2.20	1.42	3.13
9	Zr_2(**10**)$_2$(O^iPr)$_2$	3:1	6.1	1.3	2.06	0.99	2.03

Conditions: [LA]/[Cl] = 1, [M]/[I] = 100, [M] = 0.66 M, toluene, 80 °C. [a] As determined *via* $^{13}C\{^1H\}$ NMR spectroscopy. . $r_1 = \frac{k_{LALA}}{k_{LACL}}$, $r_2 = \frac{k_{CLCL}}{k_{CLLA}}$. Conversion > 99 % for all except 7-9.

Table 4.7 Average block length ($\bar{L}_m$), reactivity ratios and $r_1 \cdot r_2$ as determined by relative intensities of the carbonyl triads of the $^{13}C\{^1H\}$ NMR spectra of poly(L-lactide-*co*-ε-caprolactone) produced through the one-pot polymerisation of L-lactide and ε-caprolactone initiated by a zirconium amine tris(phenolate) alkoxide

Values determined from triad intensities for average block length and reactivity ratios are more comparable compared to those calculated from ^{1}H NMR spectroscopy diads which have significant variation (Table 4.7). Average block length was seen to increase with monomer feed mole fraction, values did not vary as widely as seen with diad-derived data and this increased sensitivity toward increasing L-lactide or ε-caprolactone in the monomer was not observed. Average block length was much closer to that expected for a random copolymer ($\bar{L}_m \sim 2$) for entries 2, 5 and 8, where the initial monomer molar ratio was 1:1. As seen with the ^{1}H NMR spectroscopic study, the use of Zr_2(**8**)$_2$(O^iPr)$_2$ as an initiator instead of Zr-*C_3^tBu* resulted in a reduction in $\bar{L}_{LA}$ and corresponding increase in $\bar{L}_{CL}$ which could be attributed to an increase in incorporation of ε-caprolactone into the growing polymer chain with respect to L-lactide. This is also observed in the respective reactivity ratios, with r_1 deacreasing and r_2 increasing. However the $r_1 \cdot r_2$ does not suggest an increase in randomness of the copolymer when Zr_2(**8**)$_2$(O^iPr)$_2$ is used over Zr-*C_3^tBu*. Similarly, replacement of the initiator with Zr_2(**10**)$_2$(O^iPr)$_2$ further reduced r_1 and increases r_2, yet $r_1 \cdot r_2$ increases further. This provides evidence of the limitation of this analysis for copolymers that appear to be significantly block-like in nature. Whilst the average block length can provide some insight the averaging with respect to reactivity ratios limits the value due to the significant drift in monomer ratio over the course of the copolymerisation to yield a tapered block copolymer.

4.3 Reactivity Ratios for the copolymerisation of *rac*-lactide / L-lactide and ε-caprolactone

Whilst analysis of the ^{1}H and ^{13}C{^{1}H} NMR spectra of polymeric material can provide insight into the microstructure on the copolymer, the averaging over the full polymer chain caused limitations as previously discussed. The Mayo-Lewis equation, as first used for the copolymerisation of styrene and methyl methacrylate combines the rate equations of the four propagation reactions of the copolymerisation allowing determination of reactivity ratios based on monomer feed ratio and the instantaneous copolymer composition.[13] The theory is discussed in detail in the introduction with both linear and non-linear methods of finding the solutions to the copolymerisation equation. Reactivity ratios have been found for the copolymerisation of lactide and other cyclic esters using both linear and non-linear methods.[6, 12] For the one-pot copolymerisation of lactide and ε-caprolactone, initiated by the series of zirconium amine tris(phenolate) alkoxides presented in this thesis, reactivity ratios were found using the linear Fineman-Ross method [14] and a non-linear least squares (NLLS) method as used by Normura *et. al*.[6] The copolymerisation of *rac*-lactide and L-lactide with ε-caprolactone were both

investigated to provide insight into the effect of high heterotactic selectivity of the microstructure of the resulting copolymer.

Multiple copolymerisations were carried out at 80 °C in toluene-d_8 and monitored *in-situ* via ^{1}H NMR spectroscopy. Initial monomer ratios and copolymer composition were calculated at low conversions (< 15%) by integrating the methine signal of the lactide and methylene signal of the corresponding lactone; this was deemed to provide an instantaneous copolymer composition, minimising the effect of monomer feed ratio drift.[6] The values acquired for F_{LA} for the various values of f_{LA} and f_{CL} were used to generate a Fineman-Ross plot that provide linear solutions for the reactivity ratios (r_1 and r_2). The Fineman-Ross approach utilises the following relationships:

$$Y = -(r_1) \cdot X + r_2$$

$$Y = \left(\frac{f_1}{(1 - f_1)}\right) \times \left(\frac{(1 - 2F_1)}{F_1}\right)$$

$$X = \left(\frac{{f_1}^2}{(1 - f_1)^2}\right) \times \left(\frac{1 - F_1}{F_1}\right)$$

Where f_1 = monomer mole fraction of lactide and F_1 = mole fraction of lactide in the resulting copolymer. An example of a Fineman-Ross plot for this copolymerisation system is included (Figure 4.7) and the reactivity ratios are summarised in Table 4.8.

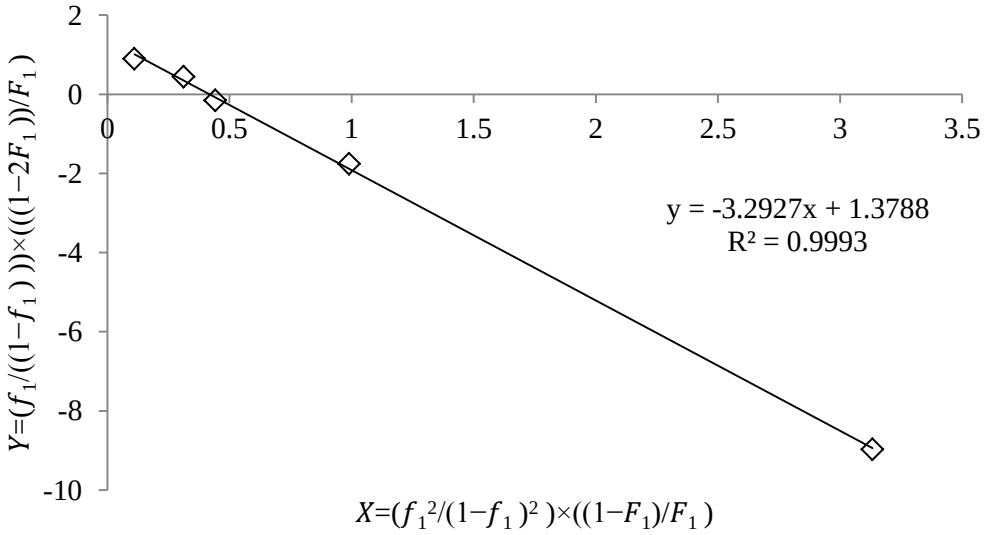

Figure 4.7 Fineman-Ross plot for the one-pot copolymerisation of L-lactide and ε-caprolactone initiated by Zr-$C_3{}^tBu$.

Initiator	M_1	M_2	r_1 [a] (S.E.) [b]	r_2 [a] (S.E.) [b]	$r_1 \cdot r_2$
Zr-C_3^tBu	*rac*-lactide	ε-caprolactone	4.78 (0.27)	0.52 (0.25)	2.49
	L-lactide	ε-caprolactone	3.29 (0.05)	1.37 (0.07)	4.51
Zr_2(**8**)$_2$(O^iPr)$_2$	*rac*-lactide	ε-caprolactone	12.23 (0.19)	0.07 (0.07)	0.86
	L-lactide	ε-caprolactone	5.88 (2.92)	0.60 (1.91)	3.53
Zr_2(**10**)$_2$(O^iPr)$_2$	*rac*-lactide	ε-caprolactone	2.15 (0.14)	0.40 (0.24)	0.86
	L-lactide	ε-caprolactone	0.91 (0.07)	0.30 (0.30)	0.27

Conditions: [M]/[I] = 100, [M] = 0.5 M, toluene, 80 °C. [a] r_1 and r_2 found using a Fineman-Ross Plot $Y = -(r_1) \cdot X + r_2$ where $Y = \left(\frac{f_1}{(1-f_1)}\right) \times \left(\frac{(1-2F_1)}{F_1}\right)$ and $X = \left(\frac{{f_1}^2}{(1-f_1)^2}\right) \times \left(\frac{1-F_1}{F_1}\right)$ F_1 calculated from ^{1}H NMR spectrum at low conversion with polymerisation carried out *in situ.* [b] Standard error calculated using the following: $S.E. = \sqrt{\frac{\sum_{s=1}^{m}\sum_{i=1}^{n} {y_{is}}^2}{(n_y-1)(n_y)}}$, where *s* = series number, *i* = point number in series s, *m* = no. of series for point y in chart, *n* = no. of points in each series, y_{is} = data value of series *s* and the i^{th} point, n_y = total no. of data values in all series.

Table 4.8 Fineman-Ross Plot reactivity ratios for the one-pot copolymerisation of lactide and ε-caprolactone

The non-linear least squares method used required the copolymer equation to be used in the following form:

$$F_1 = \frac{r_1 f_1^2 + f_1 f_2}{r_1 f_1^2 + 2 f_1 f_2 + r_2 f_2^2}$$

Where f_1 = monomer mole fraction of lactide, f_2 = monomer mole fraction of ε-caprolactone and F_1 = mole fraction of lactide in the resulting copolymer. The "Solver" add-in of Microsoft Excel was used to iteratively vary values of r_1 and r_2 to provide the best-fit of the equation to the experimental measured instantaneous mole fraction in the copolymer. The method also included a weighting factor in which $\omega = \frac{1}{{F_1}^2}$. Values are summarised in Table 4.9.

$$\sum \left(w \times \left(F_A - \frac{r_1 f_A^2 + f_A f_B}{r_1 f_A^2 + 2 f_A f_B + r_2 f_B^2} \right)^2 \right)$$

Initiator	M_1	M_2	r_1 [a]	r_2 [a]	$r_1 \cdot r_2$
Zr-$C_3{}^tBu$	*rac*-lactide	ε-caprolactone	3.55	0.51	1.81
	L-lactide	ε-caprolactone	2.83	1.24	3.51
Zr_2(**8**)$_2$(O^iPr)$_2$	*rac*-lactide	ε-caprolactone	16.59	0.23	3.82
	L-lactide	ε-caprolactone	2.54	0.23	0.58
Zr_2(**10**)$_2$(O^iPr)$_2$	*rac*-lactide	ε-caprolactone	7.10	0.13	0.92
	L-lactide	ε-caprolactone	1.07	0.18	0.19

Conditions: [M]/[I] = 100, [M] = 0.5 M, toluene, 80 °C. [a] r_1 and r_2 found through *via* a weighted linear least-squares regression model $\sum\left(\omega \times \left(F_1 - \frac{r_1 f_1{}^2 + f_1 f_2}{r_1 f_1{}^2 + 2 f_1 f_2 + r_2 f_2{}^2}\right)^2\right)$ where $\omega = \frac{1}{F_1{}^2}$ and F_1 calculated from ^{1}H NMR spectrum at low conversion with polymerisation carried out *in situ.*

Table 4.9 None-linear least squared (NLLS) solution to Mayo-Lewis Equation to provide reactivity ratios for the one-pot copolymerisation of lactide and ε-caprolactone

In order to test the robustness of the two methods for finding reactivity ratios, values found by both the Fineman-Ross plot and NLLS method were used to generate theoretical instantaneous copolymer composition values (F_1) from monomer mole fraction (f_1) using the Mayo-Lewis equation. These values were plotted for comparison with the composition measured experimentally *via* ^{1}H NMR spectroscopy. Theoretical data points that best followed the experimental line indicated the better fit of the reactivity ratios (Figure 4.8 – Figure 4.13).

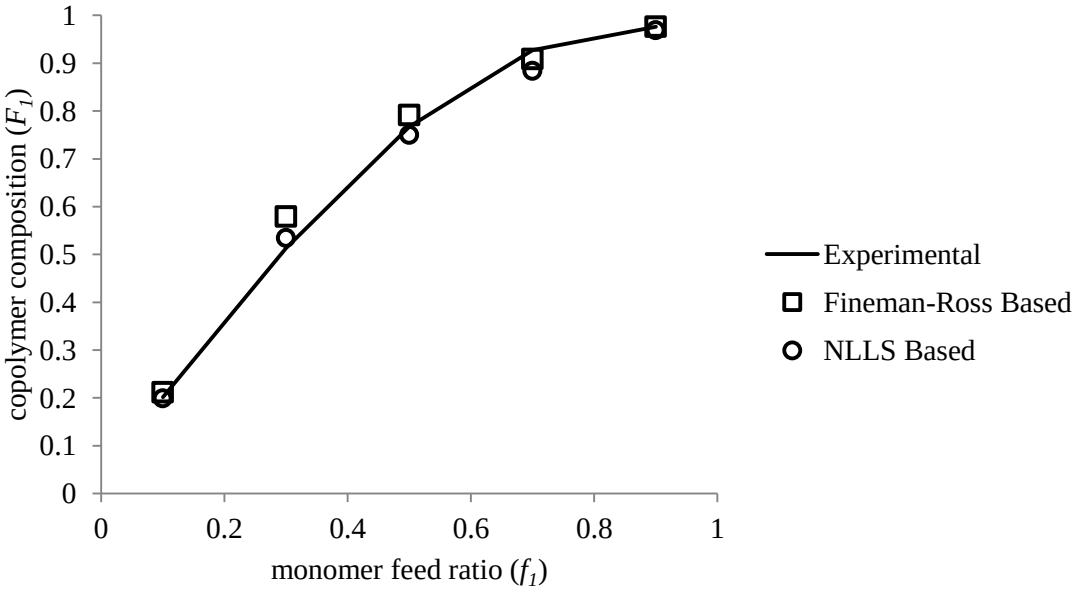

Figure 4.8 Fineman-Ross and NLLS comparison of reactivity ratios with respect to experimentally measured copolymer composition. Line for experimental is only for ease of comparison for the copolymerisation of *rac*-lactide and ε-caprolactone initiated by Zr-$C_3{}^tBu$

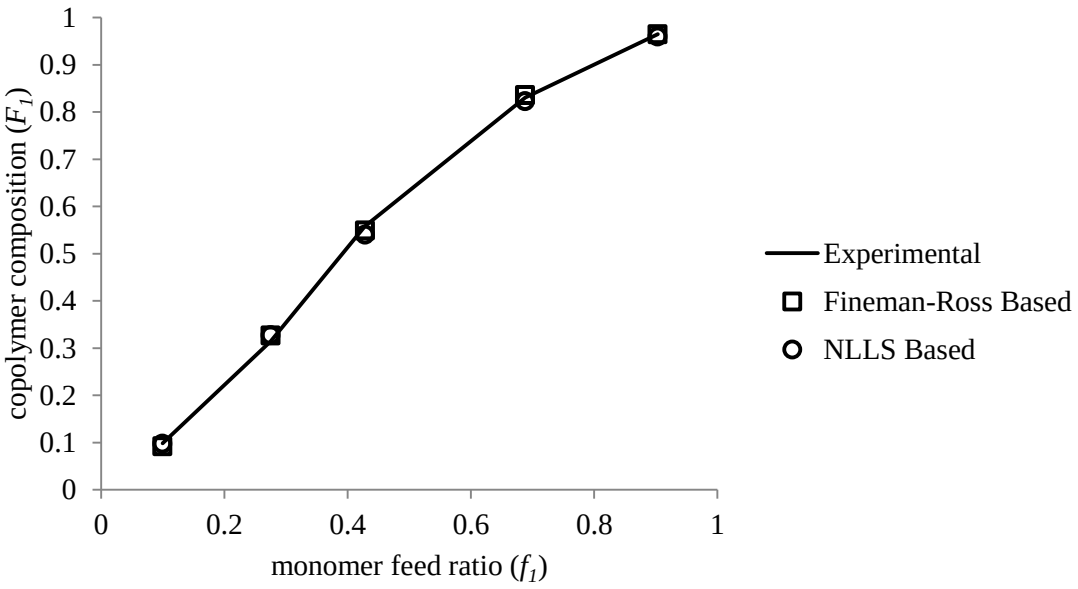

Figure 4.9 Fineman-Ross and NLLS comparison of reactivity ratios with respect to experimentally measured copolymer composition. Line for experimental is only for ease of comparison for the copolymerisation of L-lactide and ε-caprolactone initiated by Zr-$C_3{}^tBu$

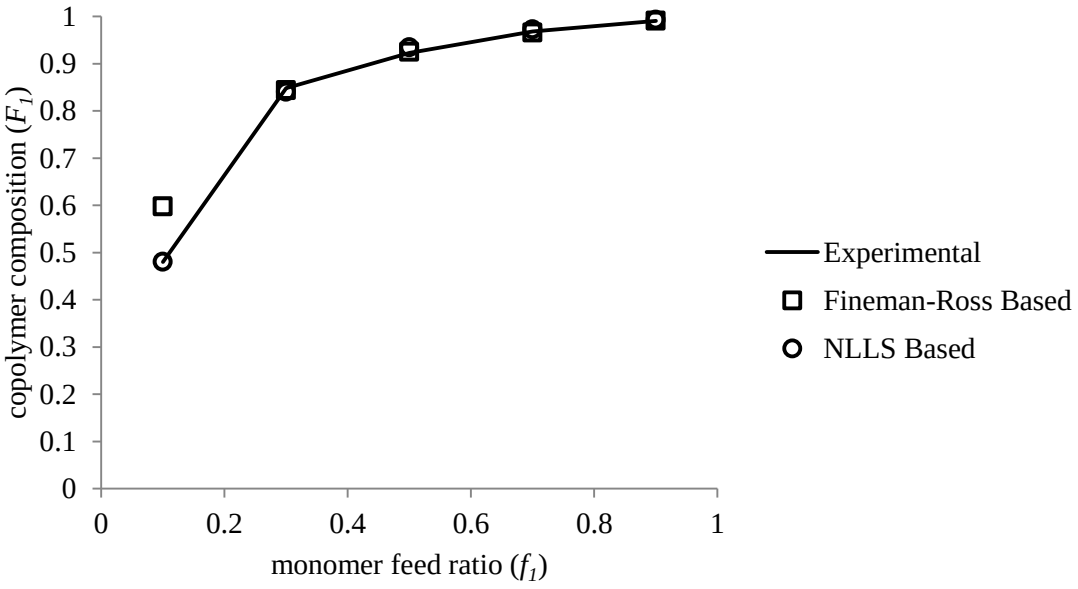

Figure 4.10 Fineman-Ross and NLLS comparison of reactivity ratios with respect to experimentally measured copolymer composition. Line for experimental is only for ease of comparison for the copolymerisation of *rac*-lactide and ε-caprolactone initiated by $Zr_2(\mathbf{8})_2(O^iPr)_2$

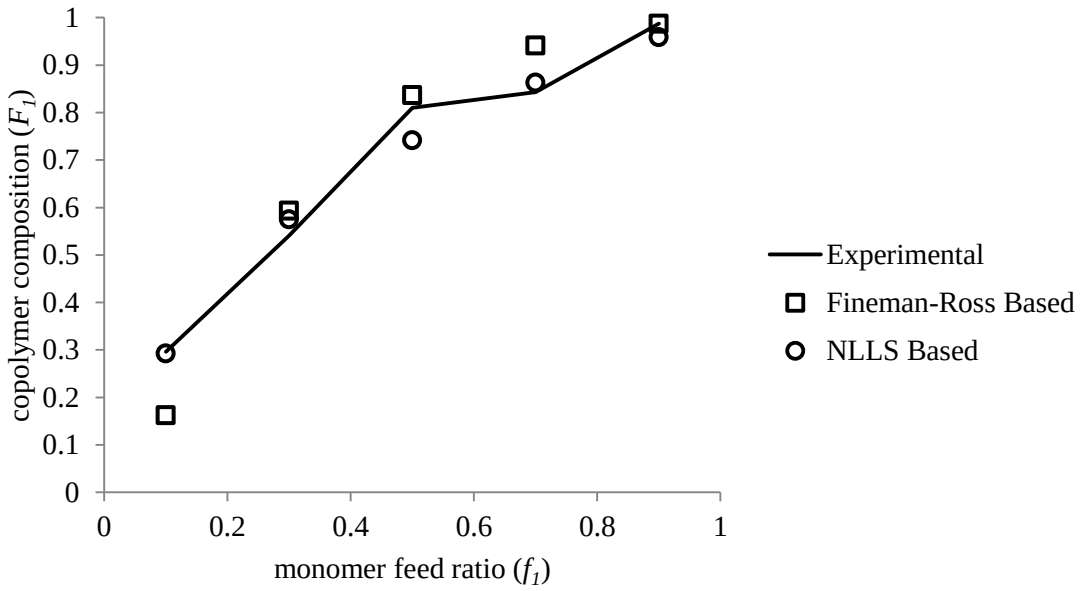

Figure 4.11 Fineman-Ross and NLLS comparison of reactivity ratios with respect to experimentally measured copolymer composition. Line for experimental is only for ease of comparison for the copolymerisation of L-lactide and ε-caprolactone initiated by $Zr_2(\mathbf{8})_2(O^iPr)_2$

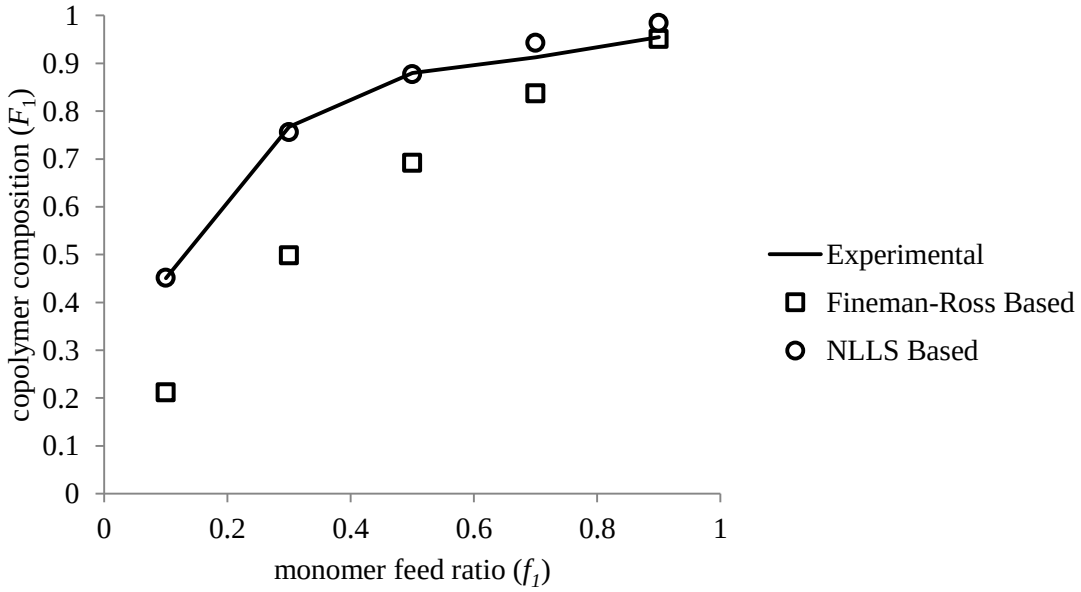

Figure 4.12 Fineman-Ross and NLLS comparison of reactivity ratios with respect to experimentally measured copolymer composition. Line for experimental is only for ease of comparison for the copolymerisation of *rac*-lactide and ε-caprolactone initiated by $Zr_2(\mathbf{10})_2(O^iPr)_2$

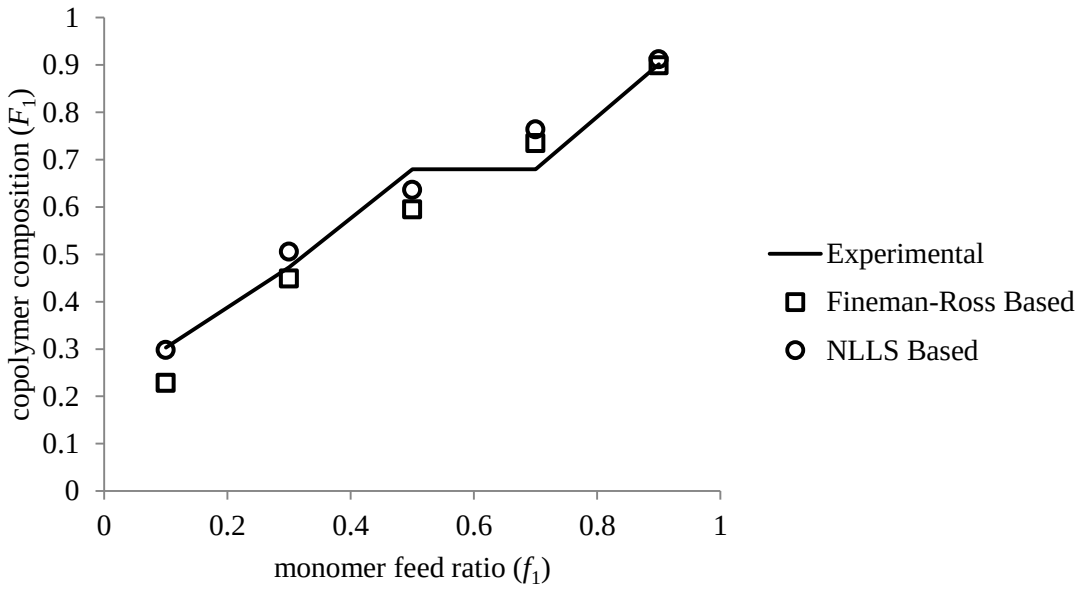

Figure 4.13 Fineman-Ross and NLLS comparison of reactivity ratios with respect to experimentally measured copolymer composition. Line for experimental is only for ease of comparison for the copolymerisation of L-lactide and ε-caprolactone initiated by $Zr_2(\mathbf{10})_2(O^iPr)_2$

The distortion of the experimentally found composition (F_1) *versus* monomer mole fraction (f_1) away from a straight line relationship for all initiators with both *rac*-lactide and L-lactide indicates a preference for the incorporation of lactide at a higher composition than in the respective monomer feed ratio. Comparison of the theoretical copolymer composition values shows that for all initiators and monomer combinations the non-linear method provided more reliable values for the reactivity ratios. A linear relationship between monomer feed (f_1) and copolymer composition (F_1) indicates a random or alternating copolymer, presuming that homopolymerisation of the two monomers is not taking place at equal rates. Visual inspection suggests that the polymerisation of L-lactide with ε-caprolactone using the Zr-$C_3{}^tBu$ initiator yields a copolymer closest to random. An equivalent copolymerisation using $Zr_2(\mathbf{10})_2(O^iPr)_2$ as the initiator also generated a pseudo-straight-line relationship however it would appear not to pass through the origin of the plot, when f_1 is equal to zero F_1 has to equal zero. This is evidence of the limitations of quantifying copolymer composition at low conversion, especially at highly biased monomer feed ratios (f_1 = 0.1 or 0.9). This is also evident in the distortion of the experimental curve seen for the copolymerisation of L-lactide and ε-caprolactone with $Zr_2(\mathbf{8})_2(O^iPr)_2$ and $Zr_2(\mathbf{10})_2(O^iPr)_2$.

Taking the values generated using the NLLS method to be most reliable, comparison of the reactivity ratio values can provide insight into the potential differences in microstructure of the

copolymer caused by variation in the initiator and removal of the stereoselective influence by replacing *rac*-lactide with L-lactide. With the reactivity ratios defined as follows:

$$r_1 = \frac{k_{LALA}}{k_{LACL}} \quad , \quad r_2 = \frac{r_{CLCL}}{r_{CLLA}}$$

Where the rate constants refer to the four possible propagation steps of the copolymerisaiton:

$$LA* + LA \rightarrow LALA* \qquad k_{LALA}$$

$$LA* + CL \rightarrow LACL* \qquad k_{LACL}$$

$$CL* + CL \rightarrow CLCL* \qquad k_{CLCL}$$

$$CL* + LA \rightarrow CLLA* \qquad k_{CLLA}$$

For all three initiators the value of r_1 drops when L-lactide is used over *rac*-lactide. This can be attributed to the slow rate of polymerisation observed for L-lactide with respect to *rac*-lactide as discussed in this thesis and reported in the literature for Zr-C_3^tBu.[7] No reduction in r_2 is observed for this copolymerisation using this set of initiators. With r_2 being the ratio of either ε-caprolactone or lactide inserting in a growing caproyl chain the effect of heterotactic selectivity enforced by the *P/M* isomer axial flipping is less influential.[15] With respect to the indication of copolymer structure based on the relationship between r_1 and r_2 as described in the introduction, all but the copolymerisation of L-lactide and ε-caprolactone by Zr-C_3^tBu have $r_1 > 1 > r_2$ suggesting a tapered block copolymer. Values of r_2 less than zero is in contradiction to reactivity ratios found using the diad and triad methods discussed previously. However, it is important to note that the Mayo-Lewis equations offers instantaneous reactivity ratios whereas the diad and triad analysis generates an average including the large blocks of poly(caprolactone) polymerised after the majority of lactide has been incorporated into the polymer chain.

The reactivity ratio product $(r_1 \cdot r_2)$ indicates that block-type copolymers are produced using Zr-C_3^tBu and for Zr_2(**8**)$_2$(O^iPr)$_2$ with *rac*-lactide and ε-caprolactone ($r_1 \cdot r_2 > 1$). With values less than one indicating an alternating copolymer. With the other evidence of the formation of block copolymers, it is suggested that as steric bulk is removed from the initiator, for the monomer feed ratios explored in this study, ε-caprolactone incorporation into the chain is limited to effectively single units with overriding preference for lactide homopolymerisaiton.

As well as determining copolymer composition at low conversion, rate constants were determined for homopolymerisations of *rac*-lactide, L-lactide and ε-caprolatone .

Initiator	Monomer	$k_{(M\text{-}M)}$ /min^{-1} [a]
Zr-C_3^tBu	*rac*-lactide	29.9×10^{-3}
	L-lactide	14.2×10^{-3}
	ε-caprolactone	39.9×10^{-3}
Zr_2(**8**)$_2$(O^iPr)$_2$	*rac*-lactide	130×10^{-3}
	L-lactide	98.9×10^{-3}
	ε-caprolactone	18.5×10^{-3}
Zr_2(**10**)$_2$(O^iPr)$_2$	*rac*-lactide	4.13×10^{-3}
	L-lactide	7.55×10^{-3}
	ε-caprolactone	23.1×10^{-3}

Conditions: [M]/[I] = 100, [M] = 0.5 M or 0.66 M, toluene-d_8, 80 °C. [a] $k_{(M\text{-}M)}$ = rate constant of homopolymerisaiton, found from the slope of $ln\left(\frac{[M]_0}{[M]_t}\right)$ vs. time.

Table 4.10 Pseudo first-order rate constants, $k_{(M\text{-}M)}$, for the ROP of *rac*-lactide, L-lactide and ε-caprolactone by: Zr-C_3^tBu and Zr_2(**8**,**10**)$_2$(O^iPr)$_2$

As seen in the full polymerisation study for these initiators in Chapter 3, the polymerisation of both *rac*-lactide and L-lactide is faster with Zr_2(**8**)$_2$(O^iPr)$_2$ than Zr-C_3^tBu but slower with Zr_2(**10**)$_2$(O^iPr)$_2$. For the polymerisation of ε-caprolactone rate decreases for Zr_2(**8**)$_2$(O^iPr)$_2$ and Zr_2(**10**)$_2$(O^iPr)$_2$. A potential cause of this is the reduced coordination potential of ε-caprolactone due to the presence of only one ester carbonyl per monomer. Coordination of the monomer was found to be important in dimer dissociation of the initiator. The reduced steric bulk of a growing poly(caprolactone) chain, with a caproyl unit adjacent to the metal centre, may allow easier combination of the dimer during propagation that would slow the rate of polymerisation.

The rate constants for the homopolymerisation can be used with the reactivity ratios to approximate the rate of insertion of ε-caprolactone into a growing poly(lactide) chain and likewise the insertion of lactide into a growing poly(caprolactone) chain (Table 4.11 and Table 4.12). Whilst the values can be used to try and infer any effect of initiator steric bulk and stereoselectivity on the microstructure of the copolymer there are limitations, including the use

of homopolymerisation rate constants derived in the absence of the respective co-monomer so there is no competing coordination to the metal centre.

Initiator	Propagation rate constants/ $\times 10^{-3}$ min^{-1}			
	k_{LALA}	k_{LACL}	k_{CLCL}	k_{CLLA}
Zr-$C_3{}^tBu$	29.9	8.42	39.9	78.2
Zr_2(**8**)$_2$(O^iPr)$_2$	130	7.84	18.5	80.4
Zr_2(**10**)$_2$(O^iPr)$_2$	4.13	0.58	7.55	58.1

Conditions: [M]/[I] = 100, [M] = 0.5 M or 0.66 M, toluene-d_8, 80 °C. k_{LACL} and k_{CLLA} found from homopolymerisation rate constants and reactivity ratios

Table 4.11 Pseudo first-order propagation rate constants for the ROP of *rac*-lactide and ε-caprolactone by: Zr-$C_3{}^tBu$ and Zr_2(**8**,**10**)$_2$(O^iPr)$_2$

Initiator	Propagation rate constants / $\times 10^{-3}$ min^{-1}			
	k_{LALA}	k_{LACL}	k_{CLCL}	k_{CLLA}
Zr-$C_3{}^tBu$	14.2	5.02	39.9	32.2
Zr_2(**8**)$_2$(O^iPr)$_2$	98.9	38.9	18.5	80.4
Zr_2(**10**)$_2$(O^iPr)$_2$	7.55	7.06	7.55	41.9

Conditions: [M]/[I] = 100, [M] = 0.5 M or 0.66 M, toluene-d_8, 80 °C. k_{LACL} and k_{CLLA} found from homopolymerisation rate constants and reactivity ratios

Table 4.12 Pseudo first-order propagation rate constants for the ROP of L-lactide and ε-caprolactone by: Zr-$C_3{}^tBu$ and Zr_2(**8**,**10**)$_2$(O^iPr)$_2$

For all initiators the rate of insertion of lactide into a caproyl growing chain is greater than the rate of insertion of caprolactone into a lactidyl growing chain. This can be attributed to the greater coordination potential of lactide and the reduced sterics of the caproyl growing chain; the growing lactide chain has pendant methyl and carbonyl groups in closer proximity to the active metal centre. As with the full polymerisation study carried out in Chapter 3, the issue of the lower solubility of L-lactide compared to *rac*-lactide may be causing issue in determining the effect of using L-lactide over *rac*-lactide and removing any stereoselectivity influence.

4.4 Utilisation of reactivity ratios

Whilst alteration of ligand structure has led to preferential formation of a random copolymer in some cases in the literature,[6] analysis would suggest that for this series of zirconium amine

tris(phenolate) alkoxide initiators there is little effect on the copolymer microstructure. With this is mind an experimental approach was taken in which monomer feed molar ratio was controlled to produce copolymers with equal encorporation of each monomer into the growing polymer chain. The Mayo-Lewis copolymerisation equation is traditionally used to calculate reactivity ratios (r_1 and r_2) when monomer feed ratios and subsequent copolymer composition is known. It is suggested that if the reactivity ratios are known then copolymer equation can be used to predict copolymer composition for particular monomer ratios. The "Solver" tool of Mircrosoft Excel was used to find values for f_{LA} and f_{CL} that would satisfy the following criteria for the polymerisation of ε-caprolactone with either *rac*-lactide or L-lactide using Zr-$C_3{}^tBu$, $Zr_2(\mathbf{8})_2(O^iPr)_2$ or $Zr_2(\mathbf{10})_2(O^iPr)_2$ as an initiator:

$$0.5 = \frac{r_1 f_{LA}^2 + f_{LA} f_{CL}}{r_1 f_{LA}^2 + 2 f_{LA} f_{CL} + r_2 f_{CL}^2}$$

Where: $r_1 = \frac{k_{LALA}}{k_{LACL}}$ and $r_2 = \frac{k_{CLCL}}{k_{CLLA}}$

And: f_{LA} = monomer mole fraction of lactide, with: $f_{LA} + f_{CL} = 1$

Monomer feed ratios to achieve an instantaneous copolymer composition of 0.5 for each initiator and copolymer system are summarised in Table 4.13.

Initiator	Copolymer System	r_1	r_2	f_{LA}	f_{CL}
Zr-$C_3{}^tBu$	*rac*-LA : ε-CL	3.55	0.51	0.28	0.72
	L-LA : ε-CL	2.83	1.24	0.40	0.60
$Zr_2(\mathbf{8})_2(O^iPr)_2$	*rac*-LA : ε-CL	16.59	0.23	0.11	0.89
	L-LA : ε-CL	2.54	0.23	0.23	0.77
$Zr_2(\mathbf{10})_2(O^iPr)_2$	*rac*-LA : ε-CL	7.10	0.13	0.12	0.88
	L-LA : ε-CL	1.07	0.18	0.29	0.71

Table 4.13 'Ideal' monomer ratio for an instantaneous copolymer composition of 50:50 for the one-pot polymerisation of either *rac*-lactide or L-lactide with ε-caprolactone using Zr-$C_3{}^tBu$, $Zr_2(\mathbf{8})_2(O^iPr)_2$ or $Zr_2(\mathbf{10})_2(O^iPr)_2$ as an initiator

To test the robustness of this method polymerisation of L-lactide with ε-caprolactone were carried out on an NMR-scale with the initial monomer ratio close to that predicted as 'ideal' using reactivity ratios and the Mayo-Lewis equation. As well as monitoring monomer

conversion, instantaneous copolymer composition was measured with a function of time (Figure 4.14 – Figure 4.16).

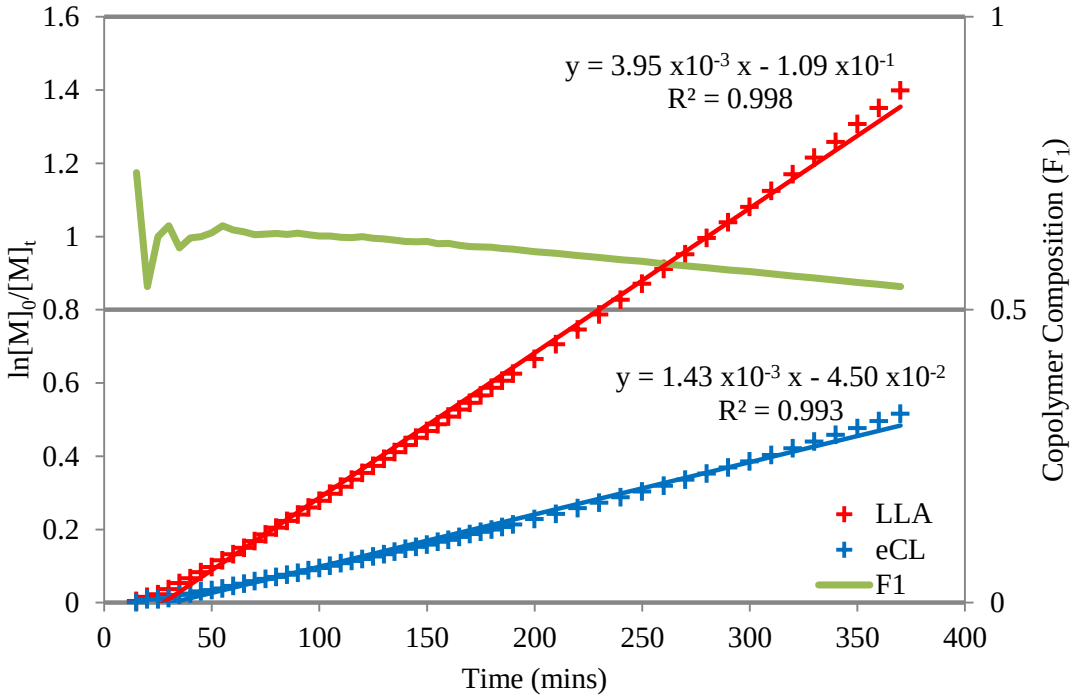

Figure 4.14 Semi-ln plot of the one-pot polymerisation of L-lactide and ε-caprolactone at an 'ideal' initial monomer ratio for 50:50 copolymer composition, initiated by Zr-$C_3{}^tBu$. Polymerisation monitored by ^{1}H NMR spectroscopy and monitored *in situ*. Conditions: [M]/[I] = 100, [M] = 0.5 M, toluene-d_8, 80 °C

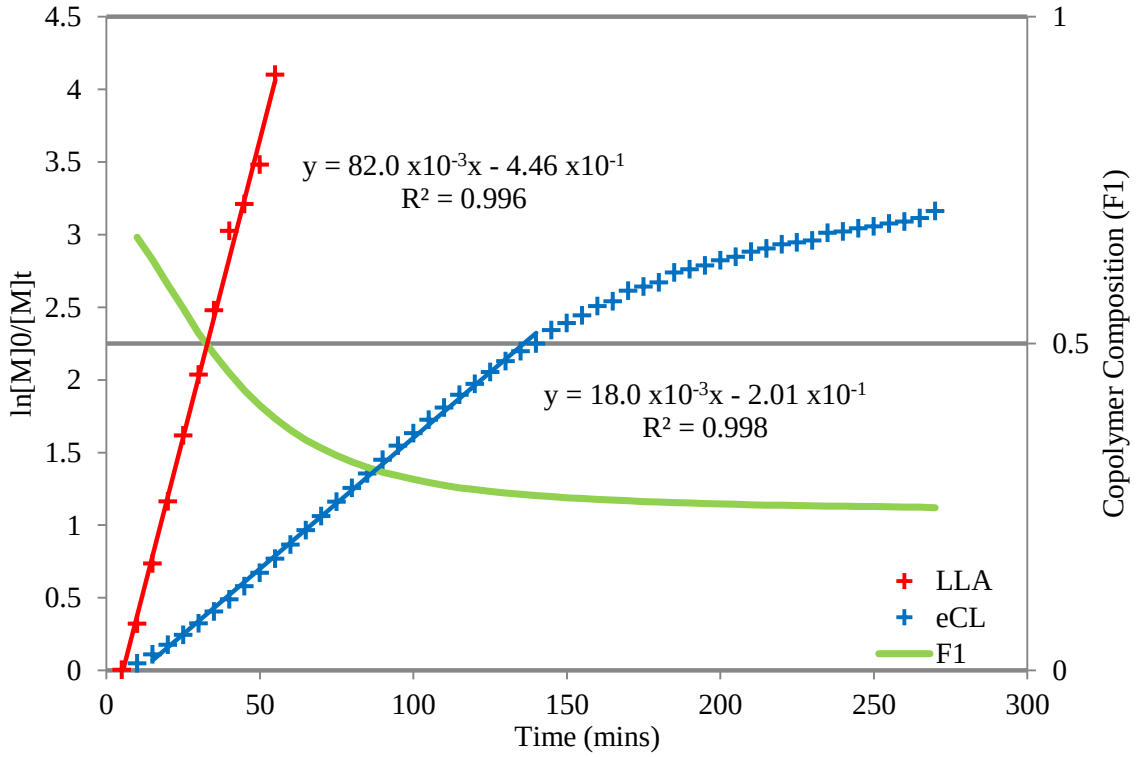

Figure 4.15 Semi-ln plot of the one-pot polymerisation of L-lactide and ε-caprolactone at an 'ideal' initial monomer ratio for 50:50 copolymer composition, initiated by Zr_2(**8**)$_2$(O^iPr)$_2$. Polymerisation monitored by ^{1}H NMR spectroscopy and monitored *in situ*. Conditions: [M]/[I] = 100, [M] = 0.5 M, toluene-d_8, 80 °C

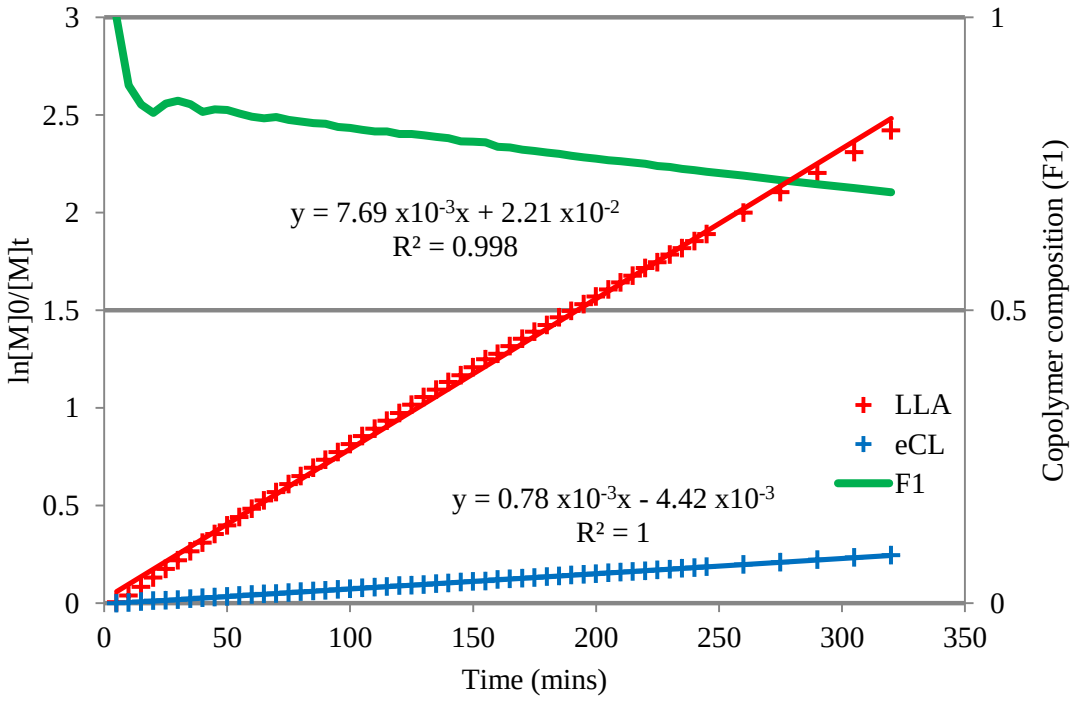

Figure 4.16 Semi-ln plot of the one-pot polymerisation of L-lactide and ε-caprolactone at an 'ideal' initial monomer ratio for 50:50 copolymer composition, initiated by Zr_2(**10**)$_2$(O^iPr)$_2$. Polymerisation monitored by ^{1}H NMR spectroscopy and monitored *in situ*. Conditions: [M]/[I] = 100, [M] = 0.5 M, toluene-d_8, 80 °C

Initial ^{1}H NMR spectroscopic reaction monitoring suggests that despite the 'ideal' monomer feed ratio the initial copolymer composition is still biased towards lactide. Copolymerisation using Zr-C_3^tBu yields a copolymer closest to a 50:50 copolymer composition and also provide the least drift in composition, attributed to the comparably slower rates of polymerisation of L-lactide and ε-caprolactone than observed for $Zr_2(\mathbf{8})_2(O^iPr)_2$. Rate of polymerisation of ε-caprolactone is greatly reduced in the copolymerisation, having initially been faster for homopolymerisation than the respective rate for L-lactide (Table 4.10). This suggests that in a copolymerisation the preference for the insertion of lactide cannot be just due to the presence of two coordinating carbonyl centres per monomer, with either Lewis basicity, energy of ring-opening, or a combination of all three playing a role. Unlike copolymerisation initiated by Zr-C_3^tBu, for $Zr_2(\mathbf{8})_2(O^iPr)_2$ rates of polymerisation of each monomer in the copolymerisation are similar to those observed in the respective homopolymerisations. Reaction monitoring indicates a rapid change in copolymer composition over 0 – 50 minutes, during which time L-lactide conversion achieves > 90 %. This suggests that whilst at reaction times < 50 minutes ε-caprolactone is incorporated, the copolymer formed is initially biased to poly(lactide) forming a block copolymer. This is also indicated by the reactivity ratios calculated (Table 4.9). The distortion observed for copolymer composition at low conversion / reaction time for copolymerisations carried out by Zr-C_3^tBu and $Zr_2(\mathbf{10})_2(O^iPr)_2$ provide evidence of the limitation of measuring copolymer composition *in situ* at low conversion using ^{1}H NMR spectroscopy. This is less noticeable in copolymerisation by $Zr_2(\mathbf{8})_2(O^iPr)_2$ due to the much faster rate of polymerisation

4.5 Conclusions and future work in utilising reactivity ratios for the controlled production of copolymers

The one-pot copolymerisation of lactide and ε-caprolactone is possible using the zirconium amine tris(phenolate) alkoxide initiators presented in this thesis. Analysis of high conversion polymeric material indicated that the copolymers had a block-type nature to them with preference to for the incorporation of lactide into the copolymer chain over ε-caprolactone.

Reactivity ratios were calculated using diad/triad NMR spectroscopy quantification of high conversion polymeric material and by finding linear and non-linear solutions to the Mayo-Lewis copolymerisation equation for low conversion data (< 15 %). Average block length values were also found through diad and triad quantification. An overwhelming preference for the polymerisation of lactide, even at ε-caprolactone-biased monomer molar ratios, lead to the

conclusion that for these initiators the preferential insertion of lactide was due to more than just the presence of two carbonyl esters per monomer. Reactivity ratios calculated from triad quantification suggested a preference for homo-polymerisation, with both r_1 and r_2 > 1. However it was deemed this was due to the large blocks of caprolactone and the averaging over the full polymer chain that triad quantification requires. The use of low-conversion data in the Mayo-Lewis copolymerisation equation was found to be more successful at providing reactivity ratios akin to that expected for a tapered block copolymer. A non-linear least squares (NNLS) method achieved a better fit to the experimental data compared to a linear Fineman-Ross solution.

Compared to early work presented by Jerome *et al.*,[3] block lengths for the zirconium initiators studied in this work are similar to that found for polymer produced using Al(O^{i}Pr)$_3$ as an initiator; $\bar{L}_{LA}$ = 2.7, $\bar{L}_{CL}$ = 2.4 for Zr-*C$_3$^{t}Bu* and $\bar{L}_{LA}$ = 3.1, $\bar{L}_{CL}$ = 3.1 for Al(O^{i}Pr)$_3$.[3] As with the work presented herein, Jerome *et al.* also reported that whilst the rate of homopolymerisation was greater for caprolactone compared to lactide, r_1 was much larger than r_2 which corresponded to a preference for the formation of a tapered-block copolymer. As proposed with studies of Al(O^{i}Pr)$_3$, it is reasonable to attribute the cause of the same behaviour in this zirconium-based series of initiators to the proximity of the carbonyl in the growing lactide chain reducing the nucleophilicity of the alkoxide species, as well the ability to chelate to the metal centre.[3] Equally, the lowest propagation rate was observed for the insertion of caprolactone into a growing lactide chain with a suggestion that incompatibility of the caprolactone monomer structure and reduced nucleophilicity play a role in hampering this step.[3]

Few examples of the one-pot copolymerisation of lactide with other lactones using zirconium-based initiators are present in the literature; with the focus primarily on Zr(acac)$_4$ for the copolymerisation of lactide with glycolide or ε-caprolactone.[16, 17] Using Zr(acac)$_4$, Kasperczyk *et al.* found that the one-pot copolymerisation of L-lactide and ε-caprolactone at a molar ratio of 3:1 produced material with an average block length of 4.29 for lactide and 1.59 for caprolactone.[17] Similar weighting in block length is observed for all zirconium initiators trialled in this work. Kasperczyk *et al*. proposed the more segmented structure was due to reduced transesterification compared to Sn(oct)$_2$;[17] likewise, little transesterification is observed for Zr-*C$_3$^{t}Bu* or Zr$_2$(**8**)$_2$(O^{i}Pr)$_2$ and Zr$_2$(**10**)$_2$(O^{i}Pr)$_2$.

It was initially proposed that the high stereoselectivity of Zr-*C$_3$^{t}Bu* may be a limiting factor in the formation of more random poly(D,L-lactide-*co*-ε-caprolatone) and that the use of the less stereoselective Zr$_2$(**8**)$_2$(O^{i}Pr)$_2$ may provide access to the desired random copolymers. Considering the reactivity ratios found using the NLLS method it was found that the use of

$Zr_2(\mathbf{8})_2(O^iPr)_2$ actually created a more block-like copolymer, deemed to be driven by the increased rate of polymerisation of lactide observed in this study and in the previous full polymerisation study (Chapter 3). Whereas the homopolymerisation of ε-caprolactone was found to be faster for the monomeric Zr-$C_3{}^tBu$ initiator, it was relatively slower for $Zr_2(\mathbf{8})_2(O^iPr)_2$ and $Zr_2(\mathbf{10})_2(O^iPr)_2$. This could be due to the reduced chelation ability of the growing poly(caprolactone) chain with respect to a growing poly(lactide) chain,[18] therefore allowing easier recombination of $Zr_2(\mathbf{8})_2(O^iPr)_2$ and $Zr_2(\mathbf{10})_2(O^iPr)_2$ into their respective inactive dimer.

The dimeric form of $Zr_2(\mathbf{8})_2(O^iPr)_2$ and $Zr_2(\mathbf{10})_2(O^iPr)_2$ and the equilibrium potentially present between an active and inactive form, as discussed in Chapter 3, adds complications to the direct comparison of these initiators for the production of copolymers. With the presence of a coordinating monomer appearing necessary to dissociate the initiator into an active species, both during the initiation and propagation steps of the polymerisation, the kinetics are not as straight forward as required for the first-order presumptions used in the Mayo-Lewis copolymerisation equation. Especially for low-conversion data and the slow initiation step for the dimeric initiators. This likely caused limitations in the utilisation of reactivity ratios for determining an ideal monomer molar ratio to achieve a 50:50 copolymer composition.

For this set initiators it is difficult to conclude if removal of the *tert*-butyl substituents has an effect on the microstructure of the copolymer produced *via* the one-pot polymerisation of *rac*-lactide / L-lactide and ε-caprolactone. This could be due to the added complexity caused by the presence of initiator dimers or the limitations of the experimental methods used in this study. The design of initiators that alter phenolate substituents whilst maintaining a monomeric geometry is desirable in the hope of providing more insight into the potential of these types of initiators for the controlled production of block or random copolymers. However, whilst phenolate substituent alteration for a homosalen-aluminium complex was found to alter copolymer microstructure,[6] it possible that the larger radius of the zirconium metal centre and the reduced steric bulk of *tert*-butyl groups over alkysilyl groups does not provide enough influence over the approach of the coordinating monomer. Higher rates of copolymerisation would offer one route to a more random copolymer structure. This could be achieved using smaller ligands such as reported by Bero *et al.* for the copolymerisaiton of lactide and glycolide or Kasperczyk *et al*. for lactide and caprolactone with $Al(acac)_3$.[16, 19] However, this would move away from the target of ligand-induced selectivity and would introduced the requirement for 'control' over secondary transesterification reactions.

With the lack of tune-ability for this series of initiators, attempts were made to direct copolymer composition through monomer feed ratio. Whilst with these initiators the success was limited, investigations could be carried out in an attempt to maintain an ideal monomer ratio through a fed polymerisation, and thus continued production of copolymer with an instantaneous 50:50 composition to higher molecular weight. The following is proposed:

- With a known 'ideal' monomer ratio for an instantaneous 50:50 copolymer composition kinetic study can provide rates of polymerisation of each monomer at low conversion.
- Rates of polymerisation / monomer consumption can be used to model the required rate of replenishment of each monomer to maintain the 'ideal' monomer ratio. Theoretically this should require a 1:1 molar mixture of the two monomers due to equal incorporation into the copolymer
- A stock solution of the two monomers can be accurately fed into the reaction vessel using a HPLC pump. This would increase the overall molecular weight of the resulting copolymer, as no further initiator is added, whilst maintaining the initial [M] to [I] ratio.

This approach to copolymer composition, whilst highly approximated in this example, may provide, with adequate reaction modelling, an effective way of controlling copolymer composition without the need for a wide range of initiators that are each developed for one copolymer. It is important to note the limitation of reaction modelling and copolymerisation studies on a Young's NMR tube scale will not necessary be applicable on larger scales. Larger scale copolymerisation studies could be carried out using *in situ* techniques such as FT-IR. There is also merit in exploring the behaviour of copolymerisations under more industrially relevant melt conditions; where the ε-caprolactone, especially in the excess required for these initiators, would act as a solvent for lactide and initiator as well as a comonomer.

4.6 References

1. Shalaby, *Biomedical polymers designed-to-degrade systems*, Hanser, Munich, 1994.
2. E. Chiellini and R. Solaro, *Adv Mater*, 1996, **8**, 305-313.
3. P. Vanhoorne, P. Dubois, R. Jerome and P. Teyssie, *Macromolecules*, 1992, **25**, 37-44.
4. F. Stassin and R. Jerome, *J Polym Sci Pol Chem*, 2005, **43**, 2777-2789.
5. H. R. Kricheldorf, K. Bornhorst and H. Hachmann-Thiessen, *Macromolecules*, 2005, **38**, 5017-5024.
6. N. Nomura, A. Akita, R. Ishii and M. Mizuno, *J. Am. Chem. Soc.*, 2010, **132**, 1750-1751.
7. A. J. Chmura, M. G. Davidson, C. J. Frankis, M. D. Jones and M. D. Lunn, *Chem. Commun.*, 2008, 1293-1295.
8. J. Fernández, A. Etxeberria and J.-R. Sarasua, *Journal of the Mechanical Behavior of Biomedical Materials*, 2012, **9**, 100-112.
9. D. Pappalardo, L. Annunziata and C. Pellecchia, *Macromolecules*, 2009, **42**, 6056-6062.
10. Y. Chen and A. Sen, *Macromolecules*, 2009, **42**, 3951-3957.
11. J. Kasperczyk and M. Bero, *Makromolekulare Chemie-Macromolecular Chemistry and Physics*, 1991, **192**, 1777-1787.
12. D. J. Darensbourg and O. Karroonnirun, *Macromolecules*, 2010, null-null.
13. F. R. Mayo and F. M. Lewis, *J. Am. Chem. Soc.*, 1944, **66**, 1594-1601.
14. M. Fineman and S. D. Ross, *J Polym Sci*, 1950, **5**, 259-262.
15. A. J. Chmura, C. J. Chuck, M. G. Davidson, M. D. Jones, M. D. Lunn, S. D. Bull and M. F. Mahon, *Angew. Chem., Int. Ed.*, 2007, **46**, 2280-2283.
16. P. Dobrzynski, J. Kasperczyk, H. Janeczek and M. Bero, *Macromolecules*, 2001, **34**, 5090-5098.
17. A. Orchel, K. Jelonek, J. Kasperczyk, P. Dobrzynski, A. Marcinkowski, E. Pamula, J. Orchel, I. Bielecki and A. Kulczycka, *Biomed Res Int*, 2013.
18. J. Lewinski, P. Horeglad, K. Wojcik and I. Justyniak, *Organometallics*, 2005, **24**, 4588-4593.
19. M. Bero and J. Kasperczyk, *Macromol. Chem. Phys.*, 1996, **197**, 3251-3258.

CHAPTER 5

EXPERIMENTAL

5 Experimental

5.1 General Procedures

$Zr(O^iPr)_4{}^iPrOH$ (99.9%, Aldrich) was used without further purification and $Hf(O^iPr)(HO^iPr)$ was purchased from Strem and used as supplied. *rac*-lactide (Aldrich) and L-lactide (Purac) were recrystallized from dry toluene and sublimed twice prior to use in polymerisation reactions. δ-valerolactone (technical grade, Aldrich) and ε-caprolactone (Aldrich) were vacuum distilled and stored under an inert atmosphere prior to polymerisation. All other starting materials were used as received and purchased from Aldrich or Acros.

Preparation of all metal complexes and subsequent ROP of *rac*-lactide and L-lactide were performed under an inert atmosphere of argon using standard Schlenk or glove-box techniques. All solvents used in the preparation of metal complexes were dry and obtained *via* an SPS (Solvent Purification System).

5.1.1 NMR Spectroscopy

Solution ^1H and $^{13}C\{^1H\}$ NMR experiments were performed at ambient temperature unless otherwise stated using a Bruker Avance-300, Bruker DRX400 or Bruker DRX500 MHz FT-NMR spectrometer with samples dissolved in $CDCl_3$, DMSO-d_6, $C_6D_5CD_3$ or C_6D_6. $CDCl_3$ for analysis of complexes was distilled from calcium hydride prior to use. C_6D_6 for complex analysis was distilled and stored over sodium. Wilmad 5 mm NMR tubes were used for ligand and polymer characterisation, while NMR tubes fitted with Young's taps were used for complexes and kinetic experiments. All chemical shifts are quoted as δ values in ppm relative to residual protio solvent resonances and all coupling constants are given in Hertz.

Homonuclear decoupled ^1H NMR spectra were recorded on a Bruker DRX400 or Bruker DRX500 MHz FT-NMR spectrometer and the methine region of the spectra analysed, as described in section 5.4.4, for the determination of the P_r value using equations given in the literature.[1]

5.1.2 Gel Permeation Chromatography (GPC)

GPC analyses were performed on a Polymer Laboratories PL-GPC 50 integrated system using PLgel 5μm MIXED-D 300 x 7.5 mm column at 35°C, using THF as the solvent at a flow rate of 1.0 ml/min. The polydispersity index (PDI) was determined from M_n/M_w where M_n is the

number average molecular weight and M_w is the weight average molecular weight. The polymers were referenced to 11 narrow molecular weight polystyrene standards with a range of M_w 615 – 568000Da.

As outlined in section 1.4.5, gel permeation chromatography (GPC) is a size exclusion technique that separates polymeric material based on hydrodynamic volume. The technique requires calibration, which in its crudest and approximate form, as carried out in this thesis, can be achieved through the use of several mono-disperse samples of polystyrene with known molecular weights. In this case a calibration curve of $\log_{10} M$ versus elution volume can be plotted, where elution volume is directly related to time *via* flow rate. Such a calibration provides molecular weight data "with respect to polystyrene standands" and is not absolute. It is important to acknowledge this when considering M_n(GPC) versus expected molecular weight based on conversion, M_n(calc.). Molecular weight data can be corrected or calculated through a number of methods depending on the type of detection method used and calibration procedure carried out. These include a Mark-Houwink correction factor and the universal calibration of the GPC system used.

It is widely accepted that for GPC, the universal calibration parameter is the hydrodynamic radius (R_e) and that it can be incorporated into the Einstein-Simha viscosity expression as follows:

$$[\eta]M = \Phi_0 {R_e}^3$$

Where [η] = intrinsic viscosity, M = molecular weight and Φ is a constant.[2] With the presumption that in dilute solutions flexible polymers behave as spheres, it is then possible to relate [η]M, through R_e, to functions of physical parameters of the polymer; such as the root-mean-square radius of gyration, molecular-expansion coefficient in solvent and end-to-end distances of the polymer chain.[2] Intrinsic viscosity, [η], can be measured through standard techniques; wherein viscosity (η) of a polymer in solution is measured at varying concentrations (c), with extrapolation to infinite dilution to give the intrinsic viscosity, [η].[3] The relationship between hydrodynamic volume and intrinsic viscosity was first used to address the issue of GPC calibration by Benoit *et al.* in 1967.[4] An approximation of the above relationship was used: $[\eta]M = 2.5A \cdot R_e$, where A = Avagadro's number. A calibration plot of $\log_{10}[\eta]$M versus elution volume can then be plotted for the standards of known molecular weight, providing a universal calibration. If the intrinsic viscosities of both the standards and fractions of unknown polymer can be measured then true molecular weight of the unknown polymer can be determined. This relationship applies to a wide number of systems, however this does have

some limitations. The polymers must have a flexible backbone and it requires the assumption that separation only occurs through size exclusion and that no other interactions take place, such as hydrogen bonding with the column material.[3]

The relationship between intrinsic viscosity and molecular weight is also presented in the Mark-Houwink equation:

$$[\eta] = \mathrm{K} \cdot M^{a}$$

Where *K* and *a* are the Mark-Houwink constants for a particular polymer and are independent of *M*.[3] The Mark-Houwink constants for different polymers can be calculated experimentally through the combination of offline viscosity data and GPC elution data.[5, 6] These constants have been widely reported for polylactide and summarised by Garlotta (Table 5.1).[7]

PDLLA	$[\eta] = 2.59 \times 10^{-4} M^{0.689}$	35 °C in THF
PDLLA	$[\eta] = 5.50 \times 10^{-4} M^{0.639}$	31.15 °C in THF
PLLA (amorphous)	$[\eta] = 6.40 \times 10^{-4} M^{0.68}$	30 °C in THF
PLLA (amor./semicryst.)	$[\eta] = 8.50 \times 10^{-4} M^{0.66}$	30 °C in THF
PLLA (semicryst.)	$[\eta] = 1.00 \times 10^{-3} M^{0.65}$	30 °C in THF

Table 5.1 Mark-Houwink constants for polylactide in THF, taken from the reference.[7]

Whilst independent of molecular weight, the values shown in Table 5.1 outline the dependence of the Mark-Houwink constants on not just temperature but also the stereochemistry and crystallinity of the polylactide. When known for both the polymer standards and the unknown samples, these constants can be used to provide the corrected molecular weight. It has already been established that [η] is related to elution volume and therefore when two polymers have the same [η] it can be stated that the following is true:

$$K_1 {M_1}^{1+a_1} = K_2 {M_2}^{1+a_2}$$

Where K_1 and a_1 are the constants of polymer 1 (standard, eg. polystyrene) and K_2 and a_2 are the constants for the unknown polymer (eg. polylactide).[6]

For the reporting of experimental molecular weight data for polylactide, a correction factor of 0.58 is widely used and accepted.[8-11] This was reported by Duda *et al.* and was based on the measurement of actual molecular weight values using a vapour pressure osmometer and its use

for GPC calibration.[12, 13] However, it is important to acknowledge that the application of a 0.58 correction factor, whilst widely used, has limitations due to the different behaviours of polylactide with different tacticities. This is also seen in the variation of Mark-Houwink constants outlined in Table 5.1. Therefore for the analysis of polymeric material of unknown tacticity, molecular weight data can be left uncorrected and expressed in terms of polystyrene standards.[1, 11, 14-20] The corrective procedure for the analysis of copolymers is further hampered due to factors including: tapering, monomer ratio and homopolymer block length.[2]

With respect to the molecular weight data presented in this thesis, molecular weights are not corrected and therefore are relative to polystyrene standards. Whilst the values are comparative for samples measured using the same system, it is important to note they are not absolute so there is a limitation to the comparison to expected molecular weight. If the widely used 0.58 correction factor is applied, it would reduce the molecular weights by ~60 %; for example, the ROP of *rac*-lactide by Zr_2(**8-10**)$_2$(O^iPr)$_2$ in the melt would be as follows:

Initiator	M_n^{calc}	M_n^{GPC}	$0.58 \times M_n^{GPC}$
Zr_2(**8**)$_2$(O^iPr)$_2$	32900	66900	38802
Zr_2(**9**)$_2$(O^iPr)$_2$	37650	19100	11078
Zr_2(**10**)$_2$(O^iPr)$_2$	34600	41900	24302

Table 5.2 'Corrected' molecular weight data (M_n) for polymeric material from the ROP of *rac*-lactide initiated by Zr_2(**8-10**)$_2$(O^iPr)$_2$

Whist the correction maintains the relationship between the three samples, its most noticeable that M_n for Zr_2(**8**)$_2$(O^iPr)$_2$ drops to being more comparable to the expected molecular weight and that Zr_2(**10**)$_2$(O^iPr)$_2$ is now below that expected, and by some margin. For true comparison analysis would be better served through the use of a viscometer detector and calibration of the GPC chromatogram to provide absolute molecular weight, as carried out by Herres-Pawlis *et al.*.[6] However, copolymer data is best left as calibrated to polystyrene standards due to the lack of reliable Mark-Houwink constants as presented in the literature.[21, 22]

5.1.3 X-ray Diffraction Studies

Data was collected at 150 K on a Nonius Kappa CCD diffractometer using Mo-Kα radiation (λ = 0.71073 Å). All structures were solved by direct methods and refined on all F^2 data using

SHELXL-97 suite of programs, with hydrogen atoms included in idealized positions and refined using the riding model.[23]

5.1.4 Mass Spectrometry

High-resolution mass spectrometry of ligands, and intermediates thereof, were recorded on a micrOTOFQ electrospray quadrupole time-of-flight (ESI-TOF) spectrometer. The samples were dissolved in methanol and the spectra recorded in positive mode. MALDI-TOF Mass Spectra of polymeric products were recorded at the EPSRC National Mass Spectrometry Service Centre, Swansea, UK. The samples were solubilised in THF and analysed by positive MALDI in linear and reflectron modes using Dithranol matrix with LiCl as an additive to promote $[M^{+}Li]^{+}$ or NaOAc.

5.1.5 Elemental Analysis

Elemental analysis was performed by Mr. A. Carver at the University of Bath, on an Exeter Analytical CE440 Elemental Analyzer, or by Mr Stephen Boyer (London Metropolitan University).

5.2 Preparation of Ligands

5.2.1 Synthesis of starting materials

Salicylammonium acetate[24] 3,5-di-*tert*-butyl-2-hydroxybenzyl bromide[25], and 3,5-dimethyl-2-hydroxybenzyaldehyde[26] were synthesised according to literature procedures.

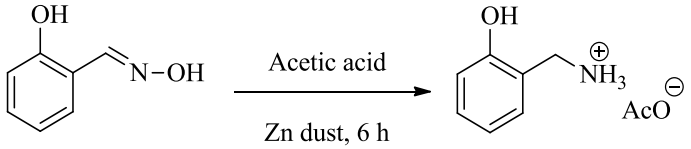

Scheme 5.1 Synthesis of Salicylammonium acetate [24]

Salicylaldoxime (5.8g, 42.3 mmol) was dissolved in Acetic acid (200ml, 3.47mmol) before the addition of zinc dust (17.0g) at a slow rate and with vigorous stirring to minimise the exotherm. (Figure 5.1) The reaction mixture was left to stir at room temperature for 6 hours before removing the zinc dust via filtration and most of the acetic acid by rotary evaporation. The resulting yellow oil was allowed to cool to room temperature before adding diethyl ether to cause a white solid to form. The white solid salicylammonium acetate (5.53g, 30.2 mmol, 71%) was isolated via filtration, washed with diethyl ether and dried under high vacuum.

^{1}H NMR (d_6-DMSO) 1.80 (3H, s, CH_3(C=O)), 3.86 (2H, s, PhCH_2N), 6.72 (1H, td J = 7.5, 0.9 Hz, Ar-H), 6.84 (1H, dd J = 7.5, 0.9 Hz, Ar-H), 7.11 (1H, td J = 7.5, 0.9 Hz, Ar-H), 7.18 (1H, dd J = 7.5, 0.9 Hz, Ar-H).

^{13}C{^{1}H} NMR (d_6-DMSO) 22.9 (H_3C(C=O)), 41.3 (PhCH_2N), 116.2, 118.2, 124.6, 129.0, 129.5 (Ar-CH), 158.0 (Ar-O), 174.1 (C=O).

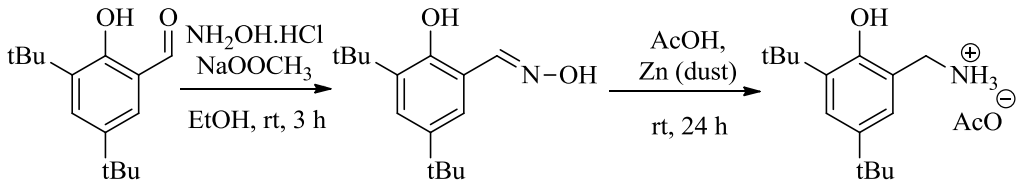

Scheme 5.2 Synthesis of 3,5-di-*tert*-butyl-2-hydroxybenzylammonium acetate

3,5-di-*tert*-butyl-2-hydroxybenzaldehyde (7.00g, 29.9 mmol) was dissolved in ethanol (75ml) before the addition of a 10% molar excess of hydroxylamine hydrochloride (2.28g, 32.9 mmol) and sodium acetate (2.70g, 32.9 mmol). The reaction mixture was stirred at room temperature

for 4 hours before the solvent was removed by rotary evaporation. Further drying under high vacuum yielded a white solid that was washed with water to remove all salts. The remaining solid was dried under vacuum to yield 3,5-di-*tert*-butyl-2-hydroxybenzyaldoxime (7.40g, 29.7 mmol, 99% yield).

^{1}H NMR ($CDCl_3$) 1.31 (9H, s, $C(CH_3)_3$), 1.45 (9H, s, $C(CH_3)_3$), 7.02 (1H, d (J = 2.4 Hz), Ar-H), 7.37 (1H, d (J = 2.4 Hz), Ar-H), 8.25 (1H, s, CH=N), 10.1 (1H, bs, Ar-OH).

^{13}C{^{1}H} NMR ($CDCl_3$) 29.8 ($C(CH_3)_3$), 31.8 ($C(CH_3)_3$), 34.5 ($C(CH_3)_3$), 35.4 ($C(CH_3)_3$), 116.0 (Ar-*C*), 125.9 (Ar-*C*), 126.6 (Ar-*C*), 136.9 (Ar-*C*H), 141.6 (Ar-*C*H), 154.5 (*C*H=N), 154.7 (Ar-O).

3,5-di-*tert*-butyl-2-hydroxybenzaldoxime (7.40g, 29.7 mmol) was dissolved in acetic acid (250 ml) and cooled in a water bath (15 °C). Zinc dust (12.0g) was added gradually to the solution and the reaction mixture stirred for 24 hours. The suspension was filtered to remove the zinc metal and acetic acid removed via rotary evaporation to give an orange oil. Further drying under high vacuum yielded a white solid (8.60g, 29.1 mmol, 98% yield)

^{1}H NMR ($(CD_3)_2SO$) 1.24 (9H, s, $C(CH_3)_3$), 1.35 (9H, s, $C(CH_3)_3$), 1.84 (3H, s, CH_3C=O), 3.89 (2H, s, N=CH_2), 7.03 (1H, d (J = 2.2 Hz), Ar-H), 7.12 (1H, d (J = 2.2 Hz), Ar-H).

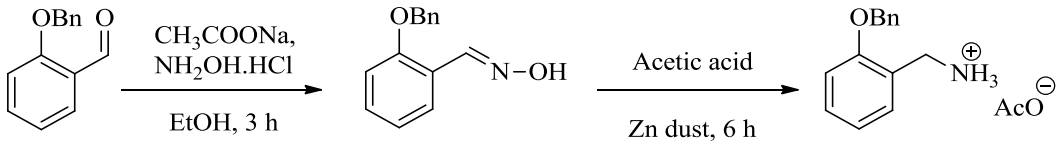

Scheme 5.3 Synthesis of 2-benzyloxybenzylammonium acetate

2-benzyloxybenzaldehyde [TCI Ltd.] (10.0 g, 47.1 mmol) was dissolved in ethanol (175 ml) before the addition of sodium acetate (4.30 g, 52.0 mmol) and hydroxylamine hydrochloride (3.60 g, 52.0 mmol). The reaction mixture was allowed to stir a room temperature for three hours before removing the solvent via rotary evaporation. The crude product was re-dissolved in toluene at 50 ° C and insoluble reagents removed via filtration. The toluene was removed via rotary evaporation and the product further dried to give a viscous oil, 2-benzyloxybenzyaldoxime (10.3 g, 45.3 mmol, 96%).

^{1}H NMR (d_6-DMSO) 5.14 (2H, s, Ph-CH_2-O), 6.96 (1H, m, Ar-H), 7.14 (1H, d (J = 8.2 Hz), Ar-H), 7.28-7.47 (6H, m, Ar-H), 7.70 (1H, dd (J = 1.6, 7.6 Hz), Ar-H), 8.36 (1H, s, CH=N).

^{13}C {^{1}H} NMR (d_6-DMSO) 70.0 (Ph-*C*H_2-O), 113.5 (Ar-*C*H), 121.3 (Ar-C), 121.7, 125.8, 127.9, 128.3, 128.9, 131.0 (Ar-*C*H), 137.2 (Ar-C), 143.7 (*C*H=N), 156.2 (Ar-O).

The isolated 2-benzyloxybenzaldoxime (10.3 g, 45.3 mmol) was dissolved in acetic acid (250 ml) before the slow addition of zinc dust (15.0 g). The reaction mixture was allowed to stir at room temperature for 18 hours before filtration to remove the zinc. The acetic acid was removed via rotary evaporation to achieve a brown oil. Subsequent washing with diethyl ether yielded a white solid 2-benzyloxybenzylammonium acetate.

^{1}H NMR (d_6-DMSO) 1.80 (3H, s, CH_3(C=O)), 3.87 (2H, s, Ph-CH_2-N), 5.16 (2H, s, Ph-CH_2-O), 6.92 (1H, dd (J = 7.2, 7.2 Hz), Ar-H), 7.04 (1H, d (J = 8.0 Hz), Ar-H), 7.19-7.41 (5H, m, Ar-H), 7.46-7.51 (2H, m, Ar-H).

^{13}C {^{1}H} NMR (d_6-DMSO) 23.0 (H_3C(C=O)), 39.5 (Ph-*C*H_2-N), 69.2 (Ph-*C*H_2-O), 112.0 (Ar-H), 120.6 (Ar-C), 127.3, 127.7, 128.5, 128.7, 128.9 (Ar-H), 137.2 (Ar-C), 155.9 (Ar-O).

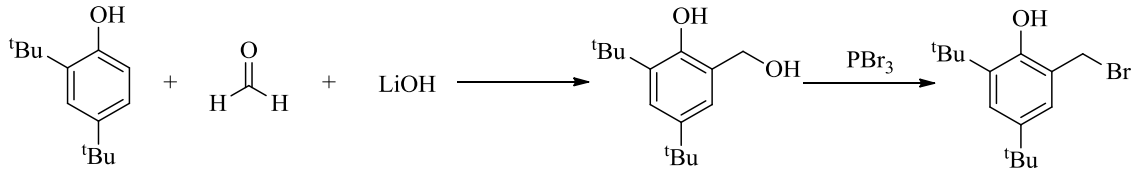

Scheme 5.4 Synthesis of 3,5-di-*tert*-butyl-2-hydroxybenzyl bromide[25]

3,4-di-*tert*-butylphenol (60g, 290 mmol) dissolved in methanol (80 ml) was charged via a dropping funnel to a reaction mixture of Lithium hydroxide monohydrate (1.0g, 24.0 mmol) and paraformaldehyde (9.0g, 300 mmol) dissolved in methanol (80ml). The reaction was refluxed (85°C) for 6 hours after which the solvent was removed via rotary evaporation to give an orange solid. The solid was dissolved in hexane (40ml), filtered and stored at 0°C overnight. The resulting green slurry was mobilized using cold hexane and filtered to yield a white solid 3,5-di-*tert*-butyl-2-hydroxybenzyl alcohol (30.5g, 129 mmol, 44%). The 3,5-di-*tert*-butyl-2-hydroxybenzyl alcohol (30.5g, 129 mmol) was dissolved in chloroform (105ml) and a solution of Phosphorus tribromide (14.1g, 52.0 mmol) in chloroform (105ml) added dropwise. (Figure 5.2) The reaction was stirred at room temperature (20°C) for 1 hour before the addition of water (175ml) and isolation of the organic fraction. The organic fraction was washed a further three

times with water (3x 175ml) before drying over anhydrous Magnesium sulphate and removing the solvent via rotary evaporation. The resulting yellow liquid was stored at 0°C over the weekend, resulting in the crystallisation of the light yellow product (28.0g, 93.6 mmol, 73%).

^{1}H NMR (*$CDCl_3$*) 1.22 (9H, s, tBu-Ph), 1.36 (9H, s, tBu-Ph), 4.51 (2H, s, Ph-CH_2-Br), 7.03 (1H, d J = 2.5 Hz, Ar-H), 7.26 (1H, d J = 2.5 Hz, Ar-H)

^{13}C{^{1}H} NMR (*$CDCl_3$*) 29.9 ((H_3C)$_3$C), 31.4 ((H_3C)$_3$C), 32.7 (Ph-CH_2-Br), 34.4 ((H_3C)$_3$C), 34.9 ((H_3C)$_3$C), 123.3 (Ar-CH), 124.7 (Ar-CH), 125.7 (Ar-C), 137.2 (Ar-C), 143.0 (Ar-C), 151.7 (Ar-O).

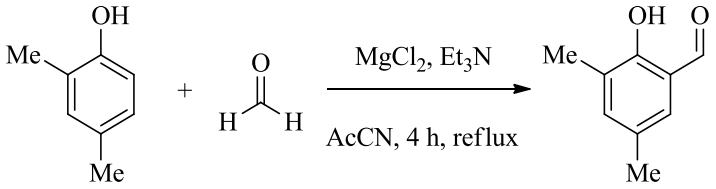

Scheme 5.5 Synthesis of 3,5-dimethyl-2-hydroxybenzyaldehyde[26]

2,4-dimethylphenol (10.0 g, 81.9 mmol), magnesium chloride (11.7 g, 123.0 mmol) and triethylamine (31.1 g, 307.0 mmol) were charged to a round-bottom flask and stirred with acetonitrile (400ml). Paraformaldehyde (16.6 g, 552.0 mmol) was added and the reaction mixture refluxed for 4 hours. (Figure 5.3) The solution was cooled before the addition of 5% aqueous hydrochloric acid (250ml). The product was extracted using diethyl ether (2x 200ml, 2x 150ml). Removal of the solvent by rotary evaporation yielded a yellow oil that was further purified via flash chromatography (9.0 g, 59.9 mmol, 73% yield)

^{1}H NMR ($CDCl_3$) 2.21 (3H, s, Me-Ph), 2.27 (3H, s, Me-Ph), 7.08 (1H, s, Ar-H), 7.15 (1H, s, Ar-H), 9.74 (1H, s, CHO), 11.08 (1H, s, OH)

^{13}C{^{1}H} NMR ($CDCl_3$) 14.6 (H_3C-Ph), 20.1 (H_3C-Ph), 119.7 (Ar-CH), 126.4 (Ar-C), 128.8 (Ar-C), 131.8 (Ar-C), 139.0 (Ar-CH), 157.9 (Ar-OH), 157.9 (*C*HO).

5.2.2 Imine bis(phenolate) ligands

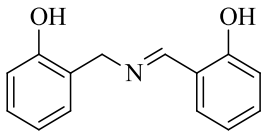

H_2**1**

Salicylammonium acetate (2.00g, 10.9 mmol) and sodium bicarbonate (3.67g, 43.7 mmol) were mixed with Ethanol (100ml) and heated to 60°C. Salicylaldehyde (1.33g, 10.9 mmol) was added drop-wise to the reaction mixture and left to stir for 2 hours. The reaction mixture was then hot filtered and washed with hot ethanol to remove insoluble $NaHCO_3$. Solvent was removed by rotary evaporation and the resulting yellow solid washed with distilled water to remove any soluble sodium salts. The disalicylaldimine, a yellow solid, was washed with hexane to remove unreacted aldehyde and dried under high vacuum (1.68g, 7.39 mmol, 68%).

^{1}H NMR (d_6-DMSO) 4.73 (2H, s, $PhCH_2N$), 6.85 (4H, m, Ar-H), 7.15 (2H, m, Ar-H), 7.32 (1H, td J = 7.5, 0.9 Hz, Ar-H), 7.45 (1H, dd J = 0.9, 7.5 Hz, Ar-H), 8.63 (1H, s, CH=N), 9.65 (1H, bs, OH), 13.72 (1H, bs, OH).

^{13}C{^{1}H} NMR (d_6-DMSO) 57.03 (CH_2N=C), 115.1, 116.5, 118.4, 118.6, 119.0, 124.4, 128.5, 129.3, 131.6, 132.3 (Ar-CH), 155.2 (Ar-O), 160.89 (*C*H=N), 166.1 (Ar-O).

m/z calc. $[C_{14}H_{13}NO_2+Na]^+$ = 250.0844, found 250.0831.

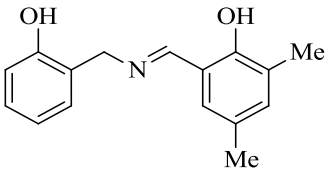

H_2**2**

Salicylammonium acetate (2.00g, 10.9 mmol) and sodium bicarbonate (3.67g, 43.7 mmol) were mixed with ethanol (80 ml) and heated to 60°C. 3,5-dimethyl-2-hydroxybenzyaldehyde (1.64g, 10.9 mmol) in ethanol (20 ml) was added drop-wise to the reaction mixture and left to stir for 2 hours. The reaction mixture was then hot filtered and washed with hot ethanol to remove insoluble $NaHCO_3$. Solvent was removed by rotary evaporation and the resulting yellow solid washed with distilled water to remove any soluble sodium salts. The yellow solid was washed

with hexane to remove unreacted aldehyde and dried under high vacuum (1.87g, 7.32 mmol, 67% yield).

^{1}H NMR (DMSO-d_6) 2.11 (3H, s, Me-Ph), 2.21 (3H, s, Me-Ph), 4.72 (2H, s, N-CH_2), 6.76-6.86 (2H, m, ^{H}Ar-H), 7.03 (1H, s, ^{Me}Ar-H), 7.05 (1H, s, ^{Me}Ar-H), 8.55 (1H, s, CH=N).

^{13}C{^{1}H} NMR (DMSO-d_6) 14.8 (H_3C-Ar), 19.7 (H_3C-Ar), 57.1 (CH_2N), 115.5, 117.9, 119.4, 125.0, 125.0, 126.7, 128.7, 129.5, 129.6, 134.3 (Ar-*C*H), 155.6, 157.2 (Ar-O), 166.6 (*C*H=N).

m/z calc. $[C_{16}H_{17}NO_2 + H]^+$ = 256.1338, found 256.1328

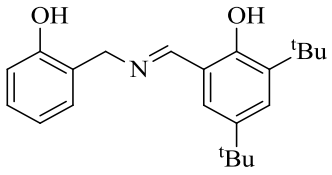

H_2**3**

Salicylammonium acetate (2.00g, 10.9 mmol) and sodium bicarbonate (3.67g, 43.7 mmol) were mixed with ethanol (80 ml) and heated to 60°C. 3,5-di-tert-butyl-2-hydroxybenzyaldehyde (2.56g, 10.9 mmol) in ethanol (20 ml) was added drop-wise to the reaction mixture and left to stir for 2 hours. The reaction mixture was then hot filtered and washed with hot ethanol to remove insoluble $NaHCO_3$. Solvent was removed by rotary evaporation and the resulting yellow solid washed with distilled water to remove any soluble sodium salts. The yellow solid was recrystallized from methanol to remove any unreacted aldehyde (1.31g, 3.86 mmol, 35% yield).

^{1}H NMR (DMSO-d_6) 1.26 (9H, s, ^{t}Bu), 1.35 (9H, s, ^{t}Bu), 4.71 (2H, s, N-CH_2), 6.77-6.86 (2H, m, ^{H}Ar-H), 7.09-7.21 (2H, m, ^{H}Ar-H), 7.28 (1H, s, ^{tBu}Ar-H), 7.29 (1H, s, ^{tBu}Ar-H), 8.63 (1H, s, CH=N).

^{13}C{^{1}H} NMR (DMSO-d_6) 29.6 (C(CH_3)$_3$), 31.7 (C(CH_3)$_3$), 34.2 (C(CH_3)$_3$), 34.9 (C(CH_3)$_3$), 57.3 (CH_2-N), 115.6, 118.1, 119.4, 124.8, 126.6, 128.5, 128.7, 129.9 (Ar-*C*H), 136.0, 139.7 (Ar-*C*), 155.7, 158.3 (Ar-O), 167.6 (*C*H=N).

m/z calc. $[C_{22}H_{29}NO_2 + H]^+$ = 340.2277, found 340.2264.

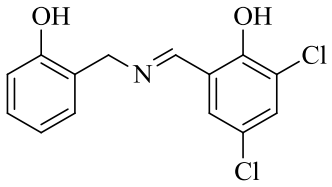

H_2**4**

Salicylammonium acetate (2.00g, 10.9 mmol) and sodium bicarbonate (3.67g, 43.7 mmol) were mixed with ethanol (80 ml) and heated to 60°C. 3,5-di-tert-butyl-2-hydroxybenzyaldehyde (2.56g, 10.9 mmol) in ethanol (20 ml) was added drop-wise to the reaction mixture and left to stir for 2 hours. The reaction mixture was then hot filtered and washed with hot ethanol to remove insoluble $NaHCO_3$. Solvent was removed by rotary evaporation and the resulting yellow solid washed with distilled water to remove any soluble sodium salts. The yellow solid was recrystallized from methanol to remove any unreacted aldehyde (1.31g, 3.86 mmol, 35% yield).

^{1}H NMR (DMSO-d_6) 4.77 (2H, s, CH_2-N), 6.79-6.89 (2H, m, ^{H}Ar-H), 7.15-7.25 (2H, m, ^{H}Ar-H), 7.44 (1H, s, ^{Cl}Ar-H), 7.55 (1H, s, ^{Cl}Ar-H), 8.64 (1H, s, CH=N).

^{13}C {^{1}H} NMR (DMSO-d_6) 53.5 (*C*H_2-N), 115.6, 117.0, 117.1, 119.5, 122.9, 125.1 (Ar-*C*H), 129.8, 130.1 (Ar-Cl), 130.7, 133.3 (Ar-*C*H), 155.9 (*C*H=N), 164.2, 165.6 (Ar-O).

m/z calc. $[C_{14}H_{11}NO_2Cl_2 + Na]^+$ = 318.0065, found 318.0066.

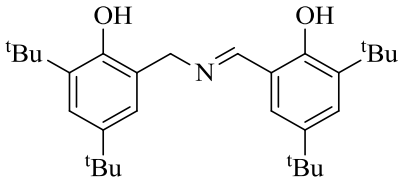

H_2**5**

3,5-di-*tert*-butyl-2-hydroxybenzylammonium acetate (2.00 g, 6.77 mmol) and sodium bicarbonate (2.28 g, 27.1 mmol) were mixed in ethanol (80 ml) and heated (70 °C). 3,5-di-*ter*-butyl-2-hydroxybenzyaldehyde (1.59 g, 6.77 mmol) was dissolved in ethanol (20 ml) and charged slowly to the reaction mixture. The reaction was stirred at temperature (70 °C) under a blanket of argon for 4 hours. The reaction was hot-filtered to remove any insoluble sodium salts before removing the solvent via rotary evaporation. The resulting yellow solid was washed with water and then dried under high vacuum. The crude product was recrystallized in minimal hot methanol and a yellow solid isolated (2.63 g, 5.82 mmol, 86 % yield).

^{1}H NMR ($CDCl_3$) 1.23 (18H, s, ^{t}Bu), 1.36 (9H, s, ^{t}Bu), 1.37 (9H, s, ^{t}Bu), 4.74 (2H, s, N-CH_2), 6.98 (1H, d (J = 2.3 Hz), Ar-H), 7.02 (1H, d (J = 2.6 Hz), Ar-H), 7.22 (1H, d (J = 7.2 Hz), Ar-H), 7.32 (1H, d (J = 2.3 Hz), Ar-H), 8.42 (1H, s, N=CH).

^{13}C{^{1}H} NMR ($CDCl_3$) 29.4, 29.9, 31.5, 31.6 (C(*C*H_3)$_3$), 34.2, 34.3, 34.8, 35.1 (*C*(CH_3)$_3$), 61.3 (N-*C*H_2), 117.9, 123.8, 124.2, 126.4, 127.5, 136.0, 136.8, 140.5, 142.6, 151.0 (Ar-*C*), 157.6, 159.1 (Ar-O), 167.8 (*C*H=N).

m/z $[C_{30}H_{45}NO_2 + Na]^+$ = 474.3348, found 474.3371.

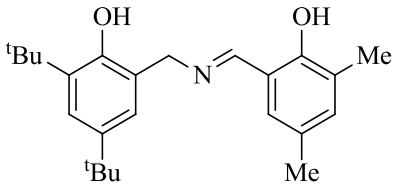

H_2**6**

3,5-di-*tert*-butyl-2-hydroxybenzylammonium acetate (2.00 g, 6.77 mmol) and sodium bicarbonate (1.71 g, 20.3 mmol) were mixed in ethanol (80 ml) and heated (70 °C). 3,5-dimethyl-2-hydroxybenzyaldehyde (1.02 g, 6.77 mmol) was dissolved in ethanol (20 ml) and charged slowly to the reaction mixture. The reaction was stirred at temperature (70 °C) under a blanket of argon for 4 hours. The reaction was hot-filtered to remove any insoluble sodium salts before removing the solvent via rotary evaporation. The resulting yellow solid was washed with water and then dried under high vacuum. The crude product was recrystallized in minimal hot methanol and a yellow solid isolated (1.63 g, 4.44 mmol, 66 % yield).

^{1}H NMR (DMSO-d_6) 1.23 (9H, s, ^{t}Bu), 1.40 (9H, s, ^{t}Bu), 2.13 (3H, s, Me), 2.22 (3H, s, Me), 4.81 (2H, s, CH_2N), 7.03-7.09 (3H, m, Ar-H), 7.16 (1H, d (J = 2.3 Hz), Ar-H), 8.56 (1H, s, N=CH).

^{13}C{^{1}H} NMR (DMSO-d_6) 15.2, 19.9 (Ar-*C*H_3), 29.8, 31.4 (C(*C*H_3)$_3$), 33.9, 34.7 (*C*(CH_3)$_3$), 57.9 (*C*H_2-N), 117.6, 122.2, 123.7, 124.6, 125.8, 126.4, 129.1, 134.0, 136.7, 141.2 (Ar-*C*), 150.8, 156.7 (Ar-O), 165.9 (N=*C*H).

m/z $[C_{24}H_{33}NO_2 + Na]^+$ = 390.2409, found 390.2404.

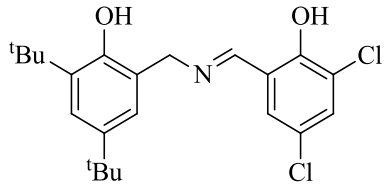

H_2**7**

3,5-di-*tert*-butyl-2-hydroxybenzylammonium acetate (2.00g, 6.77 mmol) and sodium bicarbonate (2.28g, 27.1 mmol) were mixed in ethanol (100ml) and heated (70 °C). 3,5-dichloro-2-hydroxybenzyaldehyde (1.29g, 6.77 mmol) was dissolved in ethanol (20 ml) and charged slowly to the reaction mixture. The reaction was stirred at temperature (70 °C) under a blanket of argon for 4 hours. The reaction was hot-filtered to remove any insoluble sodium salts before removing the solvent via rotary evaporation. The resulting yellow solid was washed with water and then dried under high vacuum. The crude product was recrystallized in minimal hot methanol and a yellow solid isolated (1.45g, 3.55 mmol, 52% yield).

^{1}H NMR (DMSO-d_6) 1.19 (9H, s, $C(CH_3)_3$), 1.34 (9H, s, $C(CH_3)_3$), 4.88 (2H, s, N-CH_2), 7.00 (1H, s, Ar-H), 7.11 (1H, s, Ar-H), 7.22 (1H, s, Ar-H), 7.42 (1H, s, Ar-H), 8.32 (1H, s, CH=N).

m/z $[C_{22}H_{27}NO_2Cl_2 + Na]^+$ = 430.1217, found 430.1319.

5.2.3 Amine tris(phenolate) ligands

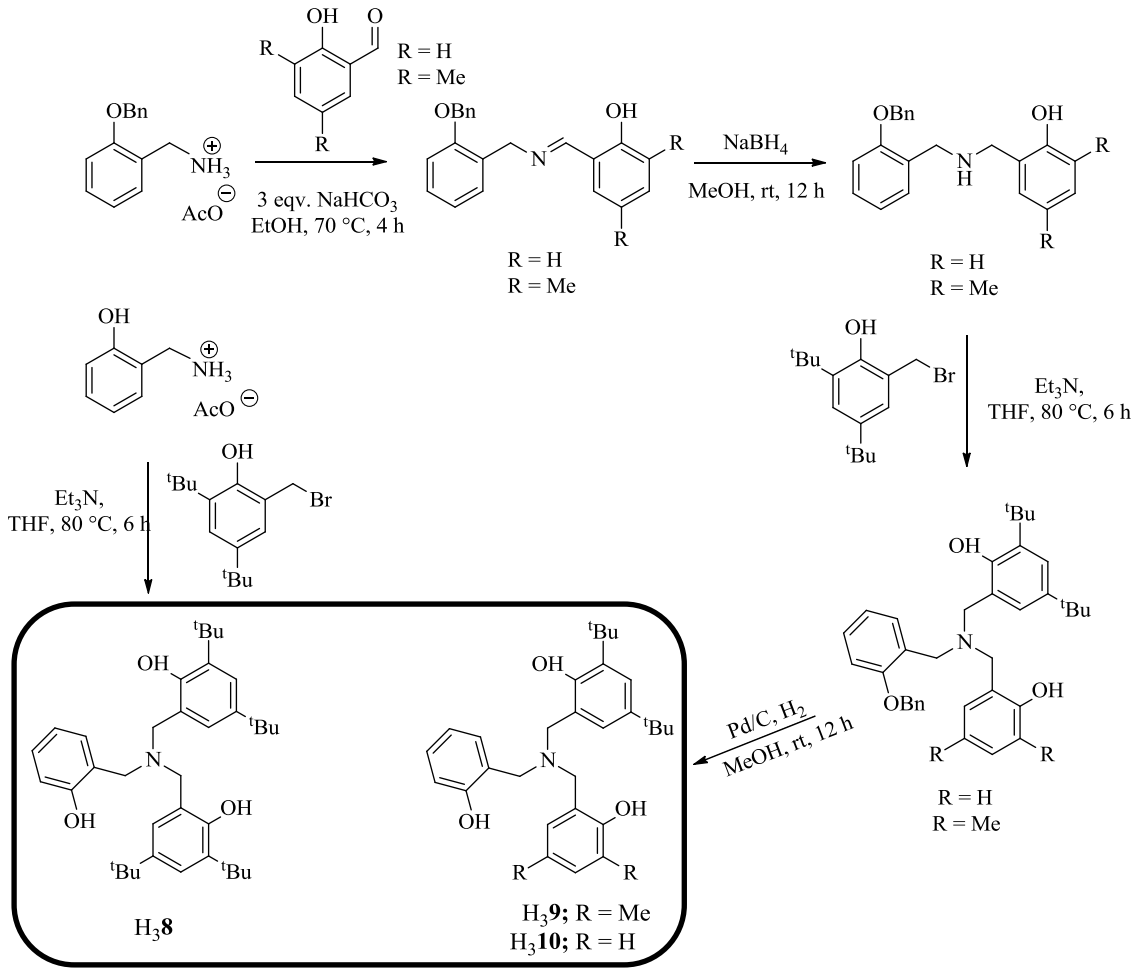

(2-hydroxybenzyl)bis(2-hydroxy-3,5-di-*tert*-butylbenzyl)amine (H_3**8**)

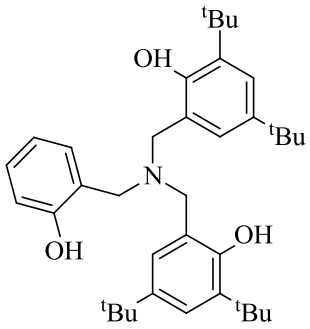

H_3**8**

Salicylammonium acetate (2.00 g, 10.9 mmol) and $NaHCO_3$ (3.66 g, 43.6 mmol) were charged to a round-bottom flask and set stirring in THF (50 ml). The reaction mixture was heated to reflux (80 °C) before adding a solution of 2-hydroxy-3,5-di-*tert*-butylbenzyl bromide (6.54 g, 21.8 mmol) in THF (25ml) drop-wise. The reaction mixture was refluxed for approx. one hour before adding triethylamine (3 ml, >21.8 mmol) drop-wise. The reaction was held a reflux for a

further five hours before cooling to room temperature. Filtration removed a white solid ($NaHCO_3$ / $Et_3NH^+Br^-$) leaving a yellow solution. Solvent was removed *via* rotary evaporation and further dried under reduced pressure to give a yellow solid. This crude product was redissolved in dichloromethane (~5ml) and subjected to flash chromatography to remove unreacted starting material and triethylamine (3.3 g, 5.9 mmol, 54% yield).

^{1}H NMR ($CDCl_3$) 1.29 (18H, s, ^{t}Bu), 1.40 (18H, s, ^{t}Bu), 3.69 (4H, s, N-CH_2-^{tBu}Ph), 3.70 (2H, s, N-CH_2-^{H}Ph), 6.81-6.89 (2H, m, ^{H}Ar-H), 6.95 (1H, s, ^{tBu}Ar-H), 6.96 (1H, s, ^{tBu}Ar-H), 7.10-7.16 (2H, m, ^{H}Ar-H), 7.22 (1H, s, ^{tBu}Ar-H), 7.22 (1H, s, ^{tBu}Ar-H).

^{13}C{^{1}H} NMR ($CDCl_3$) 28.6 ((H_3C)$_3$C), 30.6 ((H_3C)$_3$C), 33.2 ((H_3C)$_3$C), 33.8 ((H_3C)$_3$C), 54.6, 56.3 (N-*C*H_2), 115.4, 119.6 (Ar-*C*H), 121.7, 122.6 (Ar-*C*), 122.7, 124.3, 128.5, 130.5 (Ar-*C*H), 134.9, 140.8 (Ar-*C*), 150.7, 153.8 (Ar-O).

m/z calc. $[C_{37}H_{53}NO_3 + Na]^+$ = 582.3923, found 582.3945.

(2-hydroxybenzyl)(2-hydroxy-3,5-dimethylbenzyl)(2-hydroxy-3,5-di-*tert*-butylbenzyl)amine (H_3**9**)

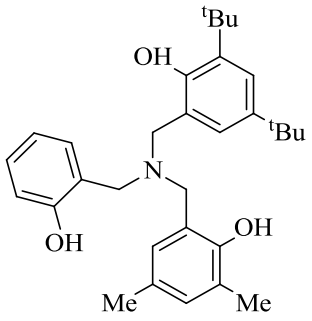

H_3**9**

2-Benzyloxybenzylammonium acetate (2.00 g, 7.23 mmol), sodium bicarbonate (2.46 g, 29.3 mmol) and ethanol (100 ml) were charged to a round-bottom flask and heated to 70 °C under a flow of argon. 3,5-dimethyl-2-hydroxybenzaldehyde (1.10 g, 7.32 mmol) was diluted with ethanol (~20 ml) and added drop-wise to the reaction mixture. The reaction mixture was stirred for four hours before hot filtering to partially remove the sodium bicarbonate. The solvent was removed via rotary evaporation to yield a yellow solid. This crude product was re-dissolved in toluene, heated and hot-filtered to remove the remaining sodium bicarbonate. The solvent was removed via rotary evaporation and further dried under vacuum to yield a yellow solid imine, *N*-(2-benzyloxybenzyl)(2-hydroxy-3,5-dimethylbenzyl)aldimine (0.80g, 2.32 mmol, 32% yield).

^{1}H NMR (d_6-DMSO) 2.11 (3H, s, CH_3), 2.20 (3H, s, CH_3), 4.78 (2H, s, Ph-CH_2-N), 5.14 (2H, s, Ph-CH_2-O), 6.89-7.13 (4H, m, Ar-H), 7.25-7.38 (5H, m, Ar-H), 7.42-7.47 (2H, m, Ar-H).

^{13}C{^{1}H} NMR (d_6-DMSO) 15.2 (H_3C-Ph), 19.9 (H_3C-Ph), 57.5 (Ph-CH_2-N), 69.2 (Ph-CH_2-O), 112.1, 117.5 (Ar-H), 120.7, 124.6, 126.4 (Ar-C), 126.5, 127.6, 127.8, 128.4, 128.8, 129.2, 129.3 (Ar-H), 134.0, 137.1 (Ar-C), 156.1, 156.7 (Ar-O), 166.9 (Ph-*C*=N).

m/z calc. $[C_{23}H_{23}NO_2 + Na]^+$ = 368.1626, found 368.1625.

N-(2-benzyloxybenzyl)(2-hydroxy-3,5-dimethylbenzyl)aldimine (0.80 g, 2.32 mmol) was dissolved in methanol before the addition of sodium borohydride (1.5 eqv.) and allowed to stir at room temperature for 12 hours / overnight. The solvent was removed via rotary evaporation and purified as above to yield the corresponding amine. This amine (0.52 g, 1.52 mmol) was dissolved in THF (80 ml) and heated to reflux (80 °C). 3,5-di-*tert*-butyl-2-hydroxybenzyl bromide (0.45 g, 1.52 mmol) was dissolved in THF (~20 ml) before being added drop-wise to the reaction mixture. The reaction mixture was refluxed for approx. one hour before adding triethylamine (0.18 ml, 1.65 mmol) .The reaction was held at reflux for a further 5 hours before cooling to room temperature. Filtration removed a white solid ($Et_3NH^+Br^-$) leaving a yellow solution. Solvent was removed *via* rotary evaporation and further dried under reduced pressure to give a yellow solid. This crude product was redissolved in dichloromethane (~5 ml) and subjected to flash chromatography to remove unreacted starting material and triethylamine. Removal of solvent under vacuum yielded an off white solid monobenzyloxy-protected amine tris(phenolate) which was subsequently dissolved in methanol and deprotected by stirring under H_2 with Pd/C. Filtration, removal of solvent *via* rotary evaporation and further drying under vacuum yielded a while solid product (0.3 g, 0.63 mmol, 41 % yield).

^{1}H NMR ($CDCl_3$) 1.27 (9H, s, ^{t}Bu), 1.39 (9H, s, ^{t}Bu), 2.19 (3H, s, Me), 2.20 (3H, s, Me), 1.97 (2H, s, CH_2-N), 3.70 (2H, s, CH_2-N), 3.71 (2H, s, CH_2-N), 6.75 (1H, s, Ar-H) 8.82-6.87 (3H, m, Ar-H), 6.92 (1H, d (J = 2.3 Hz), ^{tBu}Ar-H), 7.08-7.18 (2H, m, Ar-H), 7.20 (1H, d (J = 2.3 Hz), ^{tBu}Ar-H).

^{13}C{^{1}H} NMR ($CDCl_3$) 14.8, 19.3 (CH_3), 28.7, 30.6 ((H_3C)$_3$C), 33.1, 33.8 (H_3C)$_3$*C*), 55.0, 55.1, 56.4 (CH_2N), 155.3, 119.4, 120.7, 120.8, 122.6, 123.3, 124.1, 124.5, 128.0, 128.2, 128.4, 130.2, 130.3, 134.9, 140.6 (Ar-*C*), 149.9, 150.9, 154.0 (Ar-O).

m/z calc. $[C_{31}H_{41}NO_3 + H]^+$ = 476.3165, found 476.3159.

Bis(2-hydroxybenzyl)(2-hydroxy-3,5-di-*tert*-butylbenzyl)amine (H_3**10**)

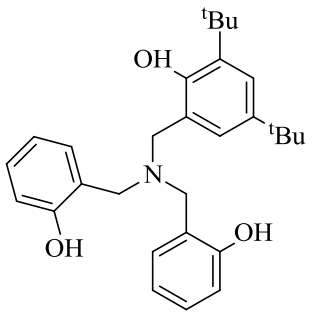

H_3**10**

2-Benzyloxybenzylammonium acetate (2.90 g, 10.6 mmol), sodium bicarbonate (3.57 g, 42.4 mmol) and ethanol (150 ml) were charged to a round-bottom flask and heated to 70 °C under a flow of argon. Salicyaldehyde (1.29 g, 10.6 mmol) was diluted with ethanol (~20 ml) and added drop-wise to the reaction mixture. The reaction mixture was stirred for four hours before hot filtering to partially remove the sodium bicarbonate. The solvent was removed via rotary evaporation to yield a yellow solid. This crude product was re-dissolved in toluene, heated and hot-filtered to remove the remaining sodium bicarbonate. The solvent was removed via rotary evaporation and further dried under vacuum to yield a yellow solid imine *N*-(2-benzyloxybenzyl)(2-hydroxybenzyl)aldimine (1.80 g, 5.64 mmol, 53% yield) .

^{1}H NMR (d_6-DMSO) 4.22 (2H, s, N-CH_2-Ph), 4.94 (2H, s, O-CH_2-Ph), 6.41-6.54 (3H, m, Ar-H), 6.75-6.79 (1H, m, Ar-H), 6.88-6.95 (2H, m, Ar-H), 7.08-7.21 (2H, m, Ar-H), 7.30-7.36 (5H, m, Ar-H), 8.18 (1H, s, Ph-CH=N).

^{13}C NMR (d_6-DMSO) 59.5 (Ph-*C*H_2-N), 69.6 (O-*C*H_2-Ph), 112.1, 113.8, 118.2, 120.5 (Ar-*C*H), 122.7, 124.5 (Ar-*C*), 128.0, 128.2, 128.7, 129.9, 130.9, 134.5, 136.2 (Ar-*C*H), 137.2 (Ar-*C*), 157.1 (Ar-OBn), 170.4 (Ar-O), 171.9 (Ph-*C*=N).

m/z calc. $[C_{21}H_{19}NO_2 + Na]^+$ = 340.1313, found 340.1310.

N-(2-benzyloxybenzyl)(2-hydroxybenzyl)aldimine (1.80 g, 5.64 mmol) was dissolved in methanol before the addition of sodium borohydride (1.5 eqv.) and allowed to stir at room temperature for 12 hours / overnight. The solvent was removed via rotary evaporation and purified as above to yield the corresponding amine. This amine (1.64 g, 5.13 mmol) was dissolved in THF (150 ml) and heated to reflux (80 °C). 3,5-di-*tert*-butyl-2-hydroxybenzyl bromide (1.54 g, 5.13 mmol) was dissolved in THF (~20 ml) before being added drop-wise to the reaction mixture. The reaction mixture was refluxed for approx. one hour before adding

triethylamine (0.8 ml, 5.64 mmol) .The reaction was held a reflux for a further 5 hours before cooling to room temperature. Filtration removed a white solid ($Et_3NH^+Br^-$) leaving a yellow solution. Solvent was removed *via* rotary evaporation and further dried under reduced pressure to give a yellow solid. The crude product was dissolved in methanol (50 ml) before the addition of Pd/C and exposure to an atmosphere of H_2. After stirring for 18 hours, the reaction was filtered through celite and the solvent removed via rotary evaporation. Further drying under vacuum yielded a yellow solid. This crude product was redissolved in dichloromethane (~5 ml) and subjected to flash chromatography to remove unreacted starting material and triethylamine. Solvent was removed under vacuum and the resulting solid recrystallized in hexane with a small amount of methanol to yield the white solid amine tris(phenolate), H_3**3** (0.98g, 2.20 mmol, 43% yield).

^{1}H NMR ($CDCl_3$) 1.26 (9H, s, ^{t}Bu), 1.36 (9H, s, ^{t}Bu), 3.74 (4H, s, N-CH_2-PH), 3.75 (2H, s, N-CH_2-Ph), 6.80-8.85 (4H, m, Ar-H), 6.93 (1H, d (J = 2.4 Hz), ^{tBu}Ar-H), 7.08-7.16 (4H, m, Ar-H), 7.20 (1H, d (J = 2.4 Hz), ^{tBu}Ar-H).

^{13}C {^{1}H} NMR ($CDCl_3$) 29.9, 31.8 (C(*C*H_3)$_3$), 34.3, 34.9 (*C*(CH_3)$_3$), 56.4, 58.1 (N-*C*H_2-Ph), 116.5, 120.5, 121.6, 122.6, 123.4, 125.4, 129.7, 131.3, 136.2, 141.9 (Ar-*C*), 152.1, 155.3 (Ar-O).

m/z $[C_{29}H_{38}NO_3 + H]^+$ = 448.2852, found 448.2880.

5.3 Synthesis of Metal Complexes

5.3.1 Aluminium imine bis(phenolate) complexes

General Procedure

Imine bis(phenolate) was usually carried out on a 0.5 g scale. Ligand H_2(**1-7**) was charged to a schlenk and placed under an inert atmosphere using standard air-sensitive techniques. Dry toluene (~10 ml) was added to the flask *via* a cannula before the addition of 1 equivalent of $AlMe_3$ (2 M in hexane) *via* syringe. The reaction was stirred at room temperature for 1 hour before the removal of solvent under reduced pressure to yield a yellow solid. Crude material was recrystallised in minimal hot toluene.

The high dilution method for the coordination of H_2**4** to $AlMe_3$ was carried out through the addition of appropriate amounts of $AlMe_3$ to dry toluene (~10 ml) in a schlenk under an inert atmosphere before the drop-wise addition of a similar solution of ligand (H_2**4**) in ~10 ml of dry toluene. Crude material was isolated by solvent removal under vacuum and recrystallisation attempted from hot toluene.

$Al_2(Me)_2$(**1**)$_1$ (5°-5° Motif, major isomer)

^{1}H NMR (C_6D_6) -0.03 (6H, s, Al-CH_3), 3.53 (2H, d (J = 14.0 Hz), CH_2-N), 5.30 (2H, d (J = 14.0 Hz), CH_2-N), 6.64 (2H, dd (J = 1.0, 6.9 Hz), Ar-H), 6.74 (2H, dd (J = 1.7, 7.7 Hz), Ar-H), 6.94 (2H, dt (J = 1.6, 7.5 Hz), Ar-H), 6.99-7.05 (4H, m, Ar-H), 7.12 (2H, dd (J = 1.9, 6.9 Hz), Ar-H), 7.29 (2H, s, CH=N), 7.37 (2H, dt (J = 1.7, 7.9 Hz), Ar-H), 8.41 (2H, dd (J = 0.7, 8.5 Hz), Ar-H).

^{13}C {^{1}H} NMR (C_6D_6) -8.10 (Al-*C*H_3), 60.8 (N-*C*H_2), 117.3, 119.9, 121.1, 122.1, 122.8, 126.3, 128.2, 129.0, 133.3, 135.4 (Ar-*C*), 154.4 (*C*H=N), 164.0, 165.2 (Ar-O).

Anal: calc. for $C_{15}H_{14}NO_2Al$: C, 67.4; H, 5.28; N, 5.24. Found: C, 66.7; H, 5.27; N, 4.72.

$Al_2(Me)_2$(**2**)$_2$ (6°-4° motif)

^{1}H NMR (C_6D_6) -0.49 (6H, s, Al-CH_3), 1.66 (6H, s, CH_3), 2.13 (6H, s, CH_3), 4.43 (2H, d (J = 17.3 Hz), CH_2-N), 5.05 (2H, d (J = 17.3), CH_2-N), 6.48-6.96 (12H, m, Ar-H), 7.70 (2H, s, CH=N).

^{13}C {^{1}H} NMR (C_6D_6) -11.6 (Al-*C*H_3), 14.5, 19.0 (*C*H_3), 61.1 (*C*H_2-N), 117.2, 119.5, 121.1, 122.0, 122.5, 127.1, 129.0, 129.2, 129.3, 135.5 (Ar-*C*), 151.9 (*C*H=N), 160.9, 167.4 (Ar-O).

$Al_2(Me)_2$(**3**)$_2$

^{1}H NMR (C_6D_6) -0.39 (6H, s, Al-CH_3), 0.98 (18H, s, C(CH_3)$_3$), 1.29 (18H, s, C(CH_3)$_3$), 4.24 (2H, d (J = 16.8 Hz), CH_2-N), 5.43 (2H, d (J = 16.8 Hz), CH_2-N), 6.72 (2H, d (J = 2.0 Hz), Ar-H), 6.80-6.87 (4H, m, Ar-H), 6.94 (2H, d (J = 2.6 Hz), Ar-H), 6.96 (2H, d (J = 2.0 Hz), Ar-H), 7.41 (2H, d (J = 2.6 Hz), Ar-H), 7.76 (2H, s, CH=N).

^{13}C{^{1}H} NMR (C_6D_6) 0.0 (Al-*C*H_3), 27.8, 30.2 (C(*C*H_3)$_3$), 32.7 (*C*(CH_3)$_3$), 33.8 (*C*(CH_3), 61.9 (*C*H_2-N), 117.6, 120.6, 121.8, 124.3, 127.1, 127.9, 128.8, 129.8, 136.8, 139.6 (Ar-*C*), 153.2, 161.9 (Ar-O), 170.2 (*C*=N).

Anal: calc for $C_{23}H_{30}AlNO_2$: C, 72.80; H, 7.97; N, 3.69. Found: C, 72.68; H, 8.12; N, 3.55.

$Al_2(Me)_2$(**4**)$_2$ (5°-5° motif, major isomer)

^{1}H NMR (C_6D_6) -0.29 (6H, s, Al-CH_3), 3.38 (2H, d (J = 13.5), N-CH_2), 5.09 (2H, d (J = 13.5 Hz), N-CH_2), 6.27 (2H, d (J = 2.5 Hz), Ar-H), 6.63 (2H, s, CH=N), 6.79 (2H, d (J = 7.2 Hz), Ar-H), 6.92 (2H, t (J = 7.2 Hz), Ar-H), 7.14 (2H, d (J = 7.2 Hz), Ar-H), 7.35 (2H, t (J = 7.2 Hz), Ar-H), 8.66 (2H, d (J = 7.2 Hz), Ar-H).

^{13}C{^{1}H} NMR (C_6D_6) 1.71 (Al-*C*H_3), 61.0 (*C*H_2-N), 121.0, 121.6, 122.1, 124.2, 126.1, 127.7, 129.9, 131.2, 134.9, 138.2 (Ar-*C*), 154.1, 158.0 (Ar-O), 164.0 (*C*H=N).

Anal: calc for $C_{15}H_{12}AlCl_2NO_2$: C, 53.6; H, 3.60; N, 4.17. Found: C, 60.85; H, 5.58; N, 3.26.

$Al_2(Me)_2$(**5**)$_2$ (6°-4° motif)

^{1}H NMR (C_6D_6) -0.20 (6H, s, Al-CH_3), 0.89 (18H, s, C(CH_3)$_3$), 1.19 (18H, s, C(CH_3)$_3$), 1.37 (18H, s, C(CH_3)$_3$), 1.371 (18H, s, C(CH_3)$_3$), 4.05 (2H, d (J = 14.7), CH_2-N), 6.14 (2H, d (J =

14.3), CH_2-N), 6.94 (2H, d (J = 2.5 Hz), Ar-H), 7.24 (2H, d (J = 2.5 Hz), Ar-H), 7.35 (2H, d (J = 2.5 Hz), Ar-H), 7.45 (2H, d (J = 2.5 Hz), Ar-H), 7.94 (2H, s, CH=N).

$^{13}C\{^1H\}$ NMR (C_6D_6) -4.44 (Al-CH_3), 29.5, 31.6, 31.7, 31.8 (C(*C*H_3)$_3$), 33.9, 34.5, 34.6, 35.2 (*C*(CH$_3$)$_3$), 66.4 (*C*H_2-N), 119.6, 124.3, 125.3, 125.7, 128.5, 129.3, 130.0, 130.2, 136.9, 139.9, 140.7, 144.8, 150.7, 163.1

Anal: calc. for $C_{31}H_{46}NO_2Al$: C, 75.7; H, 9.43; N, 2.85. Found: C, 75.2; H, 9.13; N, 2.56.

5.3.2 Titanium imine bis(phenolate) complexes

General Procedure

All procedures for the synthesis of Ti(IV) imine bis(phenolate) complexes were carried out using standard schlenk and glove box techniques to maintain an intert atmosphere. Reactions were carried out by procedure A to achieve compounds Ti(**1**)$_2$ and Ti(**3**)$_2$; procedure B was used to obtain Compound **1**B and Ti_2(**3**)$_2$(O^iPr)$_4$

Procedure A (low dilution method): On a 0.5 g scale, the imine bis(phenolate) ligand (H_2**1,3**) was dissolved in dry toluene (~10 ml) in a schlenk before the addition of 1 equivalent of Ti(O^iPr)$_4$ *via* syringe. The reaction was allowed to stir at room temperature for 1 hour before the solvent was removed under vacuum with purification to give the Ti(**X**)$_2$ complexe achieved through recrystallisation from dry toluene. Isolated material was thoroughly dried under high vacuum.

Procedure B (high dilution method): Appropriate amounts of Ti(O^iPr)$_4$ were charged to a dry schlenk with the addition of dry toluene (~10 ml). A similar solution of 1 equivalent of imine bis(phenolate) ligand (H_2**1,3**) in ~10 ml toluene was added drop-wise *via* syringe to the Ti(O^iPr)$_4$ solution. The reaction was allowed to stir for 1 hour at room temperature before the removal of solvent under vacuum and subsequent purification *via* recrystallisation in toluene.

Ti(**1**)$_2$

^{1}H NMR (CDCl): 4.84 (1H, d (J = 13.1 Hz) N-CH_2), 5.06 (1H, d (J = 13.1 Hz), N-CH_2), 6.05 (1H, dd (J = 8.2, 0.8 Hz), Ar-H), 6.46 (1H, dd (J = 8.4, 1.9 Hz), Ar-H), 6.73 (1H, td (J = 7.4, 1.2 Hz), Ar-H), 6.84 (1H, td (J = 7.6, 1.0 Hz), Ar-H), 7.02 (1H, td (J = 7.6, 1.6 Hz), Ar-H), 7.20 (1H, dd (J = 7.4, 1.6 Hz), Ar-H), 7.28-7.30 (1H, m, Ar-H), 7.43 (1H, dd (J = 7.7, 1.5 Hz), Ar-H), 8.54 (1H, s, CH=N).

^{13}C{^{1}H} NMR ($CDCl_3$): 64.0. (Ph*C*H_2N), 114.9, 116.5, 117.9, 117.9, 120.6, 124.7, 124.8, 127.2, 132.2, 134.3, 161.7(Ar-O), 162.7(Ar-O), 164.3(*C*H=N).

Anal: calc. for $C_{28}H_{22}N_2O_4Ti$: C, 67.5; H, 4.4; N, 5.6. Found: C, 67.3; H, 4.7; N, 4.3.

Ti_2(**3**)$_2$(O^iPr)$_4$

^{1}H NMR ($CDCl_3$): 1.27 - 1.32 (21H, m, 6H ($CH(CH_3)_2$), 9H ($C(CH_3)_3$)), 1.48 (9H, s, (CH_3)$_3$), 4.93 (2H, septet (J = 6.0 Hz), $CH(CH_3)_2$), 4.93 (2H, s, N-CH_2), 6.71 (1H, d (J = 8.0 Hz), Ar-H), 6.75 (1H, dd (J = 7.4, 1.0 Hz), Ar-H), 7.08 (1H, d (J = 7.5 Hz), Ar-H), 7.14 (1H, dd (J = 7.5, 1.5 Hz), Ar-H), 7.16 (1H, d (J = 2.6 Hz), Ar-H), 7.49 (1H, d (J = 2.6 Hz), Ar-H), 8.40 (1H, s, CH=N).

^{13}C{^{1}H} NMR ($CDCl_3$): 25.9, 25.8 ((CH_3)$_2$), 29.5 ((CH_3)$_3$), 31.5 ((CH_3)$_3$), 34.2 ($C(CH_3)_3$), 35.2 ($C(CH_3)_3$), 64.5 (Ph*C*H_2N), 79.2 ($C(CH_3)_2$), 116.7, 118.8, 121.2, 126.6, 127.0, 127.34, 129.0, 129.5, 137.7, 140.8(Ar-H), 160.8, 162.3(Ar-O), 165.4 (*C*H=N).

Anal: calc. for $C_{56}H_{86}N_2O_8Ti_2$: C, 66.9; H, 8.2; N, 2.8. Found: C, 66.1; H, 8.1; N, 2.7.

5.3.3 Zirconium amine tris(phenolate) complexes

General Procedure

Amine tris(phenolate) ligands (H_3**X**) could be used crude and charged to a dry Schlenk and placed under an inert atmosphere using standard Schlenk techniques. The ligand was dissolved in dry toluene before adding Zr(O^iPr)(HO^iPr). The reaction was stirred at room temperature for one hour before the solvent was removed under vacuum. Dry hexane was added, giving an

orange solution and off white solid. The solid was isolated *via* cannula filtration and dried under vacuum. The crude solid product was dissolved in minimal hot toluene and allowed to recrystallize to yield a white crystalline product.

Zr-$C_3{}^tBu$

The C_3-symmetrical amine tris(phenolate) ligand with subsequent coordination and purification according the methodologies in the literature.[14, 27]

Zr_2(**8**)$_2$(O^iPr)$_2$

^{1}H NMR ($CDCl_3$) 0.98 (6H, d (J = 6.4 Hz), $CH(CH_3)_2$), 1.00 (18H, s, $C(CH_3)_3$), 1.03 (18H, s, $C(CH_3)_3$), 1.18 (18H, s, $C(CH_3)_3$), 1.20 (6H, d (J = 6.0 Hz), $CH(CH_3)_2$), 1.28 (18H, s, $C(CH_3)_3$), 2.80 (2H, d (J = 12.8 Hz), $PhCH_2N$), 3.21 (2H, d (J = 13.2 Hz), $PhCH_2N$), 3.48 (2H, d (J = 13.2 Hz), $PhCH_2N$), 3.81 (2H, d (J = 12.8 Hz), $PhCH_2N$), 4.51 (2H, sept (J = 6.0 Hz), $CH(CH_3)_2$), 5.12 (2H, d (J = 13.2 Hz), $PhCH_2N$), 5.40 (2H, d (J = 12.8 Hz), $PhCH_2N$), 6.22 (6H, m, Ar-H), 6.52 (2H , m, Ar-H), 6.72 (2H, s, Ar-H), 6.79 (2H, s, Ar-H), 7.02 (2H, s, Ar-H), 7.12 (2H, s, Ar-H).

^{13}C{^{1}H} NMR ($CDCl_3$) 22.7 ($CH(\mathit{C}H_3)_2$), 26.4, 26.6, 29.5, 30.0 ($C(\mathit{C}H_3)_3$), 34.0, 34.3, 34.7, 34.9 ($\mathit{C}(CH_3)_3$), 61.6, 62.3, 64.9 ($Ph\mathit{C}H_2N$), 72.2 ($\mathit{C}H(CH_3)_2$), 120.8, 123.0, 123.6, 123.7, 124.2, 124.5, 125.5, 126.5, 128.3, 130.5 (Ar-*C*H), 134.8, 136.4, 140.2, 140.9 (Ar-C), 154.4, 156.7, 157.4 (Ar-O).

Anal: calc. for $C_{40}H_{57}NO_4Zr$ C, 67.9; H, 8.13; N, 1.98. Found C, 68.6; H, 8.22; N, 1.93.

Zr_2(**9**)$_2$(O^iPr)$_2$

^{1}H NMR ($CDCl_3$) 0.98 (18H, s, $C(CH_3)_3$), 1.10 (6H, d (J = 6.1 Hz), $CH(CH_3)_2$), 1.15 (6H, d (J = 6.1 Hz), $CH(CH_3)_2$), 1.29 (18H, s, $C(CH_3)_3$), 1.54 (6H, s, Ph-CH_3), 2.06 (6H, s, Ar-CH_3), 2.78 (2H, d (J = 13.0 Hz), Ph-CH_2-N), 3.12 (2H, d (J = 13.0 Hz), Ph-CH_2-N), 3.52 (2H, d (J = 13.7 Hz), Ph-CH_2-N), 3.87 (2H, d (J = 13.0 Hz), Ph-CH_2-N), 4.39 (2H, sept (J = 6.1 Hz), $CH(CH_3)_2$), 5.12 (2H, d (J = 13.7 Hz), Ph-CH_2-N), 5.24 (2H, d (J = 13.0 Hz), Ph-CH_2-N), 6.16-6.25 (6H, m, Ar-H), 6.33 (2H, s, ^{Me}Ar-H), 6.48-6.55 (2H, m, Ar-H), 6.54 (2H, s, ^{Me}Ar-H), 6.69-6.85 (2H, m, Ar-H), 7.02 (2H, d (J = 2.2 Hz), ^{tBu}Ar-H), 7.12 (2H, d (J = 2.2 Hz), ^{tBu}Ar-H).

$^{13}C\{^{1}H\}$ NMR ($CDCl_3$) 15.1 (Ar-*C*H_3), 19.4 (Ar-*C*H_3), 25.2 (CH(*C*H_3)$_2$), 25.7 (CH(*C*H_3)$_2$), 28.4 (C(*C*H_3)$_3$), 30.8 (C(*C*H_3)$_3$), 33.3 (*C*(CH$_3$)$_3$), 33.7 (*C*(CH$_3$)$_3$), 59.8 (Ph*C*H$_2$N), 60.8 (Ph*C*H$_2$N), 63.7 (Ph*C*H$_2$N), 71.4 (*C*H(CH$_3$)$_2$), 117.8, 119.7, 119.8, 122.7, 123.0, 123.3, 123.4, 123.5, 125.7, 125.8, 127.3, 128.1, 129.7, 135.5, 139.8 (Ar-H), 154.3, 155.3, 155.9 (Ar-O).

Zr_2(**10**)$_2$(O^iPr)$_2$

^{1}H NMR ($CDCl_3$) 1.06 (18H, s, C(CH$_3$)$_3$), 1.17 (6H, d (J = 6.0 Hz), CH(CH$_3$)$_2$), 1.28 (6H, d (J = 6.0 Hz), CH(CH$_3$)$_2$), 1.37 (18H, s, C(CH$_3$)$_3$), 2.96 (2H, d (J = 13.2 Hz), PhCH$_2$N), 3.24 (2H, d (J = 13.2 Hz), PhCH$_2$N), 3.64 (2H, d (J = 13.7 Hz), PhNCH$_2$), 4.02 (2H, d (J = 13.2 Hz), PhNCH$_2$), 4.45 (2H, sept (J = 6.0 Hz), CH(CH$_3$)$_2$), 5.22 (2H, d (J = 13.7 Hz), PhNCH$_2$), 5.34 (2H, d (J = 13.2 Hz), PhNCH$_2$), 5.80 (2H, d (J = 7.9 Hz), Ar-H), 6.20-6.29 (4H, m, Ar-H), 6.47-6.56 (2H, m, Ar-H), 6.60-6.72 (4H, m, Ar-H), 6.78-6.93 (4H, m, Ar-H), 7.11 (2H, d (J = 2.2 Hz), ^{tBu}Ar-H), 7.21 (2H, d (J = 2.2 Hz), ^{tBu}Ar-H).

$^{13}C\{^{1}H\}$ NMR ($CDCl_3$) 25.9 (CH(*C*H$_3$)$_2$), 26.6 (CH(*C*H$_3$)$_2$), 29.5 (C(*C*H$_3$)$_3$), 31.8 (C(*C*H$_3$)$_3$), 34.3 (*C*(CH$_3$)$_3$), 34.8 (*C*(CH$_3$)$_3$), 60.7 (Ph*C*H$_2$N), 61.9 (Ph*C*H$_2$N), 64.7 (Ph*C*H$_2$N), 72.7 (*C*H(CH$_3$)$_2$), 116.2, 118.0, 119.3, 121.1 (Ar-H), 123.8, 124.0 (^{tBu}Ar-H), 124.4 (Ar-C), 125.6, 126.5 (Ar-C), 128.3, 128.4, 129.1, 130.2 (Ar-H), 136.6, 141.1 (Ar-C), 155.0, 156.8, 160.2 (Ar-O).

Anal: calc. for $C_{32}H_{41}NO_4Zr$, C, 64.60; H, 6.95; N, 2.35. Found: C, 64.49; H, 7.05; N, 2.26.

5.3.4 Hafnium amine tris(phenolate) complexes

General Procedure

Amine tris(phenolate) ligands (H_3**X**) could be used crude and charged to a dry Schlenk and placed under an inert atmosphere using standard Schlenk techniques. The ligand was dissolved in dry toluene before adding Hf(O^iPr)(HO^iPr). The reaction was stirred at room temperature for one hour before the solvent was removed under vacuum. Dry hexane was added, giving an orange solution and off white solid. The solid was isolated *via* cannula filtration and dried under vacuum. The crude solid product was dissolved in minimal hot toluene and allowed to recrystallize to yield a white crystalline product.

Hf_2(**8**)$_2$(O^iPr)$_2$

^{1}H NMR ($CDCl_3$) 1.03 (3H, d J = 6.4 Hz, $CH(CH_3)_2$), 1.07 (9H, s, $C(CH_3)_3$), 1.11 (9H, s, $C(CH_3)_3$), 1.26 (9H, s, $C(CH_3)_3$), 1.32 (3H, d J = 6.0 Hz, $CH(CH_3)_2$), 1.37 (9H, s, $C(CH_3)_3$), 2.91 (1H, d J = 13.2 Hz, $PhCH_2N$), 3.34 (1H, d J = 13.2 Hz, $PhCH_2N$), 3.59 (1H, d J = 13.6 Hz, $PhCH_2N$), 3.95 (1H, d J = 12.8 Hz, $PhCH_2N$), 4.70 (1H, sept J = 6.0 Hz, $CH(CH_3)_2$), 5.25 (1H, d J = 13.6 Hz, $PhCH_2N$), 5.68 (1H, d J = 12.8 Hz, $PhCH_2N$), 6.28 (3H, m, Ar-H), 6.60 (1H , m, Ar-H), 6.83 (1H, s, Ar-H), 6.87 (1H, s, Ar-H), 7.09 (1H, s, Ar-H), 7.23 (1H, s, Ar-H).

^{13}C{^{1}H} NMR ($CDCl_3$) 26.6, 26.91 ($CH(CH_3)_2$), 29.5, 30.0, 31.8, 31.8 ($C(CH_3)_3$), 34.0, 34.3, 34.6, 34.8 ($C(CH_3)_3$), 61.7, 62.2, 64.8 ($PhCH_2N$), 71.4 ($CH(CH_3)_2$), 121.0, 121.2, 123.2, 123.5, 123.9, 124.4, 125.3, 126.7, 128.3, 129.1, 130.4 (Ar-CH), 135.3, 137.1, 140.0, 140.8 (Ar-C), 153.8, 156.8, 157.2 (Ar-O).

Anal.: calc. for $C_{40}H_{57}NO_4Hf$: C, 60.5; H, 7.23; N, 1.76. Found C, 60.7; H, 7.22; N, 1.71.

Hf_2(**10**)$_2$(O^iPr)$_2$

^{1}H NMR ($CDCl_3$) 0.97 (18H, s, $C(CH_3)_3$), 1.12 (6H, d (J = 6.0 Hz), $CH(CH_3)_2$), 1.18 (6H, d (J = 6.0 Hz), $CH(CH_3)_2$), 1.29 (18H, s, $C(CH_3)_3$), 2.91 (2H, d (J = 13.2 Hz), $PhCH_2N$), 3.21 (2H, d (J = 13.6 Hz), $PhCH_2N$), 3.58 (2H, d (J = 13.9 Hz), $PhCH_2N$), 4.01 (2H, d (J = 13.2 Hz), $PhCH_2N$), 4.49 (2H, sept (J = 6.0 Hz), $CH(CH_3)_2$), 5.19 (2H, d (J = 13.6 Hz), $PhCH_2N$), 5.42 (2H, d (J = 13.2 Hz), $PhCH_2N$), 5.74 (2H, dd (J = 1.1, 7.9 Hz), Ar-H), 6.11-6.23 (6H, m, Ar-H), 6.44 (2H, dt (J = 1.1, 7.2 Hz), Ar-H), 6.56 (2H, dt (J = 1.5, 7.9 Hz), Ar-H), 6.62 (2H, dt (J = 1.5, 7.5 Hz), Ar-H), 6.83 (2H, dd (J = 1.1, 7.2 Hz), Ar-H), 7.03 (2H, d (J = 2.3 Hz), Ar-H), 7.16 (2H, d (J = 2.3 Hz), Ar-H).

^{13}C{^{1}H} NMR ($CDCl_3$) 26.2 ($C(CH_3)_2$), 26.9 ($C(CH_3)_2$), 29.4 ($C(CH_3)_3$), 31.9 ($C(CH_3)_3$), 34.3 ($C(CH_3)_3$), 34.8 ($C(CH_3)_3$), 60.9 ($PhCH_2N$), 61.9 ($PhCH_2N$), 64.7 ($PhCH_2N$), 72.0 ($CH(CH_3)_2$), 116.9, 117.9, 119.4, 121.5 (Ar-CH), 123.7, 123.9 (Ar-C), 124.2, 125.4 (Ar-CH), 126.7 (Ar-C), 128.3, 129.1, 129.2, 130.1 (Ar-CH), 137.3, 141.0 (Ar-C), 154.4, 156.7, 160.4 (Ar-O).

Anal.: calc for $C_{32}H_{41}HfNO_4$: C, 56.3; H, 6.06; N, 2.49. Found: C, 56.39; H, 6.14; N, 2.51.

5.4 Polymerisation Reactions

5.4.1 Solvent-free polymerisation of *rac*-lactide

For solvent-free polymerisation of *rac*-lactide the monomer/ initiator ratio was 300:1. 0.50 g of monomer was used (recrystallised and doubly sublimed). Reactions were prepared air-sensitively and sealed before being carried out at 130 °C. After the reaction time, methanol (1 ml) was added to quench the reaction and the resulting solid dissolved in dichloromethane (~20 ml). The solvents were removed under reduced pressure and the resulting solid was analysed by ^{1}H NMR ($CDCl_3$) to determine conversion. Quantification was achieved through the integration of the monomer methine quartet (4.9 ppm) and the polymer methine multiplet (5.1 ppm) with conversion calculated using the following equation: $conv. = \frac{[PLA]}{[LA]+[PLA]} \times 100$. The solid was washed with methanol to remove all unreacted monomer. Homonuclear decoupled ^{1}H NMR spectroscopy ($CDCl_3$) was used to determine the polymer tacticity, with quantification as a P_r value (probability of racemic enchainment). GPC (THF, referenced to polystyrene standards) provided relative molecular weights (M_n) and polydispersity index (PDI) of the polymers produced. Theoretical molecular weight was calculated using the following equation: $Mw = \left(\frac{conv.}{100} \times 144 \times 300\right) + 60$, where 60 is the mass of the end groups {H/O^{i}Pr}.

5.4.2 Solvent-based polymerisations of *rac*-lactide initiated by aluminium (III) imine bis(phenolate) complexes

Solvent-based polymerisations were carried out in toluene at a lactide concentration of 0.8 M. The monomer/initator/co-initiator ratio used was 100:1:1, with benzyl alcohol acting as the co-initiator. Monomer (1 0 g) was purified through recrystallisation and double sublimation. Reactions were prepared air-sensitively and sealed before being carried out at 80 °C. After the desired reaction time, the reaction was quenched with methanol (1 ml). Solvents were then removed under reduced pressure and the resulting solid analysed by ^{1}H NMR to determine conversion. Quantification was achieved through the integration of the monomer methine quartet (4.9 ppm) and the polymer methine multiplet (5.1 ppm) with conversion calculated using the following equation: $conv. = \frac{[PLA]}{[LA]+[PLA]} \times 100$. The solid was washed with methanol to remove all unreacted monomer. Homonuclear decoupled ^{1}H NMR spectroscopy ($CDCl_3$) was used to determine the polymer tacticity, with quantification as a P_r value (probability of racemic enchainment). GPC (THF, referenced to polystyrene standards) provided relative molecular weights (M_n) and polydispersity index (PDI) of the polymers produced. Theoretical molecular

weight was calculated using the following equation: $Mw = \left(\frac{conv.}{100} \times 144 \times 100\right) + 108$, where 108 is the mass of the end groups {H/OCH_2Ph}.

5.4.3 Solvent-based polymerisations of *rac*-lactide initiated by group IV amine tris(phenolate) complexes

Solvent-based polymerisations were carried out in toluene at a lactide concentration of 0.5 M. The monomer/initator ratio used was 100:1 with monomer (1.0 g) purified through recrystallisation and double sublimation. Reactions were prepared air-sensitively and sealed before being carried out at 80 °C. After the desired reaction time, the reaction was quenched with methanol (1 ml). Solvents were then removed under reduced pressure and the resulting solid analysed by ^{1}H NMR to determine conversion. Quantification was achieved through the integration of the monomer methine quartet (4.9 ppm) and the polymer methine multiplet (5.1 ppm) with conversion calculated using the following equation: $conv. = \frac{[PLA]}{[LA]+[PLA]} \times 100$. The solid was washed with methanol to remove all unreacted monomer. Homonuclear decoupled ^{1}H NMR spectroscopy ($CDCl_3$) was used to determine the polymer tacticity, with quantification as a P_r value (probability of racemic enchainment). GPC (THF, referenced to polystyrene standards) provided relative molecular weights (M_n) and polydispersity index (PDI) of the polymers produced. Theoretical molecular weight was calculated using the following equation: $Mw = \left(\frac{conv.}{100} \times 144 \times 100\right) + 60$, where 60 is the mass of the end groups {H/O^{i}Pr}.

5.4.4 Homonuclear-decoupled ^{1}H {^{1}H} NMR spectroscopy for determining tacticity

^{1}H {^{1}H} NMR spectroscopy of polymeric material was carried out using Bruker DRX400 NMR instrument. Purified material (monomer removed through MeOH wash and subsequent drying under vacuum) was dissolved in $CDCl_3$ at a concentration of 10 mg ml^{-1}. A standard ^{1}H NMR spectrum was acquired with note taken of the chemical shift of the pendant methyl doublet signal of the lactidyl repeat unit (~1.61 ppm). The decoupled spectrum was then acquired with the secondary frequency set to that of the methyl doublet ("o2p=1.61") and the power level ("pl24=40"). Number of scans used ("ns=4") whilst fine tuning of decoupling was achieved before final acquisition of a decoupled spectrum with an increased number of scans ("ns=8"). P_r values were calculated through integration of [sis] tetrad with respect to remaining tetrads (as identified in section 1.4.3). The following equation was used to calculate probability of racemic enchainment, $P_r = \sqrt{2 \times [sis]}$, where: $[sis] = \frac{\int sis\ tetrad}{\sum(\int all\ tetrads)}$.

5.4.5 *In-situ* FT-IR studies of the polymerisation of *rac*-lactide

In-situ monitoring of the solvent-free polymerisation of *rac*-lactide was carried out using a Bruker Matrix-MF with fibre optic IR probe. A jacketed vessel was charged with monomer (25 g) and placed under a positive pressure of argon before heating to 165 °C to achieve a melt with agitation using a mechanical overhead stirrer. The probe was placed into the reaction melt and stable spectra acquired before the addition of the required amount of initiator dissolved in minimal toluene using cannula transfer under a positive pressure of argon. Spectra were collected over the length of the reaction time with the decrease in the peak attributed to the lactide acyl C-O stretch calibrated against ^{1}H NMR spectroscopy-based monomer conversion and then used to assess the kinetics.[18] All reactions were carried out to > 95 % conversion. Homonuclear decoupled ^{1}H NMR spectroscopy ($CDCl_3$) was used to determine the polymer tacticity, with quantification as a P_r value (probability of racemic enchainment). GPC (THF, referenced to polystyrene standards) provided relative molecular weights (M_n) and polydispersity index (PDI) of the polymers produced.

5.4.6 Solvent-based polymerisations of L-lactide and ε-caprolactone

Solvent-based polymerisations were carried out in toluene at an overall monomer concentration of 0.5 M. The total monomer/initator ratio used was 100:1 with the lactide/caprolactone ratio calculated on a molar basis. L-lactide was purified through recrystallisation and double sublimation, ε-caprolactone was purified *via* vacuum distillation. Reactions were prepared air-sensitively and sealed before being carried out at 80 °C. After the desired reaction time, the reaction was quenched with methanol (1 ml). Solvents were then removed under reduced pressure and the resulting solid analysed by ^{1}H NMR to determine conversion. Quantification of lactide conversion was achieved through the integration of the monomer methine quartet (4.9 ppm) and the polymer methine multiplet (5.1 ppm) with conversion calculated using the following equation: $conv. = \frac{[PLA]}{[LA]+[PLA]} \times 100$. Corresponding ε-caprolactone conversion was calculated from the integration of the acyl-methylene triplet signal for the monomer (3.95 ppm) and polymer (4.05 ppm). GPC (THF, referenced to polystyrene standards) provided relative molecular weights (M_n) and polydispersity index (PDI) of the polymers produced. Theoretical molecular weights, based on conversion, were calculated cumulatively with initial monomer ratios considered.

5.4.7 Kinetics-scale solvent polymerisations of *rac*-lactide, L-lactide & ε-caprolactone

Polymerisations were carried out in a Young's NMR tube, prepared under an inert atmosphere using standard glove-box techniques. Monomer/initiator ratio was 100:1 with a monomer concentration of 0.5 M. 0.5ml of solvent (toluene-d_8) was added to the monomer in the Young's NMR tube. A solution of initiator was prepared containing five times the amount required in 0.50 ml of toluene-d_8. 0.10 ml of this solution was then transferred to the NMR tube. Kinetic experiments were carried out at 80 °C in the NMR spectrometer. To aid accuracy, the instrument was pre-heated and shimmed to a sample of 0.5 M lactide in toluene-d_8. ^{1}H NMR spectra were obtained at regular intervals and the conversion calculated based on relative integrals of monomeric and polymeric signals for the lactide methine (4.21 ppm → 5.15 ppm) and caprolactone methylene signals (3.63 ppm → 3.96 ppm). $[M]_t = [M]_0 \times conv$. The pseudo first-order rate constant (k_{app}) was calculated from the gradient of $\ln\left(\frac{[M]_0}{[M]_t}\right) vs. t$.

5.4.8 Polymerisations to investigate reaction order

Polymerisations were carried out in a Young's NMR tube, prepared under an inert atmosphere using standard glove-box techniques. For all experiments the lactide concentration ($[LA]_0$) was 0.5 M and the monomer/initiator ratio was varied between 400:1 and 50:1. To achieve this and minimise the experimental error incurred at such a small reaction scale, the amount of initiator was calculated for a [LA]:[I] of 100:1 and six times the amount was added to a 1.2 ml of toluene-d_8. The following dilutions were used to achieve each initiator loading:

[M]:[I]	lactide	toluene-d_8	Initiator stock solution
50:1	43 mg	0.2 ml	0.4 ml
100:1	43 mg	0.4 ml	0.2 ml
200:1	43 mg	0.5 ml	0.1 ml
400:1	43 mg	0.55 ml	0.05 ml

Experiments were carried out at 80 °C in the NMR instrument. To aid accuracy, the instrument was pre-heated and shimmed to a sample of 0.5 M lactide in toluene-d_8. ^{1}H NMR spectra were obtained at regular intervals and the conversion calculated based on relative integrals of monomeric and polymeric signals for the lactide methine (4.21 ppm → 5.15 ppm). $[LA]_t = [LA]_0 \times conv$. The pseudo first-order rate constant (k_{app}) was calculated from the gradient of

$\ln\left(\frac{[LA]_0}{[LA]_t}\right) vs. t$. Order with respect to [I] was found through the plot of $\ln(k_{app})$ $vs. \ln([I])$ where the gradient of the plot is equal to the order with respect to [I].

5.4.9 *In*-situ copolymerisation studies to establish reactivity ratios

Copolymerisations were carried out in a Young's NMR tube, prepared under an inert atmosphere using standard glove-box techniques. Overall monomer/initiator ratio was 100:1 with a monomer concentration in toluene-d_8 of 0.5 M. 0.5ml of solvent (toluene-d_8) was added to the monomer in the Young's NMR tube. A solution of initiator was prepared containing five times the amount required in 0.5ml of toluene-d_8. 0.1ml of this solution was then transferred to the NMR tube. Reactions were carried out at 80 °C and to aid accuracy the instrument was pre-heated and shimmed to a sample of 0.5 M lactide in toluene-d_8. ^{1}H NMR spectra were obtained at regular intervals and the conversion calculated based on relative integrals of monomeric and polymeric signals for the lactide methine (4.21 ppm $\rightarrow$ 5.15 ppm) and caprolactone methylene signals (3.63 ppm $\rightarrow$ 3.96 ppm). Experiments were halted once conversion > 20% had been achieved. At low conversion, the mole fraction of lactide in the polymer was deemed to be an instantaneous mole fraction (F_1). Experiments were carried out at various monomer mole fractions (f_1 = 0.9, 0.7, 0.5, 0.3, 0.1). Values for the copolymer reactivity ratios were found using a Fineman-Ross plot and non-linear least squares solution to a weighted for of the Mayo-Lewis equation, as discussed in section 1.8.2.

5.5 Crystal Data and Structure Refinement

H_2**1**

Identification code	k10mdj26
Empirical formula	C_{14} H_{13} N O_2
Formula weight	227.25
Temperature	150(2) K
Wavelength	0.71073 Å
Crystal system, space group	Monoclinic, *C*2/*c*
Unit cell dimensions	a = 22.3830(16) Å alpha = 90°.
	b = 5.7810(5) Å beta = 99.915(4)°.
	c = 17.8440(16) Å gamma = 90°.
Volume	2274.5(3) $Å^3$
Z, Calculated density	8, 1.327 Mg/m^3
Absorption coefficient	0.089 mm^{-1}
F(000)	960
Crystal size	0.1 x 0.2 x 0.2 mm
Theta range for data collection	3.64° to 25.03°.
Limiting indices	-26≤h≤26, -6≤k≤6, -21≤l≤20
Reflections collected / unique	11736 / 2008 [R(int) = 0.0478]
Completeness to theta = 25.03	99.8 %
Absorption correction	None
Refinement method	Full-matrix least-squares on F^2
Data / restraints / parameters	2008 / 0 / 166
Goodness-of-fit on F^2	1.064
Final R indices [I>2sigma(I)]	R1 = 0.0372, wR2 = 0.0855
R indices (all data)	R1 = 0.0470, wR2 = 0.0923
Largest diff. peak and hole	0.129 and -0.237 $e.Å^{-3}$

H_2**2**

Identification code	k11mdj02
Empirical formula	C_{16} H_{17} N O_2
Formula weight	255.31
Temperature	150(2) K
Wavelength	0.71073 Å
Crystal system, space group	monoclinic, $P2_1/a$
Unit cell dimensions	a = 9.5050(2) Å alpha = 90°.
	B = 11.2580(2) Å beta =109.0580(10)°.
	C = 13.5330(3) Å gamma = 90°.
Volume	1368.76(5) A^3
Z, Calculated density	4, 1.239 Mg/m^3
Absorption coefficient	0.082 mm^{-1}
F(000)	544
Crystal size	0.20 x 0.15 x 0.10 mm
Theta range for data collection	3.62 to 27.49°.
Limiting indices	-12≤h≤12, -14≤k≤14, -17≤l≤17
Reflections collected / unique	25556 / 3133 [R(int) = 0.0666]
Completeness to theta = 27.49	99.6 %
Absorption correction	multi-scan
Max. and min. transmission	0.9919 and 0.9839
Refinement method	Full-matrix least-squares on F^2
Data / restraints / parameters	3133 / 0 / 182
Goodness-of-fit on F^2	1.050
Final R indices [I>2sigma(I)]	R1 = 0.0458, wR2 = 0.1046
R indices (all data)	R1 = 0.0696, wR2 = 0.1182
Largest diff. peak and hole	0.167 and -0.221 e.$Å^{-3}$

H_2**4**

Identification code	h10mdj27
Empirical formula	C_{14} H_{11} Cl2 N O_2
Formula weight	296.14
Temperature	150(2) K
Wavelength	0.71073 Å
Crystal system, space group	monoclinic, $P2_1/n$
Unit cell dimensions	a = 8.0410(5) Å alpha = 90°.
	B = 8.6470(6) Å beta = 95.121(4)°.
	C = 18.7420(10) Å gamma = 90°.
Volume	1297.94(14) A^3
Z, Calculated density	4, 1.515 Mg/m^3
Absorption coefficient	0.496 mm^{-1}
F(000)	608
Crystal size	0.20 x 0.10 x 0.10 mm
Theta range for data collection	3.57 to 27.44°.
Limiting indices	-10≤h≤10, -11≤k≤11, -24≤l≤24
Reflections collected / unique	21524 / 2946 [R(int) = 0.0503]
Completeness to theta = 27.44	99.3 %
Absorption correction	None
Max. and min. transmission	0.9521 and 0.9074
Refinement method	Full-matrix least-squares on F^2
Data / restraints / parameters	2946 / 0 / 175
Goodness-of-fit on F^2	1.031
Final R indices [I>2sigma(I)]	R1 = 0.0357, wR2 = 0.0857
R indices (all data)	R1 = 0.0482, wR2 = 0.0930
Largest diff. peak and hole	0.221 and -0.403 e.$Å^{-3}$

H_2**5**

Identification code	k13mdj01
Empirical formula	C_{30} H_{45} N O_2
Formula weight	451.67
Temperature	150(2) K
Wavelength	0.71073 Å
Crystal system, space group	Monoclinic, $P2_1/c$
Unit cell dimensions	a = 9.96000(10) Å alpha = 90°
	b = 24.2760(3) Å beta = 104.9810(10)°
	c = 12.2260(2) Å gamma = 90°
Volume	2855.64(7) A^3
Z, Calculated density	4, 1.051 Mg/m^3
Absorption coefficient	0.064 mm^{-1}
F(000)	992
Crystal size	0.30 x 0.20 x 0.20 mm
Theta range for data collection	3.55 to 27.49°.
Limiting indices	-12≤h≤12, -31≤k≤31, -15≤l≤15
Reflections collected / unique	38743 / 6517 [R(int) = 0.0509]
Completeness to theta = 27.49	99.7 %
Max. and min. transmission	0.9873 and 0.9810
Refinement method	Full-matrix least-squares on F^2
Data / restraints / parameters	6517 / 0 / 318
Goodness-of-fit on F^2	1.033
Final R indices [I>2sigma(I)]	R1 = 0.0500, wR2 = 0.1286
R indices (all data)	R1 = 0.0651, wR2 = 0.1392
Largest diff. peak and hole	0.622 and -0.282 $e.A^{-3}$

$Al_2(Me)_2(2)_2$

Identification code	k11mdj01
Empirical formula	$C_{34}\ H_{36}\ Al_2\ N_2\ O_4$
Formula weight	590.6
Temperature	150(2) K
Wavelength	0.71073 Å
Crystal system, space group	Monoclinic, $P2_1/c$
Unit cell dimensions	a = 11.55200(10) Å alpha = 90°.
	b = 12.36600(10) Å beta = 97.83°.
	c = 22.1490(2) Å gamma = 90°.
Volume	3134.55(5) $Å^3$
Z, Calculated density	4, 1.252 Mg/m^3
Absorption coefficient	0.133 mm^{-1}
F(000)	1248
Crystal size	0.50 x 0.50 x 0.40 mm
Theta range for data collection	3.56 to 27.49°.
Limiting indices	-15≤h≤14, -16≤k≤16, -28≤l≤28
Reflections collected / unique	60619 / 7141 [R(int) = 0.0474]
Completeness to theta = 27.49	99.6 %
Absorption correction	mult-scan
Max. and min. transmission	0.9488 and 0.9366
Refinement method	Full-matrix least-squares on F^2
Data / restraints / parameters	7141 / 0 / 385
Goodness-of-fit on F^2	0.997
Final R indices [I>2sigma(I)]	R1 = 0.0375, wR2 = 0.1011
R indices (all data)	R1 = 0.0475, wR2 = 0.1101
Largest diff. peak and hole	0.291 and -0.286 e.$Å^{-3}$

$Al_2(Me)_2(4)_2$

Identification code	h10mdj30
Empirical formula	$C_{102}\ H_{95}\ Al_4\ Cl_8\ N_4\ O_8$
Formula weight	1896.34
Temperature	150(2) K
Wavelength	0.71073 Å
Crystal system, space group	Orthorhombic, $Pbn2_1$
Unit cell dimensions	a = 12.0601(2) Å alpha = 90°.
	b = 22.5938(3) Å beta = 90°.
	c = 35.5013(6) Å gamma = 90°.
Volume	9673.5(3) $Å^3$
Z, Calculated density	4, 1.302 Mg/m^3
Absorption coefficient	0.327 mm^{-1}
F(000)	3948
Crystal size	0.10 x 0.10 x 0.10 mm
Theta range for data collection	3.54 to 25.02°.
Limiting indices	-14≤h≤14, -26≤k≤26, -42≤l≤42
Reflections collected / unique	77915 / 16713 [R(int) = 0.0963]
Completeness to theta = 25.02	99.1 %
Absorption correction	Semi-empirical from equivalents
Max. and min. transmission	0.9680 and 0.9680
Refinement method	Full-matrix least-squares on F^2
Data / restraints / parameters	16713 / 8 / 906
Goodness-of-fit on F^2	1.029
Final R indices [I>2sigma(I)]	R1 = 0.0836, wR2 = 0.1978
R indices (all data)	R1 = 0.1232, wR2 = 0.2241
Absolute structure parameter	0.24(8)
Largest diff. peak and hole	0.762 and -0.392 $e.Å^{-3}$

$Al_2(Me)_2(5)_2$

Identification code	h11mdj16
Empirical formula	$C_{69}\ H_{100}\ Al_2\ N_2\ O_4$
Formula weight	1075.47
Temperature	150(2) K
Wavelength	0.71073 Å
Crystal system, space group	Monoclinic, $P2_1/n$
Unit cell dimensions	a = 13.632(3) Å alpha = 90°
	b = 19.1280(17) Å beta = 99.037(7)°
	c = 25.491(2) Å gamma = 90°
Volume	6564.3(15) A^3
Z, Calculated density	4, 1.088 Mg/m^3
Absorption coefficient	0.090 mm^{-1}
F(000)	2344
Crystal size	0.10 x 0.10 x 0.05 mm
Theta range for data collection	3.52 to 25.03°.
Limiting indices	-16≤h≤16, -22≤k≤22, -30≤l≤30
Reflections collected / unique	73557 / 11493 [R(int) = 0.1273]
Completeness to theta = 25.03	99.1 %
Absorption correction	None
Max. and min. transmission	0.9955 and 0.9910
Refinement method	Full-matrix least-squares on F^2
Data / restraints / parameters	11493 / 9 / 746
Goodness-of-fit on F^2	1.040
Final R indices [I>2sigma(I)]	R1 = 0.0643, wR2 = 0.1596
R indices (all data)	R1 = 0.1107, wR2 = 0.1954
Largest diff. peak and hole	1.040 and -0.926 e.$Å^{-3}$

Ti(1)$_2$

Identification code	k11mdj40
Empirical formula	C_{35} H_{26} N_2 O_4 Ti
Formula weight	586.48
Temperature	150(2) K
Wavelength	0.71073 Å
Crystal system, space group	Monoclinic, C2/c
Unit cell dimensions	a = 20.1720(5) Å alpha = 90°.
	b = 8.0620(2) Å beta = 95.6400(10)°
	c = 17.3780(6) Å gamma = 90°.
Volume	2812.44(14) A^3
Z, Calculated density	4, 1.385 Mg/m^3
Absorption coefficient	0.348 mm^{-1}
F(000)	1216
Crystal size	0.20 x 0.10 x 0.10 mm
Theta range for data collection	3.54 to 27.48°.
Limiting indices	-26≤h≤26, -10≤k≤10, -22≤l≤22
Reflections collected / unique	18998 / 3207 [R(int) = 0.0571]
Completeness to theta = 27.48	99.2 %
Absorption correction	None
Max. and min. transmission	0.9660 and 0.9336
Refinement method	Full-matrix least-squares on F^2
Data / restraints / parameters	3207 / 0 / 204
Goodness-of-fit on F^2	1.083
Final R indices [I>2sigma(I)]	R1 = 0.0443, wR2 = 0.1019
R indices (all data)	R1 = 0.0633, wR2 = 0.1111
Largest diff. peak and hole	0.320 and -0.442 e.$Å^{-3}$

$Ti_2(3)_2(O^iPr)_4$

Identification code	k11mdj40
Empirical formula	$C_{35}\ H_{26}\ N_2\ O_4\ Ti$
Formula weight	586.48
Temperature	150(2) K
Wavelength	0.71073 Å
Crystal system, space group	Monoclinic, C2/c
Unit cell dimensions	a = 20.1720(5) Å alpha = 90°.
	b = 8.0620(2) Å beta = 95.6400(10)°
	c = 17.3780(6) Å gamma = 90°.
Volume	2812.44(14) A^3
Z, Calculated density	4, 1.385 Mg/m^3
Absorption coefficient	0.348 mm^{-1}
F(000)	1216
Crystal size	0.20 x 0.10 x 0.10 mm
Theta range for data collection	3.54 to 27.48°.
Limiting indices	-26≤h≤26, -10≤k≤10, -22≤l≤22
Reflections collected / unique	18998 / 3207 [R(int) = 0.0571]
Completeness to theta = 27.48	99.2 %
Absorption correction	None
Max. and min. transmission	0.9660 and 0.9336
Refinement method	Full-matrix least-squares on F^2
Data / restraints / parameters	3207 / 0 / 204
Goodness-of-fit on F^2	1.083
Final R indices [I>2sigma(I)]	R1 = 0.0443, wR2 = 0.1019
R indices (all data)	R1 = 0.0633, wR2 = 0.1111
Largest diff. peak and hole	0.320 and -0.442 $e.Å^{-3}$

$Zr_2(8)_2(O^iPr)_2$

Identification code	k11mdj09
Empirical formula	$C_{41.20}\ H_{58.20}\ Cl_{3.60}\ N\ O_4\ Zr$
Formula weight	850.33
Temperature	150(2) K
Wavelength	0.71073 Å
Crystal system, space group	Triclinic, $P\bar{1}$
Unit cell dimensions	a = 10.2690(2)Å alpha =83.0580(10)°.
	b = 13.0450(3)Å beta =85.0540(10)°.
	c = 18.1870(4)Å gamma =69.3200(10)°.
Volume	2260.14(8) $Å^3$
Z, Calculated density	2, 1.249 Mg/m^3
Absorption coefficient	0.493 mm^{-1}
F(000)	891
Crystal size	0.20 x 0.10 x 0.10 mm
Theta range for data collection	3.61 to 27.53°.
Limiting indices	-13≤h≤13, -16≤k≤16, -23≤l≤23
Reflections collected / unique	42935 / 10320 [R(int) = 0.0529]
Completeness to theta = 27.53	99.0 %
Absorption correction	Semi-empirical from equivalents
Max. and min. transmission	0.9524 and 0.9078
Refinement method	Full-matrix least-squares on F^2
Data / restraints / parameters	10320 / 75 / 595
Goodness-of-fit on F^2	1.106
Final R indices [I>2sigma(I)]	R1 = 0.0620, wR2 = 0.1702
R indices (all data)	R1 = 0.0800, wR2 = 0.1816
Largest diff. peak and hole	1.289 and -0.877 $e.Å^{-3}$

$Zr_2(9)_2(O^iPr)_2$

Identification code	db587
Empirical formula	$C_{41.70}\ H_{53}\ N\ O_4\ Zn$
Formula weight	697.62
Temperature	150(2) K
Wavelength	0.68890 Å
Crystal system, space group	Trigonal, $R\bar{3}$
Unit cell dimensions	a = 29.4298(6) Å alpha = 90°.
	b = 29.4298(6) Å beta = 90°.
	c = 23.4066(7) Å gamma = 120°.
Volume	17556.7(7) $Å^3$
Z, Calculated density	18, 1.188 Mg/m^3
Absorption coefficient	0.669 mm^{-1}
F(000)	6700
Crystal size	0.04 x 0.04 x 0.04 mm
Theta range for data collection	2.22 to 26.57°.
Limiting indices	-38≤h≤38, -33≤k≤38, -30≤l≤30
Reflections collected / unique	58687 / 8932 [R(int) = 0.0883]
Completeness to theta = 26.57	99.8 %
Absorption correction	None
Max. and min. transmission	0.9770 and 0.9737
Refinement method	Full-matrix least-squares on F^2
Data / restraints / parameters	8932 / 12 / 483
Goodness-of-fit on F^2	0.981
Final R indices [I>2sigma(I)]	R1 = 0.0548, wR2 = 0.1519
R indices (all data)	R1 = 0.0771, wR2 = 0.1699
Largest diff. peak and hole	0.865 and -0.384 $e.Å^{-3}$

$Hf_2(8)_2(O^iPr)_2$

Identification code	k11mdj23
Empirical formula	$C_{101}\ H_{137}\ Hf_2\ N_2\ O_8$
Formula weight	1864.11
Temperature	150(2) K
Wavelength	0.71073 Å
Crystal system, space group	Triclinic, $P\bar{1}$
Unit cell dimensions	a = 13.4420(2) Å alpha = 89.7320(10)°.
	b = 14.1900(3) Å beta = 66.6770(10)°.
	c = 15.3440(3) Å gamma = 63.7540(10)°.
Volume	2358.35(8) $Å^3$
Z, Calculated density	1, 1.313 Mg/m^3
Absorption coefficient	2.254 mm^{-1}
F(000)	965
Crystal size	0.20 x 0.15 x 0.10 mm
Theta range for data collection	3.52 to 27.45°.
Limiting indices	-17≤h≤17, -17≤k≤18, -19≤l≤19
Reflections collected / unique	28935 / 10693 [R(int) = 0.0507]
Completeness to theta = 27.45	99.2 %
Absorption correction	Semi-empirical from equivalents
Max. and min. transmission	0.8060 and 0.6614
Refinement method	Full-matrix least-squares on F^2
Data / restraints / parameters	10693 / 1 / 530
Goodness-of-fit on F^2	1.044
Final R indices [I>2sigma(I)]	R1 = 0.0334, wR2 = 0.0777
R indices (all data)	R1 = 0.0424, wR2 = 0.0821
Largest diff. peak and hole	1.967 and -1.912 $e.Å^{-3}$

$Hf_2(10)_2(O^iPr)_2$

Identification code	k12mdj11
Empirical formula	$C_{64}\ H_{82}\ Hf_2\ N_2\ O_8$
Formula weight	1364.30
Temperature	150(2) K
Wavelength	0.71073 Å
Crystal system, space group	Triclinic, $P\bar{1}$
Unit cell dimensions	a = 10.0640(5) Å alpha = 87.866(3)°
	b = 13.4640(9) Å beta = 82.346(2)°
	c = 22.6620(12) Å gamma = 75.993(3)°
Volume	2952.8(3) A^3
Z, Calculated density	2, 1.534 Mg/m^3
Absorption coefficient	3.569 mm^{-1}
F(000)	1376
Crystal size	0.10 x 0.10 x 0.10 mm
Theta range for data collection	3.51 to 27.48°.
Limiting indices	-13≤h≤13, -17≤k≤17, -29≤l≤29
Reflections collected / unique	56728 / 13345 [R(int) = 0.0776]
Completeness to theta = 27.48	98.6 %
Absorption correction	Semi-empirical from equivalents
Max. and min. transmission	0.7167 and 0.7167
Refinement method	Full-matrix least-squares on F^2
Data / restraints / parameters	13345 / 0 / 701
Goodness-of-fit on F^2	1.098
Final R indices [I>2sigma(I)]	R1 = 0.0476, wR2 = 0.1067
R indices (all data)	R1 = 0.0683, wR2 = 0.1172
Largest diff. peak and hole	1.762 and -2.672 $e.Å^{-3}$

5.6 References

1. B. M. Chamberlain, M. Cheng, D. R. Moore, T. M. Ovitt, E. B. Lobkovsky and G. W. Coates, *J. Am. Chem. Soc.*, 2001, **123**, 3229-3238.
2. E. Nichols, *Polymer Molecular Weight Methods*, American Chemical Society, 1973.
3. J. W. Nicholson, *The chemistry of polymers*, 1991.
4. Z. Grubisic, P. Rempp and H. Benoit, *J Polym Sci Pol Lett*, 1967, **5**, 753-&.
5. J. A. P. P. Vandijk, J. A. M. Smit, F. E. Kohn and J. Feijen, *J Polym Sci Pol Chem*, 1983, **21**, 197-208.
6. J. Börner, U. Flörke, K. Huber, A. Döring, D. Kuckling and S. Herres-Pawlis, *Chem. Eur. J.*, 2009, **15**, 2362-2376.
7. D. Garlotta, *J. Polym. Environ.*, 2001, **9**, 63-84.
8. A. L. Zelikoff, J. Kopilov, I. Goldberg, G. W. Coates and M. Kol, *Chem. Commun.*, 2009, 6804-6806.
9. A. Stopper, J. Okuda and M. Kol, *Macromolecules*, 2012, **45**, 698-704.
10. A. Pilone, K. Press, I. Goldberg, M. Kol, M. Mazzeo and M. Lamberti, *J. Am. Chem. Soc.*, 2014, **136**, 2940-2943.
11. N. Nomura, R. Ishii, Y. Yamamoto and T. Kondo, *Chem. Eur. J.*, 2007, **13**, 4433-4451.
12. A. Kowalski, A. Duda and S. Penczek, *Macromolecules*, 1998, **31**, 2114-2122.
13. A. Duda, Z. Florjanczyk, A. Hofman, S. Slomkowski and S. Penczek, *Macromolecules*, 1990, **23**, 1640-1646.
14. A. J. Chmura, M. G. Davidson, C. J. Frankis, M. D. Jones and M. D. Lunn, *Chem. Commun.*, 2008, 1293-1295.
15. M. D. Jones, E. L. Whitelaw and M. F. Mahon, *Inorg. Chem.*, 2010, **49**, 7176-7181.
16. B. J. Jeffery, E. L. Whitelaw, D. Garcia-Vivo, J. A. Stewart, M. F. Mahon, M. G. Davidson and M. D. Jones, *Chem. Commun.*, 2011, **47**, 12328-12330.
17. S. L. Hancock, M. F. Mahon and M. D. Jones, *New J. Chem.*, 2013, **37**, 1996-2001.
18. C. J. Chuck, M. G. Davidson, G. G. du Sart, P. K. Ivanova-Mitseva, G. I. Kociok-Kohn and L. B. Manton, *Inorg. Chem.*, 2013, **52**, 10804-10811.
19. G. W. Coates and T. M. Ovitt, *J Polym Sci Pol Chem*, 2000, **38**, 4686-4692.
20. A. P. Dove, V. C. Gibson, E. L. Marshall, A. J. P. White and D. J. Williams, *Dalton Trans.*, 2004, 570-578.
21. N. Nomura, A. Akita, R. Ishii and M. Mizuno, *J. Am. Chem. Soc.*, 2010, **132**, 1750-1751.
22. J. Fernández, A. Etxeberria and J.-R. Sarasua, *Journal of the Mechanical Behavior of Biomedical Materials*, 2012, **9**, 100-112.
23. G. M. Sheldrick, University of Gottingen, Germany, Editon edn., 1997.
24. I. Zagol-Ikapitte, V. Amarnath, M. Bala, L. J. Roberts, J. A. Oates and O. Boutaud, *Chemical Research in Toxicology*, 2009, **23**, 240-250.
25. A. Sokolowski, J. Muller, T. Weyhermuller, R. Schnepf, P. Hildebrandt, K. Hildenbrand, E. Bothe and K. Wieghardt, *J. Am. Chem. Soc.*, 1997, **119**, 8889-8900.

26. P. D. Knight, P. N. O'Shaughnessy, I. J. Munslow, B. S. Kimberley and P. Scott, *J. Organomet. Chem.*, 2003, **683**, 103-113.

27. M. Kol, M. Shamis, I. Goldberg, Z. Goldschmidt, S. Alfi and E. Hayut-Salant, *Inorg. Chem. Commun.*, 2001, **4**, 177-179.